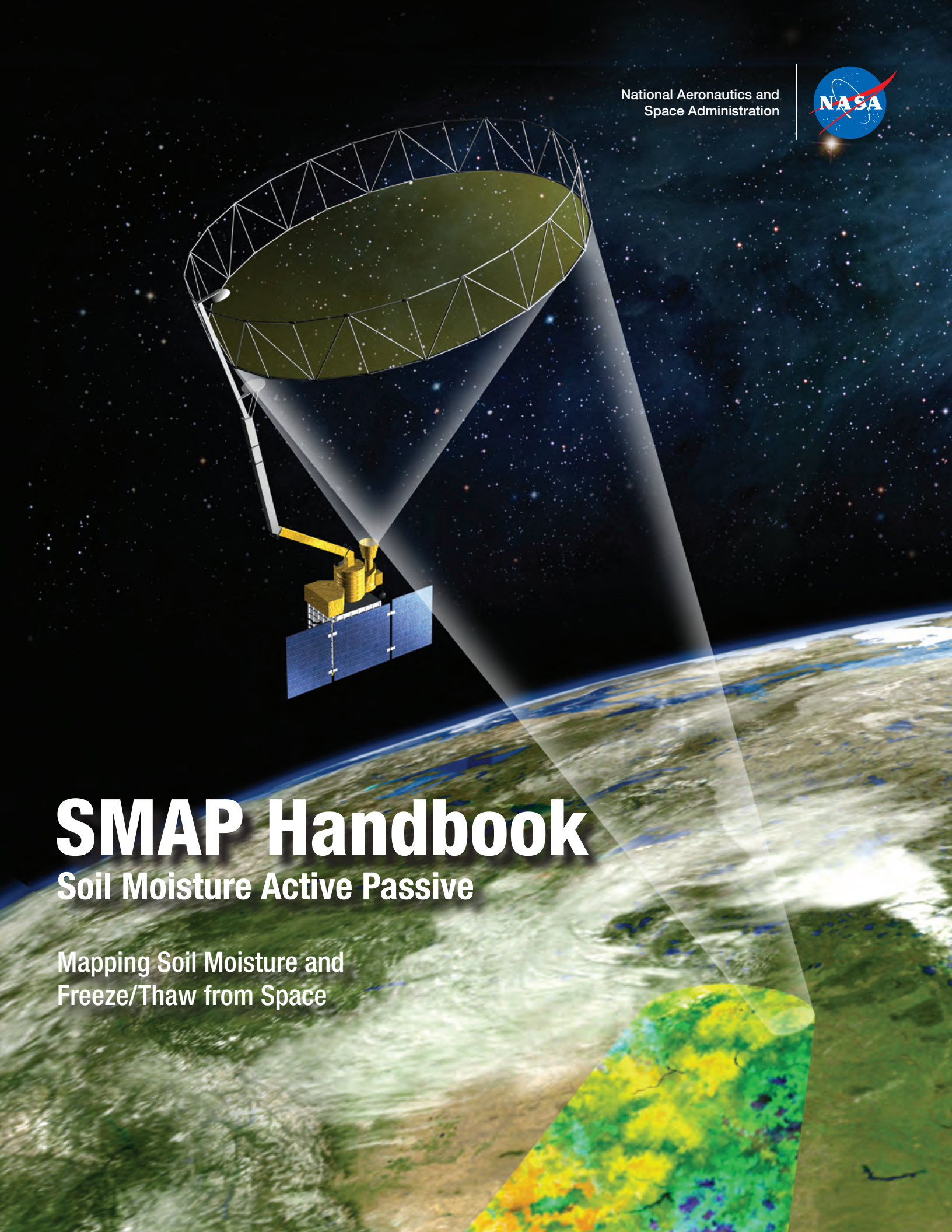National Aeronautics and
Space Administration

NASA

# SMAP Handbook
## Soil Moisture Active Passive

Mapping Soil Moisture and
Freeze/Thaw from Space

**On the cover** — The Soil Moisture
Active Passive (SMAP) mission will
provide global measurements of
soil moisture and its freeze/thaw
state from a 685-km, near-polar,
sun-synchronous orbit for a period
of 3 years. The SMAP observatory's
instrument suite includes a radiometer
and a synthetic aperture radar to make
coincident measurements of surface
emission and backscatter. SMAP data
will be used to enhance understanding
of processes that link the water, ener-
gy, and carbon cycles, and to extend
the capabilities of weather and climate
prediction models.

# SMAP Handbook
## Soil Moisture Active Passive

Mapping Soil Moisture and
Freeze/Thaw from Space

# Contents

# Key Authors

**Dara Entekhabi (SMAP Science Team Lead)**
Massachusetts Institute of Technology
Cambridge, MA 02139
E-Mail: darae@mit.edu

**Simon Yueh (SMAP Project Scientist)**
Jet Propulsion Laboratory
California Institute of Technology
Pasadena, CA 91109
E-Mail: simon.h.yueh@jpl.nasa.gov

**Peggy E. O'Neill (SMAP Deputy Project Scientist)**
NASA Goddard Space Flight Center
Greenbelt, MD  20771
E-Mail: peggy.e.oneill@nasa.gov

**Kent H. Kellogg (SMAP Project Manager)**
Jet Propulsion Laboratory
California Institute of Technology
Pasadena, CA  91109
E-Mail: kent.h.kellogg@jpl.nasa.gov

**Angela Allen**
Alaska Satellite Facility
University of Alaska
Fairbanks, AK 99701
E-Mail: arallen@alaska.edu

**Rajat Bindlish**
USDA ARS Hydrology and Remote Sensing Laboratory
Beltsville, MD  20705
Email: rajat.bindlish@ars.usda.gov

**Molly Brown**
NASA Goddard Space Flight Center
NASA GSFC Code 618
Greenbelt, MD  20771
Email: molly.e.brown@nasa.gov

**Steven Chan**
Jet Propulsion Laboratory
California Institute of Technology
Pasadena, CA 91109
E-Mail: steventsz.k.chan@jpl.nasa.gov

**Andreas Colliander**
Jet Propulsion Laboratory
California Institute of Technology
Pasadena, CA 91109
E-Mail: andreas.colliander@jpl.nasa.gov

**Wade T. Crow**
USDA ARS Hydrology and Remote Sensing Lab
Beltsville, MD 20705
E-Mail: crow@hydrolab.arsusda.gov

**Narendra Das**
Jet Propulsion Laboratory
California Institute of Technology
Pasadena, CA 91109
E-Mail: narendra.n.das@jpl.nasa.gov

**Gabrielle De Lannoy**
NASA Goddard Space Flight Center
Greenbelt, MD 20771
E-Mail: gabrielle.j.delannoy@nasa.gov

**Roy S. Dunbar**
Jet Propulsion Laboratory
California Institute of Technology
Pasadena, CA 91109
E-Mail: roy.s.dunbar@jpl.nasa.gov

**Wendy N. Edelstein**
Jet Propulsion Laboratory
California Institute of Technology
Pasadena, CA 91109
E-Mail: wendy.n.edelstein@jpl.nasa.gov

**Jared K. Entin**
NASA Headquarters
Washington, D.C. 20546
E-Mail: jared.k.entin@nasa.gov

**Vanessa Escobar**
NASA Goddard Space Flight Center
Greenbelt, MD 20771
E-Mail: vanessa.m.escobar@nasa.gov

**Shawn D. Goodman**
Jet Propulsion Laboratory
California Institute of Technology
Pasadena, CA 91109
E-Mail: shawn.d.goodman@jpl.nasa.gov

**Thomas J. Jackson**
USDA ARS Hydrology and Remote Sensing Lab
Beltsville, MD 20705
E-Mail: tom.jackson@ars.usda.gov

**Ben Jai**
Jet Propulsion Laboratory
California Institute of Technology
Pasadena, CA 91109
E-Mail: benhan.jai@jpl.nasa.gov

**Joel Johnson**
Ohio State University
Columbus, OH 43210
E-Mail: johnson.1374@osu.edu

**Edward Kim**
NASA Goddard Space Flight Center
Greenbelt, MD 20771
E-Mail: ed.kim@nasa.gov

**Seungbum Kim**
Jet Propulsion Laboratory
California Institute of Technology
Pasadena, CA 91109
E-Mail: seungbum.kim@jpl.nasa.gov

**John Kimball**
The University of Montana
Polson, MT 59860-6815
E-Mail: johnk@ntsg.umt.edu

**Randal D. Koster**
NASA Goddard Space Flight Center
Greenbelt, MD  20771
E-Mail: randal.d.koster@nasa.gov

**Amanda Leon**
National Snow and Ice Data Center
University of Colorado
Boulder, CO 80309
Email: Amanda.Leon@nsidc.org

**Kyle C. McDonald**
Jet Propulsion Laboratory
California Institute of Technology
Pasadena, CA 91109
E-Mail: kyle.c.mcdonald@jpl.nasa.gov

**Mahta Moghaddam**
University of Michigan
Ann Arbor, MI 48109
E-Mail: mmoghadd@umich.edu

**Priscilla Mohammed**
NASA Goddard Space Flight Center
Greenbelt, MD 20771
E-Mail: priscilla.n.mohammed@nasa.gov

**Susan Moran**
USDA Southwest Watershed Research Center
Tucson, AZ 85719
E-Mail: susan.moran@ars.usda.gov

**Eni G. Njoku**
Jet Propulsion Laboratory
California Institute of Technology
Pasadena, CA 91109
E-Mail: eni.g.njoku@jpl.nasa.gov

**Jeffrey R. Piepmeier**
NASA Goddard Space Flight Center
Greenbelt, MD  20771
E-Mail:  jeff.piepmeier@nasa.gov

**Rolf Reichle**
NASA Goddard Space Flight Center
Greenbelt, MD 20771
E-Mail: rolf.reichle@nasa.gov

**Francois Rogez**
Jet Propulsion Laboratory
California Institute of Technology
Pasadena, CA 91109
E-Mail: francois.p.rogez@jpl.nasa.gov

**J. C. Shi**
University of California
Santa Barbara, CA 93106
E-Mail: shi@icess.ucsb.edu

**Michael W. Spencer**
Jet Propulsion Laboratory
California Institute of Technology
Pasadena, CA 91109
E-Mail: michael.w.spencer@jpl.nasa.gov

**Samuel W. Thurman**
Jet Propulsion Laboratory
California Institute of Technology
Pasadena, CA 91109
E-Mail: sam.w.thurman@jpl.nasa.gov

**Leung Tsang**
University of Washington
Seattle, WA 98195
E-Mail: leung@ee.washington.edu

**Jakob Van Zyl**
Jet Propulsion Laboratory
California Institute of Technology
4800 Oak Grove Drive, Pasadena, CA 91109
E-Mail: jakob.j.vanzyl@jpl.nasa.gov

**Barry Weiss**
Jet Propulsion Laboratory
California Institute of Technology
Pasadena, CA 91109
E-Mail: barry.h.weiss@jpl.nasa.gov

**Richard West**
Jet Propulsion Laboratory
California Institute of Technology
Pasadena, CA 91109
E-Mail: richard.west@jpl.nasa.gov

# Preface

The SMAP Handbook was produced in 2013 as a compendium of information on the project near its time of launch. The SMAP Science Definition Team and Project personnel wrote this volume together to provide the community with the essential information on programmatic, technological, and scientific aspects of the mission.

The SMAP Handbook begins with an introduction and background that places the project in the context of other related missions and the National Research Council (NRC) Earth Science Decadal Survey report. The beginning section also includes a mission overview that introduces and traces the science goals and requirements to the measurement approach and to the data systems. The technological approaches to the instrument are also outlined and unique technical capabilities of the mission — such as radio frequency interference detection and mitigation — are highlighted.

The SMAP science products are introduced in three sections: 1) Soil Moisture, 2) Value-Added Data Assimilation, and 3) Carbon Cycle. The first science data product section defines the main attributes of the SMAP passive radiometer–based, the active radar–based, and the synergistic active-passive soil moisture products. Each of these soil moisture products has varying resolutions and different accuracies and other attributes. This section of the SMAP Handbook is meant to provide a guide to users on how to select a surface moisture product that best matches their requirements. The Value-Added Data Assimilation section of the SMAP Handbook is a guide to a unique science feature of the mission. It includes description of data products that merge the SMAP instrument measurements with other observing system data as well as models in order to produce science data products that are applicable to a much wider range of applications. The Carbon Cycle section outlines the application of the SMAP measurements to the problem of estimating the net terrestrial carbon exchange with the atmosphere that remains one of main sources of uncertainty in global change.

Calibration and validation (Cal/Val) is a necessary and major component of most Earth-observing missions. The SMAP Project has made a concerted effort to perform comprehensive pre-launch Cal/Val activities to test the retrieval algorithms for its science products. The Project also plans coordinated Cal/Val activities with collaborating partners during the early post-launch phase. These activities are outlined in a dedicated section on Cal/Val.

A rare characteristic of the SMAP Project is its emphasis on serving both basic Earth System science as well as applications in operational and practice-oriented communities. The NRC Decadal Survey identified a number of possible domains of applications with SMAP science data products. These include weather and climate prediction, agricultural and food production decision support systems, floods and drought monitoring, environmental human health assessments, and national security applications. The SMAP Project and the SMAP Science Definition Team developed formal plans to engage application users from a diversity of settings and institutions. A SMAP Early Adopter program was launched to facilitate two-way exchanges of needs and capabilities between the community and the Project. The approach to applied science is described in a dedicated section in the SMAP Handbook.

The SMAP Project is advancing rapidly as we approach launch and enter the science data acquisition phase. The material included in this volume may advance with time and updates may be necessary. The SMAP Project has taken an open approach to documentation and all major Project reports are available on line at the project website (smap.jpl.nasa.gov). The Algorithm Theoretical Basis Documents (ATBDs), Ancillary Data reports, Cal/Val Plan, and Applications Plan form a comprehensive set of Project documents that correspond to the sections of the SMAP Handbook. The posting of their most recent versions will provide the readership with updates on the contents of this volume as they become available.

The final section of the SMAP Handbook is a bibliography of papers in peer-reviewed science journals that are either about SMAP or produced in response to the development of the SMAP mission. This list of pre-launch publications is testimony to the broad and deep work that went into the design and implementation of the SMAP mission. The returns on this effort begin with the launch of the SMAP satellite mission in the very near future.

# 1. Introduction and Background

## I. Soil Moisture Observations

Soil moisture is a primary state variable of hydrology and the water cycle over land. In diverse Earth and environmental science disciplines, this state variable is either an initial condition or a boundary condition of relevant hydrologic models. Applications such as weather forecasting, skillful modeling and forecast of climate variability and change, agricultural productivity, water resources management, drought prediction, flood area mapping, and ecosystem health monitoring all require information on the status of soil moisture. The outcomes from these applications all have direct impacts on the global environment and human society. Measuring surface soil moisture with the required accuracy and resolution (spatial and temporal) is imperative to fulfill the needs of these and other applications.

Soil moisture is currently measured at scales ranging from point scale (in situ) to satellite footprint scales (~40 km) at various temporal resolutions. Measurement networks of in situ sensors (such as USDA's Soil Climate Analysis Network (SCAN) or NOAA's Climate Reference Network (CRN) in the continental United States) have potentially high soil moisture measurement accuracy but are spatially very sparse. On the other hand, satellite-based soil moisture measurements using C- and X-band channels (6 to 11 GHz or 3 to 5 cm wavelength) from the EOS Advanced Multichannel Scanning Radiometer (AMSR-E) and Navy's WindSat instruments are of coarse spatial resolution (>50 km) with shallow sensing depth (~1 cm). Satellite-based C- and X-band radiometers also have low sensitivity to soil moisture for even small amounts of vegetation, leading to high soil moisture retrieval errors. There is significant heritage from both observations and theory showing the relative advantages of lower frequency (< 5 GHz) microwave radiometry for mapping soil moisture content at the land surface. At lower frequencies the atmosphere is less opaque, the intervening vegetation biomass is more transparent, and the effective microwave emission is more representative of the soil below the surface skin layer. The European Space Agency's Soil Moisture and Ocean Salinity (SMOS) satellite, launched in November 2009, is the first wide-swath L-band soil moisture mission (operating at 1.4 GHz or ~21 cm wavelength), and retrieves soil moisture over a much higher range of vegetation conditions at a spatial resolution of ~40 km with a sensing depth of ~5 cm (Kerr et al. 2001).

Besides satellite radiometers, radar scatterometers have also been used to retrieve soil moisture. The European Remote Sensing Satellite (ERS) C-band scatterometer with resolution of ~50 km has been used to retrieve surface soil moisture over sparsely vegetated regions with moderate accuracy. Synthetic aperture radars (SARs) provide observations at much higher spatial resolution than radiometers and scatterometers. The heritage of spaceborne L-band SARs includes NASA's SIR-C and JAXA's JERS and PALSAR instruments. While SARs provide high-resolution measurements, they typically operate with narrow swaths and do not provide the frequent temporal coverage needed for global land hydrology applications.

Each of these measurement technologies on its own can only partially satisfy the criteria of high spatial and temporal resolution, wide spatial coverage, optimal sensing depth, and desired accuracy in retrieved soil moisture over moderate vegetation conditions. Therefore, soil moisture estimated from just one of these individual technologies is not matched well to the integrated needs of hydrometeorology, ecology, water resources management, and agricultural applications.

To meet these needs, NASA's Soil Moisture Active Passive (SMAP) mission uses an L-band radar and an L-band radiometer for concurrent, coincident measurements integrated as a single observation system. This combination takes advantage of the relative strengths of both active (radar) and passive (radiometer) microwave remote sensing for soil moisture mapping. At L-band the microwave emission (brightness temperature) measured by the radiometer mostly emanates from the top ~5 cm and is clearly sensitive to soil moisture in regions having vegetation water contents (VWC) up to ~5 kg m$^{-2}$ averaged over the radiometer resolution footprint of ~40 km. The SMAP L-band SAR provides backscatter measurements at higher resolution (~1 to 3 km) than the coarser resolution radiometer measurement. The accuracy of the radar is limited for soil moisture sensing, however, by the higher sensitivity of radar to surface roughness and vegetation scattering. The significant advantage provided by SMAP is the concurrent L-band radar and radiometer measurement capability, so that the radar and radiometer measurements can be effectively combined to derive soil moisture estimates with intermediate accuracy and resolution (~9 km) that meet the SMAP science requirements.

## II. Earth Science Decadal Survey

The National Research Council's (NRC) Decadal Survey Report, *Earth Science and Applications from Space: National Imperatives for the Next Decade and Beyond*, was released in 2007 after a 2-year study commissioned by NASA, NOAA, and USGS to provide consensus recommendations to guide the agencies' space-based Earth observation programs in the coming decade (NRC 2007). Several factors, including science impacts, societal benefits, and technological readiness of potential missions, were considered in the process of ranking the projects in four tiers defined by time frames for development and launch. SMAP was considered to have high science

value, diverse applications impacts, and technological readiness. The accuracy, resolution, and global coverage of SMAP soil moisture and freeze/thaw measurements have applications across several Earth and environmental science disciplines including hydrology, climate, carbon cycle, and the meteorological, environmental, agricultural, and ecological communities. Change in future water resources is a critical societal impact of climate change, and scientific understanding of how such change may affect water supply and food production is crucial for policy makers (Figure 1). Currently, uncertainties in existing climate models result in disagreement on whether there will be more or less water in any given region compared to today — the new data from SMAP should help climate models to be brought into agreement on future trends in water resource availability. For these reasons, the NRC Decadal Survey's Water Resources Panel gave SMAP the highest mission priority within its field of interest. Furthermore, other NRC Decadal Survey panels dealing with weather, climate, ecosystems, and human health also cited uses for SMAP data. The recognized broad uses of soil moisture and freeze/thaw information in Earth system science and applications resulted in the recommendation that SMAP should be considered a high-priority mission in the Decadal Survey. SMAP is one of four missions recommended by the NRC for launch in the first-tier 2010 to 2013 period, and NASA announced in early 2008 that SMAP would be one of the first two new Earth science missions (along with IceSat-2) to fly in response to the NRC Decadal Survey report and follow-on activities.

The Decadal Survey ranking and assignment of the missions to the four tiers also considered technological readiness as a factor. The SMAP mission concept was substantially derived from initial formulation studies for the Hydrosphere State (Hydros) mission (Entekhabi et al. 2004). Hydros was an Earth System Science Pathfinder satellite mission proposed to NASA in 2001. It passed through a selective approval process to enter the formulation phase but was cancelled in 2005 due to NASA budget constraints. The importance to SMAP of the early formulation work done by Hydros design studies is significant.

## III. Project Status

NASA initiated SMAP project formulation in 2008. The project went through design studies and formulation in its initial years, and successfully completed its Critical Design Review in July 2012. During May 2013 the project was approved to proceed into System Integration and Test (Phase D). The SMAP launch is currently scheduled for November 5, 2014. The SMAP mission is being developed by NASA's Jet Propulsion Laboratory, which is building the spacecraft, the instrument (except for the radiometer), and the science processing system. NASA Goddard Space Flight Center is providing the L-band radiometer and Level 4 science processing. The Canadian Space Agency (CSA) is also a mission partner to provide critical support to science and calibration/validation (pre- and post-launch). SMAP will be launched from Vandenberg Air Force Base in California on a Delta II launch vehicle, and
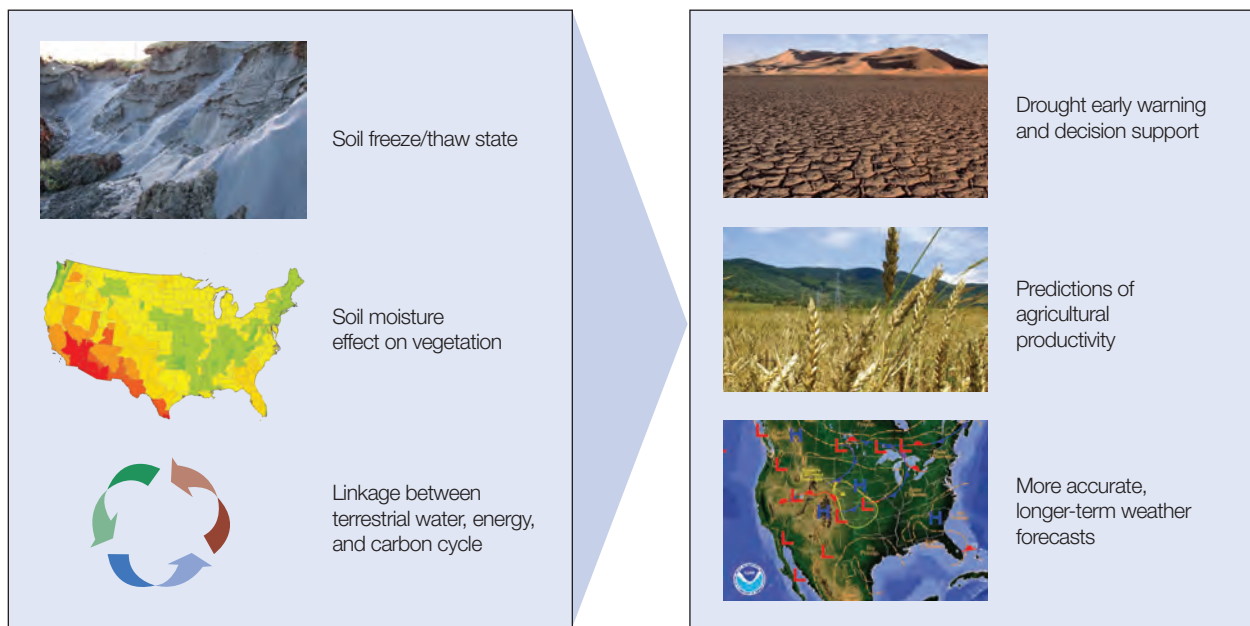


Figure 1. Some of the applications associated with SMAP data products highlighted in the Decadal Survey report.

will be placed into a polar sun-synchronous 6 AM/6 PM orbit with a 685 km altitude. The L-band SAR and radiometer share a 6-m mesh deployable offset-fed reflector antenna that rotates at 13 to 14.6 rpm to provide high spatial resolution with a 1000 km measurement swath that enables global coverage every 2–3 days (Figure 2). Major challenges that have been and are being addressed by SMAP include: (1) mitigation of L-band radio frequency interference to both radiometer and SAR measurements from terrestrial and other spaceborne sources; (2) use of a mesh reflector antenna for L-band radiometry measurements; (3) dynamics and control of a relatively large spinning payload by a comparatively small spacecraft bus; (4) cost-effective adaptation of an existing avionics architecture to accommodate the unique demands of a high-data-volume SAR; and (5) accommodating a relatively late in the design lifecycle selection of launch services and vehicle.

## References

Entekhabi, D., E. Njoku, P. Houser, M. Spencer, T. Doiron, J. Smith, R. Girard, S. Belair, W. Crow, T. Jackson, Y. Kerr, J. Kimball, R. Koster, K. McDonald, P. O'Neill, T. Pultz, S. Running, J. C. Shi, E. Wood, and J. van Zyl, "The Hydrosphere State (HYDROS) mission concept: An Earth system pathfinder for global mapping of soil moisture and land freeze/thaw," *IEEE Trans. Geosci. Rem. Sens.*, vol. 42(10), pp. 2184–2195, 2004.

Kerr, Y., P. Waldteufel, J. Wigneron, J. Martinuzzi, J. Font, M. Berger, "Soil moisture retrieval from space: The Soil Moisture and Ocean Salinity (SMOS) mission," *IEEE Trans. Geosci. Rem. Sens.*, vol. 39(8), pp. 1729–1735, 2001.

National Research Council, *Earth Science and Applications from Space: National Imperatives for the Next Decade and Beyond*, pp. 400, 2007.
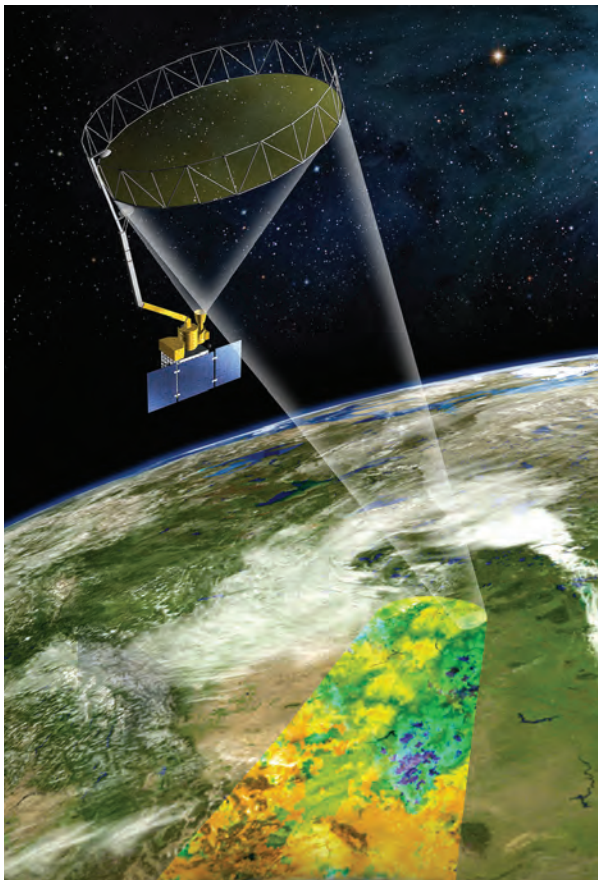
Figure 2. The SMAP observatory is a dedicated spacecraft with a rotating 6-m lightweight deployable mesh reflector. The radar and radiometer share a common antenna feed.

# 2. Mission Overview

## I. Science Objectives

SMAP observations of soil moisture and freeze/thaw state from space will allow significantly improved estimates of water, energy, and carbon transfers between the land and atmosphere. The accuracy of numerical models of the atmosphere used in weather prediction and climate projections is critically dependent on the correct characterization of these transfers. Soil moisture measurements are also directly applicable to flood assessment and drought monitoring. SMAP observations can help mitigate these natural hazards, resulting in potentially great economic and social benefits. SMAP observations of soil moisture and freeze/thaw timing will also reduce a major uncertainty in quantifying the global carbon balance by helping to resolve an apparent missing carbon sink on land at boreal latitudes.

The science objectives of the SMAP project are captured by five specific goals:

1. Understand processes that link the terrestrial water, energy, and carbon cycles,

2. Estimate global water and energy fluxes at the land surface,

3. Quantify net carbon flux in boreal landscapes,

4. Enhance weather and climate forecast skill, and

5. Develop improved flood prediction and drought-monitoring capability.

Soil moisture controls the partitioning of available energy into sensible and latent heat fluxes across regions where the evaporation regime is, at least intermittently, water-limited (as opposed to energy-limited). Since the fluxes of sensible and latent heat and moisture at the base of the atmosphere influence the evolution of weather, soil moisture is often a significant factor in the performance of atmospheric models, both in weather and in climate applications. Given the persistence of soil moisture anomalies, the initialized soil moisture can influence land fluxes, and thus simulated weather or climate, for days to months into the forecast. In this context, the metric that is used to define soil moisture measurement requirements is influenced by the need to capture soil moisture's control over land–atmosphere interactions in atmospheric models.

The above goals cover both the science impacts and applications goals of the SMAP mission. Applied science and applications have been particularly important to the development of the project. A SMAP Applications Plan has been developed and will be implemented with the cooperation of applications partners during the course of

mission life. For example, the diverse application areas directly addressed by SMAP measurements include:

- Weather forecasting through initialization of numerical weather prediction models

- Seasonal climate forecasting through use of soil moisture as model initial and boundary conditions

- Agricultural and hydrological drought monitoring through mapping of soil moisture deficits

- Flood and flashflood forecasting and hazards mitigation through soil moisture-based flood guidance

- Agricultural productivity and early famine warning through assessment of crop water stress

- Human health through monitoring and prediction of heat stress and conditions for waterborne diseases

- National security through assessment of terrain trafficability and density altitude for air transport

Chapter 8 provides more detailed explanation of these applications and outlines their traceability to SMAP data products. The SMAP project strategy for engaging with the applications community is also described.

## II. Level 1 Requirements

The SMAP Level 1 Requirements and Mission Success Criteria document specifies the SMAP baseline requirement for soil moisture and freeze/thaw measurements. This document is essentially a contract with the implementing center (Jet Propulsion Laboratory, California Institute of Technology, for SMAP) to design, build, deliver, and operate a science mission to produce science products with specified requirements. The baseline science requirement for SMAP is to provide estimates of soil moisture in the top 5 cm of soil with an error of no greater than 0.04 $cm^3$ $cm^{-3}$ volumetric (1-sigma) at 10 km spatial resolution and 3-day average intervals over the global land area, excluding regions of snow and ice, frozen ground, mountainous topography, open water, urban areas, and vegetation with water content greater than 5 kg $m^{-2}$ (averaged over the spatial resolution scale). Figure 3 shows the global regions where this requirement is expected to be met. Land regions affected by the exclusions are blank on the map in Figure 3.

The mission is additionally required to provide estimates of surface binary freeze/thaw state in the region north of 45ºN latitude, which includes the boreal forest zone, with a classification accuracy of 80% at 3 km spatial resolution
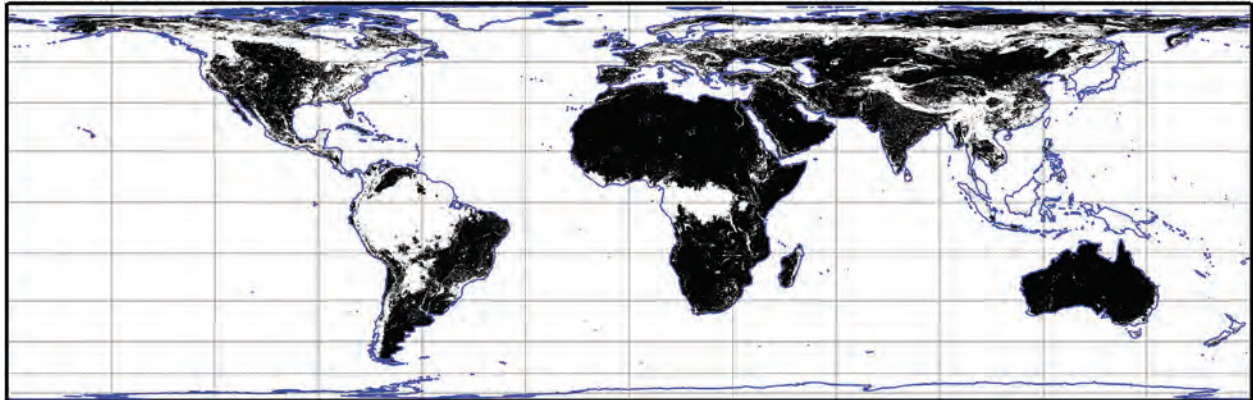
Figure 3. SMAP is expected to meet its Level 1 Requirements over the shaded regions that exclude regions of snow and ice, frozen ground, mountainous topography (areas with greater than 300 m standard devi-ation of elevation), open water (greater than 10%), urban areas (greater than 50%), and vegetation with water content greater than 5 kg m$^{-2}$.

and 2-day average intervals. The baseline science mission is required to collect space-based measurements of soil moisture and freeze/thaw state for at least three years to allow seasonal and interannual variations of soil moisture and freeze/thaw to be resolved. Finally, the document specifies that the SMAP project shall conduct a calibration and validation program to verify that its delivered data meet the requirements.

## III. Traceability Matrix

In order to meet its science measurement requirements, the SMAP approach is to integrate an L-band radar and L-band radiometer as a single observation system combining the relative strengths of active and passive microwave remote sensing for soil moisture mapping. The radar and radiometer measurements can be effectively combined to derive soil moisture maps that approach the accuracy of radiometer-only retrievals, but with a resolution intermediate between the radar and radiometer resolutions (and that can approach the radar resolution under some conditions). The SMAP mission requirements include simultaneous measurement of L-band brightness temperature and backscatter, at spatial resolutions of about 40 km across the entire swath and 3 km over outer 70% of the swath, respectively. The combined radar/radi-ometer–based soil moisture product is generated at about an intermediate 10 km resolution. Because the effects of vegetation and surface roughness are dependent on incidence angle, the SMAP mission adopted a conical scan, constant incidence angle approach. This reduces the retrieval complexity and also facilitates the use of time-series retrieval algorithms. To maximize the indepen-dent information obtainable from the polarized V and H brightness temperature channels and avoid large antenna footprints at high incidence angles, a single incidence angle in the range between 35 and 50 degrees is desired. A 40° incidence angle was adopted for SMAP as a suitable angle for both the radiometer and radar designs. The wide 1000 km swath that results from this approach enables SMAP observations to provide global coverage in 2–3 days. Table 1 is a summary of the SMAP instrument functional requirements derived from the science mea-surement needs.

## IV. Mission Concept of Operations

### A. Mission Synopsis

The goal of the SMAP mission is to establish a satellite observatory in a near-polar, sun-synchronous Earth orbit to collect a 3-year dataset that will be used to determine the moisture content of the upper soil and its frozen or thawed state, with global measurements every 3 days. This is accomplished using an instrument that combines an L-band radar and an L-band radiometer, which share a rotating 6-m-aperture reflector antenna that scans a wide 1000-km swath as the observatory orbits the Earth. The radiometer provides "passive" measurements of the microwave emission from the upper soil with a spa-tial resolution of about 40 km, and is more sensitive to near-surface soil moisture and less sensitive to the effects of surface roughness and vegetation than the radar. The radar makes "active" backscatter measurements of the surface, and the ground processing system performs the synthetic aperture radar processing to achieve a spatial resolution of 3 km across about 70% of the swath in its high-resolution mode. Utilizing a combination of the active and passive datasets provides greater accuracy and spatial resolution in measuring moisture in the upper 5 cm of soil than is possible with either of the individual instruments alone. The radar data also provide information on the frozen/thawed state of the soil, which is important to understanding the length of the vegetation growing season and the contribution of the boreal forests to the global carbon balance.

Table 1. SMAP mission requirements.

| Scientific Measurement Requirements | Instrument Functional Requirements |
|---|---|
| **Soil Moisture:**<br>~±0.04 cm$^3$cm$^{-3}$ volumetric accuracy in the top 5 cm for vegetation water content ≤ 5 kg m$^{-2}$<br><br>Hydrometeorology at ~10 km resolution<br><br>Hydroclimatology at ~40 km resolution | **L-Band Radiometer (1.41 GHz):**<br>Polarization: V, H, 3rd and 4th Stokes Parameters<br>Resolution: 40 km<br>Radiometric Uncertainty*: 1.3 K<br><br>**L-Band Radar (Tunable from 1.22–1.3 GHz):**<br>Polarization: VV, HH, HV (or VH)<br>Resolution: 10 km<br>Relative accuracy*: 0.5 dB (VV and HH)<br>Constant incidence angle** between 35° and 50° |
| **Freeze/Thaw State:**<br>Capture freeze/thaw state transitions in integrated vegetation-soil continuum with two-day precision, at the spatial scale of landscape variability (~3 km). | **L-Band Radar (Tunable from 1.22–1.3 GHz):**<br>Polarization: HH<br>Resolution: 3 km<br>Relative accuracy*: 0.7 dB (1 dB per channel if 2 channels are used)<br>Constant incidence angle** between 35° and 50° |
| Sample diurnal cycle at consistent time of day (6 AM/6 PM equator crossing)<br>Global, ~3 day (or better) revisit<br>Boreal, ~2 day (or better) revisit | Swath width: ~1000 km<br><br>Minimize Faraday rotation (degradation factor at L-band) |
| Observation over minimum of three annual cycles | Baseline 3-year mission life |

\* Includes precision and calibration stability   \*\* Defined without regard to local topographic variation

SMAP is a NASA-directed project managed by the Jet Propulsion Laboratory, with the Goddard Space Flight Center (GSFC) as a mission partner. JPL provides project management, the project scientist, systems engineering, the radar, the spacecraft, mission operations, and leads the science data processing. GSFC provides the radiometer, the deputy project scientist, the Near-Earth Network (NEN) tracking services, and supports science data processing.

Figure 4 shows the timeline for the 40-month SMAP mission based on a launch date of November 5, 2014. Four mission phases are defined to simplify description of the different periods of activity during the mission. These phases are the launch, commissioning, science observation, and decommissioning. Launch (L) is the time of liftoff of the launch vehicle.

## B. Launch Phase

The launch phase is the period of transition that takes the observatory from the ground, encapsulated in the launch vehicle fairing, to its initial free flight in the injection orbit. It begins with the start of the launch countdown at L – 5 hours. The end of the launch phase is defined at L + 24 hours to allow time to establish regular and predictable ground station contacts before the start of the commissioning activities. After ascent and separation from the launch vehicle upper stage, the spacecraft flight software controls initiation of the telemetry link, stabilization of any tipoff rates, deployment of the solar array, and establishment of a sun-pointed attitude. At this point, the ground operations team monitors the health of the observatory, collects data to establish the initial orbit, commands release of launch restraints on the stowed instrument boom and reflector, and commands playback of the launch telemetry.
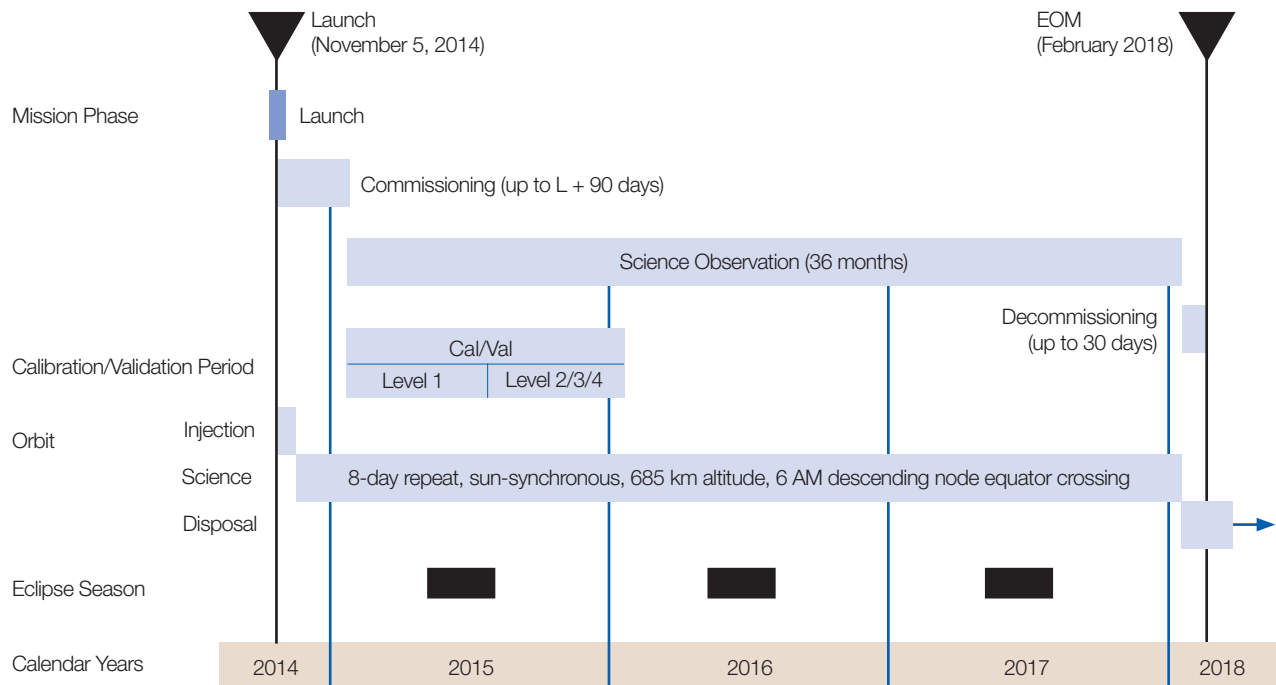
Figure 4. SMAP mission timeline.

## C. Commissioning Phase

The commissioning phase, sometimes known as in-orbit checkout (IOC), is the period of initial operations that includes checkout of the spacecraft subsystems, maneuvers to raise the observatory into the science orbit, deployment and spin-up of the instrument boom and reflector, and checkout of the full observatory. It extends from the end of the launch phase until both the ground project elements and the spacecraft and instrument subsystems are fully functional and have demonstrated the required on-orbit performance to begin routine science data collection. The Level 1 requirements call for these activities be completed by L + 90 days. During this phase, up to eight commissioning maneuvers, including two calibration burns, are executed to raise the observatory from the initial injection orbit to the 685-km science orbit.

## D. Science Observation Phase

The science observation phase is the period of near-continuous instrument data collection and return, extending from the end of the commissioning phase for 3 years. The observatory is maintained in the nadir attitude, except for brief periods when propulsive maneuvers are required to maintain the orbit and for periodic radiometer calibrations that require briefly viewing cold space. During the first year of science acquisition, a period of calibration and validation of the science data products is conducted. This includes special field campaigns and intensive in situ data acquisitions, data analysis, and performance evaluations of the science algorithms and data product quality. These activities continue at a lower level for the remainder of the science observation phase, but primarily for the purpose of monitoring and fine-tuning the quality of the science data products.

During science operations, the mission must return an average volume of 135 GB per day of science data to be delivered to the science data processing facility. SMAP does not have an onboard Global Positioning System (GPS) receiver and the associated ephemeris knowledge because the large instrument reflector in the zenith direction obscures GPS visibility. For this reason, Doppler ground tracking with frequent ephemeris table uploads to the observatory are used to maintain position and pointing accuracy.

## E. Decommissioning Phase

At the end of its useful life, the observatory is maneuvered to a lower disposal orbit and decommissioned to a functional state that prevents interference with other missions. The observatory is maneuvered to the lower disposal orbit to reduce its orbital lifetime and passivated (energy sources depleted to the extent allowed by the design)

to reduce the risk of explosion or fragmentation if struck by orbital debris. Up to 30 days have been allocated for decommissioning to end the active operations of the observatory (EOM, end of mission). The disposal orbit has been designed to ensure that the observatory re-enters the atmosphere within 15.5 years as is required to meet orbital debris probability of collision requirements after the observatory is decommissioned.

### F. Science Orbit

SMAP observes the Earth for 3 years from a sun-synchronous, near-circular science orbit with an equator-crossing altitude near 685 km and an ascending node at 6 PM local mean solar time. At this altitude, a sun-synchronous orbit has an inclination of about 98.12° and an orbit period of 98.46 minutes. The science orbit altitude has been selected to allow near-global coverage of the Earth to be obtained in 3 days (44 orbits) with an instrument swath of about 1000 km and a ground track that repeats exactly in 8 days (117 orbits). This repeat pattern provides even coverage of the planet with an ideal longitude spacing between ground tracks at the equator of 3.077° (343 km). Table 2 gives the mean orbital elements for the science orbit.

The terminator orbit was selected to allow soil moisture measurements near the morning terminator, where ionospheric effects and land–atmosphere thermal gradients are minimized. This design also minimizes thermal variations on the instrument and simplifies the spacecraft design. The 6 PM ascending node was selected so that the annual eclipse season (about 12 weeks per year from mid May to early August) occurs near the southern part of the orbit, and this minimizes thermal effects on freeze/thaw measurements in the northern hemisphere. The maximum eclipse duration is about 18.6 minutes.

Because of the asymmetric mass distribution of the Earth, a purely circular orbit cannot be maintained and a frozen-orbit geometry is used to minimize altitude variations. A frozen orbit uses a small eccentricity and locates the perigee at the northern extreme of the orbit to minimize the altitude perturbations. This approach results

in slightly higher altitudes in the southern hemisphere, but altitudes are fairly stable at each latitude. Figure 5 shows the geodetic altitude of the observatory versus latitude for the 685-km orbit. Geodetic altitude is the altitude at a point in the orbit measured normal to the reference ellipsoid for mean sea level, which has an equatorial radius of 6378.137 km (with a flattening of 1/298.257223563, resulting in a polar radius of approximately 6356.752 km). This is based on the World Geodetic System (WGS 84). The geodetic altitude is highest at the southern extreme of the orbit (711.4 km at 81.9°S) and lowest just north of the equator (684.0 km at 13.6°N). While perigee is the point closest to the center of the Earth, the geodetic altitude is increased at the northern extreme of the orbit (694.9 km at 81.9°N) because of the Earth flattening. The orbit must be maintained such that the geodetic altitude never varies by more than 1 km from this profile at any given latitude.

The altitude for the science orbit repeat pattern of 117 orbits in 8 days (Q8 = 117/8 = 14.625 orbits/day,) is selected slightly above the altitude for an exact 3-day repeat pattern (Q3 = 44/3 = 14.667 orbits/day) so that the ground track walks to the west and fills in the gap between consecutive orbits (S = 360°/Q8 = 24.615° or 2740 km). This design provides an average sampling interval of three days (spatial average) and fills in gaps in the high-resolution radar swaths, which have degraded azimuthal accuracy over the inner 30% of the swath near the ground track. The 8-day repeat pattern allows consistent spatial datasets for time histories of the measurements.

Figure 6 shows the science orbit ground track pattern in the 2740-km spacing between two consecutive orbits at the equator (orbits 1 and 2 at the descending node). Two days later, ground tracks for orbits 16 and 31 have reduced the maximum spacing at the equator to 1028 km, and over 8 days the maximum spacing is reduced to 343 km. Figure 7 shows the pattern of descending (morning) and ascending (evening) ground tracks over North America over 1 day. The ground track spacing is closer away from the equator, and coverage of boreal forest regions northward of 45°N has an average sampling interval of 2 days (spatial average). The specific values of equa-

Table 2. Science orbit mean elements.

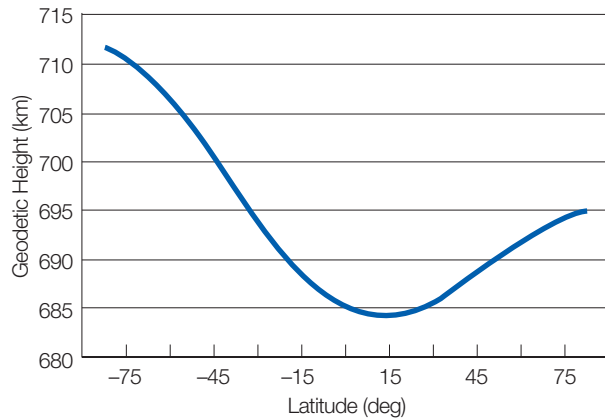| Orbital Element | Mean Element Value |
| --- | --- |
| Semi-major Axis (a) | 7057.5071 km |
| Eccentricity (e) | 0.0011886 |
| Inclination (i) | 98.121621 deg |
| Argument of Perigee (w) | 90.000000 deg |
| Ascending Node (W) | –50.928751 deg |
| True Anomaly | –89.993025 deg |

Figure 5. Science orbit geodetic altitude vs. latitude.

tor-crossing longitudes are defined after the science orbit is established near the end of the commissioning phase.

## V. Observatory

The observatory is the key implementing element of the project in space, and is defined as all hardware elements released into orbit from the launch vehicle. The observatory is made up of the spacecraft bus, which includes the engineering subsystems necessary to maintain and support operation of the spacecraft and instrument; the instrument, which includes the radar and radiometer pro-

cessing electronics and hardware, the reflector antenna and its supporting structure, and the deployment and spin mechanisms; and a portion of the launch system hardware that remains attached to the spacecraft bus after separation from the launch vehicle upper stage.

### A. Configuration

As seen in Figure 8, the observatory is made up of a rectangular bus structure, which houses the engineering subsystems and most radar components, and the top-mounted instrument, including the spin mechanism and radiometer and the reflector and its deployment structure. The three-panel solar array is part of the spacecraft bus and is folded against the bus in the launch configuration (Figure 9). The instrument hardware above the spin plane is designated the spun instrument assembly (SIA).

For science data collection, the observatory is oriented to the science orbit reference frame with the −ZSC axis pointed to the geodetic nadir and the +XSC axis coplanar with the nadir direction and the inertial velocity vector in the general direction of orbital motion, so that the +YSC axis is generally normal to the orbit plane on the sunward side of the orbit. After deployment, the instrument antenna spins about the +ZSC axis at a rate of up to 14.6 rpm in a right-handed sense (counterclockwise as viewed from above) with the antenna reflecting the transmitted and received signal 35.5° off the nadir. The instrument spin
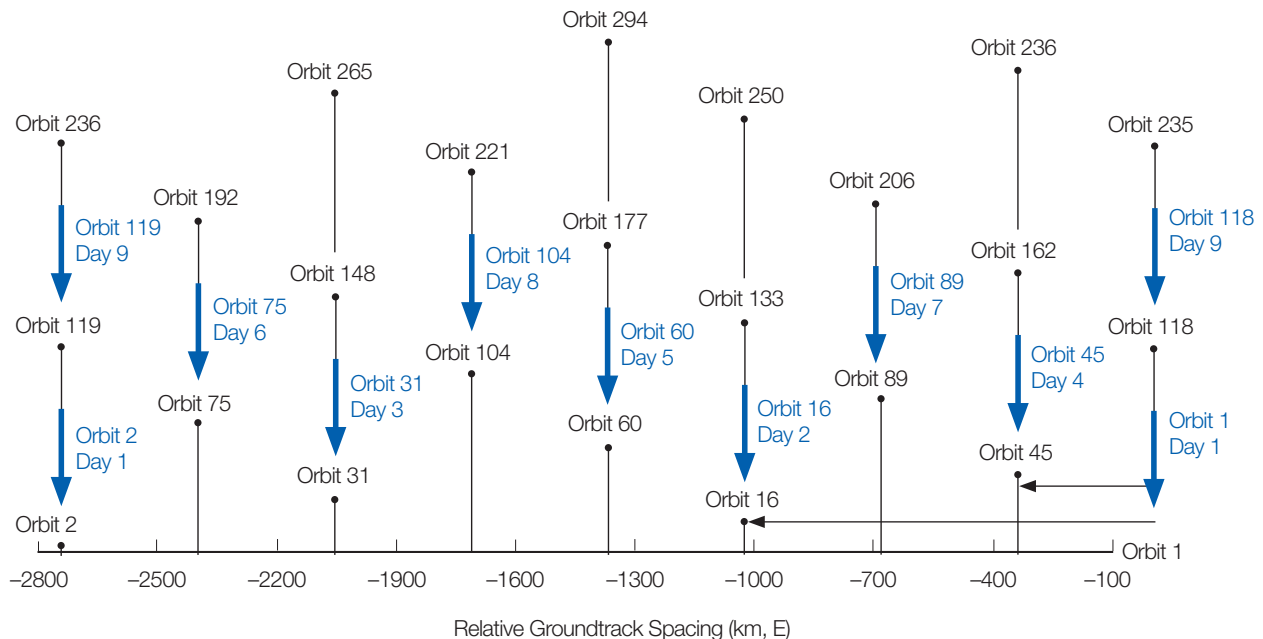


Figure 6. Science orbit ground track pattern at equator (arrows show the ideal position and spacing of the ground track equator crossings for the descending orbits).

**Figure 7. One-day ground track pattern over North America (Orbit 16 begins about 24.615 hours after Orbit 1).**

rate between 13.0 to 14.6 rpm for science will be determined before launch based on margin in the observatory pointing control authority to balance the instrument spun momentum.

The observatory transitions through three main configurations, as shown in Figure 9:

*Launch:* For launch, the solar array and reflector boom assembly (RBA) are folded against the spacecraft bus to fit within the launch vehicle fairing.

*Partially Deployed:* After separation from the Delta II second stage, the launch behavior deploys the solar array and the observatory remains in this configuration for about four weeks. During this period the initial engineering checkout is accomplished and the first commissioning maneuvers are executed to reach the science orbit.

*Fully Deployed:* Beginning about 30 days after launch, the instrument reflector boom assembly is deployed in two steps and then spun up in two steps to a rate of up to 14.6 rpm used for science data collection. (Note that there are brief transition periods of a few days, with intermediate configurations, between these steps of boom deployment, reflector deployment, and spin-up.)

## VI. Mission System

The mission system consists of the people, facilities, hardware, networks, software, and processes necessary to operate the observatory after launch and to acquire and process the returned data into scientific products. For operations, the mission system is composed of three functional elements: the Mission Operations System (MOS), the Ground Data System (GDS), and the Science Data System (SDS). Before launch, the mission system includes the mission and navigation design element, which defines the orbit design, the launch strategy, the navigation approach, and the mission plan.

### A. Mission Operations System (MOS)

The mission operations system consists of the people and processes necessary to operate the observatory after launch and to acquire the instrument and engineering data. Located at the JPL mission operations center (MOC), the MOS is organized into two teams. The flight operations team (FOT) is responsible for planning and executing all the processes necessary to operate the observatory, including the following:
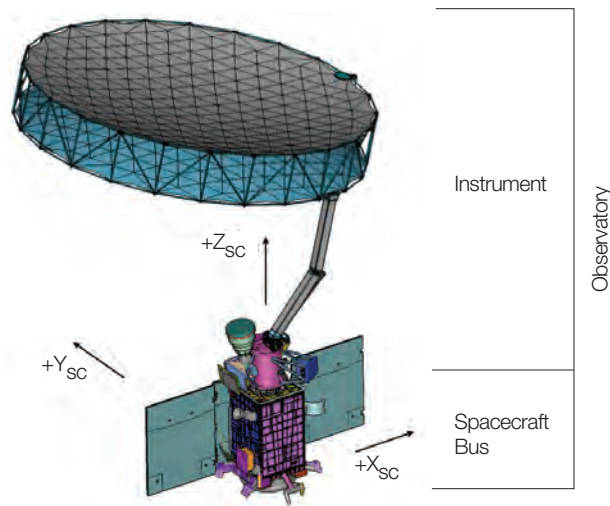
**Figure 8. Observatory fully deployed configuration.**



**Figure 9. Observatory configurations.**

- Plan, build, and execute spacecraft activities (launch, commissioning, maneuvers, calibrations, routine operations, anomaly responses)

- Monitor and operate observatory systems, subsystems, and instruments

- Manage onboard data products (file deletion)

- Schedule Near-Earth Network (NEN) and Space Network (SN) coverage and generate background sequences to manage communications

- Perform flight controller (ACE) functions (command, real time station interface) as needed [Passes are unattended during routine operations]

- Perform navigation operations (orbit determination, maneuvers)

- Perform time correlation (automated)

- Operate and maintain system testbeds

The mission data operations team (MDOT) is responsible for operating and maintaining the GDS and SDS communications networks and hardware as follows:

- Perform data accounting

- Operate GDS

- Operate SDS

- Maintain NEN/EDOS interface

- Maintain/upgrade data systems software

- Maintain hardware, communications net and facility

## B. Ground Data System (GDS)

The ground data system consists of the facilities, communications networks, hardware, and software used by the MOS. Figure 10 shows the four main facilities that support the SMAP mission and the functions executed at each facility. Figure 11 illustrates the SMAP communications paths. Operations are centered at the Mission Operations Center at JPL (MOC). Communications with the observatory are handled through the ground and space assets of the NEN and SN. Scheduling and pass reporting for the NEN and SN assets are handled through the Data Services Management Center (DSMC) at the White Sands Complex (WSC), where the primary Tracking and Data Relay Satellite (TDRS) ground terminals are located. Science telemetry from the NEN stations flows to the EOS Data and Operations System (EDOS) Level Zero Processing Facility (LZPF) at GSFC, which formats the data into files and passes the radar and radiometer data to the Science Data System. Engineering data from the NEN and SN stations flows to the MOC at JPL, which generates displays and other products to support both mission operations and science processing.

The primary path for commanding the observatory and returning science and engineering data is through three

**NEN/SN Stations**

- Antenna pointing and signal acquisition per schedule
- S-band and X-band telemetry reception, frame extraction and decoding
- S-band command reception from MOC and radiation to S/C
- Tracking data production and delivery to MOC
- High-rate science telemetry buffering and delivery to LZPF
- Real-time engineering data extraction and delivery in near-real-time to MOC
- Recorded engineering data extraction, recording to files and delivery to MOC

**SMAP Mission Ops Center (JPL)**

- Planning and sequence generation
- Command generation and radiation
- Navigation processing (OD, MD, Eph gen)
- Engineering data processing, storage, display and reporting
- S/C monitoring and maintenance
- Instrument monitoring and maintenance
- Telemetry auditing/accounting and retransmission
- On-board file management
- Time correlation
- GDS monitoring and maintenance

Commands

Real-Time Engineering Telemetry

Doppler Tracking Data

Science Telemetry Gap Reports

**DSMC (WSC)**

- Schedule NEN/SN per requests
- Provide pass reports

Schedules

State Vectors

Pass Results

Sched Reqsts

State Vectors

Schedules

Pass Reports

**LZPF and FDF (GSFC)**

- High-rate telemetry frames reception (EDOS)
- Radiometer and radar data separation into files per pass, and delivery to SDS
- End-to-end flows monitoring and problem resolution
- Store and forward recorded engineering data files to MOC
- Initial S/C tracking (first few days)

State Vectors

Recorded Engineering Telemetry Pass Files

Recorded Engineering Telemetry Pass Files

Decoded Instrument Telemetry Frames

Doppler Tracking Data

Ancillary Data

**Science Data System (JPL)**

- Radar and radiometer file reception and storage
- Level 1a through Level 3 science product generation
- Product distribution and archive
- SDS monitoring and maintenance

L0a Radar Pass Files
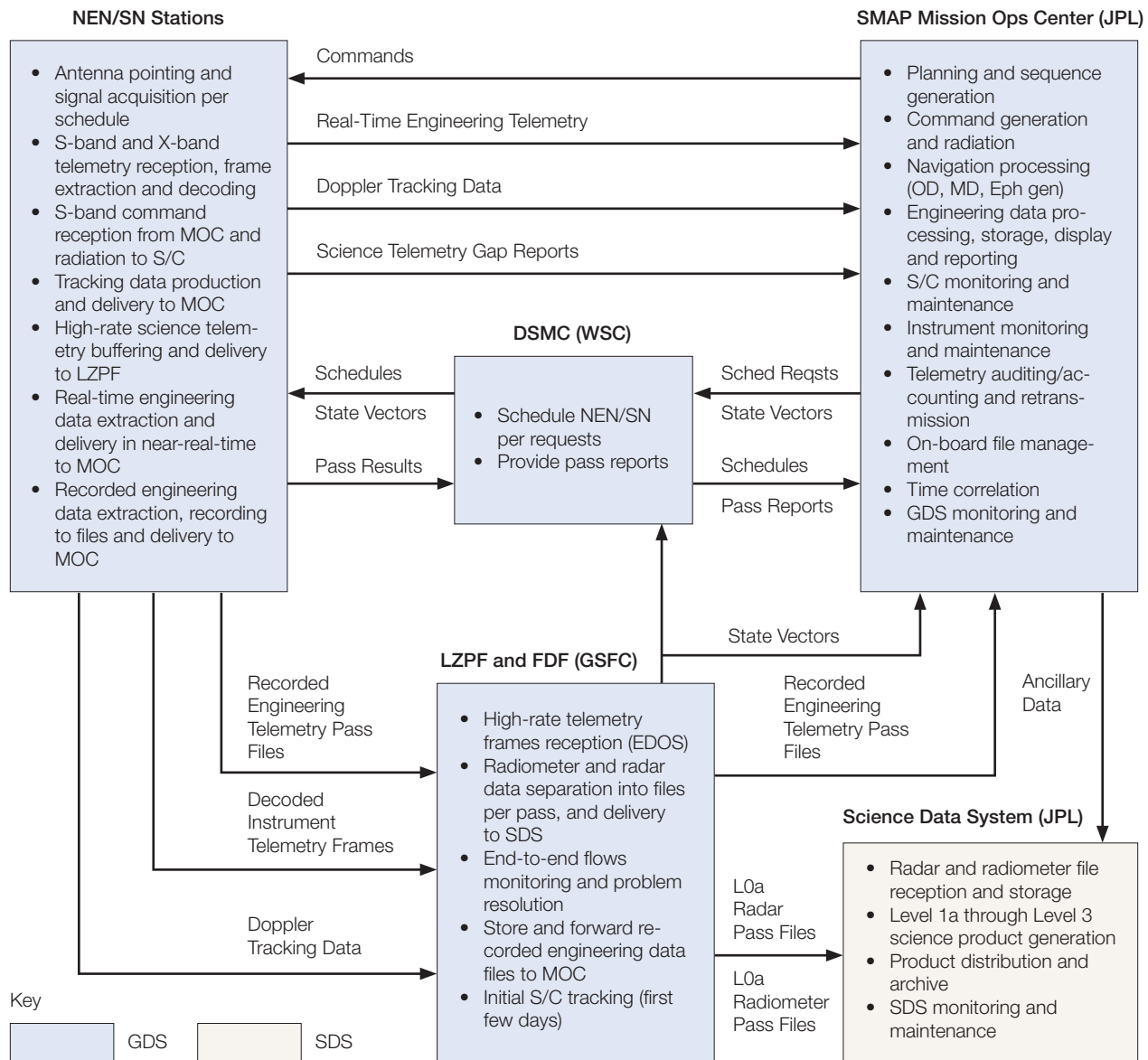
L0a Radiometer Pass Files

Key

GDS        SDS

Figure 10. Ground data system facilities and functions.

northern-hemisphere tracking stations and one southern-hemisphere station in Antarctica. Data return at the northern-hemisphere stations is via 11.3-m antennas located at Wallops, Virginia (WGS), Fairbanks, Alaska (ASF), and Svalbard Island, Norway (SGS). Data return at the southern-hemisphere station is via the 10-m antenna (MGS) at McMurdo Station, Antarctica. Table 3 gives characteristics of the four stations and average contact statistics from the science orbit. Because SMAP is in a near-polar orbit, the higher latitude stations have more frequent contact opportunities.

**C. Science Data System (SDS)**

The science data system provides the hardware and software to process the radar and radiometer instrument data and the supporting engineering data into science data products for the science team, applications users, and the public. Files of radar and radiometer data derived from the downlink telemetry are delivered from the GSFC EDOS/LZPF, and engineering ancillary data, including timing, pointing, and ephemeris information, are delivered from the MOC. Algorithms developed before launch are used to process the data into science data products. The

Table 3. Ground station characteristics (X-band).

| Ground Station | Antenna | Latitude | Average # of Contacts per day* | Average Coverage Minutes/day* |
|---|---|---|---|---|
| Svalbard (SGS) Norway | 11.3 m | 78.2ºN | 10.3 | 88.3 |
| Fairbanks (ASF) Alaska | 11.3 m | 64.9ºN | 6.8 | 53.7 |
| Wallops (WGS) Virginia | 11.3 m | 37.9ºN | 3.3 | 25.8 |
| McMurdo (MGS) Antarctica | 10.0 m | 77.8ºS | 10.4 | 90.7 |

\* These are maximum capabilities if all available passes with a duration of at least 5 minutes above 10º elevation are utilized. Horizon terrain masks not considered.

SDS has data latency requirements on delivering data products to the science team and to operational users: Level 1 products (within 12 hours of acquisition), Level 2 (within 24 hours), Level 3 (within 50 hours), and Level 4 (within 7 days for soil moisture and 14 days for carbon net ecosystem exchange). Data latency is defined here as from the time of data acquisition by the observatory to the time data products are available to the public at the NASA DAACs. SMAP data will be archived by the NASA-designated Earth science data centers at the National Snow and Ice Data Center and the Alaska Satellite Facility. During the first year of routine science collection (which comprises the formal mission cal/val period), all SMAP data product algorithms are updated as needed by comparing SMAP estimates of soil moisture and freeze/thaw state with data collected on the ground at specific cal/val sites.

The key SDS operations functions are:

- Ingest instrument and ancillary data and generate higher-level data products. The range of higher-level products is Level 1A (L1A) through Level 4 (L4). The definition of what the SDS produces is dictated by the science requirements.

- Support calibration and validation of science data products

- Provide science data accounting/auditing

- Provide data access to Project, Science, and Flight Engineering Teams

- Manage long-term data storage (products, metadata, test data, etc.); prepare and make available validated products to a public archive data center

- Maintain the SDS production and testbed systems

The SDS implementation organizations include:

- SMAP Science—responsible for the L1 radiometer and L2-L4 algorithms and science software

- JPL SDS—responsible for L1 radar algorithms and L1-L3 production code and product generation

- GSFC Global Modeling & Assimilation Office (GMAO)—responsible for Level 4 soil moisture and Level 4 carbon production code and product generation

The SDS architecture and data flow among different entities are summarized in Figure 12.

## VII. Data Products

The SMAP radiometer is capable of acquiring H and V polarization measurements as well as the third and fourth Stokes parameters. In addition, it has the capability to measure in sixteen discrete spectral subbands (each 1.5 MHz wide) within the 24 MHz fullband centered at 1.4135 GHz as an RFI mitigation approach. The subband data volume can be substantial. The radar measurements (HH, VV, and HV polarizations) have even larger volumes during each orbit. Even though the instruments are capable of acquiring the data, not all of the data can be transferred to the ground because of limitations in downlink rates. As a result, masks are applied to limit the portion of the data that can fit the downlink bandwidth. The selection of the mask is based on the science requirements.

Figure 13 shows the "Global Land" mask that is applied to the radar and radiometer instruments for downlinking the measurements needed to meet the Level 1 soil moisture requirements. Low-resolution radar measurements and fullband radiometer measurements (integrated over all the spectral subbands) are transmitted to the ground for the
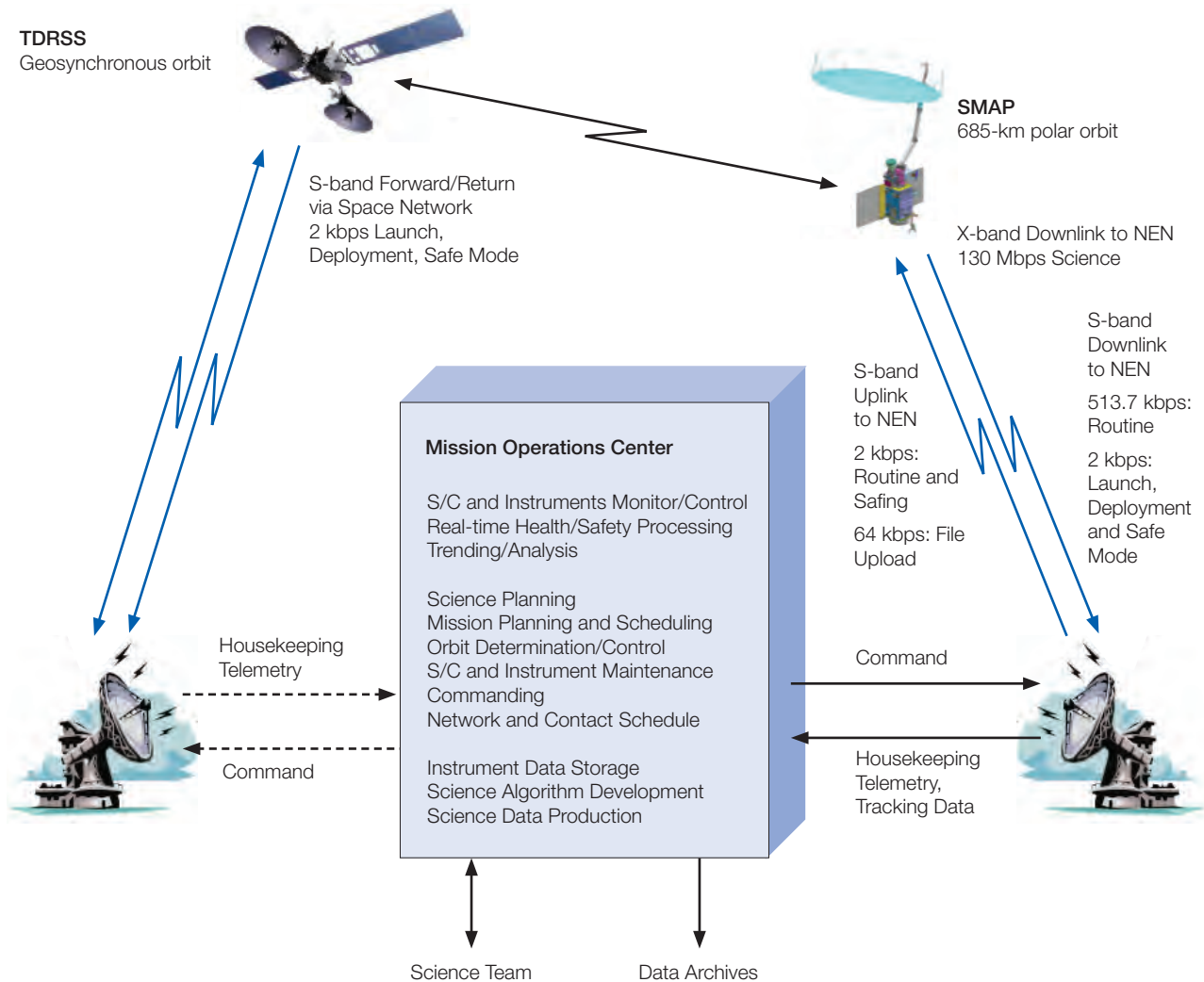
**TDRSS**
Geosynchronous orbit

**SMAP**
685-km polar orbit

S-band Forward/Return
via Space Network
2 kbps Launch,
Deployment, Safe Mode

X-band Downlink to NEN
130 Mbps Science

S-band
Downlink
to NEN

513.7 kbps:
Routine

S-band
Uplink
to NEN

2 kbps:
Routine and
Safing

64 kbps: File
Upload

2 kbps:
Launch,
Deployment
and Safe
Mode

**Mission Operations Center**

S/C and Instruments Monitor/Control
Real-time Health/Safety Processing
Trending/Analysis

Science Planning
Mission Planning and Scheduling
Orbit Determination/Control
S/C and Instrument Maintenance
Commanding
Network and Contact Schedule

Instrument Data Storage
Science Algorithm Development
Science Data Production

Housekeeping
Telemetry

Command

Command

Housekeeping
Telemetry,
Tracking Data

Science Team          Data Archives

**Figure 11. SMAP communications paths.**

fore and the aft scan, globally (land and ocean), and for both the AM and PM overpasses (additional information on the SMAP measurement approach will be given in the next chapter on Instrument Design and L1 Data Products). Over the Global Land region, subband (full spectral resolution) radiometer measurements (fore and aft scan) are transmitted to the ground network during both AM and PM overpasses. Thus, for global land areas, both fullband and subband radiometer data are available for both AM and PM overpasses — for global oceans, only fullband radiometer data will be downlinked to the ground.

The high-resolution radar data (fore and aft scan) are sent to the ground over all global land areas for the AM overpass and only over land areas north of 45°N latitude for the PM overpass. Figure 14 shows the regions where the high-resolution radar data (fore and aft) are acquired

and transmitted to the ground for the PM overpass. Over regions above 45°N, both AM and PM high-resolution radar data are available to meet the landscape freeze/thaw detection science requirement.

High-resolution radar data are also acquired (fore-look, AM overpass only) across one swath width (~1000 km) for coastal waters along continents (except Antarctica) and major islands. Figure 15 shows the extent of the high-resolution radar data downlink over oceans and open waters. These data are used for geolocation as well as potentially useful applications for the ocean and sea ice science and applications communities.

The SMAP baseline data products are listed in Table 4. Level 1B and 1C data products are calibrated and geolocated instrument measurements of surface radar
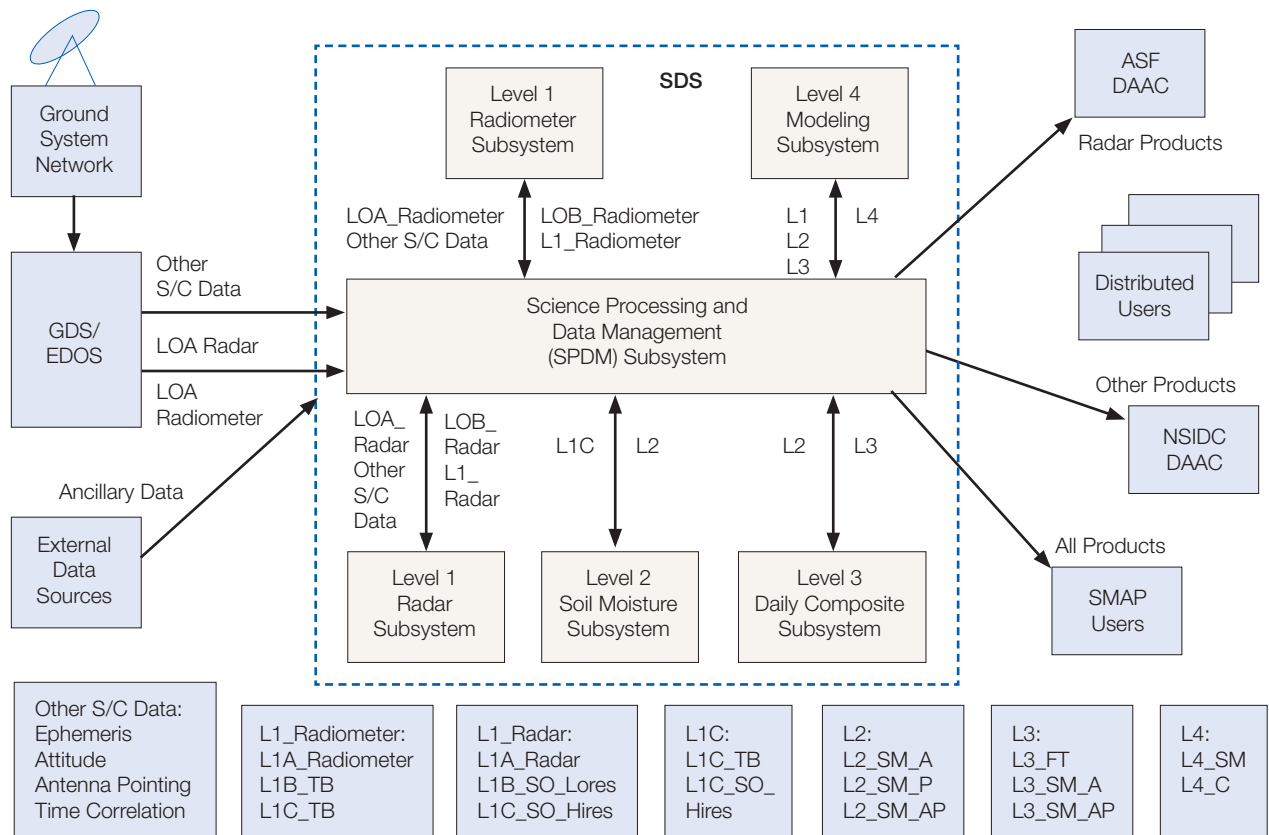
**Figure 12. SMAP Science Data System architecture and data flows.**

backscatter cross-section and brightness temperatures. Level 2 products are geophysical retrievals of soil moisture on a fixed Earth grid based on Level 1 products and ancillary information; the Level 2 products are output on a half-orbit basis. Level 3 products are daily composites of Level 2 surface soil moisture and freeze/thaw state data. Level 4 products are model-derived value-added data products of surface and root zone soil moisture and carbon net ecosystem exchange that support key SMAP applications and more directly address the driving science questions.

In total, the SMAP mission will generate 15 distributable data products representing four levels of data processing. Level 1 products contain instrument-related data and appear in granules that are based on half orbits of the SMAP satellite. The northernmost and southernmost orbit locations demarcate half orbit boundaries. Level 2 products contain output from geophysical retrievals that are based on instrument data and also appear in half orbit granules. Level 3 products are daily global composites of the Level 2 geophysical retrievals for an entire UTC day. Level 4 products contain output from geophysical models utilizing SMAP data.

There are three L2 soil moisture products resulting from the radar and radiometer data streams. L2_SM_A is a high-resolution research-quality soil moisture product that is mostly based on the radar measurements and is posted at 3 km. L2_SM_P is soil moisture derived from the radiometer brightness temperature measurements and is posted at 36 km. L2_SM_AP is a combination active and passive (radar and radiometer) product that produces soil moisture estimates at 9 km resolution.

The radar-only soil moisture (L2_SM_A) is a fine-resolution (3 km) soil moisture estimate derived from high-resolution radar backscatter data (L1C_S0_HiRes). Although the L2_SM_A data product is unlikely to be as accurate as the L2_SM_P and L2_SM_AP products, it will produce useful soil moisture information at higher spatial resolution. L2_SM_A produces radar backscatter values aggregated to 3 km during the early stages of its processing. This dataset, along with water body and freeze/thaw flags generated from the radar data, is made available during data processing to the other products as input.

The combined radar/radiometer soil moisture product L2_SM_AP is posted on a 9-km Equal-Area Scalable Earth–2

**Table 4. SMAP data products.**

| Product | Description | Gridding (Resolution) | Latency** | |
|---|---|---|---|---|
| L1A_Radiometer | Radiometer Data in Time-Order | — | 12 Hrs | Instrument Data |
| L1A_Radar | Radar Data in Time-Order | — | 12 Hrs | |
| L1B_TB | Radiometer $T_B$ in Time-Order | (36x47 km) | 12 Hrs | |
| L1B_S0_LoRes | Low-Resolution Radar $\sigma_o$ in Time-Order | (5x30 km) | 12 Hrs | |
| L1C_S0_HiRes | High-Resolution Radar $\sigma_o$ in Half-Orbits | 1 km (1–3 km)# | 12 Hrs | |
| L1C_TB | Radiometer $T_B$ in Half-Orbits | 36 km | 12 Hrs | |
| L2_SM_A | Soil Moisture (Radar) | 3 km | 24 Hrs | Science Data (Half-Orbit) |
| L2_SM_P* | Soil Moisture (Radiometer) | 36 km | 24 Hrs | |
| L2_SM_AP* | Soil Moisture (Radar + Radiometer) | 9 km | 24 Hrs | |
| L3_FT_A* | Freeze/Thaw State (Radar) | 3 km | 50 Hrs | Science Data (Daily Composite) |
| L3_SM_A | Soil Moisture (Radar) | 3 km | 50 Hrs | |
| L3_SM_P* | Soil Moisture (Radiometer) | 36 km | 50 Hrs | |
| L3_SM_AP* | Soil Moisture (Radar + Radiometer) | 9 km | 50 Hrs | |
| L4_SM | Soil Moisture (Surface and Roof Zone) | 9 km | 7 days | Science Value Added |
| L4_C | Carbon Net Ecosystem Exchange (NEE) | 9 km | 14 days | |

\# Over outer 70% of swath.
\*\* The SMAP Project will make a best effort to reduce the data latencies beyond those shown in this table.
\* Product directly addresses the mission L1 science requirements.

(EASE2) grid (Brodzik et al. 2012) that is nested consistently with the 36 km and 3 km grids used by other SMAP products. It uses both the high-resolution radar backscatter gridded at 3 km and the radiometer brightness temperature data gridded at 36 km. L2_SM_AP combines the two data streams to produce disaggregated brightness temperatures posted at 9 km. The retrieval algorithm used to estimate soil moisture from the disaggregated 9 km brightness temperatures uses the same approach as the L2_SM_P radiometer-only soil moisture product. The ancillary data inputs and implementation of the L2_SM_AP may differ from those used by L2_SM_P because of the spatial resolution differences at 9 and 36 km.

L3_FT_A, the only SMAP freeze/thaw product, consists of a daily composite of landscape freeze/thaw state for the boreal land region north of 45ºN latitude output on a polar EASE2 grid at 3 km. It is derived from high-resolution radar data (L1C_S0_HiRes half-orbits) using both the AM (descending) and PM (ascending) overpasses. The

L1C_S0_HiRes AM data will also be utilized to generate a freeze/thaw binary state flag for use in the L2/3_SM product algorithms.

SMAP measurements provide direct sensing of soil moisture in the top 5 cm of the soil column. However, several of the key applications targeted by SMAP require knowledge of root zone soil moisture in the top 1 m of the soil column, which is not directly measured by SMAP. As part of its baseline mission, the SMAP project will produce model-derived value-added Level 4 data products to fill this gap and provide estimates of root zone soil moisture that are informed by and consistent with SMAP surface observations. Such estimates are obtained by merging SMAP observations with estimates from a land surface model in a data assimilation system. The land surface model component of the assimilation system is driven with observations-based meteorological forcing data, including precipitation, which is the most important driver for soil moisture. The model also encapsulates knowledge of key land surface processes, including the vertical trans-

Figure 13. The SMAP radiometer data will include the four Stokes parameters in all spectral subbands over the 360 degrees of the antenna scan (fore and aft looks) for the AM and PM portion of the orbit over the "Global Land" region. SMAP high-resolution data will be collected over the Global Land region over the AM portion of the orbit. Low-resolution radar data and radiometer without the spectral resolution will be collected globally over land and oceans during both the AM and PM overpasses.

fer of soil moisture between the surface and root zone reservoirs. Finally, the model interpolates and extrapolates SMAP observations in time and in space, producing 3-hourly estimates of soil moisture at 9 km resolution. The SMAP L4_SM product thus provides a comprehensive and consistent picture of land surface hydrological conditions based on SMAP observations and complementary information from a variety of sources.

The L4_C algorithms utilize daily soil moisture and temperature inputs with ancillary land cover classification and vegetation gross primary productivity (GPP) inputs to compute the net ecosystem exchange (NEE) of carbon dioxide with the atmosphere over global vegetated land areas (with an emphasis on boreal areas north of 45ºN latitude). Carbon NEE is a fundamental measure of the balance between carbon uptake by vegetation and carbon losses through autotrophic and heterotrophic respiration.

Table 4 specifies several important characteristics of the SMAP baseline data products. Among these are:

- The product short name — these provide a short-hand method to differentiate among the products

- A very brief product description — additional SMAP project documents provide complete specifications of the format and the content of each data product; the

SMAP DAACs will make these documents available to the user community

- Product spatial resolution or grid posting — the resolution of some Level 1 products is based on the size of the instantaneous field of view (IFOV) of the radar or radiometer instrument, while the resolution of higher level products is based on the selected grid spacing

- Product latency to the user community — latency measures the time between the acquisition of the first element in the data product and the time the product is available for use at one of the SMAP Data Centers. Although the latencies listed in Table 4 are being used by the project to construct the data processing system, the SMAP project will do its best to deliver products sooner, whenever possible.

## A. SMAP Data Product File Format

All SMAP standard products appear in the Hierarchical Data Format version 5 (HDF5). HDF5 is a general purpose file format and programming library for storing scientific data. HDF5 functions flexibly over a wide range of computer hardware, operating systems, and software tools. Thus, users can read HDF5 files on multiple platforms regardless of the platform or data architecture. HDF5 files

are equally accessible to routines written in a large number of standard software languages, including Fortran, C, C++ and Java, and popular software packages employed by the scientific community, such as IDL and Matlab, include well established and easy to use HDF5 interfaces. Users can reference the HDF Group website at http://www.hdf-group.org to download HDF software and documentation.

## B. SMAP Data Product Organization

A critical component of data product design is the organization of the data elements within the product. To ease user interfaces, the SMAP Science Data System team devised a common data organization across all mission products. HDF5 provides a means to divide the product content into distinct groups. All products contain at least two HDF5 groups. One group, named Metadata, contains the file level metadata. The other HDF5 groups in a SMAP data product contain sets of HDF5 Datasets. Each HDF5

Dataset contains a data array. All of the arrays in the same group share a common theme and a common set of dimensions. Within any given group, the common array dimensions appear in the same order and have the same length. Thus, if two elements in different arrays in the same group have identical dimension indices, those array elements correspond to the same pixel. This standard organizational pattern enables product users to establish a clear correspondence among elements in SMAP product arrays. For example, all of the arrays in the SMAP L2_SM_AP product appear in a group named "Soil Moisture Retrieval Data." All of the HDF5 Datasets in the "Soil Moisture Retrieval Data" group contain two-dimensional arrays. The slower moving index in each array represents the pixel latitude. The faster-moving index in each array represents the pixel longitude. Thus, given longitude index m and latitude index n, a user of column major software such as Fortran, MATLAB and IDL can conclude that the disaggregated brightness temperatures in array elements



Figure 14. The SMAP high-resolution radar data will be collected during the PM overpasses across land regions above 45N in order to detect freeze/thaw transitions.



Figure 15. The SMAP high-resolution radar data will be collected one swath width across coastlines of continents and major islands for geolocation and possible use in coastal applications. In the Arctic, the Level 1 radar products may also have sea ice detection applications.

*tb_v_disaggregated (m,n)* and *tb_h_disaggregated (m,n)* were used to retrieve the soil moisture stored in array element *soil_moisture (m,n)*. Likewise, a user of row major software such as C, C++ or Python can conclude that the disaggregated brightness temperatures in array elements *tb_v_disaggregated(n,m)* and *tb_h_disaggregated (n,m)* were used to retrieve the soil moisture stored in array element *soil_moisture (n,m)*.

As previously mentioned, HDF5 usage adopts to the language the user employs to access the data. Thus, users can utilize row-major or column-major representation of arrays in their favorite software language and achieve equivalent results. To avoid confusion about array index order, SMAP documentation typically references "faster moving" and "slower moving" indices. The "faster or fastest moving" index is the one that represents contiguous storage for sequential index values. In other words, given two array elements with all indices equal except for those in the "fastest moving" position, if the fastest moving indices are consecutive numbers, one can conclude that those two elements are stored contiguously in memory and on disk.

## C. The EASE2 Grid

All of the SMAP Level 2, Level 3, and Level 4 products, as well as the Radiometer Level 1C product, employ the EASE2 grid (Brodzik et al. 2012) developed at the National Snow and Ice Data Center (NSIDC) to specify the location of data pixels. The flexible formulation of the EASE2 grid makes it ideal for SMAP use. A simple adjustment of just one scaling parameter enables generation of a family of multi-resolution grids that "nest" within one another. This nesting can be designed so that smaller grid cells are perfectly tessellated to form larger grid cells. Figure 16 displays the perfect nesting for 3-km, 9-km, and 36-km SMAP grids, while Figure 17 provides an example of SMAP NDVI ancillary data posted at these three grid resolutions.

The perfect nesting of EASE2 grids enables the SMAP team to provide data products with a convenient common projection for both the higher resolution radar observations and the lower resolution radiometer observations. EASE2 also provides the capability to generate cylindrical global grids as well as Northern and Southern Hemisphere polar grids.

The Level 1B and Level 1C radar products do not employ the EASE2 grids for data organization. Instead, these products contain an array of floating-point indices that specify either the center of the instrument IFOV or the center of the cells in an instrument swath grid. These floating point indices also reference a 1-km EASE2 grid that nests perfectly into the 3-km, 9-km and 36-km grids used in the higher-level products. This information
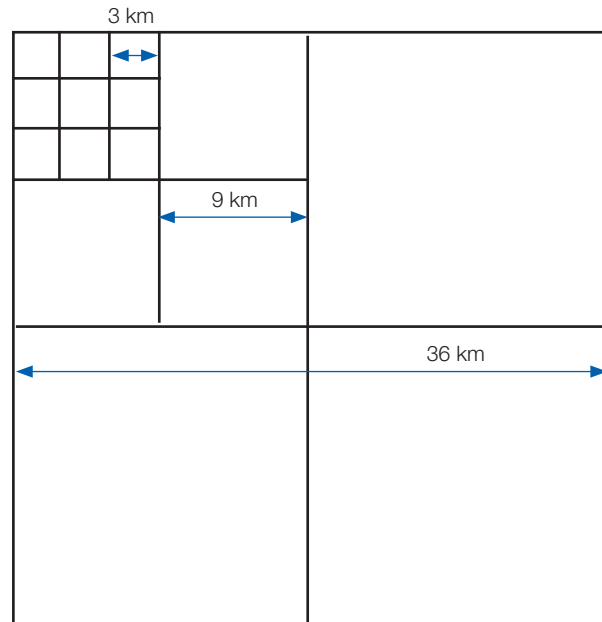


Figure 16. Nesting of SMAP 3-km, 9-km and 36-km EASE2 grids as employed in SMAP data products.

enables users to easily translate Level 1 radar data onto the EASE2 grids employed in the higher-level SMAP data products.

## D. Quality and Descriptive Information in SMAP Data Products

SMAP data products include content that enables users to assess data quality as well as gain a better understanding of geophysical conditions. This descriptive content can be classed into three identifiable categories:

- Auxiliary data elements that provide measures that enhance assessment of product content – these include statistical measures of uncertainty as well as physical measures that either impact or validate product results

- Metadata that provide an overall description of the entire product content

- Bit flags that provide quality assessments of individual pixels as well as binary indicators of existing conditions when and where the data were acquired

## E. Auxiliary Data Elements

Most SMAP products include many auxiliary arrays. Each of these arrays appears in HDF5 Datasets. Elements in these auxiliary arrays correspond directly with the elements in the arrays that specify major product output,
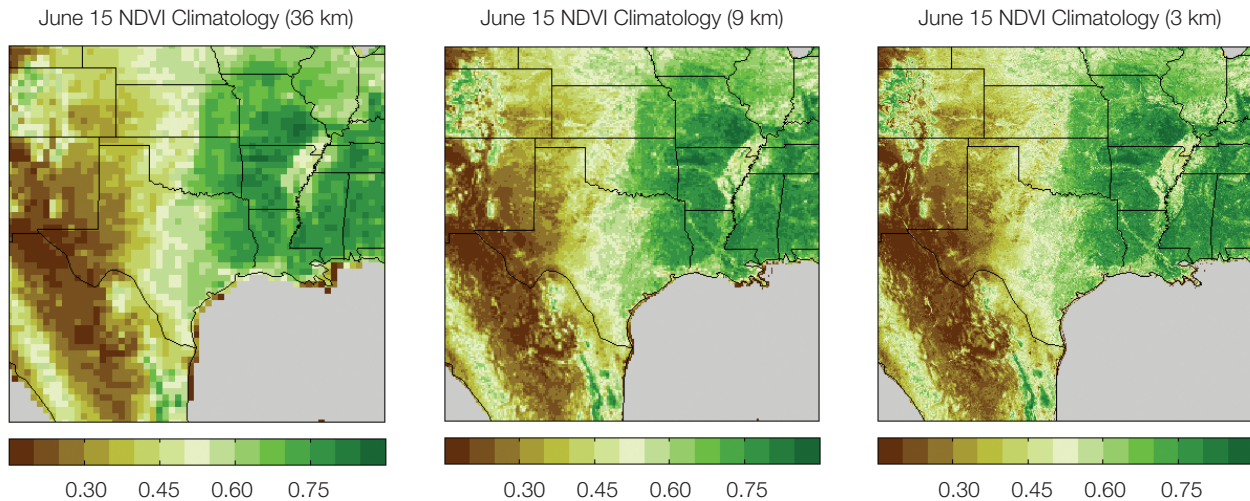
**Figure 17. Example of ancillary Normalized Difference Vegetation Index (NDVI) climatology data displayed on the SMAP 36-km, 9-km, and 3-km grids, respectively.**

such as brightness temperature or normalized backscatter in Level 1, or retrieved soil moisture in Level 2. Many of these auxiliary arrays provide a measure of noise in the major product output. Thus, the radiometer L1B product contains a noise equivalent delta temperature (NEDT) that users can employ to assess the quality of each brightness temperature measure. Likewise, the Level 1B and Level 1C radar products include a Kpc, which contains the normalized standard deviation of the backscatter measure. Based on algorithmic functions, each of the Level 2 products incorporate different uncertainty measures, which provide users with a sense of measurement noisiness for each individual pixel. Additional auxiliary arrays provide information about geophysical conditions that might impact the quality and/or the viability of data within each pixel. Examples might include the boresight angle or the Faraday rotation angle in the Level 1 data products, as well as a representative surface temperature or vegetation information from ancillary data sources in the Level 2 and Level 3 data products.

**F. SMAP Metadata**

Metadata are data that describe data. SMAP products contain two distinct types of metadata:

- File level metadata — these metadata describe the overall content of the data product and appear in an HDF5 group entitled "Metadata"

- Local metadata — these metadata describe individual arrays in the product and are provided by HDF5 Attributes associated with each array

**G. File-Level Metadata in SMAP Data Products**

SMAP file-level metadata conform to the ISO 19115 (ISO 2003) and ISO 19115-2 (ISO 2007a) standards. SMAP is the first NASA Earth science mission to employ these standards. The ISO standard provides an overarching model for metadata organization which delineates the metadata into a set of standard groups that address a common topic. Each of these metadata groups appears in a specific class. The major ISO metadata classes in SMAP products include:

- MI_Metadata — defines basic information about the metadata

- MD_DataIdentification — contains descriptive information about the output data product

- DQ_Quality — provides overall quality information about the entire data product

- LI_Lineage — covers all input data employed to generate the output data product. LI_Lineage incorporates listings of all input files as well as information about the software processing and algorithmic approach.

- EX_Extent — describes the spatial and temporal coverage of the data product

- MI_AcquisitionInformation — contains information about the flight platform and measurement instruments

The ISO standards define specific attributes within each of these classes. Each attribute provides a segment of the

necessary detail required to fully describe the entire data product. The ISO 19139 (ISO 2007b) standard provides a common XML serialization for representation of ISO model metadata. The combination of the 19115 and 19139 standards ensures that users of disparate Earth data products generated by any agency or organization can locate the metadata that they seek based on model organization and can read those metadata with reusable software tools.

**H. Local Metadata in SMAP Data Products**

SMAP standards incorporate additional metadata that describe each array within the HDF5 file. Each of these metadata elements appear in an HDF5 Attribute that is directly associated with the HDF5 Dataset that stores the array. Wherever possible, these HDF5 Attributes employ names that conform to the Climate and Forecast (CF) conventions. The Wikipedia page at http://en.wikipedia.org/wiki/Climate_and_Forecast_Metadata_Conventions provides an overview of the content and development of the CF conventions. Table 5 lists the CF names for the HDF5 Attributes that SMAP products typically employ. The table also indicates which of these local metadata elements are mandatory for all arrays, and which are optional.

**I. Bit Flags in SMAP Data Products**

Bit flags provide a compact means to specify descriptive and quality information for individual pixels represented in the data product. Bit flags serve at least three important data processing functions. These include:

- Specification of data quality and ambient information — product users can inspect these flags to determine which pixels are applicable and/or have appropriate quality for use in their research

- Provision of pre-conditions for use in subsequent data generation processes — for instance, the SMAP Level 2 executables that retrieve soil moisture will not employ Level 1 pixels that are flagged with uncorrected radio frequency interference (RFI). These same Level 2 executables will not attempt to retrieve soil moisture for pixels that are mostly or entirely over open water, since such an effort makes no sense, even if the quality of the pixel is deemed good.

- Compilation of the overall quality of a granule — at the completion of processing, SMAP executables collect the content of bit flags to perform statistical analyses of the overall data granule

In general, bit flags serve two major purposes:

- Quality indicators — indicate whether a particular quality characteristic is good or acceptable

- State indicators — indicate other states or conditions about each pixel that may be important to the product user, but not reflective of quality. A SMAP example of a state indicator might specify whether a particular instrument footprint was acquired to the fore or to the aft of the spacecraft. Another might indicate whether the results are based on high-resolution or low-resolution instrument data.

Bit flags in all SMAP data products conform to the following convention:

- SMAP products separate quality indicator bits from state indicator bits. Quality indicator bits with state indicator bits do not appear in the same bit flag variables in SMAP data products.

- Bit flags that contain quality information and bit flags that list conditions that can be classed as favorable or unfavorable adhere to the following convention:

  - Bits that indicate good quality or favorable conditions contain zeros.

  - Bits that indicate poor or unacceptable quality or unfavorable conditions contain ones.

- SMAP executables initialize bits at the beginning of each process. Software always initializes defined bits with a value of one and initializes undefined bits with a value of zero. Processing executables therefore need to actively clear all defined bits when good quality is identified or when acceptable conditions are realized. Thus, when examining flags that contain quality information or ambient condition information that can be qualified, users can choose whether they wish to parse bit flag variable contents. If the entire flag is zero, users can rest assured that no adverse conditions were detected.

## VIII. Data Archive

The Earth Observing System Data and Information System (EOSDIS) is a key core capability in NASA's Earth Science Data Systems Program. It provides end-to-end capabilities for managing NASA's Earth science data from various sources — satellites, aircraft, field measurements and various other programs. Included within the capabilities of EOSDIS are the EOSDIS Science Operations, which are managed by the Earth Science Data and Information System (ESDIS) Project. These capabilities include generation of higher level (Level 1–4) science data products for EOS missions and archiving and distribution of data products from EOS and other satellite missions, as well as data from aircraft and field measurement campaigns. The EOSDIS science operations are performed

Table 5. SMAP-specific local attributes.

| CF Compliant Attribute Name | Description | Mandatory? |
| --- | --- | --- |
| Units | Units of measure | Yes |
| valid_max | The largest valid value for any element in the associated array. The data type in valid_max matches the type of the associated array. | No |
| valid_min | The smallest valid value for any element in the associated array. The data type in valid_min matches the type of the associated array. | No |
| _FillValue | Specification of the value that will appear in the array when an element is missing or undefined. The data type of _FillValue matches the type of the associated array. | Yes for all numeric data types |
| long_name | A descriptive name that clearly describes the content of the associated array. | Yes |
| coordinates | Identifies auxiliary coordinate variables in the data product. Coordinate variables are arrays with matching shape that enable users to correlate data to spatial data or to temporal data. | No |
| flag_values | Provides a list of flag values that appear in bit flag variables. Only appears with bit flag variables. | No |
| flag_masks | Provides a list of bit fields that express Boolean or enumerated flags. Only appears with bit flag variables or enumerated data types. | No |
| flag_meanings | Provides descriptive words or phrases for each potential bit flag value. | No |

within a distributed system of many interconnected nodes (Science Investigator-led Processing Systems and distributed, discipline-specific, Earth Science Data Centers) with specific responsibilities for production, archiving and distribution of Earth science data products (NASA 2013).

The EOSDIS Data Centers serve a large and diverse user community by providing capabilities to search and access science data products and specialized services. Twelve discipline-specific EOSDIS Data Centers are collocated with science and academic institutes around the country; eight of these are referred to as Distributed Active Archive Centers (DAACs). Data Center holdings can be searched from the Reverb search and order client (http://reverb.echo.nasa.gov) powered by the EOS Clearing House (ECHO).

The ESDIS Project, through its development, management, and operation of the EOSDIS, oversees the transfer of SMAP mission data to its Data Centers for archiving and distribution to the Earth science user community. The Alaska Satellite Facility (ASF) DAAC, specializing in SAR data, and the National Snow and Ice Data Center (NSIDC) DAAC, specializing in cryospheric science and land microwave data, were selected as the co-managing Data Centers for SMAP data. ASF and NSIDC will collaboratively develop a data system strategy to provide seamless discovery and access of all SMAP and SMAP-related data.

**A. SMAP Data Management at the ASF DAAC**

The ASF of the Geophysical Institute operates the SAR Data Center for NASA at the University of Alaska in Fairbanks (UAF). For more than 20 years, ASF has worked in conjunction with the SAR research community and scientists across the globe providing near-real-time and archive data from several key Earth-observing satellites. In support of this user community, ASF offers interactive web resources for data search and download, creates custom software tools for data interpretation and analysis and provides public outreach activities (http://www.asf.alaska.edu). ASF's DAAC is one of 12 Data Centers supported by NASA and specializes in the processing, archiving, and distribution of SAR data to the global research community. In the past 2 years, ASF DAAC has moved from a process-on-demand to a download-on-demand data system that provides direct access to over 1 PB of SAR

data. The ASF data system, comparable to the EOSDIS Core System, provides ingest, cataloging, archiving, and distribution of ASF DAAC's complete data holdings. ASF distributes focused and unfocused SAR data products, browse images, and relevant metadata in multiple formats through the Vertex data search portal (https://vertex.daac.asf.alaska.edu).

**ASF DAAC Support of NASA Missions**

The ASF DAAC provides support for NASA and NASA-partner missions assigned to it by the ESDIS Project. The ASF DAAC has extensive experience managing diverse airborne and spaceborne mission data, working with various file formats, and assisting user communities to further the use of SAR data. These efforts are facilitated, in part, by ASF Scientists and Data Managers, who interact with mission teams, provide subject matter expertise, inform data and metadata formats, evaluate data structure and quality, and address data support needs. A key project component at ASF is the core product team, which provides integration of new datasets into the ASF data system and ensures efficient coordination and support of each mission. The team members have mission-specific expertise and consist of the following personnel:

- The Project Manager is the team leader who oversees mission activities at ASF and coordinates with external groups.

- The Product Owner is a primary product stakeholder and oversees ingest, archive, documentation, and distribution of data products as well as managing interactions with mission and ASF scientists and other stakeholders.

- The User Services Representative (uso@asf.alaska.edu) supports data users with products and software tools and communicates user feedback or suggestions for improvement to the Project Manager and Product Owner.

- Software Engineers design, develop, and maintain software for the acquisition, processing, archiving, and distribution of satellite and aerial remote sensing data.

- Software Quality Assurance technicians provide software and web-based-application testing prior to delivery to the production data system to ensure integrity, quality, and overall proper functionality through testing methods to uncover program defects, which in turn are reported to software engineers.

- The technical science writer composes and edits a variety of ASF materials, from newsletter articles to technical documentation.

The core product team's responsibilities for data management include:

- Ingesting, cataloging, archiving, and distributing data

- Providing guidance on file formats and integration of new file formats into the ASF data system

- Describing data products and producing user manuals and guide documents

- Creating metadata and exporting it to ECHO and GCMD (Global Change Master Directory)

- Ensuring accurate metrics are reported to EMS (ESDIS Metrics System)

- Designing, developing, and deploying specialized data portals that allow online access to data products and information

- Creating software tools for data interpretation and analysis

- Assisting users with the selection and usage of data

ASF also supports NASA and partner missions through the operation of a ground station with two 11-m antennas, providing complete services, including data downlinking, commanding, and range/Doppler tracking. ASF is part of the NASA NEN supporting a variety of low-Earth-orbit spacecraft.

**ASF DAAC Data Systems**

The ASF DAAC operates a custom data system designed, implemented, and supported by DAAC personnel. During its evolution, the ASF data system has moved from using primarily custom software on capital equipment to commodity hardware and commercial off-the-shelf (COTS) software and hardware solutions. This has greatly lowered development and maintenance costs for the data system, while simultaneously providing a higher level of performance. The ASF DAAC data system provides the following capabilities:

*Data Ingest*

- Automated data ingest occurs from the ASF ground station as well as external data providers in a variety of media and formats.

- Ingested data are pre-processed when necessary, providing browse or derivative products.

*Data Archive*

- The central ASF data system archive is provided by a Data Direct Networks gridscaler storage system.

- This system provides direct access to over 1 PB of processed data as well as the capability for automated backups to an offsite location.

- Raw data are held in a robotic silo for access by the processing system. ASF maintains a backup in an external location in case of silo failure.

*Data Distribution*

- ASF provides direct http access to DAAC data products and utilizes NASA's User Registration System (URS) for user authentication.

- NASA data are provided to public users with no restrictions. Partner data are provided to NASA-approved users through URS for authentication and ASF's internal database for access control.

- The data system provides web-based access to the archive through distribution portals Vertex and URSA (User Remote Sensing Access). Vertex supports the data pool with direct download of processed data, while URSA provides the DAAC's more advanced users with custom processing for particular science applications.

- Through custom portals and applications, the DAAC provides additional services such as mosaic subsetting, mosaicking, and time-series analysis.

*Data Support*

- ASF DAAC exports relevant metadata to NASA's ECHO system.

- ASF DAAC exports ingest, archive, and download metrics to NASA's EMS system.

- ASF DAAC assists users with data discovery and usage, maintains product documentation and use guides, and supports feedback between the ASF user community and the core product teams.

**SMAP at ASF DAAC**

ASF provides a variety of services, software tools, and user support to address the needs of the SMAP user community. The ASF core project team will leverage on-going collaborations with the SMAP Project to identify and prioritize SMAP user community needs, which in turn will inform development and implementation of data support and value-adding services for the mission. The SMAP website at ASF (https://www.asf.alaska.edu/smap) will serve as an interactive data portal, providing users with relevant documentation, custom tools and services, and ancillary data and resources.

**Post-Launch SMAP Data**

ASF will ingest, distribute, archive, and support post-launch Level 1 radar products for the SMAP mission. ASF will receive the Level 1 radar products from the SMAP Science Data System at the Jet Propulsion Laboratory (JPL) in Pasadena, California (Table 6).

**Non-SMAP Data of Interest to SMAP**

ASF will cross-link from the SMAP website to data collections that complement SMAP data and are of interest to the user community. Some of these collections are distributed by ASF, including the following:

- Airborne Microwave Observatory of Subcanopy and Subsurface (AirMOSS) data products

- Jet Propulsion Laboratory Uninhabited Aerial Vehicle SAR (UAVSAR) data products

- MEaSUREs (Making Earth System Data Records for Use in Research Environments) Inundated Wetlands data products

Table 6. SMAP science data products at ASF DAAC.

| SMAP Mission Short Name | DAAC Short Name | Description | File Size (MB) | Files per Day |
|---|---|---|---|---|
| L1A Radar | SPL1AA | Parsed Radar Telemetry | 2,965 | 30 |
| L1B_S0_LoRes | SPL1BS0 | Low-Resolution Radar $\sigma_o$ in Time Order | 300 | 30 |
| L1C_S0_HiRes | SPL1CS0 | High-Resolution Radar $\sigma_o$ on Swath Grid | 1,557 | 30 |

- Advanced Land Observing Satellite-Phased Array L-band SAR (ALOS PALSAR)

- Japanese Earth Resources Satellite-1 (JERS-1) image data and mosaics

## B. SMAP Data Management at the NSIDC

The NSIDC is a part of the Cooperative Institute for Research in Environmental Sciences (CIRES) at the University of Colorado Boulder. NSIDC supports research into the world's frozen realms: the snow, ice, glaciers, frozen ground, and climate interactions that make up Earth's cryosphere. NSIDC also manages and distributes scientific data, creates tools for data access, supports data users, performs scientific research, and educates the public about the cryosphere. NSIDC distributes more than 500 Earth science datasets collected from satellite, aircraft and ground instruments through its website (www. nsidc.org). The NSIDC DAAC within NSIDC is one of NASA's EOSDIS Data Centers and focuses primarily on the study of the cryosphere. The NSIDC DAAC (http://nsidc. org/daac/index.html) provides data support for NASA's past and current EOS satellites and field measurement programs. NASA Headquarters assigned data management of the Decadal Survey SMAP mission to the NSIDC DAAC, in collaboration with ASF, based on the center's experience managing passive microwave soil moisture data for NASA's Advanced Microwave Scanning Radiometer— EOS (AMSR-E) mission.

### NSIDC DAAC Support of NASA Missions

The NSIDC DAAC has been archiving and distributing data for NASA missions assigned to it by the ESDIS Project for more than 20 years. The DAAC has breadth and depth of experience managing heterogeneous data products, data formats, and user communities. Through early engagement with mission teams, NSIDC scientists and data managers bring significant value to the missions by providing expert counsel on data and metadata formats, data structures, and data support needs.

To aid in the efficient coordination of support, NSIDC DAAC assigns a dedicated Product Team Lead (PTL) to each mission. The PTL performs external coordination with instrument teams, data production facilities, and the ESDIS Project to develop formal agreements and define overarching operational processes and data flows. PTLs coordinate internal activities through a dedicated Product Team. The Product Team combines functional skills, such as Data Operations, Technical Writing, User Support, Science Support, and Programming, with mission-specific expertise enabling customized support of the mission data and the scientific community. The Product Team model, shown in Figure 18, provides a continuous feedback loop between the science users and the DAAC,
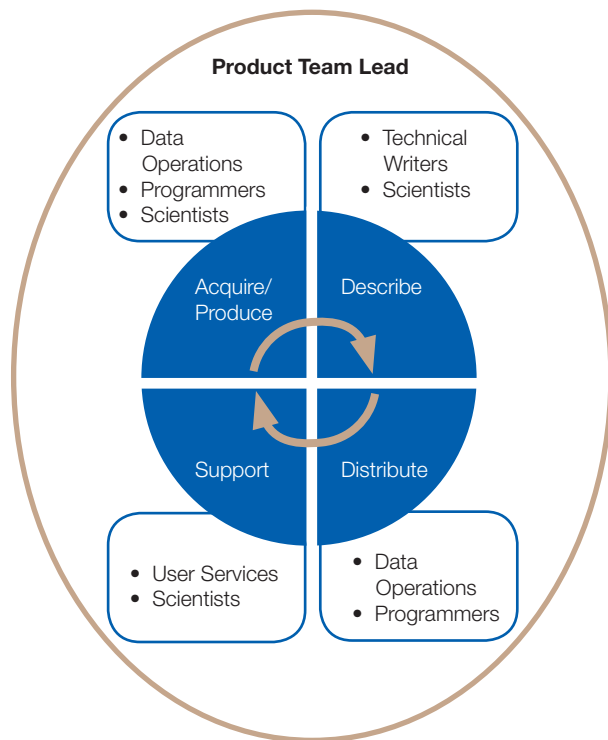


Figure 18. NSIDC DAAC mission support product team model.

which drives enhancements to documentation, data holdings, and services. The continuous feedback also extends to the external mission teams when data quality assessments or data user requests warrant involvement from the science team or data production facility.

The Product Team's core functions for data management center around four areas:

### Acquire and/or Produce Data

- Advise on data formats, structure, and delivery methods

- Establish automated processes for the transfer of data into DAAC data systems

- Develop or integrate, test, verify, and run data production code (for applicable data)

### Describe Data

- Create collection-level metadata and, when necessary, extract file-level metadata for provenance tracking and data discovery

- Export metadata to ECHO and the GCMD (Global Change Master Directory) for cross-mission, cross-sensor NASA Earth science data discovery

- Develop user documentation and supplemental information based upon the scientific community needs and NSIDC best practices

### Distribute Data

- Provide free online access to data (FTP and subscription service)

- Provide specialized portals and data services in accordance with the scientific community needs

### Support Data

- Assist user communities with the selection and usage of data and tools

- Work with user communities to identify data and tool needs

- Provide outreach and education to broaden the mission user community

**NSIDC DAAC Data Systems**

NSIDC is one of three DAACs that operate the EOSDIS Core System (ECS) for management of NASA mission data (Maurer and Leon 2009). ECS, developed and maintained by Raytheon for ESDIS, is a robust system of hardware, custom-developed software and COTS software operated and monitored by NSIDC Data Operations staff with support from on-site Raytheon contractors. ECS's flexibility to manage a wide range of Earth science data is a function of its inventory management systems. Comprehensive, accurate, and consistent metadata (i.e., data about data) provide the foundation for almost all data preservation and access functions. ECS provides a well-established and adaptable system for capturing and storing metadata. In addition to rich metadata defined by the missions stored within data files, ECS requires a separate metadata file that defines core attributes for preservation and discovery. The metadata is stored within ECS and plays a critical role in ensuring the integrity of science data. Checksums, a digital signature used to detect whether errors have occurred in transmission or storage, are recorded in the metadata and validated after files have been ingested and periodically throughout their storage life.

A portion of metadata is sent to NASA's ECHO, a metadata registry and order broker developed by ESDIS to enable the science community to more easily locate and access NASA's data and services. NSIDC DAAC utilizes NASA's Reverb (http://reverb.echo.nasa.gov/reverb) as the search and order portal for data held in the ECS. Reverb connects to ECHO and exposes data from all NASA Data Centers. This distributed discovery enables users to obtain multidisciplinary, multimission data from one portal regardless of its physical location. Orders for NSIDC data placed through Reverb are sent to the DAAC for processing and delivery. Reverb also enables the invocation of data services such as reformatting, re-projection, and subsetting. ECS provides the following capabilities:

### Data Ingest

- Automates ingest of data in multiple formats from external data providers

- Performs data transfer reconciliation and verification

- Allows for the ingest of science data, metadata, quality assurance, and production history files as well as quick-look browse images

### Data Archive

- Maintains a primary online disk copy of science data and a redundant tape backup

- Provides automated file management (e.g., duplicate file detection and deletion) and file integrity (e.g., checksum verification) functions

### Data Distribution

- Provides direct FTP access to all public data holdings

- Offers data subscriptions for automated delivery of data

- Provides data search and order through NASA's Reverb Portal (http://reverb.echo.nasa.gov/reverb)

  - Displays quick-look browse images to assist with data selection

  - Enables services for select datasets, such as spatial subsetting, reformatting, and re-projection

### Inventory Management

- Stores collection-level and file-level metadata for the following:

  - Preservation — checksums, algorithm versions, input data files

  - Data Discovery and Usage — platforms, instruments, parameters, temporal coverage, spatial coverage

- Exports inventory metadata to NASA's ECHO to enable discovery of NSIDC DAAC holdings

### SMAP at NSIDC DAAC

NSIDC supports a range of services designed to meet the needs of user communities with varying requirements and applications. Through collaboration with the SMAP Project and insight into the SMAP community through the Application Working Group and the Early Adopter program, NSIDC will strategically develop and implement data support and value-adding services for the mission. The SMAP website at NSIDC (http://nsidc.org/data/smap/index.html) serves as a gateway to data, comprehensive user documentation, tools and services, and related data and resources.

The NSIDC DAAC will provide management of three main categories of data for the SMAP mission: post-launch SMAP data, pre-launch SMAP data, and non-SMAP data of interest to SMAP. These data categories, as well as the classification of user communities and corresponding data access policies, are being formally defined by the SMAP Project with collaboration from NSIDC DAAC.

### Post-Launch SMAP Data

NSIDC is responsible for the archival, distribution, and support of post-launch Level 1 passive microwave products and Level 2–4 passive microwave and radar products (Table 7). NSIDC will receive the Level 1–3 products from the SMAP Science Data System at the Jet Propulsion Laboratory in Pasadena, California and the Level 4 products from the Global Modeling and Assimilation Office at NASA Goddard Space Flight Center in Greenbelt, Maryland.

NSIDC DAAC will also provide data access, information and support for post-launch SMAP validation datasets. The validation data suite includes data archived and distributed by NSIDC and data held at other established Data Centers. The NSIDC SMAP website will provide centralized access to validation data regardless of physical location.

Table 7. SMAP science data products at NSIDC DAAC.

| SMAP Mission Short Name | DAAC Short Name | Description | File Size (MB) | Files per Day |
|---|---|---|---|---|
| L1A_Radiometer | SPL1AP | Radiometer Data in Time-Order | 3,466 | 30 |
| L1B_TB | SPL1BTB | Radiometer $T_B$ in Time-Order | 54 | 30 |
| L1C_TB | SPL1CTB | Radiometer $T_B$ in Half-Orbits | 12 | 30 |
| L2_SM_A | SPL2SMA | Soil Moisture (Radar) | 71 | 30 |
| L2_SM_P | SPL2SMP | Soil Moisture (Radiometer) | 1 | 15 |
| L2_SM_AP | SPL2SMAP | Soil Moisture (Radar + Radiometer) | 10 | 15 |
| L3_FT_A | SPL3FTA | Freeze/Thaw State (Radar) | 1,410 | 1 |
| L3_SM_A | SPL3SMA | Soil Moisture (Radar) | 3,335 | 1 |
| L3_SM_P | SPL3SMP | Soil Moisture (Radiometer) | 15 | 1 |
| L3_SM_AP | SPL3SMAP | Soil Moisture (Radar + Radiometer) | 281 | 1 |
| L4_SM | SPL4SMGP | Soil Moisture (Surface and Root Zone ) Geophysical Data | 2,109 | 1 |
| L4_SM | SPL4SMAU | Soil Moisture (Surface and Root Zone ) Analysis Update Detail | 2,776 | 1 |
| L4_C | SPL4C | Carbon Net Ecosystem Exchange | 116 | 1 |

**Pre-Launch SMAP Data**

The SMAP Applications Working Group Early Adopter program was developed to provide a fundamental understanding of the utility and the integration of SMAP data into applications research. As part of joining the program, the SMAP Early Adopters are provided access to simulated SMAP products and pre-launch calibration and validation data from SMAP field campaigns. The NSIDC DAAC leverages its data distribution infrastructure to provide access to these pre-launch data to the Early Adopters and other approved users on behalf of the SMAP Project. After approval by the SMAP Project and acknowledgment of the pre-launch data use agreement, users are provided a login to the NSIDC SMAP Restricted Data website for convenient access to SMAP simulation and validation data, product documentation, and other resources.

**Non-SMAP Data of Interest to SMAP**

NSIDC will also provide a connection to those data collections that are complementary to SMAP data and provide value to the user community. A selection of these collections is distributed by NSIDC, such as the AMSR-E mission data and the AMSR-E Validation Soil Moisture Experiment (SMEX) field campaign data. Data collections held at other centers, including international missions such as the European Space Agency's Soil Moisture and Ocean Salinity (SMOS) data, will be referenced.

## References

Brodzik, M. J. et al., "EASE-Grid 2.0: Incremental but Significant Improvements for Earth-Gridded Datasets," National Snow and Ice Data Center, Cooperative Institute of Environmental Sciences, University of Colorado, *ISPRS International Journal of Geo-Information*, ISSN 2220-9964, 2012. dx.doi.org/10.3390/ijgi1010032

ISO 19115:2003 International Standard, Geographic Information–Metadata, International Organization for Standardization, May 1, 2003.

ISO 19115-2 ISO/TC 211 Geographic information/Geomatics, International Organization for Standardization, September 19, 2007a.

ISO 19139 Geographic information–Metadata–XML schema implementation, International Organization for Standardization, April 15, 2007b.

Maurer, J. and A. Leon, "An Introduction to EOS Data in the EOSDIS Core System (ECS) at NSIDC," *NSIDC Special Report 12*, Boulder, Colorado, USA, National Snow and Ice Data Center, 2009.

NASA, "About EOSDIS," NASA's Earth Observing System Data and Information System, 7 June 2013. http://earthdata.nasa.gov/about-eosdis

# 3. Instrument Design and L1 Data Products

## I. SMAP Instrument Overview

The SMAP instrument is required to meet the following high-level measurement objectives:

- 1000-km swath width at orbit altitude of 685 km in order to meet 3-day revisit time for soil moisture (2-day revisit time at high latitudes for freeze/thaw)

- Co-located L-band active radar measurements and passive radiometer measurements at a constant incidence angle near 40°

- Polarimetric radiometer measurements at spatial resolution of 40 km

- Dual-polarized radar measurements at spatial resolution of 3 km

To accomplish this challenging set of requirements, a 6-m conically-scanning reflector antenna architecture was selected for the instrument design. The deployable mesh antenna is shared by both the radiometer and radar instruments by using a single L-band feed. While the radiometer resolution is defined as the real aperture antenna footprint, the higher resolution radar measurements are obtained by utilizing synthetic aperture radar (SAR) processing. These are common techniques, but newly applied by the SMAP Project to a scanning mesh antenna. At the nominal SMAP altitude of 685 km, the reflector must be rotated at a minimum rate of 13.0 rpm to maintain contiguity (i.e., minimum overlap) of the measurements in the along-track direction (Figure 19).

The overall SMAP instrument architecture is shown in Figure 20. Because the rotating reflector is shared by the radiometer and radar, the RF signals from the Earth must be separated by frequency diplexers into the active and passive bands. These diplexers are located on the spun side of the observatory as shown in Figure 20. Note that all of the radiometer electronics are located on the spun side of the interface to minimize front-end losses, with slip rings providing a telemetry, signal, and power interface to the spacecraft. The more massive and more thermally dissipative radar electronics are on the fixed side, with the transmit/receive pulses routed to the spun side via a two-channel RF rotary joint.

The following sections describe in detail the radiometer and radar instruments, along with their associated processing and data products.

## II. The SMAP Radiometer

### A. Radiometer Performance Requirements

The SMAP radiometer is required to meet the following performance requirements:

- Obtain time-ordered measurements of brightness temperature at the surface of the Earth at Vertical (V) and Horizontal (H) polarizations along with the third and fourth Stokes parameters (T3 and T4) of the microwave radiation
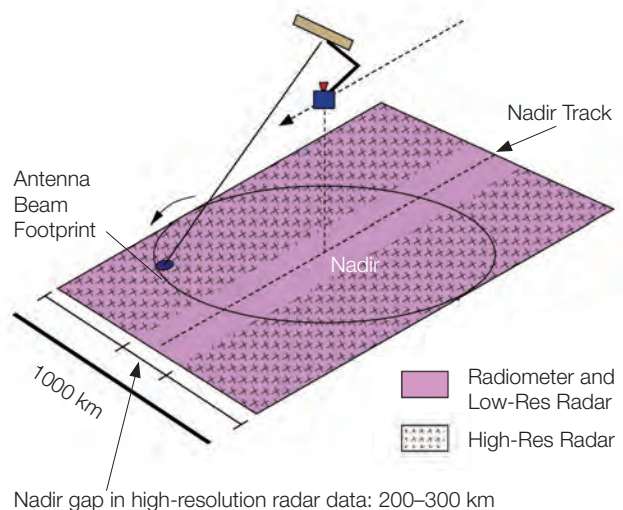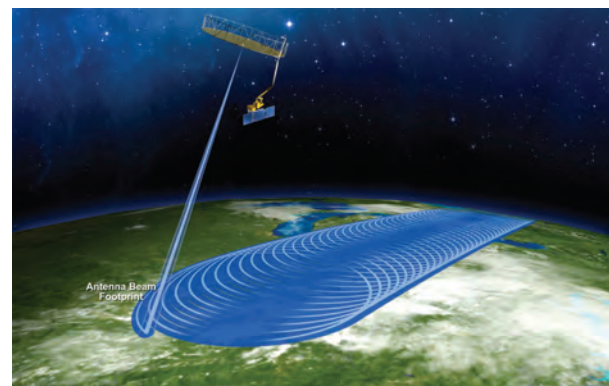




Figure 19. Schematic of the SMAP conically scanning antenna beam mapping out a swath width of 1000 km at Earth's surface. Top: Helical pattern mapped out by the conical antenna scan coupled with the forward motion of the spacecraft; light blue depicts the antenna boresight direction and intersection at the surface; dark blue depicts the 3-dB real-aperture footprint area (characteristic of the radiometer spatial resolution). Bottom: Synthetic aperture processing applied to the radar data results in variable spatial resolution across the swath, from approximately 1 km (high resolution) at the edge of the swath to approximately 30 km (low resolution) at the nadir track; the cross-hatched portion illustrates the region of the swath where the spatial resolution is between 1 and 3 km (referred to as the "hi-res" radar data region).
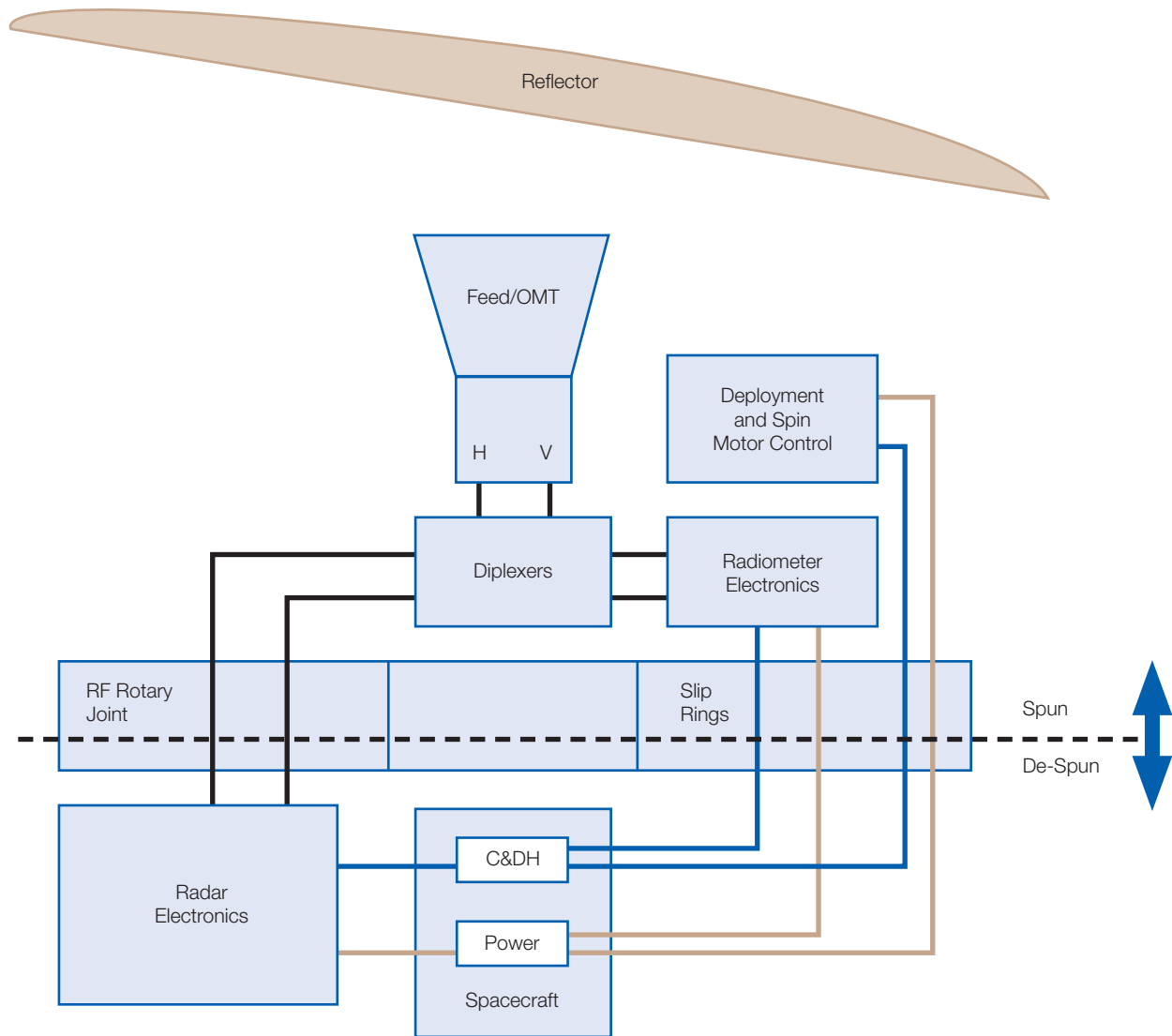
**Figure 20. Simplified instrument functional diagram.**

- Obtain time-ordered brightness temperatures at 40 km spatial resolution

- Obtain time-ordered brightness temperatures at V and H polarizations with errors from the following sources removed: antenna pattern and loss effects, Faraday rotation, atmospheric effects (excluding rain), and solar, galactic, and cosmic radiation

- Obtain geolocation information with an uncertainty (3-sigma) of less than 4 km

- Achieve radiometric accuracy for H and V brightness temperature measurements of 1.3 K or less (1-sigma) computed by binning fore- and aft-look samples into 36 km x 36 km grid cells

- Mitigate TB measurement errors due to RFI of 0.3 K (1-sigma) or less

- Collect data that meet the above requirements over all land areas of science interest

## B. Radiometer Technical Design

The SMAP instrument architecture consists of a 6-m conically-scanning reflector antenna and a common L-band feed shared by the radar and radiometer. The reflector rotates about the nadir axis at a stable rate that can be set in the range between 13–14.6 rpm, producing a conically scanning antenna beam with an approximately 40-km, 3-dB footprint at the surface with an Earth incidence angle of approximately 40º. The conical scanning sweeps out a 1000-km-wide swath with both fore and aft looks for the radiometer.

The feed assembly employs a single-horn, orthomode transducer, with V and H polarizations aligned with the Earth's surface polarization basis, and covers both radar and radiometer bands. The radiometer uses 24 MHz of bandwidth centered at 1.4135 GHz. The radar and radiometer signals are separated by frequency diplexers within the coaxial cable-based feed network and routed to the appropriate electronics for detection. The radiometer electronics are located on the spun side of the interface. Slip rings provide a signal interface to the spacecraft. The more massive and more thermally dissipative electronics of the radar are on the de-spun side, and the transmit/receive pulses are routed to the spun side via a two-channel RF rotary joint. The radiometer timing for the internal calibration switching and detection integrators is synchronized with the radar transmit/receive timing to provide additional RF compatibility between the radar and radiometer and to ensure co-alignment of the brightness temperature and backscatter cross-section measurements.

The radiometer block diagram is shown in Figure 21. The front-end comprises a coaxial cable-based feed network and radiometer front-end (RFE) box. The feed network includes a coupled noise source (CNS) for monitoring front-end losses and phase changes. The diplexers (DIP) separate the radar and radiometer bands. Internal calibration is provided by reference switches and a common noise source (Noise SRC) inside the RFE. The RF back-end (RBE) downconverts the 1413 MHz channel to an intermediate (IF) frequency of 120 MHz. The IF signals are then sampled and quantized by high-speed analog-to-digital converters in the radiometer digital electronics (RDE) box. The RBE local oscillator (PLO-OSC) and RDE sampling clocks are phase-locked to a common reference to ensure coherency between the signals. The RDE performs additional filtering, subband channelization, cross-correlation for measuring T3 and T4, and detection and integration of the first four raw moments of the signals. These data are packetized and sent to the ground for calibration and further processing.

The radiometer timing diagram is shown in Figure 22. For every pulse repetition interval (PRI) of the radar, the radiometer integrates for ~350 μs during the receive window.

(The exact amount of time can vary based on the radar PRI length and blanking time length chosen by the instrument designers.) Radiometer packets are made up of 4 PRIs. Each science data packet includes time-domain data of the entire passband (called "fullband" data) for each of the 4 PRIs, and subbanded data, which have been further integrated to 4 PRIs or ~1.2 ms. The science telemetry includes the first four sample raw moments of the fullband (24 MHz wide) and 16 subband (each 1.5 MHz wide) signals, for both polarizations and separately expressed in terms of the in-phase and quadrature components of the signals. The 3rd and 4th Stokes parameters are also produced via complex cross-correlation of the two polarizations for the fullband as well as each of the 16 subbands. Every science data packet therefore contains 360 pieces of time-frequency data.

A radiometer footprint is defined to be 12 packets long, 8 of which are for observing the scene and the 5th, 6th, 11th, and 12th for internal calibration. Figure 23(a) shows the formation of a footprint in terms of 3-dB contours. Integration of the 8 observing packets slightly enlarges the antenna's instantaneous field of view (IFOV) from 36 km x 47 km to an effective field of view (EFOV) of 39 km x 47 km. The EFOV spacing shown in Figure 23(b) is approximately 11 km x 31 km near the swath center.

## C. RFI Detection and Mitigation

SMAP's radiometer passband lies within the 1400–1427 MHz Earth Exploration Satellite Service (EESS) passive frequency allocation. Both unauthorized in-band transmitters as well as out-of-band emissions from transmitters operating at frequencies adjacent to this allocated spectrum have been documented as sources of radio frequency interference (RFI) to the L-band radiometers on SMOS (Mecklenburg et al. 2012) and on Aquarius (Lagerloef et al. 2008; Piepmeier and Pellerano, 2006; Misra and Ruf, 2008; Ruf et al. 2012). RFI impacts the amount and quality of radiometer measurements from space that are available for routine science from these missions. Since this is a serious issue that is expected to be present during the SMAP mission lifetime, SMAP will be the first spaceborne radiometer to fly a dedicated subsystem to enable detection and mitigation of RFI.

SMAP takes a multidomain approach to RFI mitigation utilizing an innovative onboard digital detector back-end with digital signal processing algorithms to characterize time, frequency, polarization, and statistical properties of received signals. Almost 1000 times more measurements than conventionally necessary are collected to enable the ground processing algorithms to detect and remove harmful interference. The SMAP radiometer instrument provides a large amount of information with time frequency diversity that is telemetered from the satellite to enable the use of multiple RFI detection methods on the ground.
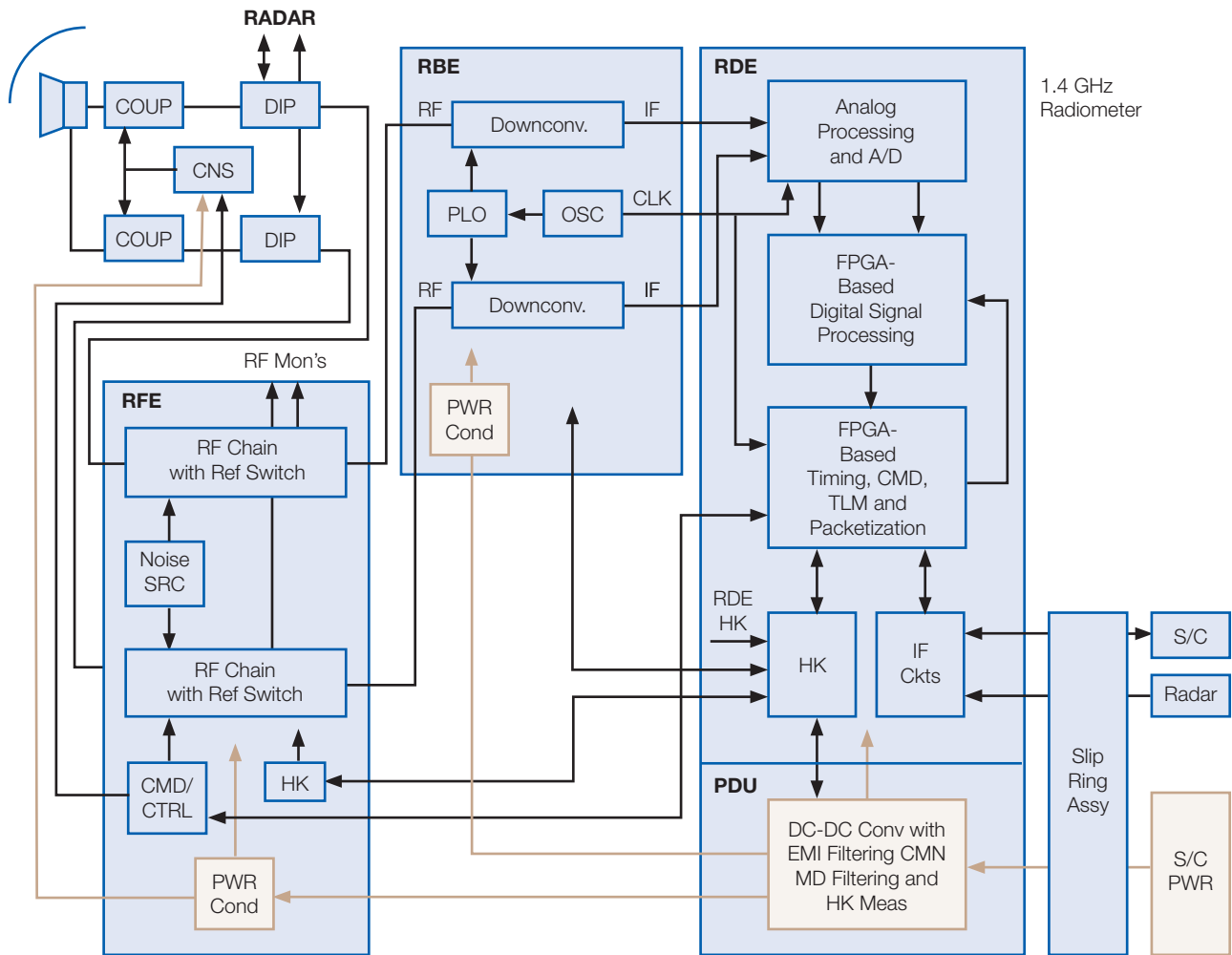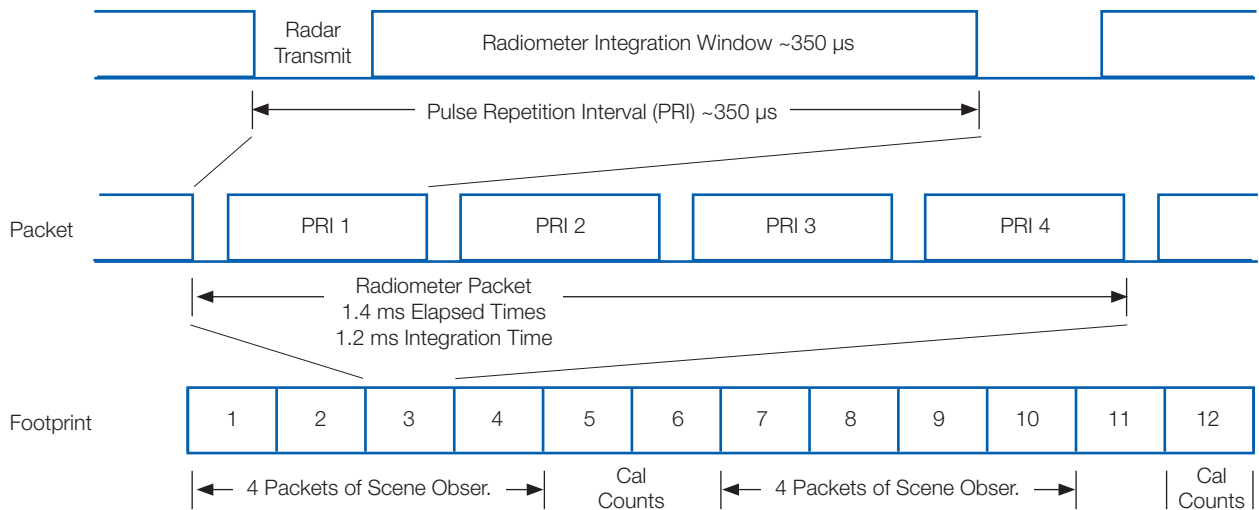
**Figure 21. Block diagram of radiometer.**



**Figure 22. Radiometer observation/internal calibration timing.**

Many of these detection techniques have been previously demonstrated; however, the SMAP radiometer is the first to enable complex RFI detection and mitigation in the ground software. The outputs of multiple RFI detection algorithms will be combined using a maximum probability of detection algorithm. Data indicated as RFI will be removed within a certain number of samples defined as a footprint and the rest of the "clean" data will be averaged to produce an RFI-free brightness temperature footprint product.

Samples measured every 350 µs over the full 24-MHz radiometer bandwidth are referred to as fullband measurements. One of the detection methods used is the time-domain or pulse-detection algorithm, which searches in time for increased levels of observed antenna temperatures above those produced by geophysical properties. This detection method is applied to the fullband time series data with an RFI detection occurring if a time sample is a certain number of standard deviations above the mean brightness temperature of the scene which is estimated by removing a certain percent of samples within a time measure (Niamsuwan et al. 2005; Johnson and Potter, 2009). The number of standard deviations, β, is defined as the threshold level and is set to accept a certain number of false alarms, which are detected RFI samples when RFI is not present. Each detection method has an associated threshold level, β, which varies geo-
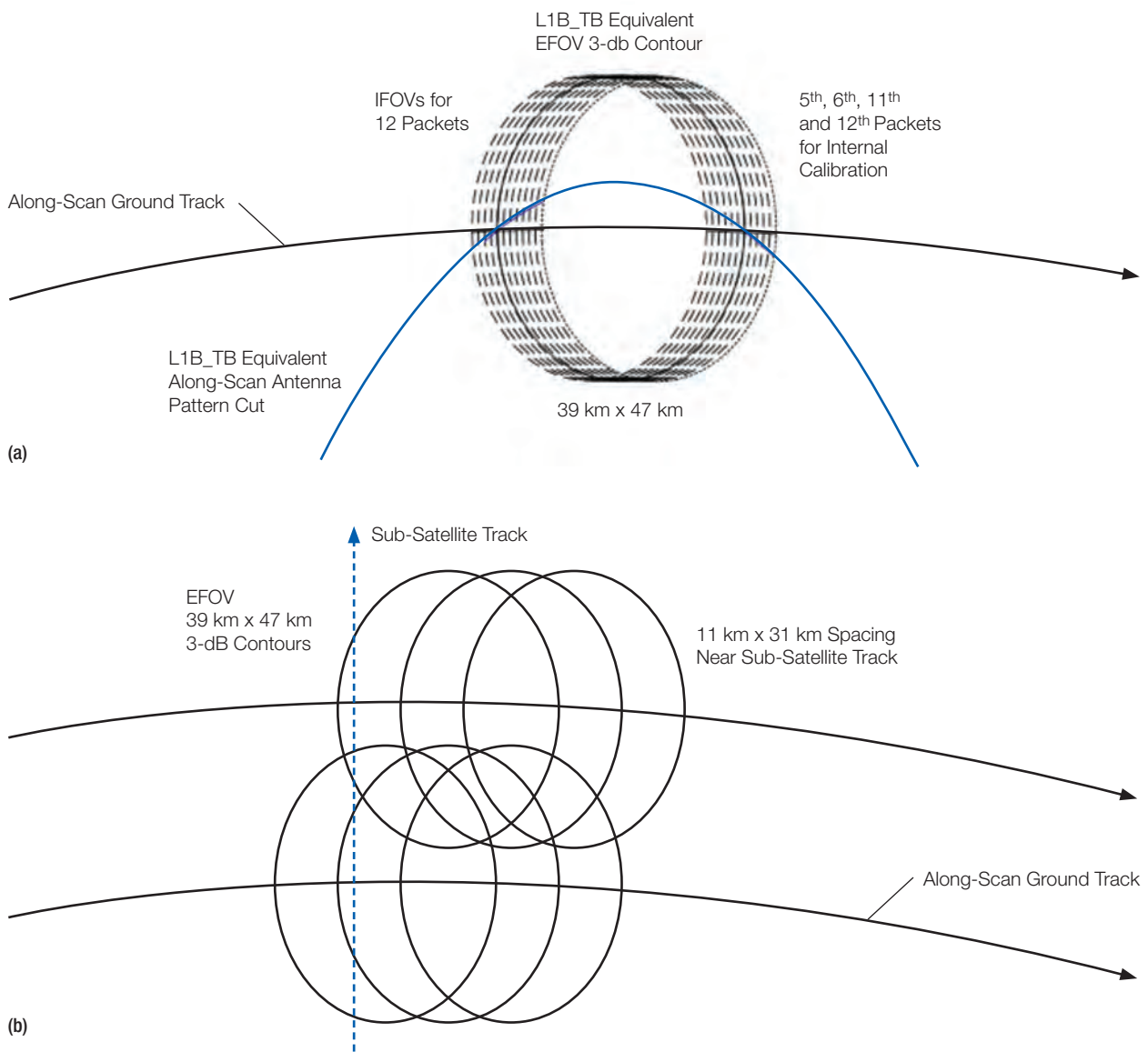


**L1B_TB Equivalent EFOV 3-db Contour**

IFOVs for 12 Packets

5th, 6th, 11th and 12th Packets for Internal Calibration

Along-Scan Ground Track

L1B_TB Equivalent Along-Scan Antenna Pattern Cut

39 km x 47 km

(a)

Sub-Satellite Track

EFOV 39 km x 47 km 3-dB Contours

11 km x 31 km Spacing Near Sub-Satellite Track

Along-Scan Ground Track

(b)

Figure 23. Radiometer EFOV formation (a) and spacing (b).

graphically with a 1x1° resolution in latitude and longitude — this is consistent with the Aquarius approach and grid for β. The 1x1° resolution grid was also chosen because it includes the full null-to-null beamwidth of the SMAP radiometer on the ground. This approach allows aggressive lower thresholds to be set in areas of persistent RFI and higher thresholds in RFI "quiet" areas, thereby reducing loss of "good" samples due to false alarms. In the ground processing, each detection algorithm produces a set of flags, with 1 indicating RFI detected for a particular sample and 0 indicating no RFI detected.

To produce more sensitive RFI detections, the measurement bandwidth is divided into 16 subbands, each with a 1.5-MHz bandwidth. These data are sampled every 1.4 ms and are referred to as subband measurements. One detection method that uses these data is called the cross-frequency detector. It is similar to the pulse detector except that it searches for increased levels of antenna temperatures in any subband relative to other subbands (Guner and Johnson 2010; Guner et al. 2007). The cross-frequency detection method has been shown to be more sensitive to wideband interfering sources than other methods.

Another detection method employed is a standard test for normality. The SMAP instrument produces the first four raw moments of the radiometer signal voltage in both the time and frequency domain. These moments are used to compute the kurtosis statistic, which has the unique property of being equal to 3 if the input is Gaussian in nature, such as thermally generated radiometric sources measured by SMAP. If the kurtosis statistic deviates from a value of 3, this is a clear indicator of the presence of man-made RFI sources which tend to have a non-Gaussian distribution (Ruf et al. 2006).

Included in the SMAP radiometer data are the 3rd and 4th Stokes parameters, which are produced via complex cross-correlation of the vertical and horizontal polarizations for the fullband as well as each of the 16 subbands. Polarization detection uses the 3rd and 4th Stokes parameters to search for variations greater than a fixed number of standard deviations away from reasonable geophysical values to identify RFI (Kristensen et al. 2012).

Since each of these detection methods is sensitive to different kinds of RFI, a complex method of integrating multiple detection results was developed. A single maximum probability of detection (MPD) flag, which minimizes the probability of missing the detection of RFI, is formed by a logical OR of each of the individual RFI detector outputs. Due to the logical OR operation, no RFI that is detected by any individual algorithm can ever be missed by the MPD algorithm. For this reason, the MPD flag minimizes the probability of missed detection — in other words, the probability of RFI detection is maximized given the available individual detectors. The MPD algorithm operates on both the fullband data (350 µs samples) and the 16-subband data (1.4 ms samples). The philosophy of using a logical OR operation to combine individual flags is used to combine the outputs of the two versions. If a fullband MPD flag is set high (indicating the presence of RFI), then all 16 subbands that include that time interval are considered contaminated with RFI. This methodology is illustrated in Figure 24. RFI removal is accomplished by including in the final product average (over the 8 time sample by 16 subchannel spectrogram) only those second moment subband counts for which the composite MPD flag is not set. Thus, the final product is an average of the RFI-free samples forming an RFI-free footprint.

## D. Radiometer Processing

The radiometer processing algorithms are described more completely in the L1B_TB ATBD. The L1B_TB Radiometer processing subsystem consists of four separate executable programs:

- L0a preprocessor — collects metadata from each downlink telemetry file

- L0b preprocessor — organizes the downlink telemetry files into half-orbit granules

- L1A processor — unpacks telemetry data, sorts data into various radiometric states, and performs digital numbers to engineering units conversions

- L1B processor — performs calibration, RFI detection and mitigation, and removes error sources to produce brightness temperature products

The L0a and L0b preprocessors prepare the incoming downlinked telemetry files by stitching and splitting them into half-orbit granules. Some overlap is included at the beginning and end to ensure that all data are included in the final L1B_TB product files. The L1A processor unwraps the CCSDS packets which make up the telemetry files, parses the radiometer science data into various radiometric states, and creates and stores the time stamps for science data. Housekeeping telemetry such as temperature, voltage, and current monitor points are converted to engineering units for each scan. These telemetry points are stored before and after unit conversion.

Each record of the resulting L1A file contains both fullband and subband data in high-rate mode (over land and calibration targets) and only fullband data in low-rate mode (over ocean). The L1A file is stored in HDF format and will be submitted for archival storage along with the output data products. The L1A file becomes the primary
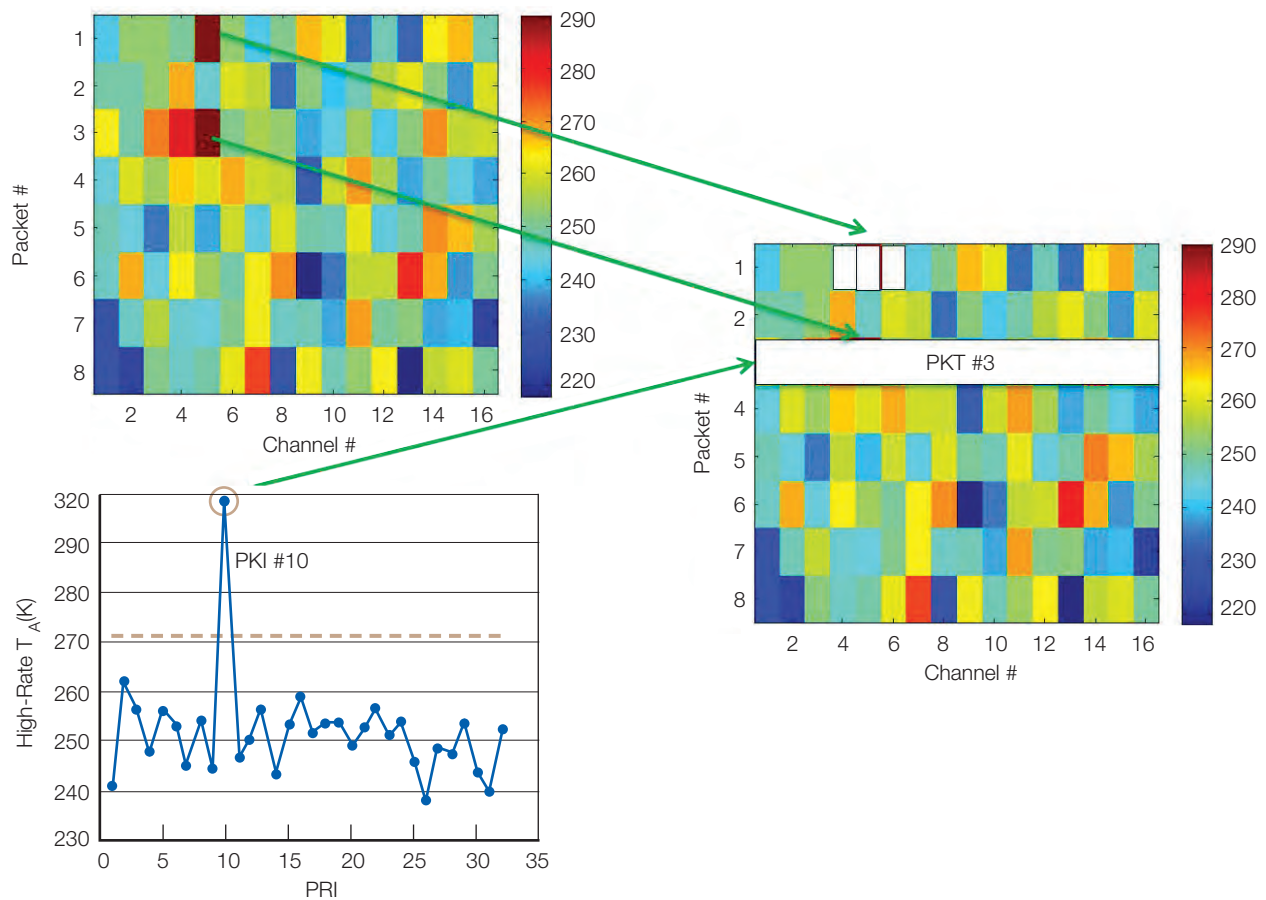
Figure 24. Example of the MPD operation. The bottom left plot shows the pulse-detection algorithm detecting RFI in the time domain and the corresponding time slice in the time-frequency data is flagged for removal, shown on the right plot. The cross-frequency algorithm detects RFI in the time-frequency data shown on the top left and that spectrogram element in addition to the elements of adjacent subbands are flagged for removal. All time-domain and frequency-domain detection methods similarly flag elements in the time-frequency data for removal. The remaining clean elements are then averaged to form a product.

input to the L1B processor. The L1A file provides the first four raw moments of the science telemetry needed for processing. In addition to the radiometer telemetry data, these processors will also require ancillary data to support geolocation and calibration. Processing radiometer data and locating them accurately on the Earth's surface will require precise data on the location of the spacecraft and the attitude of the spacecraft and of the spinning antenna. All of these data will be supplied in the form of standardized SPICE kernel files by the navigation element of the project in coordination with the Navigation and Ancillary Information Facility (NAIF) at JPL. SPICE files follow format standards used by many JPL planetary missions and include a software library to access and manipulate them. More detailed information about NAIF and SPICE is available at http://naif.jpl.nasa.gov. Some additional instrument parameters and processing parameters will be supplied to the processors in instrument parameter files read by each of the executable programs.

## E. L1B Product Description

The output L1B file in HDF format contains five main sections of data. The first is a metadata block, which contains information about the entire file. Metadata are divided into two groups: a general group present in all SMAP data products (including higher levels), and a product-specific group that contains more specialized fields appropriate to the corresponding product. The general fields include input and output file names, types, and versions, time ranges of the contained data, generating software names, versions, dates of modification, and producer description information. The product-specific group for L1B_TB includes bounding coordinates on the Earth for contained data, orbital parameters and times, output projection used, antenna rotation rate, product resolution, algorithm version, and thresholds applied during processing. Following the metadata is the spacecraft data group,

which records basic geometric fields once every revolution of the antenna. Included are the spacecraft position and attitude, and the nadir track position on the surface. Following the spacecraft data group is the high-resolution calibration data group, which consists of values for instrument component losses and noise temperatures for the vertical and horizontal polarizations for all 16 radiometer subbands used in the internal calibration part of the algorithm.

The next group is the calibration data group, which contains values for instrument component losses and noise temperatures for the vertical and horizontal polarizations for the radiometer fullband. The brightness temperature group contains the products that are required based on science objectives. It contains time-ordered footprint averaged brightness temperatures ($T_B$s) referenced to the Earth's surface with error sources removed. This group also includes geolocation information, antenna temperatures referenced to the feedhorn before and after radio frequency interference mitigation, error sources, quality flags, $T_B$ error, and noise-equivalent delta temperature (NEDT) along with relevant bit flags.

## F. Calibration

Calibration of the radiometer science data reported in the L1B_TB product requires measuring and characterizing the gain and noise contributions from every part of the radiometer system from the antenna radiation pattern all the way through to the radiometer back-end. Most of these elements will have nominal values determined pre-launch during system integration and testing. Ground processing will incorporate these nominal values through an instrument parameter file read by the L1B processor. These parameters provide an initial calibration. The radiometer is designed to meet stability requirements over a time span of 1 month in its gain and noise parameters that satisfy the measurement error budget. Long-term trends, biases, and systematic errors are corrected through the viewing of external calibration target areas that exhibit spatial uniformity and/or temporal stability.

Since a full end-to-end calibration of the SMAP radiometer including the reflector (effects of mesh emission and certain other reflector-related effects) can only be performed on orbit after the main reflector has been deployed, end-to-end $T_B$ calibration shall be performed on orbit using external calibration targets. Desirable external calibration targets should be beamfilling, spatially homogeneous, temporally stable, and have a $T_B$ value that is independently known via measurement or calculation to a useful level of uncertainty. SMAP is considering several natural targets for use in external calibration: Antarctica, Amazon rain forests, the ocean, and cold space.

Aquarius and SMOS are using Antarctica to verify the calibration stability of the radiometer. Measurements across East Antarctica show subkelvin temporal stability. SMAP's polar orbit will allow viewing of East Antarctica during ~6 orbits every day. Amazon rain forests have been useful for trending the Aquarius radiometer's calibration as well as the Aquarius scatterometer, although the temporal coverage is much less than for the Antarctic, and independently determining the Amazon forest $T_B$ is still a research area. SMAP has defined an area in the South Pacific that, based on oceanographic and climatological considerations, should serve as a good external calibration target and that is viewable ~2 times per day. Knowing the ocean $T_B$ accurately requires knowledge of the sea state over the viewed area, as well as sea surface temperature (SST) and sea surface salinity (SSS). The Aquarius forward simulator will be used to help with this calculation. (The globally averaged open ocean is also relatively stable, with a $T_B$ around ~100 K. The global ocean TB requires global coverage, which means it would be available every 7 days.) Together, the ocean, East Antarctica, and the Amazon will be complementary external calibration targets covering brightness temperatures from about 100 K to 300 K. For absolute $T_B$ calibration, the ocean and cold space (described next) remain the primary calibration targets since their $T_B$s can be determined through independent means with the smallest uncertainty. East Antarctica and the Amazon forest will be used initially as stability references.

Monthly cold space calibration (CSC) is part of the SMAP mission baseline. A pitch maneuver will allow the entire conical scan to view space. In contrast to the other three external target candidates, the expected $T_B$ of cold sky can be computed in an absolute sense from basic physical principles and L-band brightness temperature maps of cold sky. For calibration purposes, L-band maps of the radio sky from radio astronomers will be used to avoid "hot spots" and to calculate the $T_B$ seen when integrating over the SMAP radiometer solid angle. The back lobe contributions from the Earth will be computed using the antenna gain of back lobes and expected brightness temperatures of Earth. Other uses of CSC include: (a) drift detection, (b) scan bias detection because the brightness temperatures of cold space are known quite well, and (c) on-orbit characterization of nonlinearity together with the other three external calibration targets. SMOS was able to use CSC to detect and correct for drift that took 7 months to diminish as well as to use CSC for flat-field purposes. The SMAP L1B_TB simulator already incorporates the data and analysis tools to analyze the optimum locations over the Earth for the cold space viewing.

## G. Heritage and Data Continuity (Aquarius and SMOS)

As mentioned in Chapter 1, the SMAP mission was developed in response to the NRC's Earth Science Decadal Survey and has significant roots in the Hydros Earth System Science Pathfinder (ESSP) mission, which was initially selected as an alternate ESSP mission and subsequently cancelled in late 2005 prior to Phase A. One significant feature SMAP adopted from Hydros is the footprint oversampling used to mitigate RFI from terrestrial radars. The Aquarius/SAC-D project, a NASA ESSP ocean salinity mission launched in June 2011, also influenced the SMAP hardware and calibration algorithm. The radiometer front-end design is very similar to Aquarius; for example, the external correlated noise source (CNS) is nearly an exact copy of that from Aquarius. Features of the Aquarius calibration algorithm, such as calibration averaging and extraterrestrial radiation source corrections, are incorporated into the SMAP algorithm. Finally, the SMAP orbit simulator is a modification of the Aquarius simulator code.

SMAP's antenna is conical scanning with a full 360° field of regard. However, there are several key differences (some unique) from previous spaceborne conical scanning radiometers. Most obvious is the lack of external warm-load and cold-space reflectors, which normally provide radiometric calibration through the feedhorn. Rather, SMAP's internal calibration scheme is based on the Dicke-Switching design used by Aquarius/SAC-D and Jason Advanced Microwave Radiometer (AMR) pushbroom radiometers, and uses a reference load switch and a coupled noise diode. The antenna system is shared with the SMAP radar, which requires the use of a frequency diplexer in the feed network. Like the Naval Research Laboratory's WindSat instrument, SMAP measures all four Stokes parameters, although unlike WindSat, SMAP uses coherent detection in a digital radiometer back-subend. The first two modified Stokes parameters, TV and TH, are the primary science channels; the T3 and T4 channels are used to help detect RFI, which has recently proven quite valuable for the SMOS mission (Skou et al. 2010). The T3 channel measurement can also provide correction of Faraday rotation caused by the ionosphere. Overall, the most significant difference SMAP has from all past spaceborne radiometer programs is its aggressive hardware and algorithm approach to RFI mitigation.

## III. The SMAP Radar

### A. Radar Performance Requirements

The SMAP radar is required to meet the following performance requirements:

- Obtain measurements of surface backscatter cross-section for HH and VV polarizations (co-polarized measurements)

- Obtain measurements of surface backscatter cross-section at HV or VH polarizations (one cross-polarized measurement selectable by ground command)

- Obtain measurements of co- and cross-polarized surface backscatter cross-section consistent with a multi-look data product at 3-km resolution over 70% of the approximately 1000-km scanned instrument swath using synthetic aperture processing

- Achieve radiometric accuracy of 1 dB for co-polarized (HH and VV) measurements multi-looked/averaged to 3-km spatial resolution

- Achieve radiometric accuracy of 1.5 dB for cross-polarized (HV or VH) measurements multi-looked/averaged to 3 km

- Collect data that meet the above requirements over all land areas of science interest

- Collect data continually at a reduced, real-aperture resolution of 30 km continuously over the entire Earth (including oceans)

### B. Radar Technical Design

Figure 25 displays a simplified block diagram of the SMAP radar functions. As the antenna rotates, the SMAP radar emits H-polarized and V-polarized pulse pairs at a pulse-repetition frequency (PRF) of approximately 2850 Hz (Figure 26). The exact PRF varies slightly around the orbit to account for Earth's oblateness. Each pulse is 15 μs in length, and is modulated to a linear-FM chirp of 1-MHz bandwidth. The H-polarized and V-polarized signals are transmitted in succession with a separation of 9 μs using a single high-power transmitter, and routed respectively to the H-pol and V-pol ports of the antenna by a polarization selection switch. The H-polarized and V-polarized transmit signals are at two different frequencies, $f_H$ and $f_V$, separated by 3 MHz. This frequency separation allows the resultant echoes from each transmit polarization to be distinguished during their simultaneous reception (Figures 26 and 27). In essence, the SMAP radar can be thought of as two simultaneously operating dual-polarized systems: one measuring HH and VH polarization echoes, the other measuring VV and HV polarization echoes (where the convention of the notation used here is ordered first "receive polarization" then "transmit polarization").

Upon receive, the signals from the V- and H-polarized antenna ports are routed to two identical receivers. After downconversion and sampling, each receiver applies a set of three digital filters (Figure 27). In the H-channel receiver, there is a 1-MHz filter centered on fH to measure

the HH co-polarized backscatter, and a filter centered on $f_V$ to measure the $H_V$ cross-polarized backscatter. The situation is reversed in the V-channel receiver, where $f_V$ and $f_H$ measure the VV co-polarized backscatter and VH cross-polarized backscatter, respectively. The output samples from the co-polarized and cross-polarized filtering operations are telemetered to the ground for SAR processing. In both receivers, there is also a 1-MHz "noise-only" filter in between the transmit frequencies for the purpose of measuring the thermal noise background. Note that SMAP is a relatively narrow-band radar compared to other spaceborne SARs. This is consistent with the SMAP mission's moderate spatial resolution requirements. Following a standard technique utilized in radar scatterometry, a measurement of the receiver's thermal noise power is subtracted from the signal power in ground data processing. This is a necessary step to prevent biasing the backscatter measurement at low signal levels. All of the filters are designed with high out-of-band rejection to ensure suppression of RFI signals at frequencies outside the filter pass bands.



**Figure 25. Simplified block diagram of SMAP radar functions.**

To obtain the required 3-km resolution for the freeze/thaw and soil moisture products, the radar employs pulse compression in range as well as Doppler discrimination in azimuth to subdivide the antenna footprint. This is equivalent to the application of SAR techniques to the conically scanning radar case. Due to squint angle effects, the high-resolution products will be somewhat degraded within the 300-km region of the swath centered on the nadir track, with azimuth resolution capability decreasing over this region as the pixel location approaches the spacecraft sub-satellite track (Figure 28).

Radiometric calibration is accomplished by using a "loop-back" approach whereby some of the energy in the transmit pulse is coupled into the receiver to continuously track the transmit power–receiver gain product, which is used in the radar equation. Radiometric calibration "outside of the loopback" is accomplished by careful measurement of transmission losses (through cables, diplexer, rotary joint, etc.) over temperature pre-launch. A summary of the SMAP radar parameters is given in Table 8.

### C. RFI Detection and Mitigation

The L-band region of the electromagnetic spectrum is heavily used, and it is well known that Earth remote sensing at this frequency is subject to significant RFI. In order to meet radiometric accuracy requirements, the SMAP project has taken aggressive measures to both identify and mitigate the effects of RFI. Because SMAP is a global mapping mission with continuous, near-real-time generation of data products, any RFI mitigation techniques must lend themselves to reliable automation in ground processing software. The SMAP radar operates in a "shared" band between 1215 and 1300 MHz with other services such as long-range aircraft tracking systems and satellite global positioning systems. The most dominant sources of interference globally are ground-based radiolocation radars used for long-range surveillance and tracking of aircraft. This category of systems employs rotating or electrically scanning antennas with transmit powers anywhere from kilowatts to megawatts. These radiolocation systems operate over the entire 1215–1300 MHz remote sensing allocation, and conspicuously appear in all previously flown L-band radar missions (e.g., JERS, ALOS PALSAR, Aquarius, and the airborne NASA UAVSAR). In addition to these radiolocation systems, a variety of "other" services are observed less frequently, most notably near a few specific urban centers. These other emissions range from very low-power tonal signals to coded signals of unknown purpose. Finally, there are space-based systems, the largest of which are the global radio navigation satellites (GNSS) such as GPS. These systems are low power, but transmit a continuous broadband coded signal.
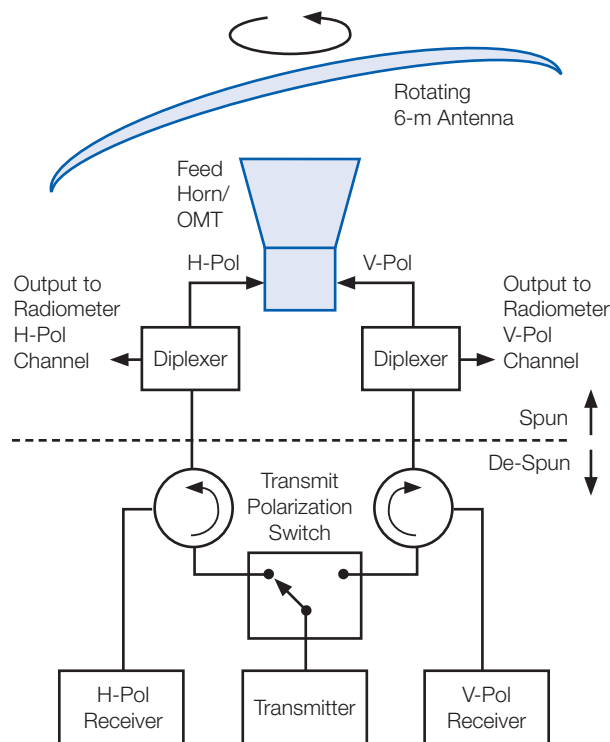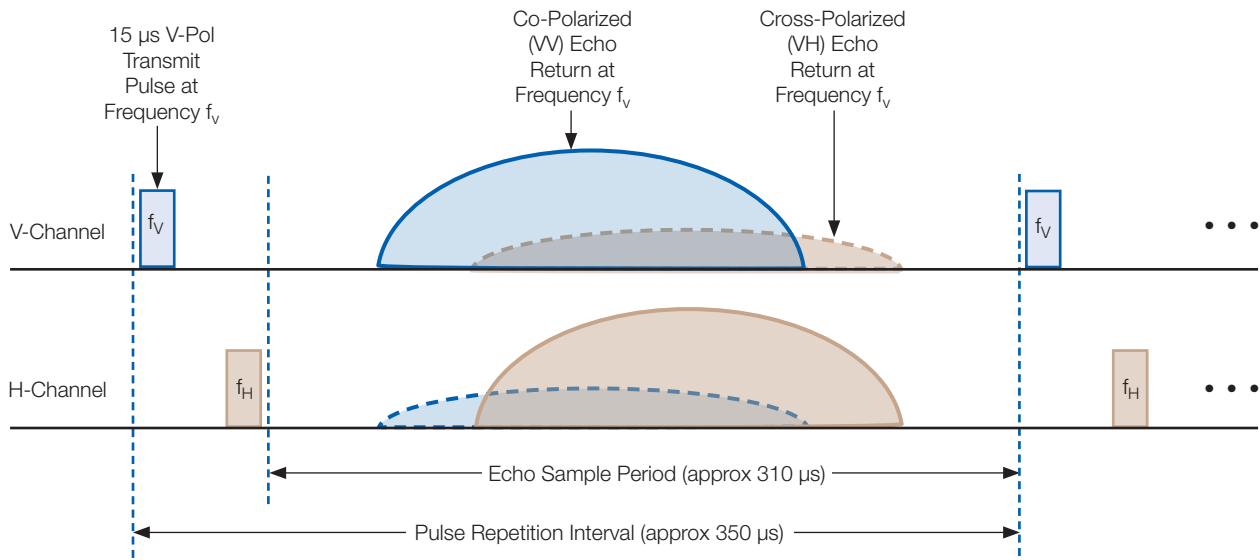
Figure 26. Time-domain illustration of the SMAP radar transmit, reception, and polarization scheme.
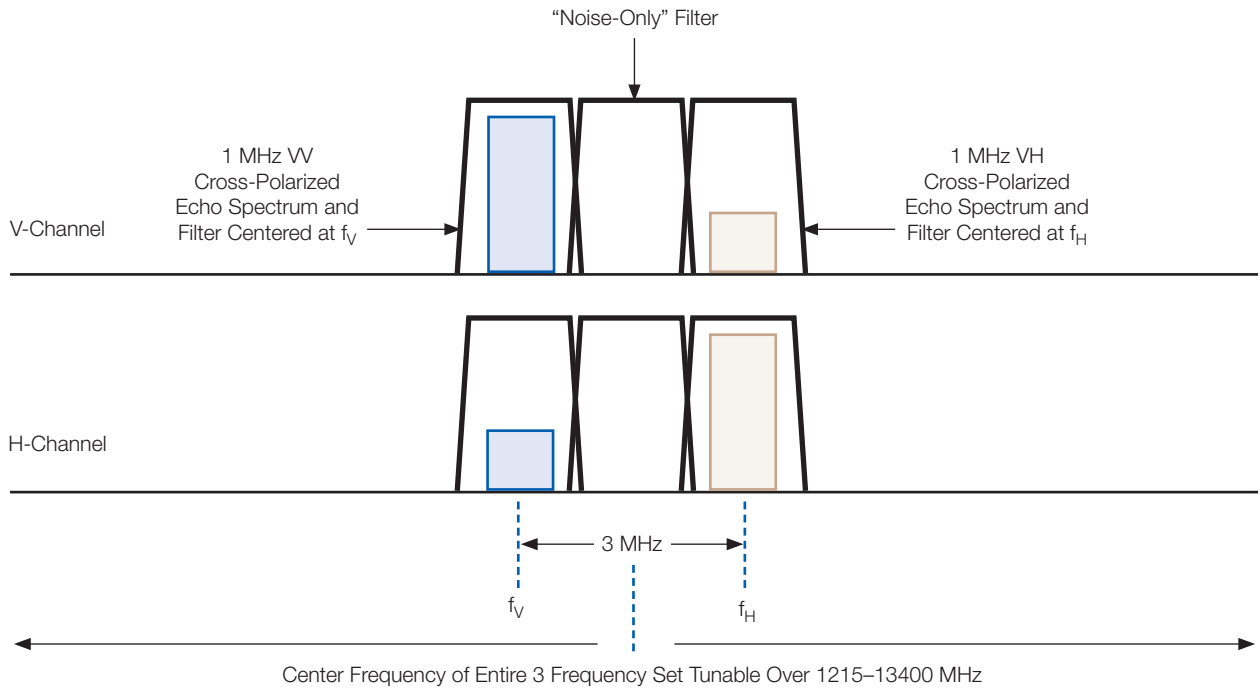
Figure 27. Frequency-domain representation of the SMAP receiver showing filtering and tuning.
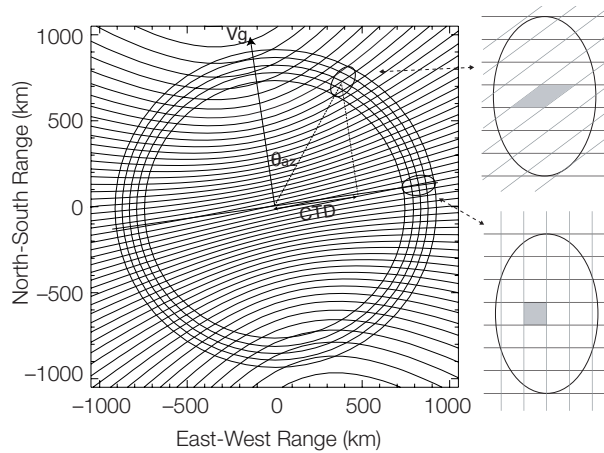
**Figure 28. Range-Doppler geometry of rotating radar antenna beam, showing azimuth resolution degradation in the upper right panel at high squint angles.**

For the SMAP radar, the most severe RFI issue will be from surface-based systems. In order to quantify this effect for the specifics of the SMAP design and to test mitigation algorithms, a simulation that consists of the many known emitters on the ground was constructed. This simulation of terrestrial RFI compares extremely well

with actual Aquarius data observed over North America, validating the model. Studies have shown that a slow-time thresholding (STT) approach is effective for detecting and excising terrestrial RFI (Belz et al. 2011; Chan and Spencer 2009; Spencer et al. 2013). This approach involves the excision of raw radar data samples whose power exceeds a threshold that is set relative to the median power over a sliding window in the slow-time or azimuth dimension for each range bin. Excised samples can be filled with statistically representative data in order to avoid an additional radiometric bias. RFI mitigation studies with SMAP parameters indicate that, under nominal assumptions, the overall measurement errors due to RFI will be within the budgeted allocation of 0.4 dB RMS. The errors due to RFI are expected to show great temporal and spatial variability; they will be undoubtedly quite large for some small fraction of measurements, and some geographical areas will likely be characterized by larger errors than others. However, the range of global variation seen in the Aquarius data suggest that even over challenging geographic areas, reasonable measurements will still be possible.

Interference from satellite-based GNSS sources is expected to be much lower than that from terrestrial sources. Whereas Earth-based sources can generate interference many decibels above the expected echo signal levels, satellite sources typically generate interference below the

**Table 8. Approximate SMAP radar parameters.**

**Antenna Key Parameters**

| | |
|---|---|
| Beamwidth (1-way, 3 dB) | 2.7° |
| Look Angle, Incidence Angle | 35.5°, 40.0° |
| Peak Gain | 36 dBi |
| Rotation Rate | 13.0 to 14.6 rpm |

**Radar Key Parameters**

| | |
|---|---|
| Transmit Carrier Frequencies | Tunable from 1217.25 MHz to 1275.75 MHz |
| Channels | HH, VV, HV (or VH) |
| PRF, Pulse Length | 2.9 kHz, 15 μsec |
| Azimuth Dwell Time | 42 ms |
| Transmit Bandwidth | 1 MHz |
| Peak Transmit Power | 500 W (at output of amplifier) |
| Single-Look Res (broadside) | 250 m x 400 m |
| Noise Equiv. $\sigma^o$ (broadside) | <–30 dB |

receiver noise-floor level. The low-level "hum" associated with this interference can be significant for low-echo signal levels, but is readily removed by the use of the noise-only value in the noise subtraction process. The noteworthy exception to this is when there is a strong specular reflection off of a very smooth surface. The percentage of measurements that will experience strong specular events above the noise floor, however, is much less than 2%. Such specular cases should have a readily recognizable "profile" in the noise-only measurement, and should be easy to flag in the radar data product.

If unexpected interference is encountered that is substantially different from the readily mitigated RFI, the SMAP radar still has the ability to selectively tune the receiver to avoid these sources. A key feature of the SMAP radar design is that the transmit frequencies, along with the associated filter center frequencies, can be tuned anywhere within the 1217.25 MHz to 1275.75 MHz remote-sensing allocation (Figure 28) in steps of 1.25 MHz. Tuning to the desired frequency is accomplished by using a look-up table that is dependent on geographic location. This tuning capability was implemented to allow frequency adjustments in response to persistent interferers operating at a specific location, or in response to new emitters that may appear over time. During the early post-launch period, an "RFI survey" will be conducted. During this survey, the SMAP transmitter will be disabled, the radar frequency will be continuously tuned up and down the 1215–1300 MHz allocation, and the SMAP receiver will simply listen to the RFI environment. Results from this survey will be analyzed to determine the best frequencies to use for the SMAP radar during the science acquisition phase of the mission.

## D. Radar Processing

The radar processing algorithms are described more completely in the L1 Radar ATBD. The L1 radar processing subsystem consists of six separate executable programs:

- L0a preprocessor — collects metadata from each downlink telemetry file

- L0b preprocessor — organizes the downlink telemetry files into half-orbit granules

- L1A processor — unpacks telemetry data and performs unit conversions

- Calibration Preprocessor — collects calibration data and updates calibration models

- L1B processor — Low-resolution radar processor

- L1C processor — High-resolution (SAR) processor

The L0a and L0b preprocessors prepare the incoming downlinked telemetry files by stitching and splitting them into half-orbit granules. Some overlap is included at the beginning and end to ensure that all data are included in the final L1B and L1C product files. The L1A processor unpacks the telemetry files, assembling radar records and decoding the raw telemetry data. Decoding includes all the necessary bit-level decoding and conversion of fields to floating-point values with standard SI units where needed.

Each record of the resulting L1A file contains data from one pulse-repetition interval (PRI) when the instrument is in high-resolution mode, and from one 48-PRI-long low-resolution interval when the instrument is operating in low-resolution mode. The block floating-point quantized (BFPQ) encoded high-resolution samples are left unchanged at this stage so that diagnostic tools can examine the raw data using the L1A file. The L1A file is stored in HDF format and will be submitted for archival storage along with the output data products. The L1A file becomes the primary input to the L1B (low-resolution, real-aperture) processor, the L1C (high-resolution, synthetic aperture) processor, the calibration preprocessor, and various diagnostic and support tools. The L1A file provides the echo samples measured by the radar along with the corresponding timing and frequency parameters needed for processing. In addition to the radar telemetry data, these processors will also require ancillary data to support geolocation and calibration. Processing radar data and locating them on the Earth's surface will require precise data on the location of the spacecraft, the attitude of the spacecraft and of the spinning antenna, and the topography of the Earth. All of these data will be supplied in the form of standardized SPICE kernel files by the navigation element of the project in coordination with the Navigation and Ancillary Information Facility (NAIF) at JPL. SPICE files follow format standards used by many JPL planetary missions and include a software library to access and manipulate them. More detailed information about NAIF and SPICE is available at http://naif.jpl.nasa.gov. Some additional instrument parameters and processing parameters will be supplied to the processors in algorithm parameter files read by each of the executable programs.

## E. L1B Product Description

The output L1B file in HDF format contains four main sections of data. The first is a metadata block that contains information about the entire file. Metadata are divided into two groups: a general group present in all SMAP data products (including higher levels), and a product-specific group that contains more specialized fields appropriate to the corresponding product. The general fields include input and output file names, types, and versions, time ranges of the contained data, generating software names,

versions, dates of modification, and producer description information. The product-specific group for L1B includes bounding coordinates on the Earth for contained data, orbital parameters and times, output projection used, antenna rotation rate, product resolution, algorithm version, the DEM used, and thresholds applied during processing. Following the metadata is the spacecraft data group, which records basic geometric fields once every revolution of the antenna. Included are the spacecraft position and attitude, and the nadir track position on the surface. Following the spacecraft data group is the sigma0 data group, which consists of vectors of data organized in time-order. The primary field is the radar normalized backscattering cross-section with one value per 48-PRI low-resolution interval. 1-D arrays with shapes of one value per low-resolution interval are called sigma0 arrays. Included are vectors of data providing:

- Geographic coordinates

- Equal-Area Scalable Earth–2 (EASE2) grid coordinates

- Topographic data for the beam center point

- Geometric look vector data (e.g., azimuth and incidence angles, range)

- Surface type flag

- Number of looks

- Data quality flags

- Normalized radar cross-section (NRCS) for all channels

- NRCS standard deviations for all channels

- Calibration factors used

- Signal-to-noise ratio (SNR)

- Spatial resolution

Because the vectors are organized in time-order, the spatial locations follow the scanning motion of the antenna and the orbital motion of the spacecraft. These measurements are real-aperture results that apply to the full beam footprint on the surface (about 40 km across). The EASE2 grid is a set of standard projections used by many Earth science missions. Following the sigma0 data group is another set of 2-D arrays called the sigma0 slice data group. These arrays divide the beam footprint into 9–14 range slices with sizes of about 6 km by 40 km. The same fields are present here as in the sigma0 data group, but with higher range resolution. The range binning is actually done by the instrument before downlink to reduce data volume. These 2-D arrays called sigma0 slice arrays will have a second dimension size determined by the L1B processor to accommodate the data take.

### F. L1C Product Description and Swath Grid

The output L1C product in HDF format is spatially organized (unlike the time-ordered L1B product) using a 2-D swath grid. A special coordinate system developed at JPL called SCH coordinates defines the swath grid used to project the output data. SCH coordinates are a spherical coordinate system that best approximates the WGS84 ellipsoid in the along-track direction. This coordinate system is readily referenced to conventional geodetic coordinates (latitude and longitude) and these coordinates are also supplied in the output swath format. Level 2 and higher SMAP products are also spatially organized, but they will use EASE2 grid projections instead of a swath-oriented projection. To aid in translating data between the radar swath grid and the EASE2 grids, the L1C product will include the index coordinates of the cylindrical and one of the polar EASE2 grids along with the WGS84 latitude and longitude for each swath grid point. The swath grid will have approximately 1 km posting; however, it should be noted that all performance requirements are specified for the corresponding 3-km grid obtained by averaging the 1-km grid. The L1C product uses the swath grid rather than one of the EASE2 grids because the swath grid is more space efficient (fewer empty array positions in a half-orbit), and suffers from much less distortion. Furthermore, many important performance characteristics of the radar data such as the number of looks, the effective resolution, and the random error are functions of cross-track position but not of along-track position. Using a swath grid makes validation of the data an easier task.

The L1C product contains three sections of data. The first is the same metadata present in the L1B file. The second is the spacecraft data group that contains time-ordered geometry data (spacecraft position, velocity, and attitude) at the times when the spacecraft nadir point crosses each swath row. The third is the sigma0 data group organized as 2-D swath grid arrays. The primary field again is the sigma0 field. The L1C SAR processing algorithms will geolocate sigma0 results with respect to the 3-D ellipsoidal surface of the Earth as defined by the WGS84 Earth model. These data are then projected onto the 2-D swath grid. The same basic data fields listed earlier for the L1B file are also present in L1C files, but they will be 2-D spatially organized arrays rather than 1-D time-ordered vectors.

## G. SAR Processing Algorithm

The L1C processor begins with the formation of the output swath grid tailored for the current data granule. A full-resolution grid with 250 m spacing is generated to accumulate the correlation contributions that each pulse makes to its illuminated grid points. The processor works through the input data in time order, computing the illuminated area for each pulse echo, and accumulating results in 2-D arrays over the swath grid. The basic processing flow follows the rectangular algorithm, which breaks the general 2-D correlation required for SAR processing into two successive 1-D matched filtering steps. First is range compression, which correlates the echo data with a replica of the transmitted FM chirp waveform. Second is azimuth compression, which correlates the range compressed data with the computed Doppler history for each grid point. Azimuth compression is implemented using time domain correlation with back projection. A time-domain approach is favored because it easily accommodates the varying squint angle around the conical scan. The scan is fast enough that the beam dwell time over any given grid point is relatively small (38 ms) compared to other SAR systems. This decreases the computational burden of a time domain algorithm. Nonetheless, latency requirements are a challenge since SMAP processing runs in real time. The three polarization channels and the fore and aft data are processed in parallel to reduce processing times. Contributions to each grid point are scaled with the effective area of a resolution cell at that point and the beam gain in the look direction. Noise subtraction and gain calibration using an internal loop back measurement are applied to produce calibrated sigma0 values for the output. The full-resolution grid is averaged to 1-km spacing and written into the output HDF product. The L1C processor also applies RFI filtering described earlier to each pulse echo, and a Faraday rotation correction based on externally supplied measurements of the ionosphere.

## H. Calibration

Calibration of the co-polarized and cross-polarized backscatter measurements reported in the L1C product requires measuring and characterizing the gain and noise contributions from every part of the radar system from the antenna radiation pattern all the way through the ground processing algorithms. Most of these elements will have nominal values determined pre-launch during system integration and testing. Ground processing will incorporate these nominal values through an algorithm parameter file read by the L1C processor. These parameters provide an initial calibration. The radar system is designed to meet stability requirements over a time span of about 1 month in its gain and noise parameters that satisfy the measurement error budget. Long-term trends, biases, and systematic errors are corrected through the use of external calibration target areas that exhibit spatial uniformity and temporal stability. Examination of backscatter data from other missions such as JERS-1, PALSAR-1, QuikSCAT, and Aquarius shows that suitable target areas fall into three broad geophysical categories: rain forests in the Amazon, Congo, and parts of Indonesia; ice sheets in Greenland and Antarctica; and a wind-corrected globally averaged ocean. The specific target areas for operational use will be selected during the post-launch SMAP cal/val period. The Amazon is particularly suitable because other missions like ALOS/PALSAR have used and future ALOS-2 PALSAR will use it as a calibration reference, so there will be larger amounts of high-resolution data available. The ocean is also a suitable target for SMAP because the low-resolution radar data cover it frequently, and a wind correction using externally supplied wind fields can be applied similar to the approach used by the Aquarius mission.

The stable external target areas provide a cross-calibration reference for the SMAP L1 radar backscatter, which will be used to set a global bias correction for the backscatter measurements. The bias correction will minimize the differences between the SMAP backscatter over these target areas and the measurements made by the ALOS/PALSAR mission. PALSAR is a high-resolution, fully polarimetric L-band SAR system that made extensive use of man-made calibration references such as corner reflectors and transponders to establish an absolute calibration level. The relatively lower resolution of the SMAP radar does not allow accurate calibration against corner reflectors because the effective areas of these targets are too small relative to the SMAP resolution cell. By cross-calibrating with PALSAR, SMAP can indirectly make use of the PALSAR corner reflector based absolute calibration.

The radar system is designed to meet short-term stability requirements that add up to a relative calibration error of 0.35 dB. Here, "short term" means about 30 days, which is the time scale that pre-launch testing can test and verify. The radar error budget includes an additional 0.2 dB of relative error due to long term variations in system gain. Long-term variations are expected due to component aging effects, seasonal temperature variation, and imperfections in the short-term temperature calibration models. Detecting and correcting long-term variations is performed using external targets with good long-term stability. The best candidate identified so far is the globally averaged wind-corrected ocean. Aquarius ocean data have shown backscatter stability around 0.1 dB over a 2-year time span. Selected areas of the Amazon rain forest are another candidate. These have shown long-term stability of 0.2 dB if data are separated between dry and rainy seasons.

The choice of external target to use for long-term detrending will be made during the SMAP post-launch cal/val period. Pre-launch studies are performed using PALSAR and Aquarius data to provide initial target areas. During the L1 cal/val period, measurements from different target types will be compared for consistency and one will be chosen. A mixture of two target types may also be used for the final SMAP calibration.

## References

Belz, J. E. et al., "A Study of Radio Frequency Interference in the Space-to-Earth Exploration Allocation at L-Band," *Proceedings of the IEEE Aerospace Conference*, Big Sky, MT, 2011.

Chan, S. and M. Spencer, "RFI Study for the SMAP Radar," *Proceedings of the IEEE Radar Conference*, Pasadena, CA, May, 2009.

Guner, B. and J. T. Johnson, "Performance study of a cross-frequency detection algorithm for pulsed sinusoidal RFI in microwave radiometry," *IEEE Trans. Geosc. Rem. Sens.*, vol. 48, pp. 2899–2908, 2010.

Guner, B., N. Niamsuwan, and J. T. Johnson, "Time and frequency blanking for RFI mitigation in microwave radiometry," *IEEE Trans. Geosc. Rem. Sens.*, vol. 45, pp. 3672–3679, 2007.

Johnson, J. T. and L. C. Potter, "A study of detection algorithms for pulsed sinusoidal interference in microwave radiometry," *IEEE Trans. Geosc. Rem. Sens.*, vol. 47, pp. 628–636, 2009.

Kristensen, S., J. E. Balling, N. Skou, and S. S. Søbjœrg, "RFI in SMOS data detected by polarimetry," in Proc. *IEEE Int. Geosci. Remote Sensing Symp. (IGARSS)*, Munich, 2012.

Lagerloef, G., F. R. Colomb, D. Le Vine, et al., "The Aquarius/SAC-D Mission: Designed to Meet the Salinity Remote-Sensing Challenge," *Oceanography*, vol. 21, no. 1, pages 68–81, March 2008.

Mecklenburg, S., M. Drusch, Y. H. Kerr, et al., "ESA's Soil Moisture and Ocean Salinity Mission: Mission Performance and Operations," *IEEE Trans. Geosci. Rem. Sens.*, vol. 50, no. 5, part 1, pp. 1354–1366, May 2012.

Misra, S. and C. S. Ruf, "Detection of radio frequency interference for the Aquarius radiometer," *IEEE Trans. Geosc. Rem. Sens.*, vol. 46, pp. 3123–3128, 2008.

Niamsuwan, N., J. T. Johnson, and S. W. Ellingson, "Examination of a simple pulse blanking technique for RFI mitigation," *Radio Science*, vol. 40, June 2005.

Piepmeier, J. R., J. T. Johnson, P. N. Mohammed, D. Bradley, C. Ruf, M. Aksoy, R. Garcia, D. Hudson, L. Miles, and M. Wong, "Radio-Frequency Interference (RFI) Mitigation for the Soil Moisture Active Passive (SMAP) Microwave Radiometer," *IEEE Trans. Geosc. Rem. Sens.*, vol. 56, no. 1, part 2, pp. 761–775, January 2014.

Piepmeier, J. R. and F. Pellerano, "Mitigation of Terrestrial Radar Interference in L-Band Spaceborne Microwave Radiometers," *Proc. IEEE Int. Geosci. Remote Sensing Symp. (IGARSS)*, Denver, CO, pp. 2292–2296, July 30–August 4, 2006.

Ruf, C. S., D. Chen, D. LeVine, P. deMatthaeis, and J. R. Piepmeier, "Aquarius radiometer RFI detection, mitigation, and impact assessment," *Proc. IEEE Int. Geosci. Remote Sensing Symp. (IGARSS)*, Munich, Germany, July, 2012.

Ruf, C. S., S. M. Gross, and S. Misra, "RFI Detection and Mitigation for Microwave Radiometry with an Agile Digital Detector," *IEEE Trans. Geosc. Rem. Sens.*, vol. 44, no. 3, 694-706, March 2006.

Skou, N. et al., J. E. Balling, S. S. Søbjœrg, and S. S. Kristensen, "Surveys and analysis of RFI in the SMOS context," *Proc. 2010 IEEE International Geoscience and Remote Sensing Symposium*, Honolulu, HI, July 2010.

Spencer, M., C. Chen, H. Ghaemi, S. Chan, and J. Belz, "RFI Characterization and Mitigation for the SMAP Radar," *IEEE Trans. Geosci. Remote Sens.*, vol. 51, no. 10, pp. 4973–4982, October 2013.

# 4. Soil Moisture Data Products

## I. Passive, Active-Passive, and Active Products Overview

The SMAP Project produces three soil moisture products (see Chapter 2, Table 4). These products at Level 2 are titled L2_SM_P, L2_SM_A, and L2_SM_AP. They are half-orbit retrievals of soil moisture (SM) posted on nested fixed Earth grids of different spacing (36, 3, and 9 km, respectively). In the equivalent Level 3 products, individual half-orbit granules acquired over 24 hours are composited to produce daily multi-orbit global maps of retrieved soil moisture. Each of these soil moisture products has different attributes and uses the SMAP instrument data in different ways. The SMAP instrument package will deploy an L-band SAR and an L-band radiometer for concurrent coincident measurements. The L2_SM_P product is principally based on the passive (P) radiometer measurements and hence its resolution and other data attributes are related to the radiometer brightness temperature characteristics. The L2_SM_A product uses the SMAP radar backscatter cross-sections and hence its data attributes and resolution are compatible with the active (A) instrument measurements. The active-passive (AP) soil moisture product combines the radar and radiometer measurements and hence its resolution is intermediate between the two. Besides their characteristic spatial gridding (36 km for the passive, 3 km for the active, and 9 km for the active-passive), the three soil moisture products will have other varying attributes owing to which instrument data are the primary input to their retrieval algorithms. These attributes additionally include accuracy because of the differences in the sensitivity of active and passive measurements to soil moisture. Factors such as vegetation water content and canopy density as well as surface roughness affect data from the two SMAP instruments to varying degrees. Also, differences in retrieval algorithms affect the products. A good understanding of these considerations is critical to the selection of the most appropriate soil moisture product by SMAP users. In this chapter these three soil moisture products are described in detail, and the material presented should provide a valuable guide to their eventual use in diverse science and applications research.

At L-band, the observed radiometric brightness temperature represents emission determined mainly by the physical temperature and dielectric constant of the observed scene (related to soil moisture in the top ~5 cm). The sensitivity to soil moisture decreases significantly for surfaces with vegetation water content (VWC) above ~5 kg m$^{-2}$. The SMAP radiometer instrument is designed to provide measurements of brightness temperature with better than 1.3 K uncertainty (1-sigma). Given that the brightness temperature difference across the dynamic range of surface soil moisture can be many tens of K (up to ~70 K and higher), the L-band radiometer is a highly sensitive indicator of surface soil moisture content. As a result, based on multiple airborne and other field campaigns over the last two decades, passive microwave soil moisture retrieval algorithms have evolved to be reasonably robust and reliable. However, spaceborne radiometer measurements, including those by SMAP, suffer from coarse spatial resolution. The SMAP real-aperture antenna, with a 6 m-diameter lightweight deployable mesh reflector, can yield ~40-km resolution (3 dB) measurements at the elevation of the SMAP low-Earth orbit. Because of this, SMAP brightness temperature measurements and derived products are posted on a 36-km fixed Earth grid. The SMAP L2_SM_P is a soil moisture product based on brightness temperature measurements that are sensitive to soil moisture. Given the extensive heritage of L-band passive microwave soil moisture retrieval algorithms, this product is expected to be reliable and robust (better than 0.04 cm$^3$ cm$^{-3}$ (1-sigma) accuracy) with about 40 km resolution, which is compatible with hydroclimatological applications.

Using the same antenna system but with synthetic aperture radar (SAR) processing, the SMAP L-band radar provides backscatter cross-section measurements at much higher spatial resolution (~1 to 3 km over the outer 70% of the swath; measurements approach 3 to 30 km resolution in the 30% area along the nadir flight track directly beneath the satellite). The high-resolution advantage of SAR is diminished for soil moisture sensing by the higher sensitivity of SAR to surface roughness and scattering by vegetation. Owing to these latter factors, SAR-based algorithms used for soil moisture retrieval have relatively more uncertainty. It is anticipated that the L2_SM_A will have a lower accuracy (up to 0.06 cm$^3$ cm$^{-3}$) over regions with VWC below ~3 kg m$^{-2}$. Thus, the L2_SM_A soil moisture product has the advantage of increased spatial resolution but with less accuracy for regions with higher vegetation cover. Depending on the specific application and requirements for the levels of discrimination of soil moisture in its dynamic range, certain users may prefer to have soil moisture information at higher resolution and will accept the higher error and reduced sensitivity that may be present with the radar-only-based soil moisture products.

Concurrent SMAP SAR and radiometer measurements and their respective advantages can be effectively combined to derive soil moisture estimates with intermediate accuracy and at intermediate resolution (~9 km) that meet the SMAP project requirements (see next section). The SMAP L2_SM_AP soil moisture product uses the coarse resolution but sensitive (to soil moisture) passive radiometer measurements and the high resolution but relatively less sensitive active radar measurements to produce an intermediate resolution soil moisture product. The algorithm for this product uses the SAR backscatter cross-section measurements to disaggregate the radiometer brightness temperatures. The spatially higher

resolution disaggregated brightness temperatures and the instrument radiometer brightness temperature fields are compatible in that their field averages are identical. The brightness temperature retrieval algorithm used for L2_SM_P (with ancillary information of the right type and at the right scale [9 km]) is then utilized to retrieve intermediate-resolution soil moisture fields based on the disaggregated brightness temperature fields. The L2_SM_AP accuracy is equal to or better than 0.04 cm$^3$ cm$^{-3}$ (1-sigma) for regions with VWC below ~5 kg m$^{-2}$. This soil moisture data product is unique to SMAP and is possible given that the SMAP radar and radiometer share the same antenna and data acquisition strategy. The resolution scale of this soil moisture product is 9 km, which is compatible with hydrometeorological applications.

## II. Requirements and Validation Metrics

The SMAP Level 1 Requirements and Mission Success Criteria document specifies the SMAP baseline requirement for soil moisture as estimates of soil moisture in the top 5 cm of soil with an error of no greater than 0.04 cm$^3$ cm$^{-3}$ volumetric (1-sigma). This accuracy must be met at 10 km spatial resolution and with 3-day average intervals over the global land area (see Chapter 2 for more detail). The SMAP soil moisture data products suite must include a product that meets these requirements, which must be demonstrated within the cal/val (calibration/validation) phase of the project (the first 12 months of science data acquisition). The soil moisture accuracy requirement applies over global coverage but excludes regions of snow and ice, frozen ground, mountainous topography, open water, urban areas, and vegetation with water content greater than 5 kg m$^{-2}$. The SMAP Project has a Calibration/Validation (Cal/Val) Plan (Chapter 7) that is designed to demonstrate that SMAP baseline products meet the requirements over sites with diverse climate and land cover.

The "1-sigma" specification on the accuracy requirement is a quadratic performance statistical metric. The root mean square error (RMSE) is such a statistical measure and it is the one adopted by the SMAP Project. Entekhabi et al. (2010) provide a detailed definition of this metric and relate it to time series correlation, bias, and other metrics that are often used to assess the accuracy of geophysical retrievals from satellite measurements with respect to true fields. Each of these metrics has advantages and disadvantages. Entekhabi et al. (2010) explore the relationship between RMSE and correlation metrics in the presence of biases in the mean as well as in the amplitude of fluctuations (standard deviation) between estimated and true fields. They also introduce an approach for converting a requirement in an application product into a corresponding requirement for soil moisture accuracy.

Even with the specification that RMSE is to be used to measure accuracy, there are still many important consid-

erations in evaluating this statistic. The most challenging issue with the validation is the representativeness of the in situ validation measurements. The validation measurements themselves can only provide an estimate of the true surface soil moisture. There may be bias and amplitude errors in the estimates because of in situ sensor errors, but also, and perhaps more importantly, due to undersampling of the true field mean soil moisture based on a finite number of point samples. The heterogeneity in soil moisture fields, due to spatial variations in soil texture, in topography, in land cover, and in other factors, commonly results in undersampling of the true field. Hence, statistical errors are also a characteristic of the estimates to be considered ground truth. This is the problem of "upscaling," which is defined further in Chapter 7. Validation of satellite retrievals with ground truth will include the upscaling error. If the errors in upscaling are considered independent of the retrieval algorithm errors, the RMSE of retrievals (with truth as reference) will additively include the upscaling error (RMSE of estimate ground truth with truth as reference).

Beyond upscaling, the RMSE has several other subtle issues that affect its use. If the true surface volumetric soil moisture (at a given scale) is defined as $\theta_{true}$ (actually the upscaling estimate of the truth) and the corresponding estimated retrieval is $\theta_{est}$, then the root mean square error (RMSE) metric is simply

$$RMSE = \sqrt{E\left[\left(\theta_{est} - \theta_{true}\right)^2\right]} \qquad (1)$$

where $E[.]$ is the expectation or linear averaging operator. This metric quadratically penalizes deviations of the estimate with respect to the true soil moisture (in units of volumetric soil moisture) and is a compact and easily understood measure of estimation accuracy. This metric, however, is severely compromised if there are biases in either the mean or the amplitude of fluctuations in the retrieval. If it can be estimated reliably, the mean bias

$$b = E\left[\theta_{est}\right] - E\left[\theta_{true}\right]$$

can easily be removed by defining the unbiased RMSE

$$ubRMSE = \sqrt{E\left[\left(\left(\theta_{est} - E\left[\theta_{est}\right]\right) - \left(\theta_{true} - E\left[\theta_{true}\right]\right)\right)^2\right]} \qquad (2)$$

that characterizes random errors.

The RMSE and the unbiased RMSE are related through

$$RMSE^2 = ubRMSE^2 + b^2 \qquad (3)$$

which implies $RMSE \geq |b|$ and underscores the shortcomings of the $RMSE$ metric in the presence of mean bias. The bias in soil moisture may vary with season.

The validation of SMAP soil moisture products will report the unbiased *ubRMSE* and bias *b* separately for more complete diagnoses of the accuracy of the soil moisture products.

A final issue to consider is related to where and over what period the accuracy RMSE is applied. A validation site may be composed of one or more grid cells in the data product grid. The SMAP cal/val activity is based on a number of sites distributed across the globe covering representative climates and land covers. At each site the RMSE statistics may be estimated. The accuracy requirement implies that for the $N_i$ validation sites (within the global land area excluding regions of snow and ice, frozen ground, mountainous topography, open water, urban areas, and vegetation with water content greater than 5 kg m$^{-2}$) for which validating in situ observations are available from verified sites, the SMAP surface (0–5 cm) soil moisture products must satisfy

$$\frac{1}{N_i} \sum_{i=1}^{N_i} \left[ ubRMSE(i) \right] \leq 0.04 \ \left[ \text{cm}^3 \ \text{cm}^{-3} \right] \qquad (4)$$

that is, the mean of the anomaly RMSE of the SMAP product *(ubRMSE)* across all $N_i$ validation areas must be less than 0.04 cm$^3$ cm$^{-3}$. For the purposes of assessing the accuracy of SMAP baseline products in meeting mission L1 requirements, the SMAP Science Definition Team has decided that data will be binned over 6-month time-domain periods globally within the SMAP mask to capture seasonal extremes.

## II. Radiometer-Only Soil Moisture Retrievals (L2/3_SM_P)

### A. Overview

This section covers the two coarse spatial resolution soil moisture products which are based on the SMAP radiometer brightness temperatures: L2_SM_P, which is derived surface soil moisture in half-orbit format at 40-km resolution output on a fixed 36-km Equal-Area Scalable Earth–2 (EASE2) grid, and L3_SM_P, which is a daily global composite of the L2_SM_P surface soil moisture, also at 40-km resolution output on a fixed 36-km EASE2 grid. Utilizing one or more of the soil moisture retrieval algorithms to be discussed later in the chapter, SMAP brightness temperatures are converted into an estimate of the 0–5 cm surface soil moisture in units of cm$^3$/cm$^3$.

As mentioned earlier in this Handbook, the SMAP science objectives are based in part on the requirements of the hydrometeorology, hydroclimatology, and carbon flux communities. To resolve hydrometeorological water and energy flux processes and extend weather and flood

forecast skill, a spatial resolution of 10 km and temporal resolution of 3 days are required. To resolve hydroclimatological water and energy flux processes and extend climate and drought forecast skill, a spatial resolution of 40 km and temporal resolution of 3 days are required. The SMAP L2/3_SM_P products will meet the needs of the hydroclimatology community. Although generated at a coarser 40-km spatial resolution, the L2/3_SM_P radiometer-based data products should still satisfy the 0.04 cm$^3$/cm$^3$ volumetric soil moisture retrieval accuracy specified in the mission Level 1 requirements. Additional details can be found in the SMAP Level 2 & 3 Soil Moisture (Passive) Algorithm Theoretical Basis Document (O'Neill et al. 2012).

### B. Science Basis for Baseline Algorithm

The microwave portion of the electromagnetic spectrum (wavelengths from a few centimeters to a meter) has long held the most promise for estimating surface soil moisture remotely. Passive microwave sensors measure the natural thermal emission emanating from the soil surface. The intensity of this radiation depends on the dielectric properties and temperature of the target medium, which for the near surface soil layer is a function of the amount of moisture present. Low microwave frequencies (at L-band or ~1 GHz) offer additional advantages: (1) the atmosphere is almost completely transparent, providing all-weather sensing; (2) transmission of signals from the underlying soil is possible through sparse and moderate vegetation layers (up to at least 5 kg/m$^2$ of vegetation water content); and (3) measurement is independent of solar illumination which allows for day and night observations.

At microwave frequencies, the intensity of the observed emission is proportional to the product of the temperature and emissivity of the surface (Rayleigh-Jeans approximation). This product is commonly called the brightness temperature ($T_B$). If the microwave sensor is in orbit above the Earth, the observed $T_B$ is a combination of the emitted energy from the soil as attenuated by any overlying vegetation, the emission from the vegetation, the downwelling atmospheric emission and cosmic background emission as reflected by the surface and attenuated by the vegetation, and the upwelling atmospheric emission (Figure 29).

At L-band frequencies, the atmosphere is essentially transparent, with the atmospheric transmissivity $\tau_{atm} \approx 1$. The cosmic radiation at the radio astronomy band ($T_{sky}$) is on the order of 2.7 K. The atmospheric emission is also small, about 2.5 K. These small atmospheric contributions will be accounted for in the L1B_TB ATBD, since the primary inputs to the radiometer-derived soil moisture retrieval process described in this chapter are atmospherically corrected surface brightness temperatures.
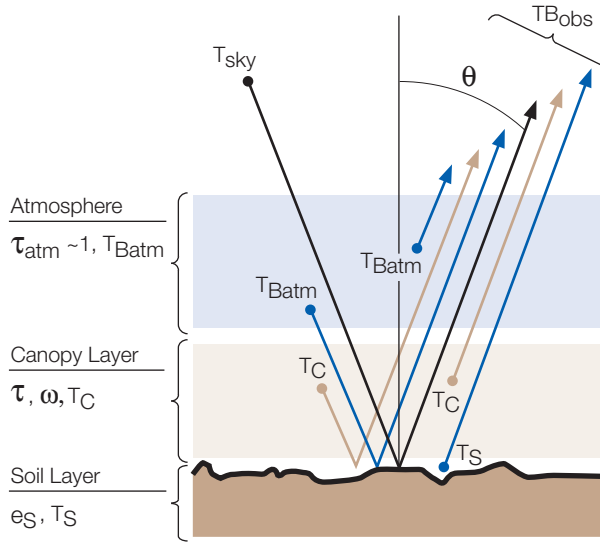
**Figure 29. Contributions to the observed brightness temperature $T_B$ from orbit. From SMOS ATBD (Kerr et al. 2006).**

Retrieval of soil moisture from SMAP surface $T_B$ observations is based on a well-known approximation to the radiative transfer equation, commonly known in the passive microwave soil moisture community as the tau-omega model. A layer of vegetation over a soil attenuates the emission of the soil and adds to the total radiative flux with its own emission. Assuming that scattering within the vegetation is negligible at L-band frequencies, the vegetation may be treated mainly as an absorbing layer. A model following this approach to describe the brightness temperature of a weakly scattering layer above a semi-infinite medium was developed by Basharinov and Shutko (1975) and described in Ulaby et al. (1982). The equation includes emission components from the soil and the overlying vegetation canopy (Jackson and Schmugge 1991):

$$T_{Bp} = T_s e_p exp(-\tau_p sec\theta) + T_c(1-\omega_p)$$
$$[1-exp((-\tau_p sec\theta)][1+r_p exp(-\tau_p sec\theta)] \quad (5)$$

where the subscript $p$ refers to polarization (V or H), $T_s$ is the soil effective temperature, $T_c$ is the vegetation temperature, $\tau_p$ is the nadir vegetation opacity, $\omega_p$ is the vegetation single scattering albedo, and $r_p$ is the rough soil reflectivity. The reflectivity is related to the emissivity ($e_p$) by $e_p = (1 - r_p)$, and $\omega_p$, $r_p$, and $e_p$ are values at the SMAP look angle of $\theta = 40°$. The transmissivity $\gamma$ of the overlying canopy layer is $\gamma = exp(-\tau_p sec \theta)$. Equation (5) assumes that vegetation multiple scattering and reflection at the vegetation–air interface are negligible. The surface roughness effect is modeled as $r_p = r_{p\,smooth} exp (-h cos^2 \theta)$ where the parameter $h$ is assumed linearly related to the root mean square surface height (Choudhury et al. 1979; Wang 1983). Nadir vegetation opacity is related to the total columnar vegetation water content (VWC, in

kg/m2) by $\tau_p = b_p$*VWC with the coefficient $b_p$ dependent on vegetation type and microwave frequency (and probably polarization) (Jackson and Schmugge 1991).

If the air, vegetation, and near-surface soil are in thermal equilibrium, as is approximately the case near 6:00 AM local time (the time of the SMAP descending pass), then $T_c$ is approximately equal to $T_s$ and the two temperatures can be replaced by a single effective temperature ($T_{eff}$). Soil moisture can then be estimated from $r_{p\,smooth}$ using the Fresnel and dielectric-soil moisture relationships.

The smooth surface reflectivity $r_{p\,smooth}$ is defined by the Fresnel equations, which describe the reflection of an electromagnetic wave by a smooth dielectric boundary. At horizontal polarization, the electric field of the wave is oriented parallel to the reflecting surface and perpendicular to the direction of propagation. At vertical polarization, the electric field of the wave is on the incidence angle plane, which is spanned by two vectors corresponding to the surface normal and the direction of wave propagation. In the Fresnel equations below, $\theta$ is the SMAP incidence angle of $40°$ and $\varepsilon$ is the complex dielectric constant of the soil layer:

$$r_H(\theta) = \left| \frac{cos\theta - \sqrt{\varepsilon - sin^2 \theta}}{cos\theta + \sqrt{\varepsilon - sin^2 \theta}} \right|^2 \quad (6)$$

$$r_V(\theta) = \left| \frac{\varepsilon cos\theta - \sqrt{\varepsilon - sin^2 \theta}}{\varepsilon cos\theta + \sqrt{\varepsilon - sin^2 \theta}} \right|^2 \quad (7)$$

In terms of dielectric properties, there is a large contrast between liquid water (real part of dielectric $\varepsilon_r \sim 80$) and dry soil ($\varepsilon_r \sim 5$). As soil moisture increases, the soil dielectric constant increases. This leads to an increase in soil reflectivity or a decrease in soil emissivity ($1 - r_p$). Note that low dielectric constant is not uniquely associated with dry soil. Frozen soil, independent of water content, has a similar dielectric constant to dry soil. Thus, a freeze/thaw flag is needed to resolve this ambiguity. As $T_B$ is proportional to emissivity for a given surface soil temperature, $T_B$ decreases in response to an increase in soil moisture. It is this relationship between soil moisture and soil dielectric constant (and hence microwave emissivity and brightness temperature) that forms the physical basis of passive remote sensing of soil moisture. Given SMAP observations of $T_B$ and information on $T_{eff}$, $h$, $\tau_p$, and $\omega_p$ from ancillary sources (section VI) and using single-channel or multichannel algorithm approaches (later in this chapter), Eq. (5) can be solved for the soil reflectivity $r_p$, and Eq. (6) or (7) can be solved for the soil dielectric $\varepsilon$. Soil moisture can then be estimated using one of several dielectric models and ancillary knowledge of soil texture. SMAP production software will include the option of using the dielectric models of Mironov et al. 2009, Dobson et al. 1985, or Wang and Schmugge 1980.

## C. Rationale for the Use of L-Band 6 AM Data

Within the microwave portion of the electromagnetic spectrum, emission from soil at L-band frequencies can penetrate through greater amounts of vegetation than at higher frequencies. Figure 30 shows microwave transmissivity as a function of increasing biomass at L-band (1.4 GHz), C-band (6 GHz), and X-band (10 GHz) frequencies, based upon modeling. The results show that L-band frequencies have a significant advantage over the C- and X-band frequencies (and higher) provided by current satellite instruments such as AMSR-E and WindSat, and help explain why both SMOS and SMAP are utilizing L-band sensors in estimating soil moisture globally over the widest possible vegetation conditions. Another advantage of measuring soil moisture at L-band is that the microwave emission originates from deeper in the soil (typically 5 cm or so), whereas C- and X-band emissions originate mainly from the top 1 cm or less of the soil (Figure 31).
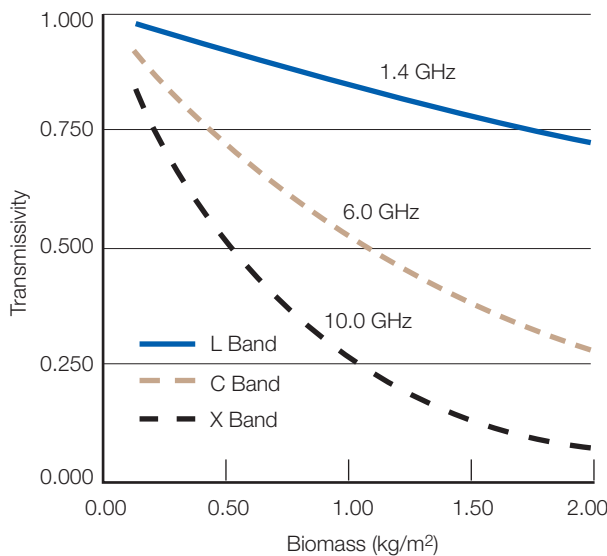


Figure 30. Vegetation transmissivity to soil emission at L-band frequencies (1.4 GHz) is much higher than at C- (6 GHz) or X-band (10 GHz) frequencies. (Adapted from Ulaby et al. 1996.)

Although the above arguments support the use of low frequencies, there is, however, a lower frequency limit for optimal $T_B$ measurements for soil moisture. The microwave observations made by a satellite radiometer will be affected by ionospheric Faraday rotation effect and emission. Faraday rotation is a phenomenon in which the polarization vector of an electromagnetic wave rotates as the wave propagates through the ionospheric plasma in the presence of the Earth's static magnetic field. The phenomenon is a concern to SMAP because the polarization rotation increases as the square of wavelength. At frequencies lower than L-band, the ionospheric

Faraday rotation will become more significant. Thus, L-band frequency is an optimal choice for orbiting satellite radiometers with balanced vegetation and ionospheric effects. Within the L-band, radiometric measurements could be significantly degraded by man-made and galactic noise. Since there is a protected band at L-band at 1.400–1.427 GHz that is allocated exclusively for radio astronomy use, the SMAP radiometer operates in this band.
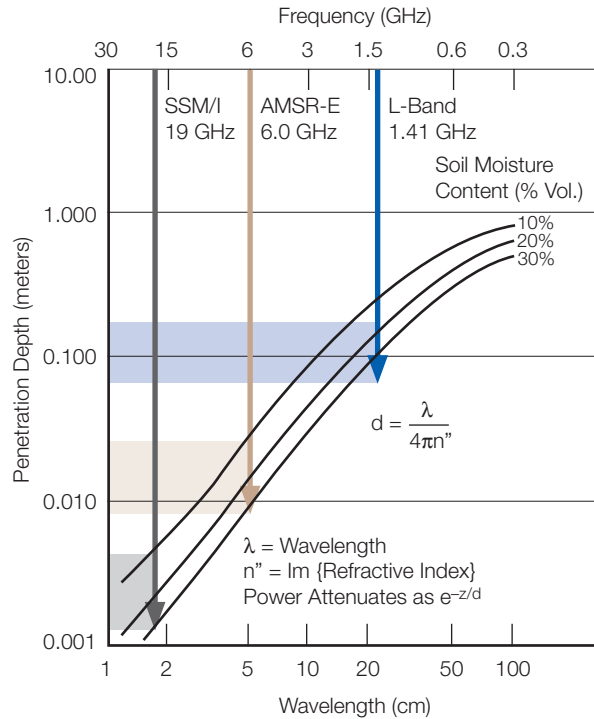


Figure 31. L-band TB observations are sensitive to emission from deeper in the soil than at higher frequencies (adapted from Njoku and Kong 1977). Soil moisture curves are given for 10, 20, and 30% (or in absolute units, 0.10, 0.20, 0.30 cm³/cm³).

The decision to place SMAP into a sun-synchronous 6:00 AM / 6:00 PM orbit is based on a number of science issues relevant to the L2_SM_P product (Fagerlund et al. 1970; Jackson and Kimball 2009). Faraday rotation depends on the total electron content (TEC) in the ionosphere. If the Faraday rotation is uncorrected, the SMAP polarized (H and V) radiometer measurements will contain errors that translate to soil moisture error. The TEC (or Faraday rotation) varies greatly during the day, reaching a maximum during the afternoon and a minimum in the pre-dawn hours. By using $T_B$ observations acquired near 6:00 AM local solar time as the primary input to the L2_SM_P product, the adverse impacts of Faraday rotation are minimized. Faraday rotation correction to SMAP $T_B$ is described in the L1B_TB ATBD.

At 6:00 AM, the vertical profiles of soil temperature and soil dielectric properties are likely to be more uniform (Basharinov and Shutko 1975) than at other times of the day (Figure 32). This early morning condition will minimize the difference between canopy and soil temperatures and thermal differences between land cover types within a pix-

el (Figure 33). These factors help to minimize soil moisture retrieval errors originating from the use of a single effective temperature to represent the near surface soil and canopy temperatures. This same effective temperature can be used as the open-water temperature in the water-body correction to $T_B$ that will be discussed in section VI.
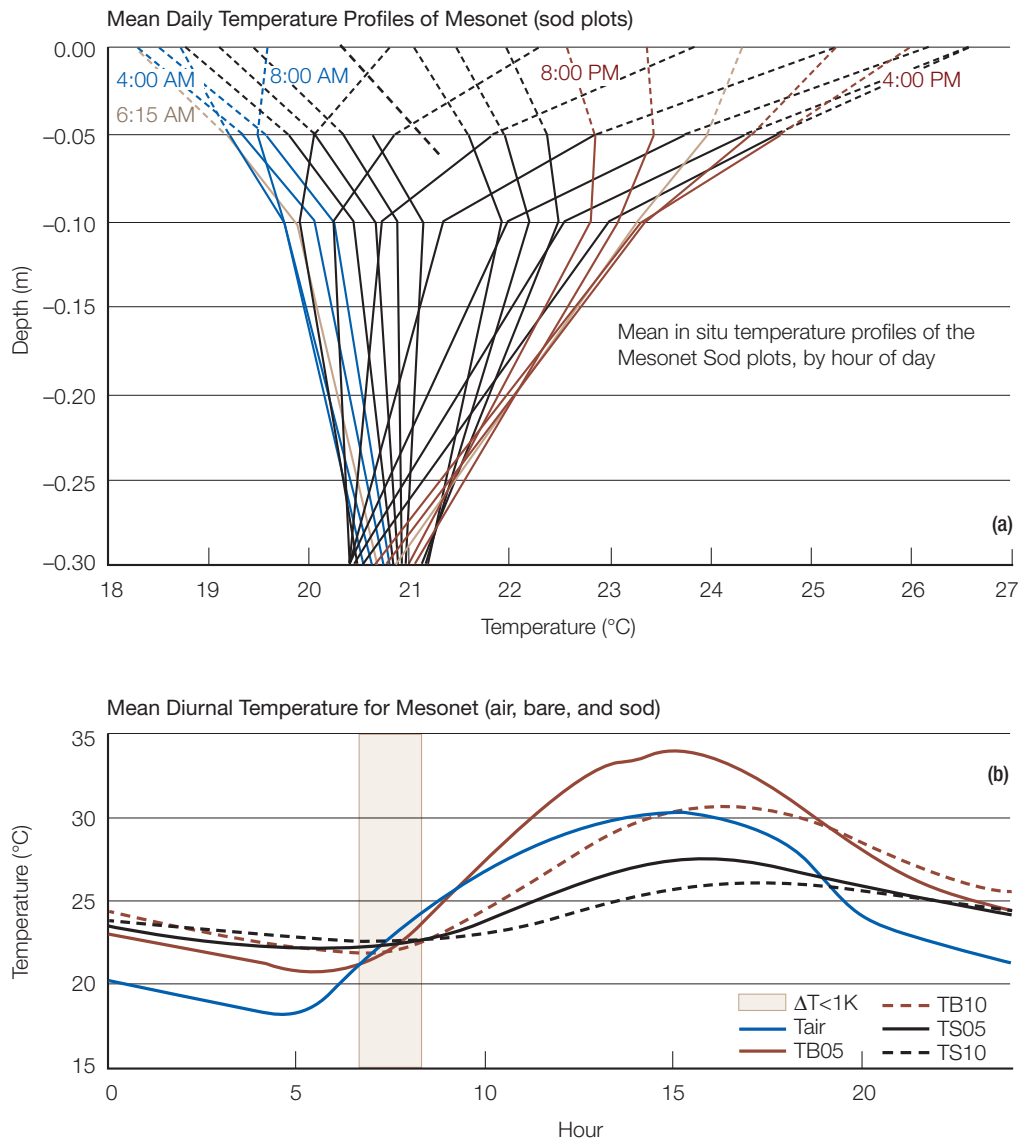


Figure 32. Soil temperature as a function of time based on June 2004 Oklahoma Mesonet data: (a) vertical profiles for a sod-covered site and (b) the mean soil temperatures for bare soil (TB05 at 5 cm below the surface, TB10 at 10 cm below the surface), and sod (TS05, TS10). The shaded region identifies the period of the day when these effects result in less than 1 °C difference among the four temperatures (T. Holmes, personal communication).
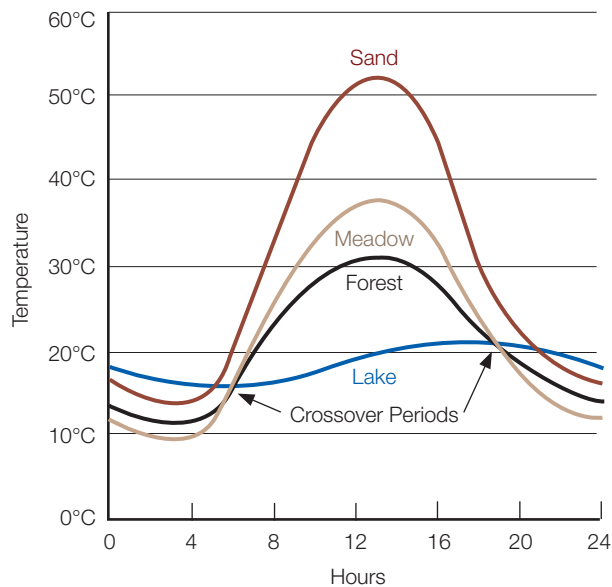
Figure 33. Schematic showing diurnal variation in temperature and thermal crossover times at approximately 6:00 AM / 6:00 PM local time for various broad classes of land surface covers. (Modified from Fagerlund et al. 1970.)

As will be discussed in the next section, the current approach to generation of the baseline L2_SM_P product will be restricted to input data from the 6:00 AM descending passes because of the thermal equilibrium assumption and near-uniform thermal conditions of surface soil layers and overlying vegetation in the early morning hours. Accurate soil moisture retrievals using data from 6:00 PM ascending passes may require use of a land surface model and will be generated as part of the L4_SM product (see ATBD for L4_SM).

## D. Soil Moisture Retrieval Process

From a broad perspective, there are five steps involved in extracting soil moisture using passive microwave remote sensing. These steps are normalizing brightness temperature to emissivity, removing the effects of vegetation, accounting for the effects of soil surface roughness, relating the emissivity measurement to soil dielectric properties, and finally relating the dielectric properties to soil moisture. Decades of research by the passive microwave soil moisture community have resulted in a number of viable soil moisture retrieval algorithms that can be used with SMAP $T_B$ data. ESA's SMOS mission currently flies an aperture synthesis L-band radiometer which produces $T_B$ data at multiple incidence angles over the same ground location. The baseline SMOS retrieval algorithm is based on the tau-omega model described earlier, but utilizes the SMOS multiple incidence angle capability to retrieve soil moisture. SMAP retrievals will also be based on the tau-omega

model, but will use the constant incidence angle $T_B$ data produced by the SMAP conically-scanning radiometer. Other needed parameters in the retrieval will be obtained as ancillary data.

For the SMAP L2_SM_P product, four soil moisture retrieval algorithms are currently being evaluated:

- Single-channel algorithm at H polarization (baseline) (SCA-H)

- Single-channel algorithm at V polarization (SCA-V)

- Dual-channel algorithm (DCA)

- Microwave Polarization Ratio Algorithm (MPRA)

Figure 34 illustrates the conceptual process used in retrieving soil moisture from SMAP radiometer brightness temperature measurements. The process begins with the ingestion and merging of the fore- and aft-look gridded brightness temperature data from the SMAP L1C_TB product. It then identifies grid cells where the $T_B$ quality and surface conditions (brown diamonds in the figure) are considered favorable for soil moisture retrieval and sets the retrieval quality flag accordingly. The observed $T_B$s are then corrected for the presence of standing water prior to being converted into soil moisture estimates by the baseline retrieval algorithm.

In order for soil moisture to be retrieved accurately, a variety of global static and dynamic ancillary data are required (section VI). Static ancillary data do not change during the mission, while dynamic ancillary data require periodic updates in time frames ranging from seasonally to daily. Static data include parameters such as permanent masks (land/water/forest/urban/mountain), the grid cell average elevation and slope derived from a DEM, permanent open water fraction, and soils information (primarily sand and clay fraction). The dynamic ancillary data include land cover, surface roughness, precipitation, vegetation parameters, and effective soil temperatures. Measurements from the SMAP radar will be the primary source of information on open water fraction and frozen ground, supplemented by water information from a MODIS-derived surface water data base and temperature information from the GMAO model used in L4_SM. Ancillary data will also be employed to set flags which help to determine either specific aspects of the processing or the quality of the retrievals. All input data to the L2_SM_P process are pre-mapped to the 36-km EASE2 grid.

The SMAP L2_SM_P product contains two 16-bit integer data flags that enable users to examine (a) the surface conditions of a grid cell and (b) the quality of soil moisture estimate when retrieval is attempted.
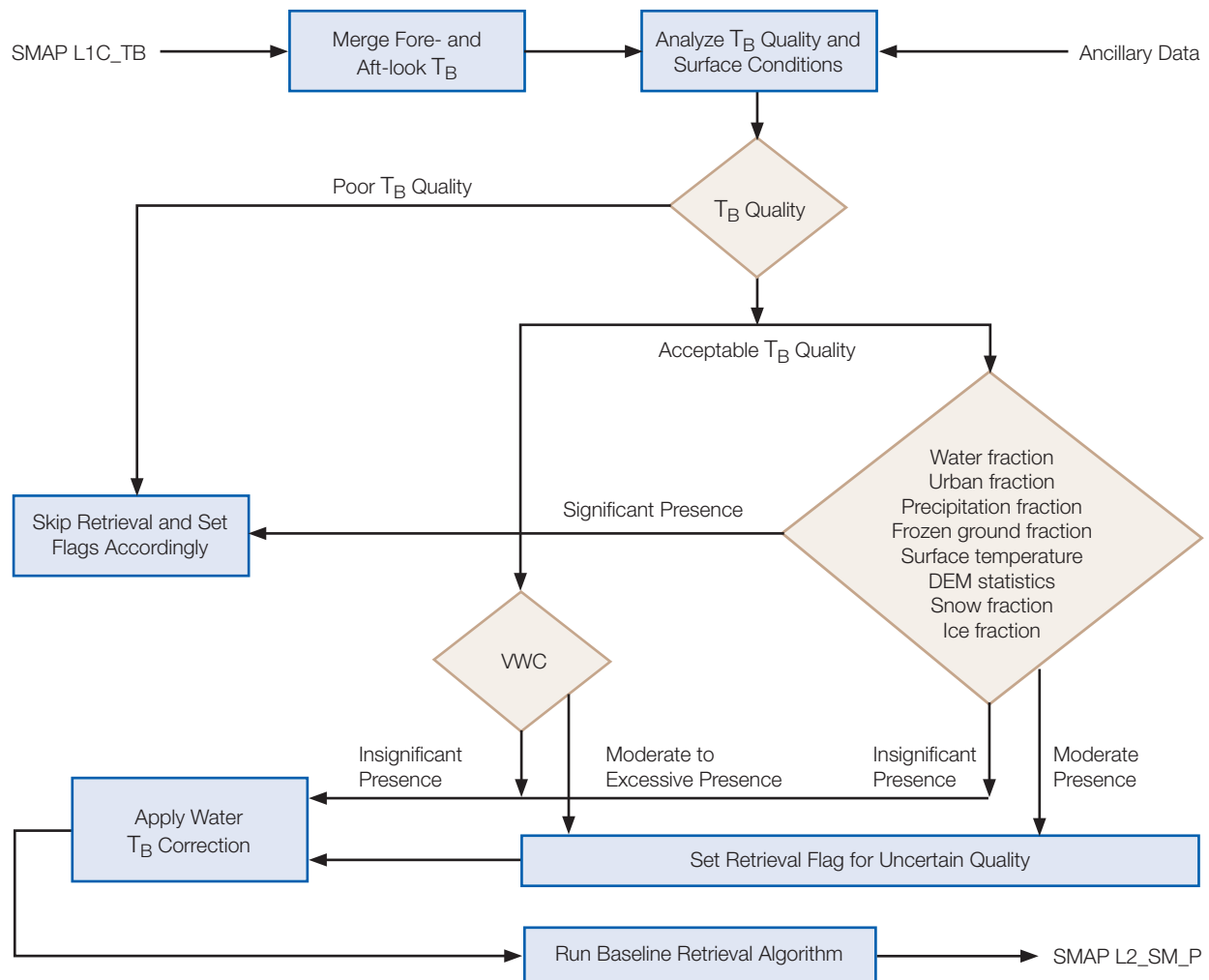
**Figure 34. A simplified schematic of the processing flow used to produce the L2_SM_P products.**

**a. surface_flag:** The surface_flag field is a 16-bit integer field whose binary representation consists of bits that indicate the presence or absence of certain surface conditions at a grid cell. Each surface condition is numerically compared against two non-negative thresholds: T1 and T2, where T1 < T2. When a surface condition is found to be below T1, retrieval is attempted and flagged for recommended quality. Between T1 and T2, retrieval is still attempted but flagged for uncertain quality. Above T2, retrieval is skipped. The definitions of surface conditions and their thresholds are included in the algorithm ATBD and data product guides that are accessible along with the data products at the DAACs. The updated documents will include changes to the flag definitions and to their thresholds.

**b. retrieval_qual_flag:** The retrieval_qual_flag field is a 16-bit integer field whose binary representation consists of bits that indicate whether retrieval is performed or not at a given grid cell. When retrieval is performed, it contains additional bits to further indicate the exit status and quality of the retrieval. A summary of bit definition of the retrieval_qual_flag field is listed in Table 9.

At the 40-km footprint resolution scale of the SMAP radiometer, a significant percentage of footprints within the SMAP land mask will contain some amount of open fresh water due to the presence of lakes, rivers, wetlands, and transient flooding. It is assumed that all ocean pixels will be masked out using the SMAP ocean/land mask. For soil moisture retrieval purposes, the presence of open water within the radiometer footprint (IFOV) is undesirable

Table 9. Retrieval_qual_flag bit information.

| Bit | Retrieval Information | Bit Value and Interpretation |
|-----|----------------------|------------------------------|
| 0 | Recommended Quality | 0: Retrieval has recommended quality |
| | | 1: Retrieval does not have recommended quality |
| 1 | Retrieval Attempted | 0: Retrieval was attempted |
| | | 1: Retrieval was skipped |
| 2 | Retrieval Successful | 0: Retrieval was successful |
| | | 1: Retrieval was not successful |
| 3–15 | Undefined | 0 (not used in L2_SM_P) |

since it dramatically lowers the brightness temperature and results in anomalously high retrieved soil moisture for that grid cell if soil moisture is retrieved without knowledge of the presence of open water. This results in a bias that degrades the overall soil moisture retrieval accuracy. It is therefore important to correct the SMAP Level 1 $T_B$ observations for the presence of water, to the extent feasible, prior to using them as inputs to the L2_SM_P soil moisture retrieval. Fortunately, this bias can be corrected, especially when it occurs at dawn near inland water/land boundaries where the temperature of water can be reasonably approximated as the temperature of land (as shown in Figure 33).

The procedure to correct for water $T_B$ is quite simple. Given a mixture of land and water within the antenna IFOV, the observed $T_B$ is an areal weighted sum of the $T_B$ contributions from the water and from the land:

$$T_B^{IFOV} = \alpha T_B^{water} + (1-\alpha)T_B^{land} \tag{8}$$

where $\alpha$ denotes the areal fraction of water within the antenna IFOV, and $T_B^{water}$ denotes the $T_B$ emission from water computed from a theoretical model (for example, the Klein-Swift model) (Klein and Swift 1977) with an estimated physical temperature obtained from ancillary sources. At the 6 AM SMAP overpass time, the temperature of the water is approximately the same as the temperature of the surface soil layer, so the same ancillary temperature data can be used for both. Once $\alpha$ and $T_B^{water}$ are known, $T_B^{land}$ can be solved for and then used to retrieve soil moisture in the non-open water part of the IFOV.

### E. Baseline Algorithm

In the single-channel algorithm (SCA) (Jackson 1993), horizontally polarized (H-pol) $T_B$ data are traditionally used due to their sensitivity to soil moisture, but the same algorithm can also be applied to V polarization $T_B$. The use of H-pol $T_B$ with the SCA is the current SMAP baseline algorithm. In this approach, brightness temperatures are converted to emissivity using a surrogate for the physical

temperature of the emitting layer. The derived emissivity is corrected for vegetation and surface roughness to obtain the soil reflectivity. The Fresnel equation is then used to determine the dielectric constant. Finally, a dielectric mixing model is used to obtain the soil moisture. Additional details on these steps follow.

At the L-band frequency used by SMAP, the brightness temperature of the land surface is proportional to its emissivity ($e$) multiplied by its physical temperature ($T$). It is typically assumed that the temperatures of the soil and the vegetation are the same, especially at the SMAP overpass time of 6 AM. The microwave emissivity at the top of the soil surface or vegetation canopy is given by (the polarization subscript $p$ is suppressed in the following equations):

$$e = \frac{T_B}{T} \tag{9}$$

If the physical temperature is estimated independently, emissivity can be determined. SMAP will use GMAO modeled temperatures to represent the temperature of the near surface soil layer (see "SMAP Ancillary Data Report: Surface Temperature," JPL D-53064). The emissivity retrieved above is that of the soil as modified by any overlying vegetation and surface roughness. In the presence of vegetation, the observed emissivity is a composite of the soil and vegetation. To retrieve soil water content, it is necessary to isolate the soil surface emissivity ($e^{surf}$). Following Jackson and Schmugge (1991), the emissivity can be represented by:

$$e = [1-\omega][1-\gamma][1+(1-e^{surf})\gamma] + e^{surf}\gamma \tag{10}$$

Both the single scattering albedo ($\omega$) and the one-way transmissivity of the canopy ($\gamma$) are dependent upon the vegetation structure, polarization, and frequency. The transmissivity is a function of the optical depth ($\tau$) of the vegetation canopy where $\gamma = \exp(-\tau \sec\theta)$. At L-band, the single scattering albedo tends to be very small, and sometimes is assumed to be zero in order to reduce dimensionality for computational purposes. For SMAP,

the capability for a nonzero $\omega$ will be retained. Substituting $\gamma$ into Eq. 10 and rearranging yields

$$e^{surf} = \frac{e-1+\gamma^2+\omega-\omega\gamma^2}{\gamma^2+\omega\gamma-\omega\gamma^2} \qquad (11)$$

The vegetation optical depth is dependent upon the vegetation water content (VWC). In studies reported in Jackson and Schmugge (1991), it was found that the following functional relationship between the optical depth and vegetation water content could be applied:

$$\tau = b*VWC \qquad (12)$$

where $b$ is a proportionality value that depends on both the vegetation structure and the microwave frequency. Since $b$ is related to the structure of the overlying vegetation, it is likely that $b$ will also vary with microwave polarization. The variation of the $b$ parameter with polarization is currently being studied by the SMAP team — it is expected that analysis of SMOS data and other field data will resolve whether a polarization dependence is needed to improve soil moisture retrieval accuracy.

For SMAP implementation of the SCA, values of $b$ and $\omega$ will be provided by means of a land cover look-up table that is currently under review (a very preliminary version of this table can be found in the L2_SM_P ATBD, which will be updated prior to launch). The baseline approach to estimating vegetation water content utilizes a set of land cover–based equations to estimate the combined foliage and stem VWC from values of the Normalized Difference Vegetation Index (NDVI) (an index derived from visible-near infrared reflectance data from the EOS MODIS instruments now and the NPP/JPSS VIIRS instrument in the SMAP time frame) (see additional details and Eq. 18 in O'Neill et al. 2012). A 10-year MODIS-based NDVI vegetation climatology has been used in pre-launch studies for vegetation correction which results in robust and stable soil moisture retrievals. This climatology will be updated to cover 14 years (through 2013) by the time of the SMAP launch. Methods are currently under evaluation to tie this long-term climatology to real-year NDVI conditions for more accurate retrievals under anomalous conditions.

The emissivity that results from the vegetation correction is that of the soil surface, including any effects of surface roughness. These roughness effects must be removed in order to determine the smooth surface soil emissivity ($e^{soil}$) which is required for the Fresnel equation inversion. One approach to removing this effect is a model described in Choudhury et al. (1979) that yields the bare smooth soil emissivity:

$$e^{soil} = 1 - [1 - e^{surf}]\,\exp[h\cos^2\theta] \qquad (13)$$

Some studies drop the $\cos^2\theta$ term or change it to $\cos\theta$ to avoid overcorrecting for roughness. The parameter $h$ is dependent on the polarization, frequency, and geometric properties of the soil surface and is related to the surface height standard deviation $s$. $h$ values for different land cover types will be included in the look-up table used in SMAP retrievals (O'Neill et al. 2012).

Emissivity is related to the dielectric properties ($\varepsilon$) of the soil and the viewing or incidence angle ($\theta$). For ease of computational inversion, it can be assumed that the real component ($\varepsilon_r$) of the dielectric constant provides a good approximation of the complex dielectric constant; however, the more complex formulation can also utilized, and both approaches produce very similar results. The Fresnel equations link the dielectric constant to emissivity — for horizontal (H) polarization (Eq. 6 rewritten for emissivity):

$$e_H(\theta) = 1 - \left|\frac{\cos\theta - \sqrt{\varepsilon_r - \sin^2\theta}}{\cos\theta + \sqrt{\varepsilon_r - \sin^2\theta}}\right|^2 \qquad (14)$$

and for vertical (V) polarization (Eq. 7 rewritten for emissivity):

$$e_V(\theta) = 1 - \left|\frac{\varepsilon_r\cos\theta - \sqrt{\varepsilon_r - \sin^2\theta}}{\varepsilon_r\cos\theta + \sqrt{\varepsilon_r - \sin^2\theta}}\right|^2 \qquad (15)$$

The dielectric constant of soil is a composite of the values of its components — air, soil, and water, which have greatly different values. In the final step of the soil moisture retrieval process, one of three dielectric mixing models is used to relate the estimated dielectric constant to the amount of soil moisture (Mironov et al. 2009; Dobson et al. 1985; and Wang and Schmugge 1980). The SMAP algorithm team is currently evaluating the relative merits of these dielectric models and their impact on overall soil moisture retrieval accuracy. The SMAP processing software will retain coding for all three dielectric model options.

In terms of soil moisture retrieval performance, the Hydros OSSE (Crow et al. 2005) revealed that the SCA could produce biased retrievals based on linear VWC correction aggregated from high-resolution vegetation data. However, two relatively simple approaches were developed to create an effective VWC using nonlinear aggregation that helps to reduce the bias and overall RMSE in retrieved soil moisture (O'Neill et al. 2006; Zhan et al. 2008). Figure 35 demonstrates the effectiveness of these nonlinear vegetation aggregation methods in improving the accuracy of retrieved soil moisture, especially in areas with heavier vegetation.

### F. Alternate Algorithms

The **Dual-Channel Algorithm** (DCA) is an extension of the SCA described in the previous section — it uses both H-polarized and V-polarized $T_B$ observations to simultaneously retrieve soil moisture and VWC (Njoku and Li 1999).

The inversion mechanism of the DCA starts with feeding the tau-omega model (Eq. 5) with initial guesses of soil moisture and VWC. The quantities are then adjusted iteratively until the difference between the computed and observed $T_B$ observations is minimized in a least square sense. Similar to the SCA, estimates of model parameters (e.g., surface temperature, surface roughness, and vegetation single scattering albedo) must be provided using ancillary datasets in the inversion process. The DCA has been used with reasonable success in a number of cases, including the 2007 CLASIC field campaign conducted in Oklahoma, USA (Yueh et al. 2008).

The ability of the DCA to simultaneously estimate two geophysical parameters may come with a penalty. While the additional channel allows for estimation of VWC, it also brings in additional $T_B$ errors (uncorrelated between V and H channels) that may adversely affect retrieval accuracy. Also, an assumption implicit in this algorithm is that the optical depth is identical for both polarizations, which is not likely to be true for structured vegetation. Exactly which effect outweighs the other is under investigation.

The **Microwave Polarization Ratio Algorithm** (MPRA) is based on the Land Parameter Retrieval Model (LPRM)

(Owe et al. 2001). The LPRM is an index-based retrieval model that uses dual polarization channels at a single low microwave frequency (typically C- or X-band) to derive soil moisture and vegetation optical depth. As implemented on multifrequency satellites such as AMSR-E, it also uses the Ka-band V-polarized channel to retrieve physical temperature of the surface. Only a few studies (de Jeu et al. 2009) have examined the applicability of this model at L-band frequencies, although analysis of SMOS data with LPRM is currently underway [R. de Jeu, personal communication, 2011]. Because there are no Ka-band V-polarized $T_B$ observations available from the SMAP instruments, surface temperature will be obtained using ancillary datasets as with the other L2_SM_P algorithms.

In the MPRA, the radiative transfer model operates on two assumptions: (1) the soil and canopy temperatures are considered equal (T), and (2) the vegetation transmissivity ($\gamma$) and the single-scattering albedo ($\omega$) are the same for both H and V polarizations. If $e_s$ is the soil emissivity, the $T_B$ can be expressed by the tau-omega model (Equation 5) with $T_C = T_S = T$:

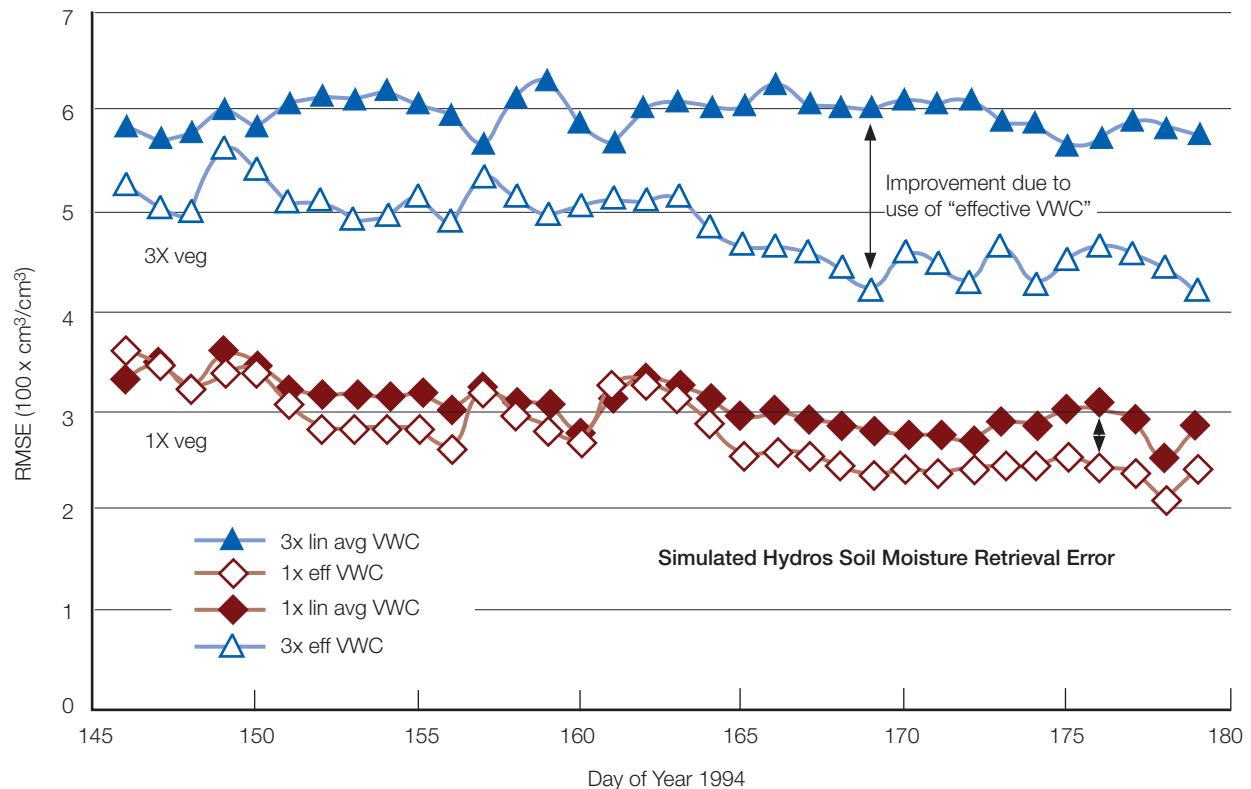$$T_B = e_S\gamma T + (1-\omega)(1-\gamma)T + \gamma(1-e_S)(1-\omega)(1-\gamma)T \qquad (16)$$



Figure 35. Improvement in simulated Hydros soil moisture retrieval error using a simple effective VWC correction with the SCA algorithm for existing vegetation (1X) and for artificially increased simulated vegetation amounts (3X) (O'Neill et al. 2006).

The single scattering albedo ω represents the loss of energy in the canopy and is assumed by MPRA to be constant globally (such as ω = 0.05), in contrast to the other L2_SM_P algorithms where a nonzero ω is assumed to be a function of land cover type and is input as an ancillary parameter.

The Microwave Polarization Difference Index (MPDI) and the observed emissivity ($e_H$ and $e_V$) are used in MPRA to derive the vegetation optical depth (Meesters et al. 2005), which is used to calculate the transmissivity (γ). The MPDI and vegetation optical depth are calculated as follows:

$$MPDI = \frac{T_{BV} - T_{BH}}{T_{BV} + T_{BH}} \tag{17}$$

$$\tau = \cos\theta \ \ln \left[ ad + \sqrt{(ad)^2 + a + 1} \right] \tag{18}$$

where $a = 0.5 * [(e_V - e_H) / MPDI - e_V - e_H]$ and $d = 0.5 * \omega / (1 - \omega)$.

With this set of equations, soil moisture is retrieved in an optimization routine that minimizes the error between the modeled and observed H-polarized brightness temperatures. The vegetation optical depth at this optimized soil moisture value is an additional retrieval result.

## G. Algorithm Performance

One measure of algorithm performance is determining the accuracy of the retrieved soil moisture in a root square sense. Different algorithms respond differently to uncertainty in a given model / ancillary parameter. One test performed by the SMAP team involved retrieving soil moisture from one year of global simulated SMAP bright-

ness temperatures (GloSim1), varying one parameter in turn while keeping the other parameters constant with no error. Table 10 lists the error in retrieved volumetric soil moisture in cm³/cm³ for each of the four SMAP L2_SM_P candidate algorithms over the full range of soil and vegetation water content (VWC) conditions encountered in the global simulation. The first column lists the parameter and its assigned error. Across this full range of conditions, with error only in one parameter at a time, all of the algorithms appear to perform to acceptable levels in retrieving soil moisture (last line in Table 10 is Total RSS).

A more stringent simulation is to assign some error to all parameters simultaneously and then assess the accuracy in retrieved soil moisture. Figure 36 shows the results obtained when the indicated errors were applied to the indicated parameters and soil moisture was retrieved for one year and compared to the "true" soil moisture. The soil moisture retrieval error was plotted for all of the algorithms as a function of VWC. As expected, retrieval errors went up as the vegetation increased. The baseline single-channel H pol algorithm shows the smallest error and meets the required accuracy even at the highest VWC bin that is included in the accuracy statistics. Results for the SCA-V pol are similar. However, the RMSE for the DCA and MPRA options exceed the target accuracy of 0.04 cm³/cm³ when VWC >~ 4 kg/m² based on the simulated data. When the RMSE is averaged across all of the VWC bins, all retrieval algorithm options meet the required accuracy. For this simulation, parameters such as b and h were assumed to be the same for both H and V polarization. This assumption is being re-examined as new information is obtained (through analysis of SMOS and other field data) regarding quantification of any polarization dependence of any of the algorithm parameters.

Table 10. Simulated retrieval error by parameter for each algorithm.

| Model/Ancillary Uncertainty | Baseline<br>Single Pol (H)<br>RMSE (cm³/cm³) | Option 1<br>Single Pol (V)<br>RMSE (cm³/cm³) | Option 2<br>Dual Pol<br>RMSE (cm³/cm³) | Option 3<br>MPRA<br>RMSE (cm³/cm³) |
|---|---|---|---|---|
| Gridding + aggregation | 0.0061 | 0.0058 | 0.0059 | 0.0058 |
| 5% h | 0.0065 | 0.0060 | 0.0060 | 0.0058 |
| 5% omega | 0.0063 | 0.0061 | 0.0062 | 0.0061 |
| 5% sand fraction | 0.0073 | 0.0070 | 0.0070 | 0.0070 |
| 5% clay fraction | 0.0062 | 0.0059 | 0.0059 | 0.0059 |
| 2K T5 | 0.0087 | 0.0100 | 0.0112 | 0.0120 |
| 5% VWC | 0.0066 | 0.0061 | — | — |
| 10% VWC | 0.0072 | 0.0065 | — | — |
| 5% water fraction | 0.0061 | 0.0059 | 0.0059 | 0.0058 |
| 10% water fraction | 0.0061 | 0.0058 | 0.0059 | 0.0058 |
| 20% water fraction | 0.0061 | 0.0058 | 0.0059 | 0.0058 |
| 1.3 K TB | 0.0068 | 0.0067 | 0.0083 | 0.0095 |
| **Total RSS Error** | 0.0203 | 0.0201 | 0.0205 | 0.0214 |

| L2_SM_P Error Analysis | | | | | | | |
| --- | --- | --- | --- | --- | --- | --- | --- |
| | h | omega | sandfrc | clatfrc | T5 | VWC | watrfrc | TB |
| RMSE | 5% | 5% | 5% | 5% | 2K | 5% | 10% | 1.3K |

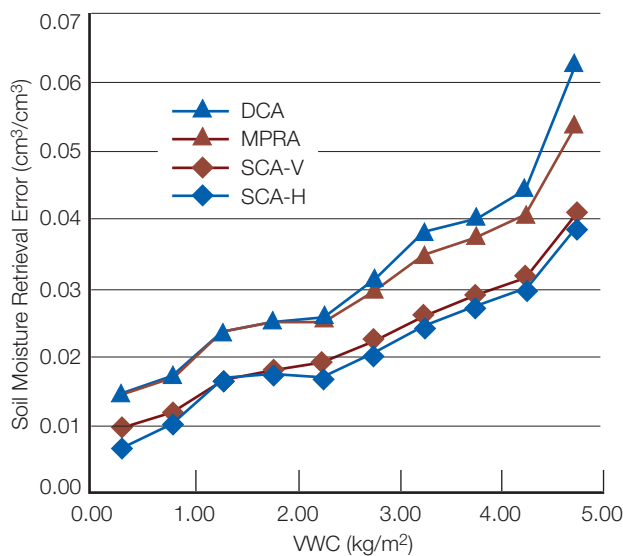| RMSE Averaged Across All VWC Bins | | | |
| --- | --- | --- | --- |
| SCA-H | SCA-V | DCA | MPRA |
| 0.0213 | 0.0227 | 0.0323 | 0.0305 |



Figure 36. Simulated error performance of all L2_SM_P candidate retrieval algorithms given the indicated RMSE in the algorithm input parameters listed above.

Microwave observations from the SMOS mission have been reprocessed to simulate SMAP observations at a constant incidence angle of 40° (details of this reprocessing are explained in the L2_SM_P ATBD) (O'Neill et al. 2012). This procedure provides a brightness temperature dataset that closely matches the observations that will be provided by the SMAP radiometer. SMOS brightness temperatures provide a global real-world, rather than simulated, input for evaluating the different SMAP radiometer-only soil moisture algorithm alternatives. Initial results

using the SCA with a SMOS-based simulated SMAP $T_B$ dataset and MODIS-based vegetation (NDVI) climatology data are presented here. For this preliminary analysis, the roughness parameter ($h$), vegetation parameter ($b$), and the single scattering albedo ($\omega$) were assumed constant for all land cover classes ($h = 0.1$, $b = 0.08$, $\omega = 0.05$). In subsequent analyses, these parameters will be further refined for different land cover classes as information becomes available. Figure 37 shows the average soil moisture estimated using the SCA algorithm with the SMAP-simulated SMOS TB data for the ascending orbits (overpass time of 6 AM) for July 1–10, 2011. The soil moisture spatial patterns are consistent with geographical features. Soil moisture retrieved using the SCA with SMOS-simulated SMAP TB for January 2010–May 2013 was compared to data from in situ soil moisture networks in USDA ARS watersheds that have previously been extensively used in satellite-based soil moisture validation (Jackson et al., 2010, 2012). Figure 38 shows the comparison between observed and estimated soil moisture over the Little River (LR), Little Washita (LW), Walnut Gulch (WG), and Reynolds Creek (RC) watersheds for SMOS ascending orbits (overpass time of 6 AM). Table 11 shows the statistical performance of the SCA algorithm over these watersheds. Despite the presence of two obvious outliers which did not get thrown out during routine flagging, the overall RMSE and the individual watershed ubRMSEs meet mission requirements. All of these results are encouraging for the potential of SMAP to meet its required soil moisture accuracy of 0.04 cm3/cm3 for the L2_SM_P product.

## H. Level 3 Radiometer-Only Soil Moisture Product (L3_SM_P)

The L3_SM_P product is a daily global product. To generate the product, individual L2_SM_P half-orbit granules acquired over one day are composited to produce a daily multi-orbit global map of retrieved soil moisture.

The L2_SM_P swaths overlap poleward of approximately ±65° latitude. Where overlap occurs, three options are considered for compositing multiple data points at a given grid cell:

Table 11. Statistical summary of the SMOS/SMAP/SCA retrieval algorithm results over USDA watersheds for SMOS ascending orbits (6 PM overpass time), January 2010–May 2013.

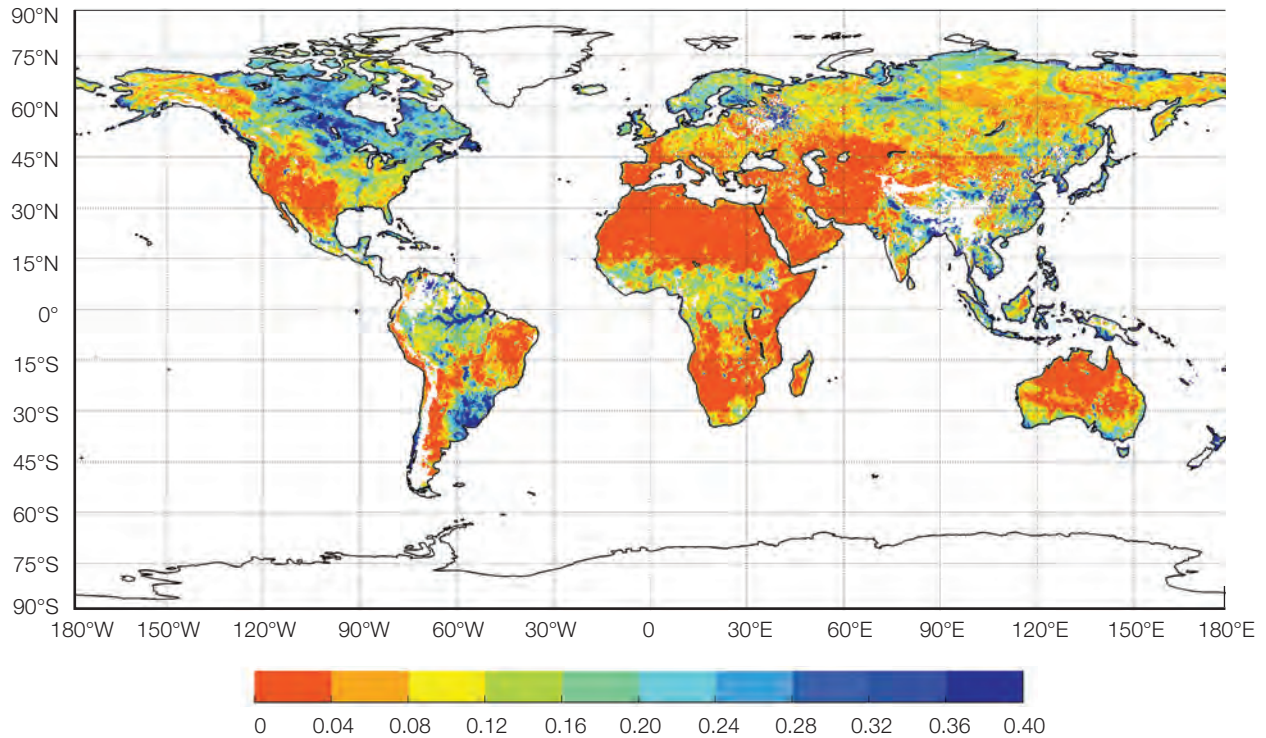| Watershed | Count | RMSE | R | Bias | ubRMSE |
| --- | --- | --- | --- | --- | --- |
| Little River, GA | 247 | 0.028 | 0.767 | −0.003 | 0.028 |
| Little Washita, OK | 245 | 0.047 | 0.841 | −0.028 | 0.037 |
| Walnut Gulch, AZ | 231 | 0.025 | 0.789 | −0.008 | 0.024 |
| Reynolds Creek, ID | 74 | 0.050 | 0.219 | −0.045 | 0.022 |
| Overall | 797 | 0.037 | 0.745 | −0.016 | 0.033 |

**Figure 37. Average estimated soil moisture using the single-channel algorithm (SCA) for SMOS ascending orbits for the period of July 1–10, 2011.**

1. Use the most recent (or "last-in") data point

2. Take the average of all data points within the grid cell

3. Choose the data point observed closest to 6:00 AM local solar time

The current approach for the L3_SM_P product is to use the nearest 6:00 AM local solar time (LST) criterion to perform Level 3 compositing. According to this criterion, for a given grid cell, an L2 data point acquired closest to 6:00 AM local solar time will make its way to the final Level 3 granule; other "late-coming" L2 data points falling into the same grid cell will be ignored. For a given granule whose time stamp (yyyy-mm-ddThh:mm:ss) is expressed in UTC, only the hh:mm:ss part is converted into local solar time. For example:

| UTC Time Stamp | Longitude | Local Solar Time |
|---|---|---|
| 2011-05-01T23:19:59 | 60E | 23:19:59 + (60/15) hrs = 03:19:59 |
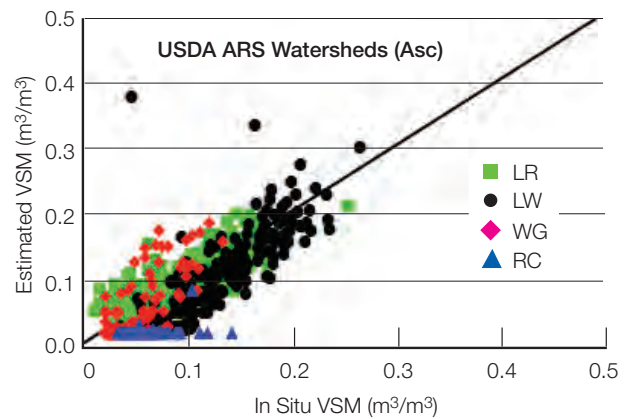


**Figure 38. Comparison of estimated soil moisture using SMOS-simulated SMAP $T_B$ with in situ observations over USDA ARS watershed sites for ascending orbits (6 AM overpass time) for January 2010–May 2013. Two outliers can be explained: on 2/25/2011, the surface temperatures were very low and there is likely some wet snow in the SMOS footprint that ECMWF did not predict; on 9/16/2011, there is an active rain event that ECMWF did not predict (so these two points did not get thrown out during routine flagging).**

The local solar time 03:19:59 is then compared with 06:00:00 in Level 3 processing for 2011-05-01 to determine if the swath is acquired closest to 6:00 AM local solar time. If so, that data point (and only that data point) will go to the final Level 3 granule. Under this convention, an L3 composite for 2011-05-01 has all Level 2 granules acquired within 24 hours of 2011-05-01 UTC and Level 2 granules appearing at 2011-05-02 6:00 AM local solar time at the equator. Note that this is also the conventional way to produce Level 3 products in similar missions and is convenient to users interested in global applications. Figure 39 shows an example of the L3_SM_P soil moisture output for one day's worth of simulated SMAP descending orbits (6 AM) globally and over just the continental U. S. (CONUS).
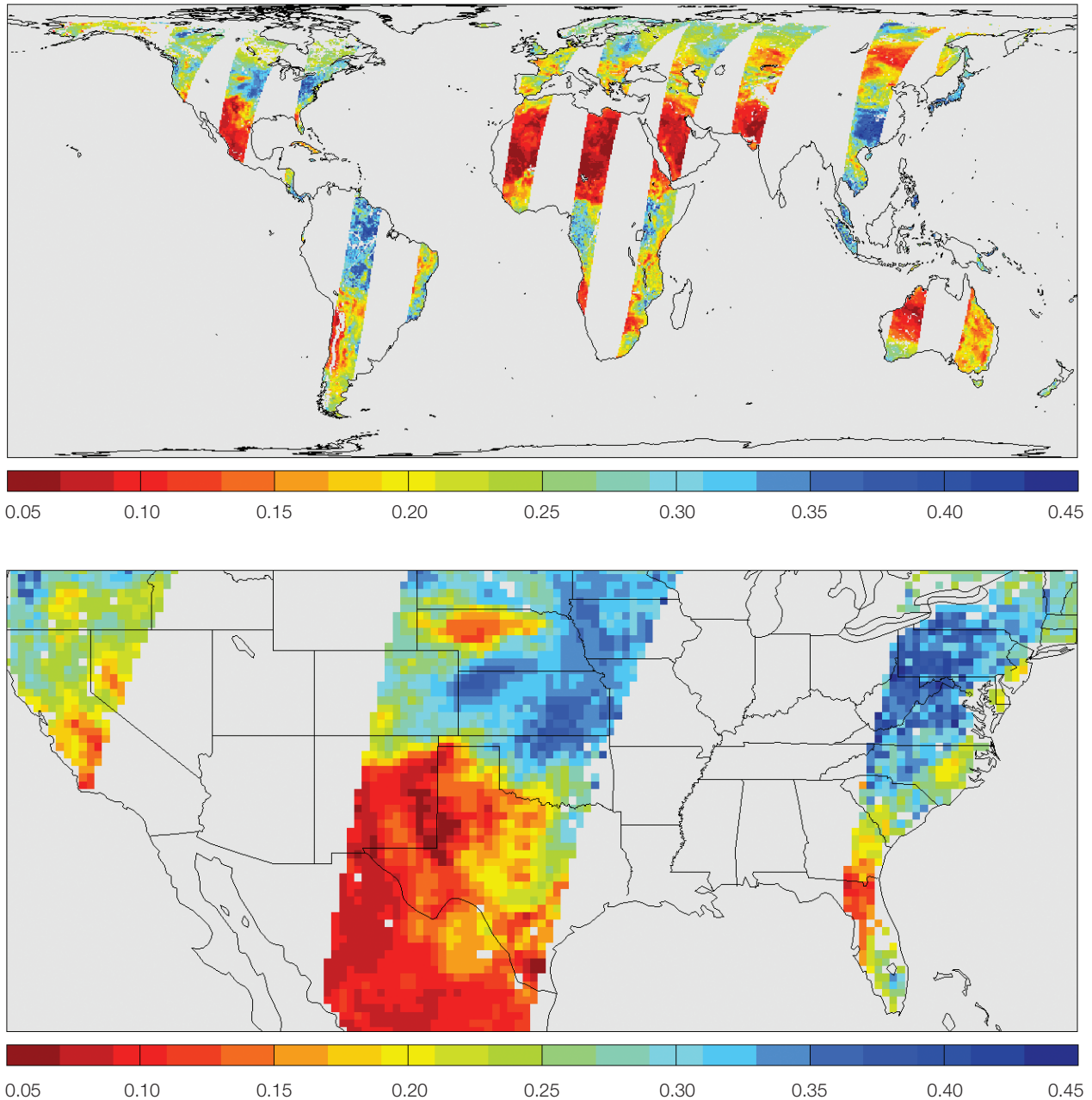


Figure 39. Simulation of L3_SM_P retrieved soil moisture in cm³/cm³. This example is based on the single-channel algorithm operating on H-polarized T_B observations simulated using geophysical data from a land surface model.

## IV. Combined Radar-Radiometer Soil Moisture Retrievals (L2/3_SM_AP)

### A. Science Basis for Baseline Algorithm

The SMAP instrument package will deploy an L-band SAR and an L-band radiometer for concurrent coincident measurements. By combining the relative advantages of active and passive microwave remote sensing, more robust soil moisture mapping is possible (Entekhabi et al., 2010). Due to the concurrent SAR and radiometer measurements and their respective advantages, they can be effectively combined to derive soil moisture estimates with intermediate accuracy and at intermediate resolution (~9 km) that meet the SMAP science requirements. The SMAP L2_SM_AP surface soil moisture baseline retrieval algorithm takes advantage of unique features of the SMAP dual-instrument measurement approach and first produces estimates of brightness temperature at an intermediate scale between the SMAP SAR and radiometer, using the SAR backscatter measurements to disaggregate the radiometer brightness temperature. The disaggregated and the true radiometer brightness temperature fields are compatible in that their field averages are identical. The brightness temperature retrieval algorithms with ancillary information of the right type and at the right scale are then utilized to retrieve intermediate-resolution soil moisture fields based on the disaggregated brightness temperature fields.

An L-band radiometer measures the natural microwave emission in form of the brightness temperature ($T_B$) of the land surface, while the L-band SAR measures the energy backscattered ($\sigma$) from the land surface after transmission of an electromagnetic pulse. If the L-band radiometer and L-band SAR make a concurrent and constant look angle measurement over a particular region on the Earth, then the influence of azimuthal and viewing-angle dependent factors are minimized. Over short periods of time, the land surface vegetation and surface roughness factors remain stable, whereas variability in soil moisture status exists due to wetting and dry down of the soils. In such a scenario, the increase of surface soil moisture or soil dielectric constant will lead to a decrease in radiometer $T_B$ (at polarization $v$ or $h$) and an increase in SAR co-pol ($hh$ or $vv$) $\sigma$ measurements, and vice-versa (Njoku and Entekhabi 1996; Ulaby et al. 1996). During this short time period, $T_B$ and co-pol $\sigma$ are negatively correlated due to soil moisture variations in time. The time period should be much shorter than the seasonal phenology of vegetation. It should be noted that in some agricultural land use regions the vegetation can grow and change attributes rapidly over a few days,which may be a source of error. Also, precipitation and associated surface disturbances can change the soil roughness characteristics that may introduce another source of error. Despite these sources of uncertainty, within this region of interest over a short period of time the measured $T_B$ and co-pol $\sigma$ are expected to have a functional relationship, and thus a hypothesis of linear functional relationship is established on the same spatial scale:

$$T_B = \alpha + \beta \cdot \sigma \qquad (19)$$

The linear dependence in (19) is based on units of dB for the SAR backscatter cross-section. The unknown parameters $\alpha$ [K] and $\beta$ [K/dB] are dependent on the dominant vegetation and soil roughness characteristics, and the $T_B$ polarization can either be $v$ or $h$ and the $\sigma$ polarization is either $vv$ or $hh$. To overcome the limitations of existing active-passive algorithms, a new algorithm is proposed that disaggregates the radiometer-based brightness temperature using high-resolution SAR backscatter by implementing Eq. (19).

SMAP grid configurations used in the algorithm are shown in Figure 40, where "$C$" represents coarse-scale (36 km), "$F$" represents fine-scale (3 km), and "$M$" represents medium-scale (9 km) for the radiometer, SAR, and combined product grid spacing, respectively. This convention is used throughout the text. The SMAP grid configurations are nested: within a single ($nc$ = 1) 36 km x 36 km pixel of grid C there are $nm$ = 16 pixels of grid $M$ and nf = 144 pixels of grid $F$. SAR backscatter cross-sections are averaged in power to obtain the coarse-resolution (M & C) backscatter cross-sections.

Equation (19) evaluated at scale $C$ (36 km) is:

$$T_B(C) = \alpha(C) + \beta(C) \cdot \sigma(C) \qquad (20)$$

Here $\sigma(C) = \frac{1}{nf} \sum_{i=1}^{nf} \sigma(F_i)$ where F = 3 km grid resolution and $nf$ is the number of $F$ grid cell within $C$. $T_B(C)$ and $\sigma(F)$ are available in the SMAP L1C_TB and L1C_S0_HiRes data products, respectively. [Note: $\sigma(F_i)$ while averaging is in linear units.] The parameters $\alpha(C)$ and $\beta(C)$ can be statistically estimated based on the time-series regression in (20), i.e., pairs of SMAP radiometer $T_B(C)$ and spatially-averaged SAR data $\sigma(C)$ from successive overpasses over the same Earth grid are used in the statistical linear regression $T_B(C)$ = intercept + slope $\cdot \sigma(C)$.

Das et al. (2014) test the robustness of the assumption of the linear functional relationship (20) between brightness temperature and radar backscatter cross-section, using data from the Passive Active L-band System (PALS) aircraft instrument taken during the Soil Moisture Experiment 2002 (SMEX02) to show the strength of linear functional dependence (i.e., R2) between the time-series of $T_{B_v}$ (4 km) and $\sigma_{vv}$ (4 km) specific to a particular location or coarse radiometer pixel (Figure 2 in Das et al. 2014; also see Colliander et al. 2012). The explained variance (high R2) of the linear approximation $T_{B_v} = \alpha + \beta.\sigma_{vv}$ is between 65% and 93% for the SMEX02 PALS observations. There
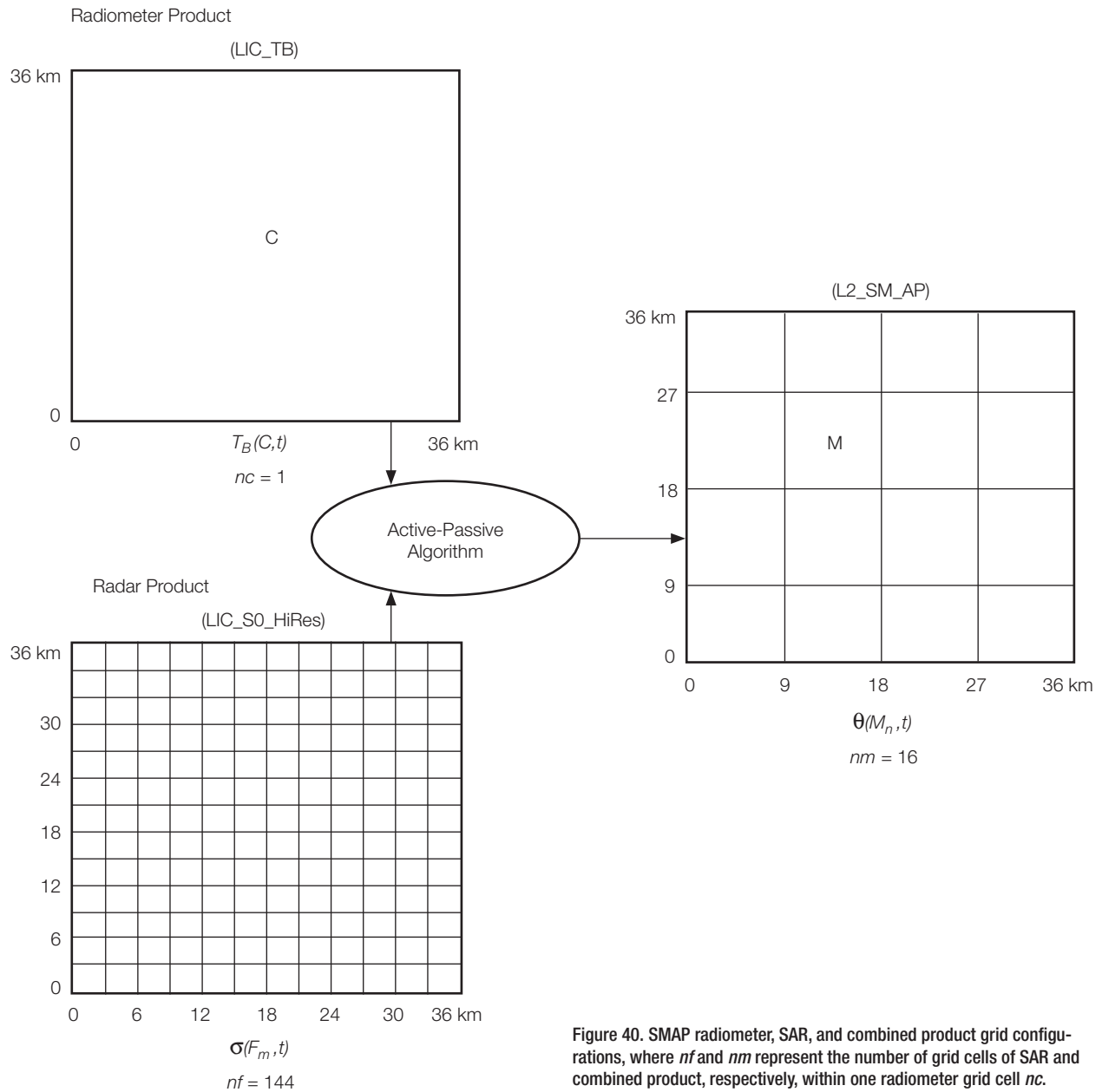
**Figure 40. SMAP radiometer, SAR, and combined product grid configurations, where *nf* and *nm* represent the number of grid cells of SAR and combined product, respectively, within one radiometer grid cell *nc*.**

were only 8 days of PALS flights during SMEX02 and in some locations of the flight domain not enough soil moisture change was observed.

To confirm the fidelity of the linear functional relationship between $T_B$ ($C$) and $\sigma$ for different hydroclimatic regions and various land covers, PALS data from multiple field campaigns (SGP99, SMEX02, CLASIC, and SMAPVEX08) are consolidated and analyzed. The $T_B$ ($C$) and $\sigma$ mean values from each field experiment are removed from the observations of each experiment in order to remove ex-

periment-to-experiment instrument calibration differences. Figure 2 in Das et al. (2011 and 2014) shows the explained variance between the various radar and radiometer polarization measurements from the combined SGP99, SMEX02, CLASIC, and SMAPVEX PALS field campaigns (Colliander et al. 2012). The results are segmented based on the magnitude of vegetation cover. The explained variance ranges from 0.4 to 0.6 (for various polarization combinations) for low vegetation conditions and diminishes to zero for full vegetation cover.

The amount of vegetation cover is quantified using the radar measurements and the Radar Vegetation Index (RVI) that is defined as

$$RVI = \frac{8\sigma_{hv}}{\sigma_{hh} + \sigma_{vv} + 2\sigma_{hv}} \qquad (21)$$

with the radar backscatter values in units of power (Kim and van Zyl 2009). RVI is an index that is directly proportional to the amount of vegetation on the land surface, and is influenced by the geometric structure of vegetation. It can be derived directly from SMAP radar measurements. When the vegetation cover is dense and there is complete unpolarized volume scattering from the vegetation canopy, which consists of randomly oriented dipoles, RVI has the upper limit of unity. If the vegetation cover consists of dipoles oriented at 45° with respect to the V polarization, then the scattering from vegetation alone will have RVI=2; however, natural vegetation cover is unlikely to have only uniformly oriented dipoles. For bare smooth surfaces, the cross-pol radar backscatter cross-section is much smaller than the co-pol values. This leads to a near-zero RVI. Conveniently, the RVI is nominally between zero and unity.

The parameter β is estimated for the measurements from the combined SGP99, SMEX02, CLASIC, and SMAPVEX PALS field campaign datasets (Colliander et al., 2012). The brightness temperature change sensitivity to backscatter change is highly dependent on vegetation density (Figure 41). Values of β for different classes of RVI show that dense vegetation cover masks the soil moisture sensitivity of radar measurements (β approaches zero for RVI approaching unity). Across low vegetation cover regions (low RVI), the changes in radiometer brightness temperature are also reflected in changes in radar backscatter, leading to large (negative) values of the statistically-estimated β.
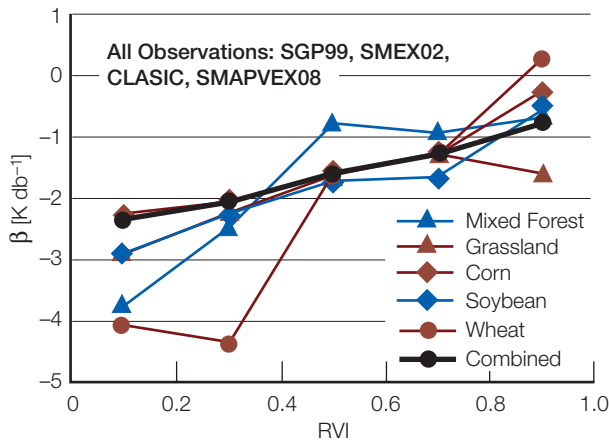


**Figure 41. Parameter β estimated from consolidated PALS data taken over four field experiments and for different landcover types.**

The statistically estimated slope parameter β(C) in (20) (when based on SMAP measurements) is specific for a given location. This is because β(C) is a sensitivity parameter relating $T_{B_v}$ (C) and $\sigma_{vv}$ (C) and it is a function of surface characteristics like the local vegetation cover and soil roughness. The parameter varies seasonally as well as geographically depending upon land cover.

To develop the satellite-based active-passive algorithm, (19) can also be conceptually evaluated at the 9-km scale $M$ [same as was done for 36-km scale $C$ in (19)] within the radiometer footprint $C$:

$$T_{B_v}(M_j) = \alpha(M_j) + \beta(M_j) \cdot \sigma_{vv}(M_j) \qquad (22)$$

where $\sigma_{vv}(M_j) = \frac{1}{nm}\sum_{i=1}^{nm_j} \sigma_{vv}(F_i)$ obtained from the SMAP high-resolution (3 km) SAR data product. Here $T_{B_v}(M_j)$ is the unknown brightness temperature at scale $M_j$. This scaled brightness temperature is not available given the SMAP radiometer instrument resolution. In fact, this variable is the target of our estimation and it is referred to as the disaggregated/downscaled brightness temperature. The first step in developing the algorithm is to subtract (20) from (22):

$$T_{B_v}(M_j) - T_{B_v}(C) = \{\alpha(M_j) - \alpha(C)\} + \\ \{[\beta(M_j) \cdot \sigma_{vv}(M_j)] - [\beta(C) \cdot \sigma_C(C)]\} \qquad (23)$$

Because $T_{B_v}(M_j)$ is not available, the parameters $\alpha(M_j)$ and $\beta(M_j)$ cannot be estimated in the manner that was followed at scale $C$. The path forward to incorporate the effects of the variations of these parameters at scale $M_j$ with respect to the coarser scale $C$ begins with rewriting (23) algebraically as

$$T_{B_v}(M_j) = T_{B_v}(C) + \{\beta(C) \cdot [\sigma_{vv}(M_j) - \sigma_{vv}(C)]\} + \\ \{[\alpha(M_j) - \alpha(C)] + \beta(M_j) - \beta(C)] \cdot \sigma_{vv}(M_j)\} \qquad (24)$$

The left-hand side of (24) is the target variable of the active-passive algorithm, i.e., the disaggregated brightness temperature at the 9 km scale $M_j$. The first term on the right-hand side (RHS), $T_{B_v}(C)$, is the radiometer-measured brightness temperature at 36 km or scale $C$. The second RHS term, $\{\beta(C) \cdot [\sigma_{vv}(M_j) - \sigma_{vv}(C)]\}$, can be calculated based on the regression parameter $\beta(C)$ that is estimated through the time-series of radiometer brightness temperature measurements and SAR measurements aggregated to scale $C$. The remainder of this second RHS term is also based on the SAR measurements aggregated to scales $M_j$ and $C$. The third RHS term accounts for the deviations/heterogeneity of the parameters α and β within the grid $C$. The term $\{[\alpha(M_j) - \alpha(C)] + \beta(M_j) - \beta(C)] \cdot \sigma_{vv}(M_j)\}$ is in units of brightness temperature and represents the subgrid scale heterogeneity effects. The parameters α and β depend

on vegetation and surface roughness. The SMAP SAR also provides high-resolution cross-polarization backscatter measurements that are principally sensitive to vegetation and surface characteristics. The cross-polarization backscatter at scale $M_j$ deviations from its coarse-scale aggregate $[\sigma_{hv}(C) - \sigma_{hv}(M_j)]$ are indicators of the subgrid heterogeneity in vegetation and surface physical characteristics.

This heterogeneity indicator $[\sigma_{hv}(C) - \sigma_{hv}(M_j)]$ can be converted to variations in co-polarization backscatter through multiplications by the sensitivity $\left[\frac{\delta\sigma_{vv}(M_j)}{\delta\sigma_{hv}(M_j)}\right]_C$. This sensitivity, denoted by the scale $C$ parameter $\Gamma \equiv \left[\frac{\delta\sigma_{vv}(M_j)}{\delta\sigma_{hv}(M_j)}\right]_C$, is specific to each grid $C$ and the particular season for this grid $C$. It can be estimated using high-resolution SMAP co-polarization and cross-polarization SAR measurements through statistical regression. For any scale $C$ data granule there will be a reasonable number of scale $M_j$ SAR data pairs to estimate the sensitivity parameter $\Gamma$. The parameter $\Gamma$ derived from consolidated PALS data taken over four field experiments (Colliander et al. 2012) for different land covers is shown in Figure 42. Except for low vegetation cover, the parameter $\Gamma$ tends to converge among different land covers.

The term $\Gamma \cdot [\sigma_{hv}(C) - \sigma_{hv}(M_j)]$ is the projection of the variations due to the heterogeneity in parameters $\alpha$ and $\beta$ in the SAR co-polarization space. It can be converted to brightness temperature units for use in (23) through multiplication by $\beta(C)$, i.e., $\beta(C) \cdot \Gamma \cdot [\sigma_{hv}(C) - \sigma_{hv}(M_j)]$, where $\beta(C)$ is the particular radiometer grid scale C conversion factor relating co-polarization backscatter variations to brightness temperature variations. Therefore,

$$\beta(C) \cdot \Gamma \cdot [\sigma_{hv}(C) - \sigma_{hv}(M_j)] \approx \{[\alpha(M_j) - \alpha(C)] + [\beta(M_j) - \beta(C)] \cdot \sigma_{vv}(M_j)\}$$

The SMAP active-passive brightness temperature disaggregation algorithm is complete by substituting this term for the third RHS term in (24),

$$T_{B_v}(M_j) = T_{B_v}(C) + \{\beta(C) \bullet [\sigma_{vv}(M_j) - \sigma_{vv}(C)]\} + \beta(C) \cdot \Gamma \cdot [\sigma_{hv}(C) - \sigma_{hv}(M_j)] \quad (25)$$

which can be written more compactly as

$$T_{B_v}(M_j) = T_{B_v}(C) + \beta(C) \bullet [\sigma_{vv}(M_j) - \sigma_{vv}(C)] + \Gamma \cdot [\sigma_{hv}(C) - \sigma_{hv}(M_j)] \quad (26)$$

The disaggregated brightness temperatures $T_{B_v}(M_j)$ from (26) are expected to have more noise than $T_{B_v}(C)$ due to inherent errors in $T_{B_v}(C)$, $\sigma_{vv}(M_j)$, and $\sigma_{hv}(M_j)$, and the degree of uncertainty associated with parameters $\beta(C)$ and $\Gamma$ that are derived from regressions. The disaggregated brightness temperature $T_{B_v}(M_j)$ at 9 km is an intermediate product of the proposed active-passive algorithm. Since the second and third terms in (26) are deviations

of the backscatter from the 36-km pixel mean values, the statistical expectation of the disaggregated brightness temperature will necessarily always be equal to the radiometer measurement. Thus, there is a built-in consistency between the L2_SM_AP and L2_SM_P soil moisture products.
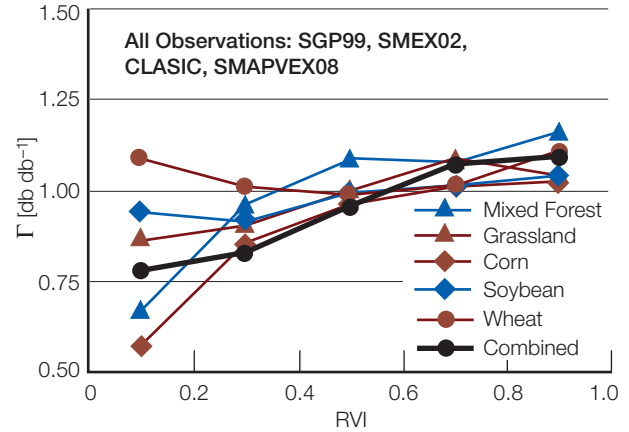


Figure 42. Parameter $\Gamma$ determined using $\sigma_{vv}$ and $\sigma_{hv}$ from consolidated PALS data taken over four field experiments and for different land cover types.

## B. Baseline Algorithm Implementation

The L2_SM_AP algorithm is implemented on the SMAP Science Data System (SDS). The two primary inputs into the baseline algorithm are 36-km radiometer-based brightness temperature and the 3-km radar-based backscatter cross-sections. These data are derived from the L2_SM_P and L2_SM_A processing stream instead of the lower-level (Level-1) data products suite. The water-body correction and the freeze/thaw flags derived from the SMAP radar measurements are available at the early stages of Level 2 product processing. The water-body corrected brightness temperature at 36 km ($T_{B_p}(C)$ for polarizations $p=v$ and $h$) along a swath with associated QC flags is available as part of the L2_SM_P product, and is a direct input to the L2_SM_AP algorithm. The 3-km gridded $\sigma_{pq}$ (F) data for polarizations $pq=vv$, $hh$, and $hv$, 3-km transient water body and freeze/thaw flags produced during the L2_SM_A processing are also input to the L2_SM_AP algorithm. The fine-resolution 3-km radar backscatter cross-section data contained in the coarse-scale (36-km) grid are averaged to the intermediate and coarse-scale resolutions. The results are $\sigma(C)$ and $\sigma(M_j)$.

## C. Algorithm Flow

There are two main derived parameters based on the water-body corrected and flagged radar backscatter cross-section ($\Gamma(C)$ and $\beta(C)$). Each is a scalar for the 36-km grid. These are estimated statistically from $\sigma_{pp}(F)$, $\sigma_{pq}$ (F), and $T_{B_p}(C)$. The parameter $\Gamma(C)$ is the slope of the

linear regression between deviations of $\Gamma \equiv \left[\frac{\delta\sigma_{pp(Mj)}}{\delta\sigma_{pq(Mj)}}\right]_c$ where $\delta$ is defined as the deviation $\alpha(Mj) - \sigma(C)$. The parameter $\beta(C)$ is estimated as the regression slope of a time-series of $\sigma_{pp}(C)$ and $T_{Bp}(C)$. The time window over which the statistical regression is implemented must balance the sample size (favoring longer windows) and changes in the linear slope due to changing vegetation phenology (favoring shorter windows). Trade-off studies on the size of this time window are ongoing, and early indications (based on Aquarius active-passive data) are that a 3-month window is applicable in most climate zones.

Prior values for $\Gamma(C)$ and $\beta(C)$ are also available in data files during processing. The priors are established using the field experiment-based parameterizations of the parameters as a function of RVI (Figures 41 and 42) as well as Aquarius heritage observations. The standard error of estimation of slope is also derived during the regression steps described above. The same is available for the archive prior values for the parameters. The statistical regression values and the priors are combined in a Bayesian framework based on their respective errors of estimation. This leads to more robust estimates for $\Gamma(C)$ and $\beta(C)$.

At this point the disaggregated brightness temperatures at the intermediate 9-km scale can be calculated using (26). At this stage the same baseline algorithm used for L2_SM_P is applied to estimate surface soil moisture. The ancillary data used in the process will be at a finer resolution than those used in L2_SM_P. But the architecture of the algorithm and the parameterizations used will be the same. This ensures a high level of consistency among all the SMAP soil moisture products. Documentation for these static and dynamic ancillary datasets can be found at http://smap.jpl.nasa.gov/science/dataproducts/ATBD/.

## D. Alternate Algorithms

The alternate algorithms for the active-passive soil moisture product are variations of the brightness temperature disaggregation of the baseline algorithm. In the first alternative, the brightness temperature disaggregation is performed at the fine scale $F_i$ instead of the intermediate scale $Mj$ ( Figure 40). Then the brightness temperature values are aggregated to 9 km and soil moisture values are retrieved at the 9-km scale. The performance of this alternate implementation is highly dependent on the impact of increased radar noise at the higher resolution. In a second alternate implementation, the soil moisture retrievals are performed on the estimates of 3-km disaggregated brightness temperatures. Then the soil moisture values are averaged to the intermediate 9-km resolution. Since over the dynamic range of surface soil moisture and brightness temperature the variations are nearly linear, the nonlinearity of the tau-omega model is not expected to affect the relative performance of this (second) alternate

algorithm. Aggregation of soil moisture to 9 km is also affected by the quality of the ancillary data such as land cover, physical temperature, and soil classification. These alternate implementations of the baseline algorithm are currently undergoing testing using simulated SMAP data products (see next section).

## E. Algorithm Performance

The performance of the baseline algorithm is evaluated using the PALS datasets from SMEX02. The reason for using the PALS SMEX02 dataset is the availability of wet and dry soil moisture conditions and the range of vegetation conditions within the PALS flight domain for the campaign duration. PALS was flown over the SMEX02 region (the Walnut Creek watershed, Iowa) for eight days during the months of June and July, 2002.

Although the PALS L-band radar and radiometer have similar frequencies to SMAP, the PALS instruments have much finer spatial resolution (approximately ~0.8 km depending on flight altitude). To apply the L2_SM_AP algorithm to PALS data, the data are gridded for the radiometer at ~4 km and for the radar at ~0.8 km. Equation (8) is implemented to obtain the disaggregated/downscaled $T_{B_v}$ at ~0.8 km, and the L2_SM_P algorithm (see L2_SM_P algorithm description in this chapter) is then used to retrieve soil moisture from disaggregated $T_{B_v}$ at ~0.8-km resolution. Das et al. (2014) report that the RMSE of the brightness temperature disaggregation (4 km to 0.8 km) is 1.8 K. When the 4-km radiometer data are resampled (using just simple assignment) to 0.8 km, the RMSE is 2.75 K. The improvement 2.75 to 1.8 K is due to the inclusion of heterogeneity information from the radar in the disaggregation process. The higher resolution and accuracy of the disaggregated brightness temperature enables soil moisture retrieval at high resolution.

Soil moisture retrievals on disaggregated $T_{B_v}$ are performed using the $\tau$-$\omega$ algorithm with ancillary data measured/sampled during the SMEX02 experiment. To validate the retrieved soil moisture estimates at ~0.8 km resolution, the field averaged soil moisture calculated from in situ measurements in 31 fields over 4 days are used (Figure 43a–c). The representative spatial resolution of a field is near ~0.8 km, making the comparison between field measurements of soil moisture and retrieved soil moisture from disaggregated $T_B$ at 0.8 km compatible. Figure 43(a) results indicate that the proposed algorithm (RMSE: 0.033 cm$^3$/cm$^3$) outperforms the minimum performance (RMSE: 0.056 cm$^3$/cm$^3$) as shown in Figure 43(b). The Minimum Performance intermediate-resolution soil moisture values are the retrieval results from $T_{B_v}$ resampled at ~0.8 km. They are obtained by direct resampling of $T_{B_v}$ at ~4 km to high-resolution ~0.8 km pixels. The Minimum Performance is a reference

for comparison. It is essentially a resampling of brightness temperature to finer scale without use of information from the radar. Results from this study establish the applicability of the algorithm (26) by clearly outperforming the results from Minimum Performance. The baseline algorithm also captured the spatial variability in soil moisture with reasonable accuracy for vegetation having ≤ 5 kg/m$^2$ VWC. The baseline algorithm reduces the Minimum Performance algorithm error by 40%.

Another test was performed to evaluate the contribution of radar cross-pol backscatter measurements ($\sigma_{pq}$) on the algorithm (26). The radar $\sigma_{pq}$ addresses the heterogeneity especially due to vegetation within the coarse radiometer footprint. The test was conducted by ignoring the radar cross-pol measurement ($\sigma_{pq}$) in the algorithm (25) or essentially $\Gamma = 0$. Therefore (26) becomes

$$T_{B_p}(M_j) = T_{B_p}(C) + \beta(C) \cdot [\sigma_{pp}(M_j) - \sigma_{pp}(C)] \quad (27)$$

The retrieval using (27) is shown in Figure 43(c). The RMSE (0.043 cm$^3$/cm$^3$) in this scenario is greater than the RMSE (0.033 cm$^3$/cm$^3$) obtained from the baseline algorithm (26). This test clearly captures the important contribution of $\sigma_{pq}$ in capturing sub-radiometer measurement scale vegetation heterogeneity for the baseline algorithm. However, (27) performed better than the Minimum Performance and hence strengthens the applicability of radar measurements to disaggregate the coarse radiometer measurement.

In order to test the algorithm across a wider range of conditions than those encountered in the limited airborne field campaigns, simulation environments are used. A global-scale simulation (GloSim) for the SMAP mission is developed and implemented on the SMAP Testbed at JPL. The GloSim orbit simulator on SDS mimics the SMAP configuration and follows an 8-day exact repeat pattern that provides total global coverage in 2–3 days. GloSim includes the capability of generating orbital files of simulated radiometer and radar observations of T$_B$ and $\sigma$, respectively. Description of models used in forward simulation of T$_B$ and $\sigma$ are beyond the scope of this paper; however, details are available at the SMAP webpage (http://smap.jpl.nasa.gov/science/dataproducts/ATBD/). Geophysical data (e.g., soil moisture and soil temperature) obtained from GMAO MERRA at 9-km resolution covering a 1-year period and ancillary data (e.g., model parameters, soil texture, land cover, water bodies, and VWC) at high resolution are used as underlying truth maps to sample forward observations of T$_B$ and $\sigma$ to mimic SMAP-like measurements. GloSim also applies realistic instrument/antenna beam sampling and orbital sampling to simulate the footprint-averaged observations within swaths acquired by the SMAP instruments. These simulated observations, along with their noise-perturbed versions,
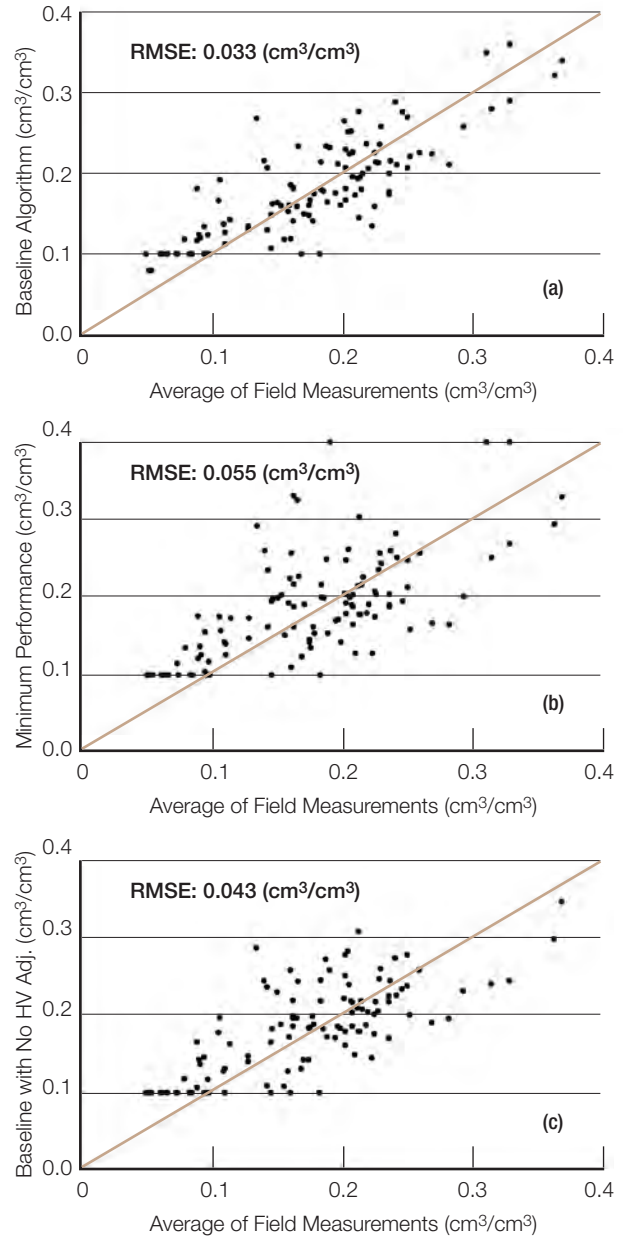


**Figure 43.** Comparison of field averaged soil moisture and retrieved soil moisture estimated from PALS data for 8 days: (a) Baseline Algorithm, (b) Minimum Performance, and (c) Baseline Algorithm soil moisture retrieval with no heterogeneity information provided by cross-pol $\sigma_{hv}$ radar backscatter information.

are essential to the testing, development, and operational implementation of all SMAP Level 2 and Level 3 soil moisture and freeze/thaw algorithms.

L2_SM_AP retrieval is performed on the simulated SMAP half orbit granules of L2_SM_P and L2_SM_A generated

from GloSim. The algorithm is implemented for extensive analyses. These analyses help to understand and develop solutions and risk reduction of various important operational and algorithm related issues such as: a) determine size of temporal window required over valid land pixels of radiometer and radar data to derive high-fidelity algorithm parameters; b) identify regions of the world where updates to the temporal window are essential due to changing vegetation phenology and ground conditions; c) develop and mature algorithm parameters database; d) develop and mature L2_SM_AP error budget table;

e) highlight the sensitivities of various ancillary data, masks and flags on the retrievals; and f) assess the limitations of the algorithms and help to tune the algorithms.

For discussion and illustration of L2_SM_AP retrievals, the particular swath as shown in Figure 44 is selected because it covers a wide range of conditions in soil moisture state (dry–wet), soil texture (sand–clay), land covers (rainforest–desert), and different hydroclimatic domains. Along with the SMAP products as inputs, the L2_SM_AP processor implemented in the SMAP SDS also ingests
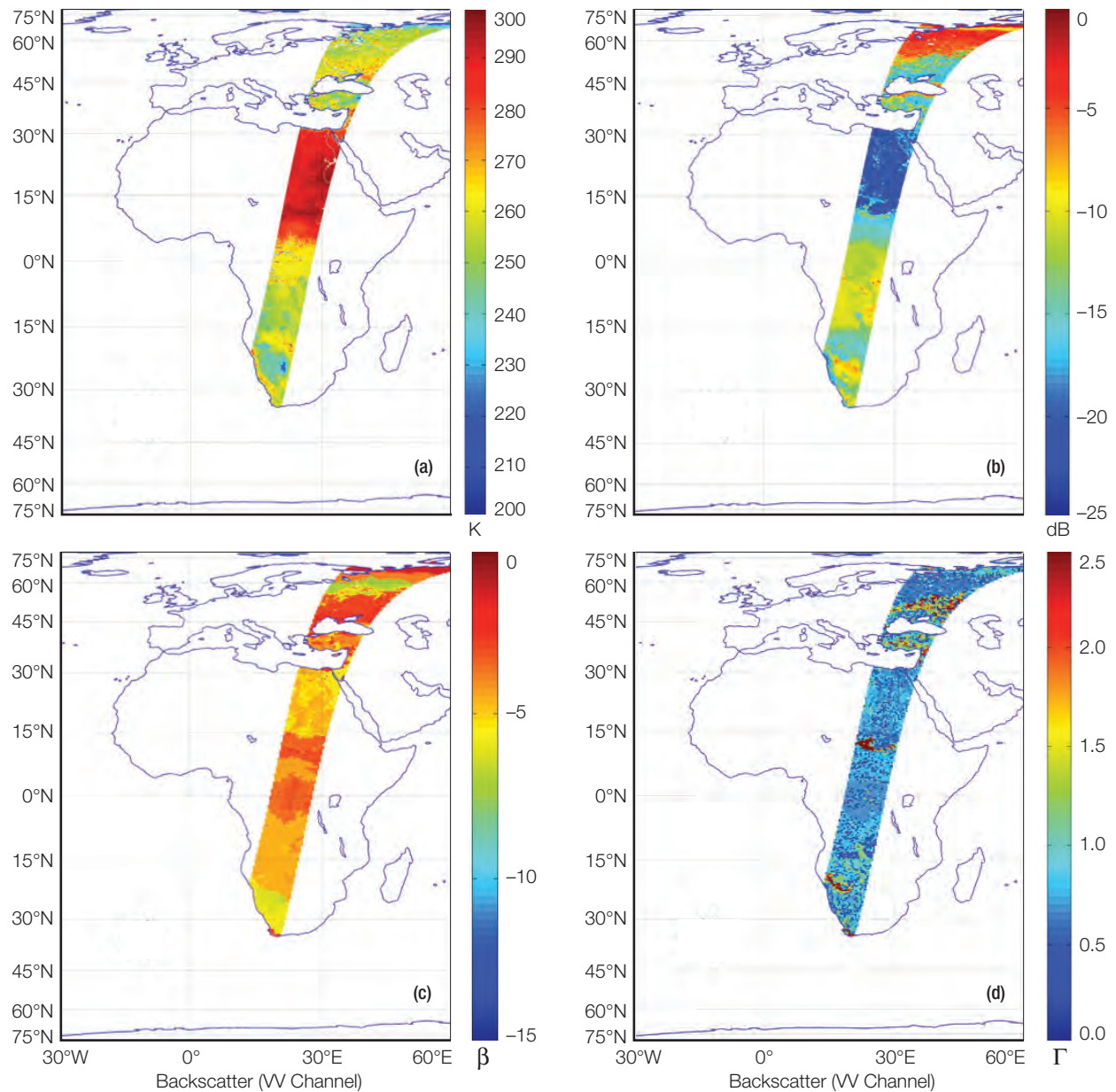


**Figure 44. (a)** $T_{B_V}$ **(C) data gridded at 36 km from GloSim for 1 day in June; (b) Swath of aggregated** $\sigma_{vv}$ **at 9-km grid from GloSim for 1 day in June; (c) Beta (β) parameter used for the swath from GloSim for 1 day in June; (d) Gamma (Γ) parameter used for the swath from GloSim for 1 day in June.**

static (e.g., soil) and dynamic (e.g., VWC and soil temperature) ancillary datasets, and global masks (e.g., urban, inland water bodies) at 9-km Earth fixed grid. For the GloSim L2_SM_AP retrievals, the parameter ($\beta$) estimation is conducted using time series of $T_{B_v}(C)$ and $\sigma_{VV}(C)$ for all grid cells. Figure 44(c) illustrates the state of parameter $\beta$ (derived from a 3-month time series) used over the swath that clearly exhibits dependency of $\beta$ with respect to land cover. The land cover mostly influences the dynamic range of $T_{B_v}(C)$ and $\sigma_{VV}(C)$, and hence the parameter $\beta$. Another parameter $\Gamma$ in (26) that detects the heterogeneity

within $C$ is determined on the fly over the swath and is shown in Figure 44(d) for a particular day in the month of June. Typically, very high correlation is observed between $\sigma_{VV}$ and $\sigma_{hV}$, and that is well captured (Figure 44d). The parameter $\Gamma$ also displays dependency for land cover.

The L2_SM_AP algorithm (26) is applied on data obtained from L2_SM_P and L2_SM_A. Figure 45(a) shows that the disaggregated $T_B$ at 9 km that captures the spatial heterogeneity detected by the SMAP radar that would otherwise be masked by the coarse-resolution scale of
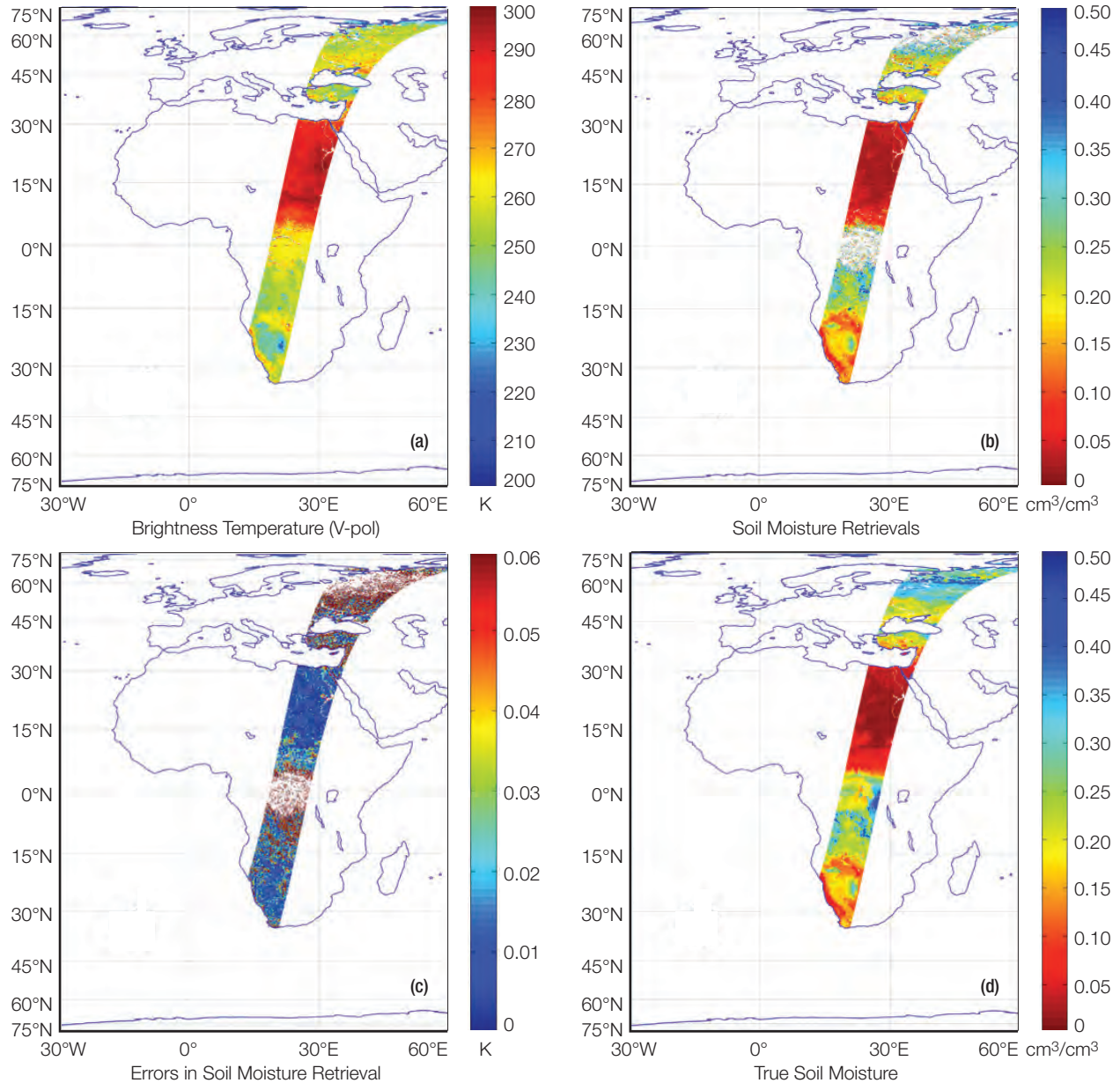


**Figure 45. (a) Swath of disaggregated $T_{B_v}$ at 9-km grid from GloSim for 1 day in June; (b) Swath of retrieved soil moisture at 9-km grid from GloSim for 1 day in June; (c) Errors in soil moisture at 9-km grid from GloSim for 1 day in June; (d) True soil moisture at 9-km grid from GloSim for 1 day in June.**

the brightness temperature measurements. Soil moisture retrieval is conducted on the disaggregated $T_{B_v}$ using the tau-omega ($\tau$-$\omega$) model (SCA). Figure 45(b) and Figure 45(d) show the retrieved and truth soil moisture at 9 km, respectively. Applicable noise is introduced in the ancillary data while performing the retrievals. Comparisons of Figure 45(b) and Figure 45(d) show similar spatial patterns of soil moisture for most of the regions. However, over highly-vegetated regions (e.g., rain forest), the $\tau$-$\omega$ model did not converge and therefore a null value is assigned during the retrieval process. To get an initial assessment of retrievals, errors are computed for the swath and are shown in Figure 45(c), with higher error for regions having high vegetation as expected.

Nearly ~5300 half-orbit granules of L2_SM_P and L2_SM_A are processed for a 1-year period for the GloSim L2_SM_AP retrievals. RMSE is computed for each 9 km grid cell. The global spatial pattern of RMSE is shown in Figure 46 for a 6-month period (April–September) period. The spatial pattern of RMSE in Figure 46 matches with the global VWC spatial distribution. RMSEs are not computed for the 9 km grid cells having more than 5% water fraction within the 9 km, more than 25% urban areas, open water bodies, and mountainous regions. These threshold values are currently being evaluated and harmonized for consistency across all SMAP Level 2 soil moisture products. Quantitative values of RMSE with respect to a range of VWC over the global extent is shown in Figure 47. The RMSE curve in this plot clearly meets the SMAP L1 requirements.

## V. Radar-Only Soil Moisture Retrievals (L2/3_SM_A)

### A. Science Basis for Baseline Algorithm

Retrieval of soil moisture from measured backscatter data typically implies an inversion of the radar forward scattering process. It has been common in the literature to use radar measurements to develop empirical or semi-empirical models for scattering or for inversion for bare surfaces (Dubois et al. 1995; Oh et al. 1992) and for vegetated surfaces (Bindlish et al. 2009; Joseph et al. 2008; Kim and van Zyl 2009). The empirical models face challenges when compared with datasets not used in the original model development (Zribi et al. 1997). Analytical inversion of a complex forward model is not feasible; iterative numerical inversion often requires significant computing time, especially for the global and frequent mapping to be done by SMAP (Verhoest et al. 2007), although the iterative techniques have become more effective and computationally efficient (Tabatabaeenejad et al. 2012). Forward model fits (e.g., using polynomials) were inverted analytically (Shi et al. 1997), iteratively (Moghaddam et al. 2000), using a genetic algorithm approach (Oh 2006), or

through neural-network training (Paloscia et al. 2008). The performance of all these methods is dependent on the fidelity of the inversion formulas, the accuracy of the model fitting, and the inherent accuracy of the forward model. As a different strategy, the effects of time-invariant surface roughness and vegetation were corrected by deriving the relative change index (Wagner and Scipal 2000) or through temporal differencing (Balenzano et al. 2011). Such approaches are susceptible to errors caused by changes in vegetation or other geophysical conditions over the time series of data used.

Recently, a look-up table representation of a complicated forward model was demonstrated to be an accurate and fast tool for retrieval (Kim et al. 2012a; Kim et al. 2014). Bare rough surfaces can be characterized in terms of their root mean square (rms) roughness height, correlation length, and moisture content (a surrogate for dielectric constant). The use of time-series data makes the retrieval a well-constrained estimation problem, under the assumption of a time invariant surface roughness (Verhoest et al. 2007). By taking a co-polarized ratio (Shi et al. 1997) or its equivalent (Kim et al. 2012a), the soil moisture retrieval becomes insensitive to the correlation length except for very rough surfaces, which enables an accurate retrieval of soil moisture without correlation length information. This approach has been extended to the vegetated surface by introducing a vegetation axis to the lookup table (Kim et al. 2014). One axis representation of the vegetation effect is clearly a simplification, considering that different sets of vegetation parameters result in different backscattering coefficients. However, with SMAP's three measurement channels (HH, VV, HV), at most three independent parameters can be uniquely estimated, and therefore simplified forward models must be represented in terms of at most three dominant parameters. The simplification will result in some errors in soil moisture retrieval, especially in heavily vegetated areas such as forests. Allometric relationships, if available, reduce the number of unknowns and may improve the retrievals (Tabatabaeenejad et al. 2012). The three parameters used to simplify the scattering model are then the dielectric constant of soil, soil surface roughness, and VWC. Accordingly, the lookup table is referred to as a "data cube" (van Zyl 2011), shown in Figure 48.

The merits of using a data cube to estimate the desired unknowns are summarized below:

- It avoids numerical or analytical inversion that is often not feasible for a sophisticated forward model

- It achieves similar inversion accuracy as the numerical or analytical inversion by adopting a fine interval for the data cube axis, as demonstrated by van Zyl 2011
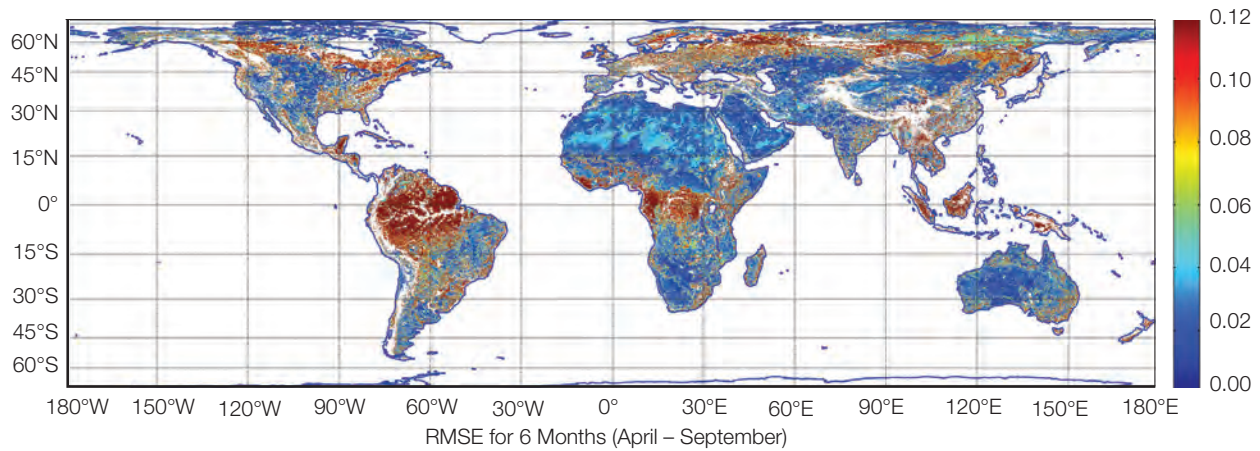
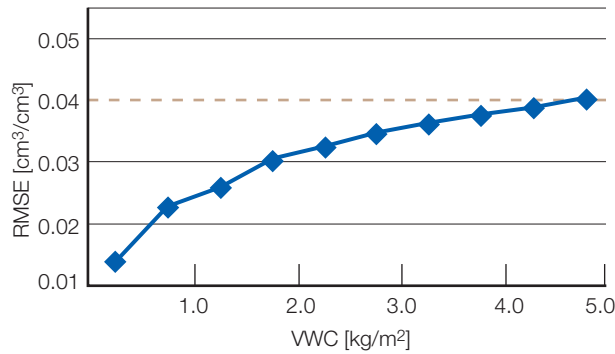**Figure 46. RMSE in soil moisture estimates at 9-km grid from GloSim for 6-month period (April–September)**



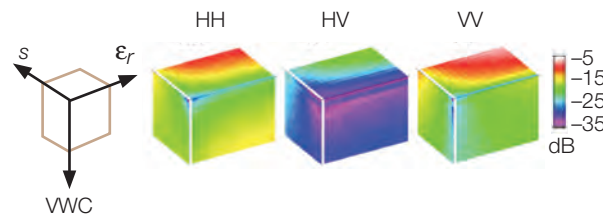**Figure 47. RMSE stratified by the mean VWC contained within 9 km from GloSim for a 6-month period (April–September).**



**Figure 48. An example of data cubes for grass surfaces.** *s* refers to rms height of isotropic surface, and rages from 0.5 to 5 cm. $\varepsilon_r$ is the real part of relative permittivity (3 to 30). VWC denotes vegetation water content (0 to 5 kg/m²).

- It simplifies forward model modification or replacement while retaining the same retrieval formula

- A new data cube can be added for a new vegetation/forest class or for the same vegetation class but at a different season

Forward models are developed for each land cover class of the International Geosphere-Biosphere Programme

(IGBP). All crops belong to one class according to the IGBP classification although their scattering characteristics may not be the same. Considering that SMAP's 3-km resolution radar will be useful in monitoring croplands that have relatively small spatial extent, four dominant crop classes of the world were selected according to the statistics provided by the Food and Agriculture Organization of the United Nations and regional crop maps. The SMAP project initially employs data cubes for 17 classes (13 IGBP classes plus 4 crops), and will expand the classes in the future if needed.

The distorted Born approximation (DBA) scattering theory is applied to model radar backscattering for a vegetation-covered soil layer, which can be qualitatively decomposed into a sum of three dominant contributions:

$$\sigma_{pq}^{t} = \sigma_{pq}^{S}(\varepsilon, s, l) \, exp \, (-2\tau_{pq}(VWC)) + \sigma_{pq}^{v}(VWC) + \sigma_{pq}^{SV}(VWC, \varepsilon, s, l) \tag{28}$$

In this expression, $\sigma_{pq}^{t}$ represents the total radar scattering cross-section in polarization pq (HH, VV, or HV for SMAP radar), $\sigma_{pq} \, exp(-2\tau_{pq})$ denotes the scattering cross-section of the soil surface modified by the two-way vegetation attenuation, $\sigma_{pq}^{v}$ is the scattering cross-section of the vegetation volume, and $\sigma_{pq}^{SV}$ represents the scattering interaction between the soil and vegetation. The quantity $\varepsilon$ is the complex dielectric constant of bare soil, $s$ and $l$ are the rms height and the correlation length for surface roughness, respectively, $\tau$ is the vegetation opacity along the slant path of the radar beam, and *VWC* is the vegetation water content. The latter two parameters can be derived from specific geometric and dielectric properties of the discrete scatterers contained within the vegetation canopy. Full details of the forward model development are provided in Burgin et al. (2011), Duan and Moghaddam (2011), Huang and Tsang (2012), Huang et al. (2010), and Kim et al. (2014).

The range of the VWC axis varies by each land cover class. To determine the range in VWC, a 10-year climatology of global VWC for each IGBP class was constructed using a 10-year climatology of MODIS normalized difference vegetation index (NDVI) information, which was subsequently converted into VWC using a set of land cover–based equations to estimate the combined foliage and stem VWC (Jackson et al. 2004; Hunt et al. 2011). The full details of the VWC estimation are available in the SMAP Vegetation Water Content Ancillary Data Report (http://smap.jpl.nasa.gov/science/dataproducts/ATBD/). The resulting VWC values range from zero to the maximum specified in Table 12.

The evaluation of the data cubes was presented elsewhere by comparing with field campaign datasets and satellite data. The list of the field campaigns used is shown in Table 12. The evaluation results are summarized as:

- Bare surface (Duan and Moghaddam 2011; Oh et al. 2002). Compared with the in situ data over a wide range of soil moisture, roughness, and correlation length, the data cubes are in good agreement for both co-pol and cross-pol with an RMSE smaller than 1.5 dB (co-pol) and 2.2 dB (cross-pol).

- Woody vegetation (Burgin et al. 2011). The fidelity of training the data cubes is such that the model predictions of evergreen needleleaf forest match the concurrent overflight observations by the Uninhabited Aerial Vehicle Synthetic Aperture Radar (UAVSAR) with a RMS difference of 0.13 (HH) and 0.09 (VV) dB. For old Jack pines, their relatively simple geometry, smooth and dry ground, and absence of thick and wet understory helped achieve the very small training error (the errors do not represent validation using independent data at present). The same modeling approach was validated for a variety of mixed forests

Table 12. Specification of the data cubes.

| IGBP class ID, class name | VWC percentile (50th, 95th, Max, kg/m$^2$) | % cover of global land | Training or Validation Reference |
|---|---|---|---|
| 1 Evergreen needleleaf | 13.2, 14.7, 16.8 | 4.0 | CanExSM10 |
| 2 Evergreen broadleaf | 17.9, 18.5, 20.1 | 10.0 | CanExSM10 |
| 3 Deciduous needleleaf | 7.3,  7.9,  8.7 | 0.6 | CanExSM10 |
| 4 Deciduous broadleaf | 12.0, 12.9, 13.6 | 1.6 | CanExSM10 |
| 5 Mixed forest | 12.0, 12.7, 13.7 | 4.7 | CanExSM10 |
| 6 Closed shrub | 1.6,  2.9,  4.1 | 0.5 | Tara Downs |
| 7 Open shrub | 0.5,  1.9,  2.8 | 18.3 | Tara Downs |
| 8 Woody savanna | 3.6,  4.4,  5.4 | 7.5 | Tara Downs |
| 9 Savanna | 2.4,  3.2,  4.2 | 7.0 | Not available |
| 10 Grassland | 0.5,  1.7,  2.9 | 9.3 | SGP99 |
| 11 Wetlands | 3.5,  4.3,  5.4 | 0.2 | CanExSM10 |
| 12 Crop  : wheat | | | Not available |
| 12        : corn | 2.5,  3.8,  4.8 | 9.0 | SMEX02 |
| 12        : soybean | | | SMEX02 |
| 12        : rice | | | Not available |
| 14 Crop/natural vegetation | 3.3,  3.9, 4.7 | 2.1 | Not available |
| 16 bare surface | n/a | 13.7 | Michigan92 |

Vegetation Water Content (VWC) was derived from the 10-year MODIS NDVI climatology. % cover of each class is compiled by the MODIS-IGBP product. "urban" and "ice" (ID=13 and 15, respectively) were not simulated. Further details of the validation datasets and results can be found in material related to various field experiments: Canadian Experiment for Soil Moisture in 2010 (CanEx-SM10) (Tabatabaeenejad et al. 2012), Southern Great Plains (SGP) 1999 (Njoku et al. 2002), Michigan 92 (Oh et al. 2002), Soil Moisture Experiment 2002 (SMEX02) (Jackson et al. 2004), Tara Downs (Burgin et al. 2011).

in Australia using independent data (JPL's Airborne SAR, AIRSAR): the co-pol RMSE is smaller than 3.4 dB even without removing any biases (Figure 5 of Burgin et al. 2011). The models for woody savanna were validated by comparison with independent spaceborne data (Phased Array type L-band SAR, PALSAR): the co-pol RMSE is better than 2.7 dB (Figure 4, Burgin et al. 2011).

- Non-woody vegetation (Kim et al. 2014). Co-pols are simulated with an accuracy of better than 1.8 dB RMSE (pasture and grass). Both co-pols are simulated with an accuracy of better than 2.9 dB RMSE (corn).

- The backscatter predictions by the data cubes were compared with observations of the scatterometer on-board the Aquarius/SAC-D satellite (Kim et al. 2013). The co-pols compare well with a mean difference of 3 dB for bare surface and 2 dB for the other classes. Part of the bias may be explained by the difference in incidence angle, a bias in input data used by the evaluation process, and the terrain slope (note the Aquarius spatial resolution is nominally 80–120 km). The standard deviation of the difference between simulation and observation is about 2.5 dB (shrubland, savanna, and grassland) and 4 dB (cropland and bare soil). Parts of the 4 dB standard deviation error may be caused by the terrain slope and diversity of crops.

## B. Baseline Retrieval Algorithm

The SMAP radar provides three independent channels (HH, VV, and HV). HV-channel measurements are reserved for possible use in correcting vegetation effects. The remaining two co-pol measurements (HH and VV) are not always sufficient to determine $s$ and $\varepsilon$. One of the main causes is the ambiguity in bare surface scattering — a wet and smooth surface may have the same backscatter as a dry and moderately rough surface. Very often the time scale of the change in $s$ is longer than that of $\varepsilon$ (Jackson et al. 1997). Then $s$ may be constrained to be a constant in time, thus resolving the ambiguity (Kim et al. 2014). The concept of a time-invariant $s$ has also been utilized in other studies (Joseph et al. 2008; Mattia et al. 2009; Verhoest et al. 2007). The SMAP baseline algorithm differs from these studies in that no ancillary or ground measurements or statistical assumptions are required to constrain $s$ and in that the algorithm may apply generally to temporally changing vegetation.

The SMAP baseline approach (Kim et al. 2012a; Kim et al. 2014) is a multichannel retrieval algorithm that searches for a soil moisture solution such that the difference between modeled and observed backscatter is minimized in the least squares sense. The algorithm estimates $s$ first

and then retrieves $\varepsilon_r$ using the estimated $s$. Vegetation effects are included by selecting the forward model's $\sigma^0$ at the VWC level given by an ancillary source or the SMAP HV measurements. The algorithm retrieves $s$ and the real part of the dielectric constant ($\varepsilon_r$) using a time series of $N$ co-pol backscatter measurements: $\sigma^0_{HH}(t_1)$, $\sigma^0_{VV}(t_1)$, $\sigma^0_{HH}(t_2)$, $\sigma^0_{VV}(t_2)$, ... , $\sigma^0_{HH}(t_N)$, and $\sigma^0_{VV}(t_N)$. There are thus $2N$ independent input observations and $N+1$ unknowns consisting of $N$ $\varepsilon_r$ values and one $s$ value. Note that the VWC provided by ancillary information is allowed to be varying throughout the time series.

Radar backscattering coefficients before conversion to decibels can be modeled as Gaussian random variables (Ulaby et al. 1986a) to account for speckle and thermal noise effects. Assuming sufficient integration following power detection, the backscattering coefficient after conversion to decibels can also be modeled as a Gaussian random variable. Because SMAP will observe HH and VV returns at slightly different center frequencies, the effects of speckle and thermal noise on these measurements are statistically independent. Statistical independence of speckle in measurements at differing time steps is also expected. These facts and a maximum likelihood formulation motivate least-squares retrieval approaches based on the average of individual error terms. It is noted that calibration, radio frequency interference, and other error sources may produce correlated error terms. The systematic and correlated components from these sources will be corrected. Any residuals may impact overall algorithm performance and are modeled as uncorrelated Gaussian noise (although they may still contain correlated noise).

The retrieval algorithm therefore minimizes the cost function ($C$):

$$C (s, n, \varepsilon_{r1}, \varepsilon_{r2}, ..., \varepsilon_{rN})$$
$$= w_{1,HH} (\sigma^0_{HH} (t_1) - \sigma^0_{HH, fwd} (s, n, \varepsilon_{r1}))^2$$
$$+ w_{1,VV} (\sigma^0_{VV} (t_1) - \sigma^0_{VV, fwd} (s, n, \varepsilon_{r1}))^2$$
$$+ w_{1,HH} (\sigma^0_{HH} (t_2) - \sigma^0_{HH, fwd} (s, n, \varepsilon_{r2}))^2$$
$$+ w_{1,VV} (\sigma^0_{VV} (t_2) - \sigma^0_{VV, fwd} (s, n, \varepsilon_{r2}))^2$$
$$+ ..$$
$$+ w_{1,HH} (\sigma^0_{HH} (t_N) - \sigma^0_{HH, fwd} (s, n, \varepsilon_{rN}))^2$$
$$+ w_{1,VV} (\sigma^0_{VV} (t_N) - \sigma^0_{VV, fwd} (s, n, \varepsilon_{rN}))^2$$
$$= \frac{1}{N} \left[ \begin{array}{l} E_1 (\sigma^0_{HH} (t_1), \sigma^0_{VV} (t_1), s, n, \varepsilon_{r1}) + \\ E_2 (\sigma^0_{HH} (t_2), \sigma^0_{VV} (t_2), s, n, \varepsilon_{r2}) + .. \\ E_N (\sigma^0_{HH} (t_N), \sigma^0_{VV} (t_N), s, n, \varepsilon_{rN}) \end{array} \right]$$

(29)

where values from observations and from the forward model are denoted as $\sigma^0$ and $\sigma^0_{fwd}$ (both in dB), respec-

tively. An additional parameter $n$ is included above (so that a total of $N+2$ parameters are now involved) to account for bias discrepancies between data-cube simulations and actual vegetation properties. Again, note that the above formulation can accommodate temporal change in VWC, because $\sigma^0_{fwd}$ is chosen by the VWC value available at each time. The weights $w_i$ in the cost function are associated with differing errors in the cross-section measurement as a function of time or polarization, and the subscript $i$ indexes the time sequence. Uniform weights are utilized in the results to be shown, based on the measurement errors of each channel at each time step (Kim et al. 2012a). The cost function then is an average of terms $E_i$ that depend individually on only three (e.g., $s$, $n$, and $\varepsilon_{r1}$) of the $N+2$ parameters. This allows the minimum of the cost function to be located without a search over the complete $N+2$ dimensional space.

Because $s$ and $n$ are the only parameters in common among the terms of the cost function, the retrieval algorithm considers all possible values of $s$ and $n$. For each $s$ value, values of $\varepsilon_{ri}$ are found that minimize each $E_i$ term individually (i.e., $N$ one dimensional searches are performed), and the resulting average of $E_i$ values is the minimum value of the cost function for the assumed value of $s$, notated $C_{min}(s)$. The retrieved estimate of $s_{rtr}$ is determined as the value of $s$ that minimizes $C_{min}(s)$, and retrieved estimates of soil moisture are the corresponding $\varepsilon_{ri}$ values determined when constructing $C_{min}(s_{rtr})$. Because $\sigma^0$ is a monotonic function of $s$, the minimum is unique with respect to $s$. $\sigma^0$ is also a monotonic function with respect to $\varepsilon_r$. Therefore, the minimum associated with $\varepsilon_{ri}$ is unique for a given $s$.

The least-square minimization of Eq. 29 is implemented using the forward model data cube (generated using the models described in Figure 48). The current baseline retrieval is generally independent of the correlation length (that therefore is not a part of the data cube) as long as the soil surface is not too rough (Kim et al. 2012a).

## C. Algorithm Flow

The algorithm flow is presented in Figure 49. The processor reads in 1-km resolution $\sigma^0$ from the SMAP L1C_S0 (1-km radar data). The 1-km data in natural units are aggregated onto a 3-km EASE2 grid, during which various quality flags are applied. The complete set of the quality flags is presented in the SMAP Data Specification Document. Among these, three quality flags are derived using the 3-km $\sigma^0$: freeze/thaw (F/T) state (see Chapter 6 for details), radar vegetation index (RVI), and transient water body. Described briefly, these three parameters contribute to SMAP's soil moisture retrieval as follows:

- Based on the F/T state, soil moisture will be retrieved only for unfrozen ground

- The RVI is the normalized ratio of cross-pol $\sigma^0$ to the total power (Kim and van Zyl 2001), and is designed as a normalized index of the vegetation amount. For rice and soybeans, the RVI may provide an estimate of VWC (Kim et al. 2012b), which in turn is under consideration for use in choosing the vegetation axis of the data cube during the retrieval.

- The spatial coverage of inland open water bodies is not yet well monitored (Alsdorf et al. 2007) and highly variable in time. Due to the difference in brightness temperature and $\sigma^0$ between water and land surfaces, accurate knowledge of a transient water body is important for SMAP's soil moisture retrieval. The presence of transient water bodies may be retrieved with multi-polarized L-band radar observations (Kim et al. 2011). Accordingly, water-body information that is synchronized and simultaneous to SMAP's soil moisture retrieval will be derived with SMAP's radar data.

Static and dynamic ancillary data are sampled for each pixel. The complete set of the ancillary data is defined in "SPS-SPDM Interface Memorandum for the L2_SM_A" (SMAP JPL document, SMAP-860-026-12 D, May 20, 2013). $\sigma^0$ values from past time stamps are sampled and used by the time-series algorithm. For each 3-km pixel, land cover class information is obtained from annual ancillary data. The land cover information allows the determination of an appropriate data cube for each pixel. Finally, the retrieval over all land cover classes is spatially assembled to create a half-orbit output, followed by the conversion from the dielectric constant to soil moisture.

## D. Alternate Algorithms

Two alternative algorithms have been implemented. The official product will include only the retrieval output from the baseline algorithm. However, internally the soil moisture retrieval outputs from the baseline and alternative algorithms will be continuously assessed and compared with one another.

### Change detection by Wagner et al.

A radar-only time-series algorithm (Wagner et al. 1999) was proposed to retrieve an index of $m_v$ change using C-band ERS scatterometer data. The index ($M_s$) is given by

$$M_S = (\sigma^0 (t) - \sigma^0_{dry}) / (\sigma^0_{wet} - \sigma^0_{dry}), \qquad (30)$$
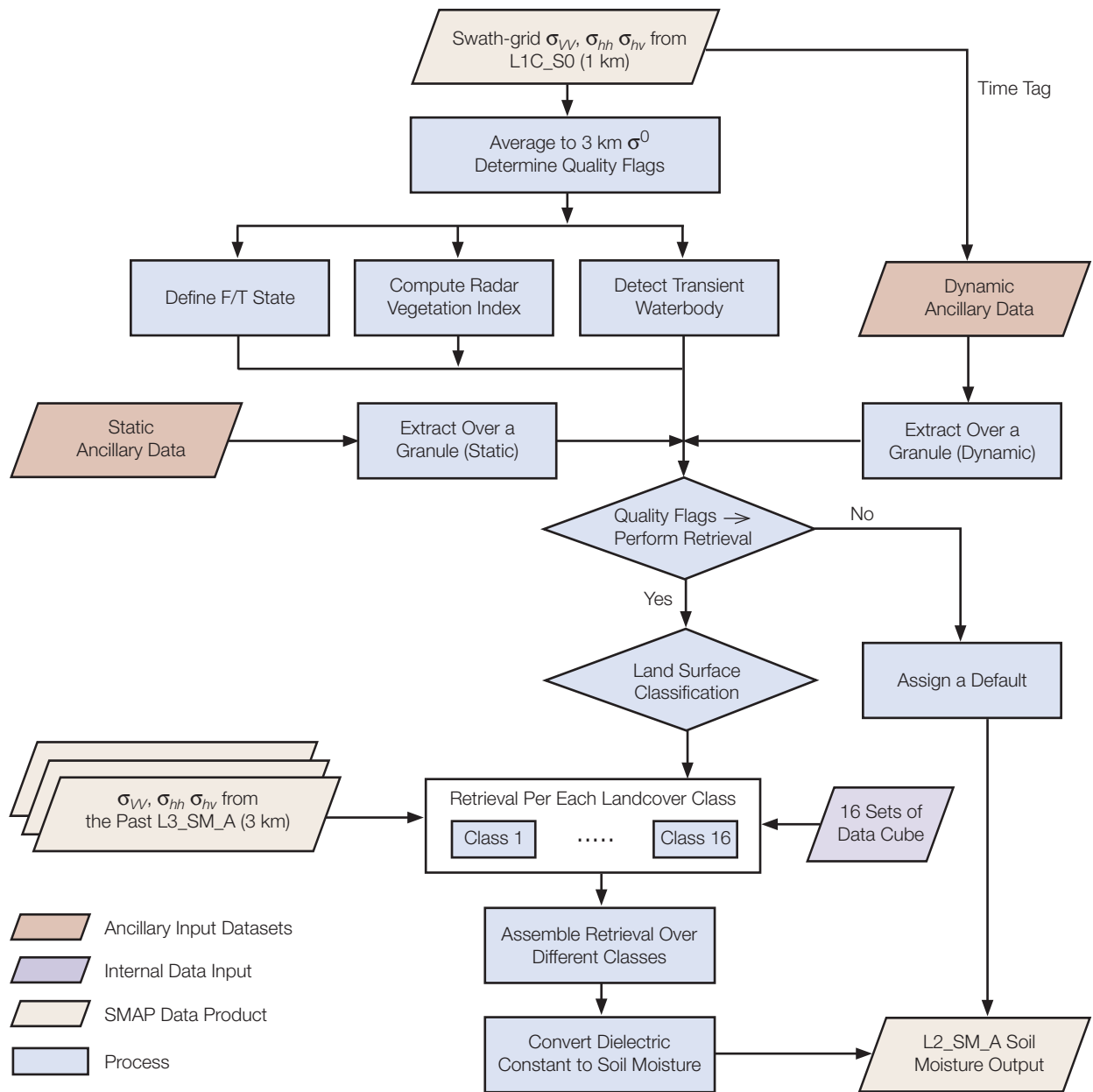
**Figure 49. Flow of the baseline algorithm. F/T stands for freeze/thaw.**

where $\sigma^0(t)$ is the observation at one time. $\sigma^0_{wet}$ and $\sigma^0_{dry}$ are two extreme values of $\sigma^0$ of a pixel, which may be derived from a multi-year database of radar records. At least one year worth of the SMAP data are needed to derive the two extreme values of $\sigma^0$. $M_S$ is an index ranging from 0 to 1, and can distinguish 5 different levels of soil moisture states. Later studies retrieved the index varying continuously, and correction of the vegetation effects was applied (Naeimi et al. 2009). Most of the studies were applied to low-speckle scatterometer data with the spatial resolution of 25 km or larger. When applied to the 1-km resolution data from the ENVISAT Advanced SAR (ASAR), the speckle began to impact the performance even at 3-km resolution; 3–10 km resolution was recommended for reliable retrieval of the index (Pathe et al. 2009). The algorithm has so far been implemented with vertical polarization due to availability. The sensitivity to soil moisture may be stronger with horizontal polarization thanks to the double-bounce process than with vertical polarization. Both polarizations will be studied for SMAP.

### Change-detection based on Kim and van Zyl

The algorithm is based on concepts developed in Kim and van Zyl 2009. After the SMAP radar data are accumulated for a moderate time period (nominally 6 months), an expression will be derived to relate the backscattering cross-section to soil moisture as

$$m_v = f(\sigma_{hh}, \sigma_{vv}) \tag{31}$$

where the normalized radar cross-sections are expressed in decibels. Since this expression depends on the biomass level, the cross-polarization will be used to compensate the biomass variation over time; how this will be implemented is being studied. $f()$ is given by

$$f(\sigma_{hh}, \sigma_{vv}) = C_0 + C_1 \frac{\sigma_{hh} + \sigma_{vv}}{2} \tag{32}$$

The two coefficients for each pixel will be determined using the expected minimum and maximum values for soil moisture and the time-series backscattering cross-section data. The minimum and maximum values for soil moisture may be estimated using soil porosity models that are commonly available. Accommodating different vegetation phenology during the implementation of the above relationship remains as a task. The obvious assumption contained in Equation 32 is that there is a linear relationship between the radar cross-sections and the soil moisture. However, simulated data suggests that this relationship is nonlinear. Ground radar and airborne data will be used to derive the final expression for the function $f(\sigma_{hh}, \sigma_{vv})$. The slowly varying backscattering cross-section component due to the biomass variation will be estimated and compensated using the cross-polarization backscattering cross-section. Ground radar measurements will help derive the expression before the SMAP instrument is launched. However, since the ground measurements are limited, various vegetation environments will be considered with simulated data. When the two extreme conditions (completely dry and wet) of the soil moisture and radar backscatter are known exactly, a test with a corn field experiment shows that the soil moisture may be retrieved with an error of 0.026 cm³/cm³. When the errors in the two extreme values are simulated with the random noise, the retrieval error reaches 0.05 cm³/cm³ (Kim and van Zyl 2009).

### E. Algorithm Performance and Error Budget

The performance of the baseline algorithm is evaluated in the pre-launch phase using (1) global representative simulations on the SMAP Testbed at JPL and (2) field experiment data that offer the radar backscatter and ground truth observations. The implementation of the complete pre-launch Cal/Val process is described in the "SMAP Calibration and Validation Plan" (JPL D-52544, Apr. 2011).

The performance of the retrieval approach is evaluated below. The main sources of retrieval error are (a) radar measurement error (speckle and calibration of thermal effect after removing any drift), (b) data-cube modeling error including the contribution from the scheme of using the VWC to represent many vegetation parameters, (c) dielectric model error that is estimated to be about 0.02 cm³/cm³ (Mironov et al. 2009), and (d) spatial heterogeneity in vegetation. The source (a) is simulated below by modeling the radar measurement error as a Gaussian random variable (Figure 7.15, Ulaby et al. 1986b) with a Monte Carlo approach, because an operating SMAP-like radar is not available at present. The assessment of the sources (b–c) will be presented below using a field campaign dataset over grass vegetation. Unlike the radar measurement uncertainty, statistical characterization (e.g., zero-mean Gaussian distribution) of data-cube error and dielectric model error is not straightforward. Furthermore, separating the field validation result into the contributions by the individual sources (data cube, VWC, and dielectric conversion) would require dedicated experiments that are not available at present. The source (d) may occur within a 3-km SMAP pixel, but not in the homogeneous field environment used below. The retrieval algorithm to be implemented for SMAP will allow for pixel heterogeneity by modeling heterogeneous pixel scattering as a combination of each of the component class data cubes.

For the performance analysis through simulation, the specified error allocation of SMAP radar measurements was used. The total error in $\sigma^0$ measurement for a 3-km × 3-km pixel is 0.71 dB (HH and VV) and 1.06 dB (HV) at the worst-case cross-track position after combining fore-scan and aft-scan records, and for a scene $\sigma^0$ of –25 dB (HH and VV) and –30 dB (HV). At the best-case cross-track position, $\sigma^0$ errors are 0.58 dB (HH and VV) and 1.01 dB (HV). The "total" error includes speckle, residual calibration, and residual radio-frequency contamination. The noise floor allocation varies from –28.5 dB to –31.5 dB (very similar between co- and cross-polarization) depending on the swath position. The "current best estimate" of radar measurement errors is better than the allocation. According to the analysis of the theoretical antenna pattern for SMAP, the cross-coupling of co-polarization into cross-polarization is estimated to 0.2 dB.

The details of the Monte Carlo simulation are available in Kim et al. (2013). The retrieval results are presented in Figure 50 for the grass and shrub data cubes. Each case of the Monte Carlo analyses is defined by different values of dielectric constant, surface roughness, and VWC. In the grass case, the retrieval error is better than 0.06 cm³/cm³ except for VWC greater than 2 kg/m² and $m_v$ larger than 0.3 cm³/cm³. Generally the $m_v$ retrieval error increases with the surface soil moisture, reflecting

the reduced sensitivity (Kim et al. 2012a). Similarly, the $m_v$ retrieval error increases with VWC as a result of the attenuation by vegetation. In the shrub case (Figure 50), in comparison, the woody stems produce double-bounce scattering that becomes stronger when the soil surface becomes wet and a sizable amount of stems exist. As a result, at $m_v$ of about 0.3 cm³/cm³ in the shrub case, the $m_v$ retrieval becomes more accurate for higher VWC; such is not the case for grass or the dry-soil shrubs.

The results of the Monte Carlo study are organized as a function of VWC in Figure 51 covering a large variety of

land cover classes. For non-woody classes such as grass and soybean, the $m_v$ retrieval error increases with VWC due to the vegetation attenuation; for woody-vegetation (shrub and woody savanna), the $m_v$ retrieval improves with VWC, by benefiting from the double bounce process. The double-bounce process depends strongly on ground soil moisture and ground reflectivity, thus allowing the soil moisture retrieval. Corn, evergreen needle, and deciduous broadleaf classes also have a dominant vertical structure for trunks or stems, and the double-bounce mechanism again helps the retrieval. The two forest classes (evergreen broadleaf and deciduous needle) were modeled to have
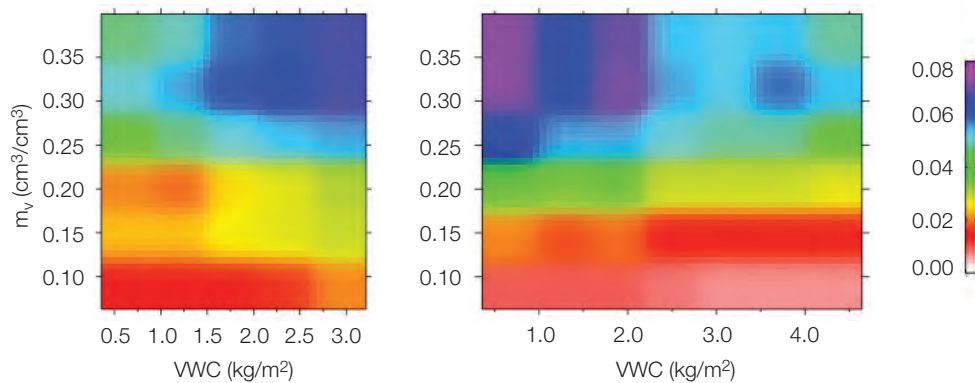


Figure 50. RMS errors in $m_v$ retrieval (cm³/cm³) given by the Monte Carlo simulation of the radar measurement error (13% for the signal, 1σ) and VWC uncertainty (10%, 1σ): (left) grass (right) shrub. The cases represent $s$ of 1 cm and the correlation length to the RMS height has the ratio of 10. (From Kim et al. 2013.)
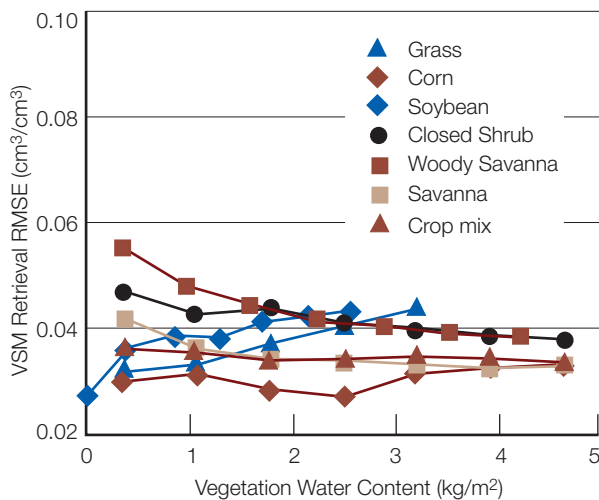


Figure 51. Monte Carlo simulation of the radar measurement error (13% for the signal, 0.5 dB) on the data-cube $m_v$ retrieval. Each point on a curve is an average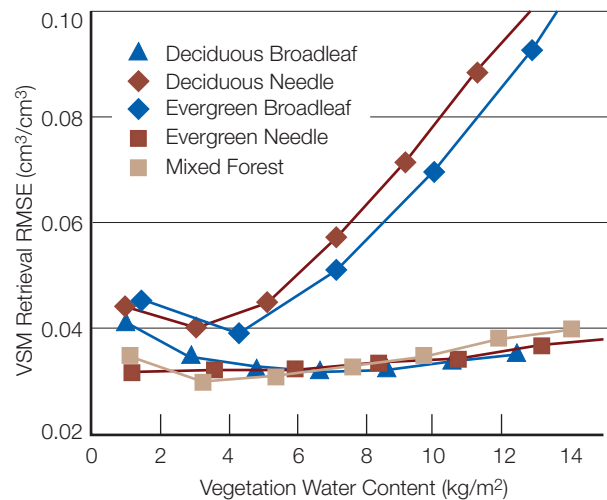 of $m_v$ RMSE from the Monte Carlo simulation (e.g., Figure 50) over roughness values of 0.5 cm to 4 cm, and soil moisture truth ranging from 0.05 to 0.45 cm³/cm³. (From Kim et al. 2013.)

prominent non-vertical trunk structures according to the current simulation, producing a weak double-bounce return. Furthermore, the geometry of the branch structure within the canopy layer becomes much denser as VWC increases, compared with the conifer case. As a result, the attenuation of the soil moisture signal by the canopy layer increases with VWC. Therefore, the sensitivity of $\sigma^0$ to $m_v$ decreases and $m_v$ retrieval deteriorates. The apparent difference in retrieval performance among the five forest classes is due also to representing a forest class with only a few species (because of limited experimental data). In the future, the forest classes will be further divided into more specific ones and the retrieval results fine-tuned. The bare surface case shows retrieval performance better than the above vegetated cases (0.028 cm³/cm³ at 0 kg/m² VWC for the soybean class in Figure 51). The retrieval errors increase with VWC for grass and soybean, because $\sigma^0$ becomes less sensitive to $m_v$ towards high VWC. The worst-case scenario for SMAP radar measurement noise is 0.7 dB, in which case the retrieval RMSE in Figure 51 increases slightly by about 0.005 cm³/cm³ for most of the IGBP classes, when model errors are not considered in the budget.

### F. Algorithm Evaluation: Field Campaign Data

The baseline algorithm was tested with

- Scatterometer data collected over four bare surface sites near Ypsilanti, Michigan during a 2-month period (Oh et al. 2002). The observed $m_v$ at four sites ranges from 0.06 to 0.3 cm³/cm³. The surface roughness is time-invariant at each site, but changes from 0.55 cm to 3.5 cm rms height from site to site and the ratio of correlation length to the roughness varies from 4 to 15.

- The airborne Passive/Active L-band Sensor (PALS) data collected over pasture fields during the 1999 Southern Great Plains (SGP99) experiment in the Little Washita watershed region, Chichasha, Oklahoma, USA (Colliander et al. 2012; Jackson et al. 1999). Across six fields, surface roughness changed from 0.3 to 0.9 cm, and VWC varied from 0.1 to 0.5 kg/m². In situ soil moisture varied from 0.05 to 0.3 cm³/cm³ temporally and spatially.

- UAVSAR data over seven agricultural types and 50 fields in Winnipeg, Canada in 2012 (McNairn et al. 2013) (SMAPVEX12). Over the 2-month period, the soil moisture was recorded from dry to 0.6 cm³/cm³. The surface roughness is time-invariant at each site, but varies from 0.3 cm to 2.0 cm RMS height from site to site and the ratio of correlation length to the roughness varies from 6 to 88. The crops grew fully from seeds and the VWC reached maximum (e.g., 4.2 kg/m² for corn) during the observed time series.

Figure 52(a) shows that the bare surface retrieval has an RMSE of 0.044 cm³/cm³ after compiling the retrievals over the four in situ locations. The retrieval over the pasture surface has an RMSE of 0.054 cm³/cm³ (Figure 52b). The slightly larger error for the pasture surface may reflect the effect of vegetation.
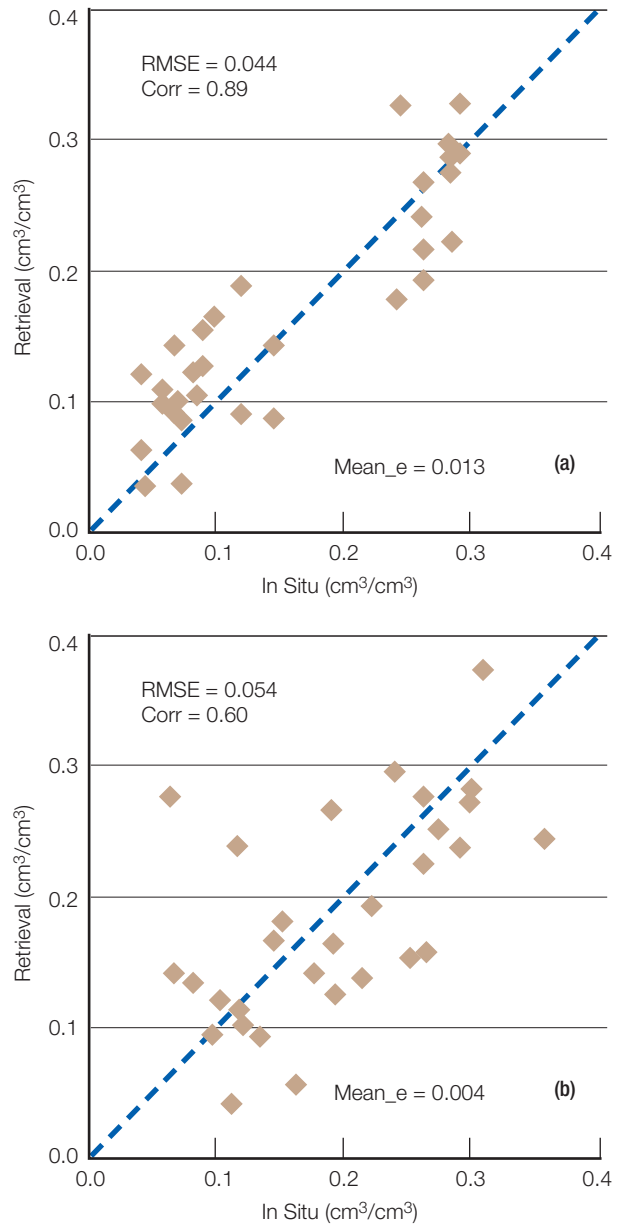


Figure 52. RMS errors in soil moisture retrieval using the baseline algorithm, assessed with (a) the Ypsilanti bare surface data and (b) the SGP99 pasture surface data. (From Kim et al. 2012a; Kim et al. 2014.)

Two of SMAP's candidate algorithms were applied to the data from the SMAPVEX12 campaign, the baseline and the change index method by Wagner et al. (Figure 53). To apply the baseline algorithm, the UAVSAR data were normalized to SMAP's 40° angle by the histogram method of Mladenova et al. (2012). The correlation between retrieved and measured $m_v$ was higher when biomass was stable over time (spring wheat). For bean crop, the retrieved index (based on VV) correlated with the measured $m_v$ better than the data-cube retrieval (based on HH and VV). This suggests that VV backscatter responds to relative changes in in situ $m_v$ more strongly than when dual-polarizations are used together. However, both VV and HH backscatter are needed to retrieve absolute soil moisture. Corn data cubes were able to correct for the effect of the significant temporal change in vegetation; as a result, the correlation of its retrieval is better than that of the index approach. The errors in the baseline retrieval ranged from 0.037 to 0.086 cm³/cm³ over these four fields.

Based on the above results, the error budget is derived in Table 13. The Monte Carlo analyses presented in Figure 51 assess the errors due to the $K_p$ noise and the vegetation water content uncertainty. However, the analysis does not capture forward model errors. The conversion from dielectric constant to soil moisture is accurate to about 0.02 cm³/cm³ (Mironov et al. 2009), which would not affect the total error budget when added to the total error by root square sum. The in situ evaluation with the airborne radar data described in Figure 52 and Figure 53 accounts for the errors associated with data-cube modeling and dielectric conversion (as well as the errors in in situ measurements of soil moisture, both instrumental and scaling). A small degree of heterogeneity exists within the airborne radar footprint, which would also contribute to the in situ evaluation result. The effect of scaling and heterogeneity within the 3-km pixel will be studied further.
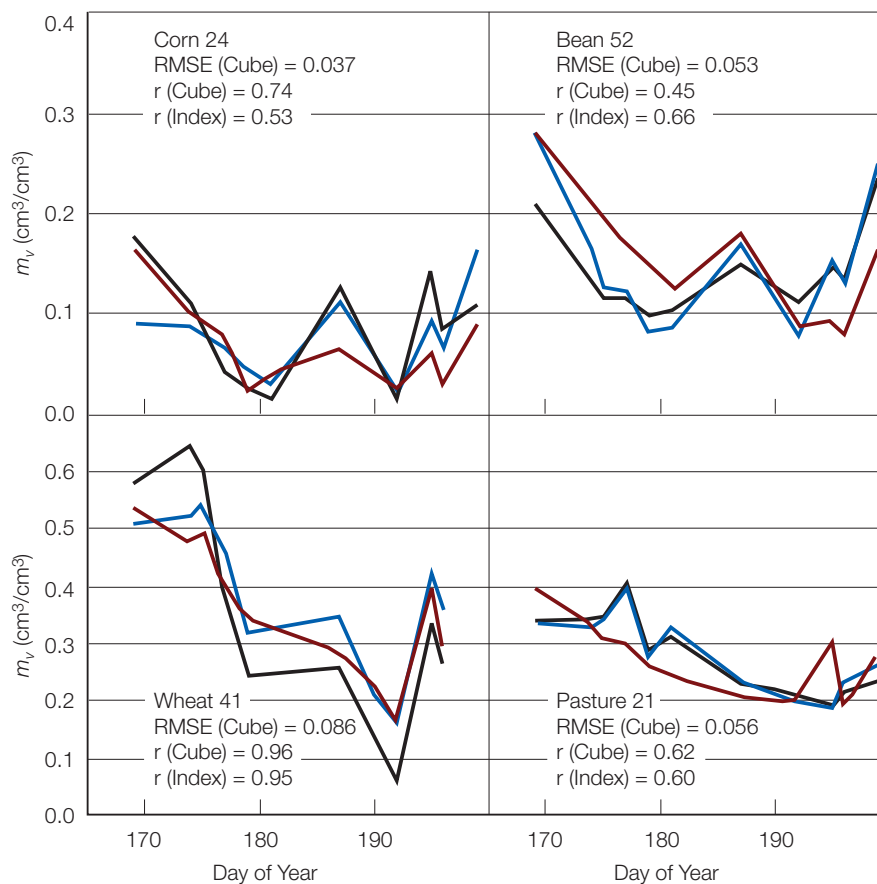


Figure 53. Preliminary retrieval of soil moisture for one field per crop type where SMAP's forward scattering models are available: in situ moisture (red), baseline retrieval (black), and change index (blue). The legend (top to bottom) reads: crop type and field number, RMS error of the data-cube retrieval in cm³/cm³ units, and correlation (r) between retrieval and in situ $m_v$. The retrieved change index was scaled to match in situ $m_v$. (From McNairn et al. 2013.)

**Table 13. Error budget for the baseline algorithm.**

| Error sources | Budget ($cm^3$/$cm^3$) | |
| --- | --- | --- |
| | Outer swath edge | Inner swath edge |
| A) Kp 0.75-1.0 dB 1$\sigma$ error (1$\sigma$, co-pol, fore look) | 0.035 | 0.043 |
| B) Vegetation water content error (1$\sigma$, 10%) | 0.01 | |
| C) Forward model error (data cubes and heterogeneity) | 0.04 | |
| D) Dielectric model uncertainty | 0.02 | |
| E) Soil texture: 5% error | 0.004 | |
| $m_V$ retrieval error up to VWC of ~3 kg/$m^2$ | 0.058 | 0.063 |

The $K_p$ and VWC errors are modeled with Gaussian random variables with zero mean. The soil moisture retrieval error is obtained from the Monte Carlo analysis in Figure 51. Number of the pair of HH and VV radar backscatter used as time-series input (6, equivalently 18 days).

## VI. Ancillary Data

Ancillary data are data acquired from external sources that are required as inputs to the SMAP retrieval algorithms in generation of the SMAP data products. Ancillary data needed by the SMAP mission fall into two categories: (a) static ancillary data, which do not change substantially over the course of the mission, and (b) dynamic ancillary data that require periodic updates on time frames ranging from seasonal to daily. Static data include parameters such as permanent masks (land / water / forest / urban / mountain), the grid cell average elevation and slope derived from a DEM, permanent open water fraction, and soils information (primarily sand and clay fraction). Dynamic ancillary data include land cover, surface roughness, precipitation, vegetation parameters, and effective soil temperatures. Ancillary data are by definition external to SMAP. However, there is some sequential transfer of parameters between algorithms as needed for downstream processing. For example, the SMAP HiRes radar data product provides key pieces of dynamic information to the L2_SM_P algorithms such as open water fraction and a frozen ground flag (see L2_SM_A and L3_FT_A ATBDs).

Table 14 lists the 14 ancillary data parameters required by one or more of the SMAP L2/3 product algorithms along with the primary source of information for that parameter (in all cases, there are alternative options for these parameters from climatological datasets, forecast models, or datasets acquired in past or current missions). The choice of which ancillary dataset to use for a particular SMAP product is based on a number of factors including its availability and ease of use, its inherent error and resulting impact on the overall soil moisture or freeze/thaw retrieval accuracy, and its compatibility with similar choices made by the SMOS mission. Latency, spatial resolution, temporal resolution, and global coverage are also important. The choice of a primary source for each of the fourteen ancillary data parameters is fully documented in individual SMAP Ancillary Data Reports which are available to the user community.

In most cases, the raw ancillary data must go through a number of pre-processing steps to convert them to the appropriate quantity and format for use by the SMAP algorithms. For example, the NDVI must be converted into vegetation water content, ECMWF or GMAO temperatures must be temporally interpolated to the time of SMAP observations, and all of the static ancillary data must be resampled to the same 3-, 9-, and 36-km EASE grids as the SMAP output products. While the exact types of ancillary datasets needed are specific to a given retrieval algorithm, all standard L2/3 products require some ancillary datasets to meet the specified retrieval accuracies.

## References

Alsdorf, D. E., E. Rodriguez, and D. P. Lettenmaier, "Measuring surface water from space," *Rev. Geophys.*, 45, RG2002, 2007. dx.doi.org/10.1029/2006RG000197

Balenzano, A., F. Mattia, G. Satalino, and M. W. J. Davidson, "Dense temporal series of C- and L-band SAR data for soil moisture retrieval over agricultural crops," *IEEE J. Sel. Topics Appl. Earth Observ.*, 4, pp. 439–440, 2011.

Basharinov, A. and A. Shutko, "Simulation studies of the SHF radiation characteristics of soils under moist conditions," *NASA Tech. Transl.*, TT F-16, 1975.

Bindlish, R., T. J. Jackson, R. Sun, M. Cosh, S. H. Yueh, and S. Dinardo, "Combined passive and active microwave observations of soil moisture during CLASIC," *IEEE Geosci. Remote Sens. Lett.*, 6, pp. 644–648, 2009.

Burgin, M., D. Clewley, R. Lucas, and M. Moghaddam, "A generalized radar backscattering model based on wave theory for multilayer multispecies vegetation," *IEEE Trans. Geosci. Rem. Sens.*, 49, pp. 4832–4845, 2011.

Choudhury, B. J., T. J. Schmugge, A. Chang, and R. W. Newton, "Effect of surface roughness on the microwave emission from soil," *J. Geophys. Res.*, 84(C9), pp. 5699–5706, 1979.

**Table 14. Ancillary data parameters and primary sources.**

| 1 | Soil Temperature | GMAO (or ECMWF) forecast temperatures |
|---|---|---|
| 2 | Surface Air Temperature | GMAO (or ECMWF) forecast temperatures |
| 3 | Vegetation Water Content  (VWC) | MODIS NDVI |
| 4 | Sand and Clay Fraction | Combination of HWSD (global), regional datasets (STATSGO-US, ASRIS-Australia, NSD-Canada), FAO |
| 5 | Urban Area | GRUMP dataset — Columbia University |
| 6 | Open Water Fraction | A priori static-water fraction from MODIS MOD44W to be used in conjunction with open-water fraction from SMAP HiRes radar |
| 7 | Crop Type | Combination of USDA Cropland Data Layer, AAFC-Canada, Ecoclimap-Europe |
| 8 | Land Cover Class | MODIS IGBP; crop class will be further subdivided into four general crop types |
| 9 | Precipitation | ECMWF total precipitation forecasts (or GPM once launched) |
| 10 | Snow | Snow and Ice Mapping System (IMS) — NOAA |
| 11 | Mountainous Area | Combination of SRTM, Alaska USGS DEM, Canada Geobase DEM, and GTOPO30 |
| 12 | Permanent Ice | MODIS IGBP class |
| 13 | Vegetation Parameters ($b$, $\omega$, and $\tau$) | Land cover-driven table lookup |
| 14 | Roughness Parameter ($h$) | Land cover-driven table lookup |

Colliander A., S. Chan, S. Kim, N. Das. S. Yueh, M. Cosh, R. Bindlish. T. Jackson, and E. Njoku, "Long Term Analysis of PALS Soil Moisture Campaign Measurements for Global Soil Moisture Algorithm Development," *Remote Sensing of Environment*, 121, pp. 309–322, 2012.

Crow, W., T. Chan, D. Entekhabi, P. Houser, T. Jackson, E. Njoku, P. O'Neill, JC Shi, and X. Zhan, "An observing system simulation experiment for SMAP radiometer soil moisture products," *IEEE Trans. Geosci. Rem. Sens.*, 43(6), pp. 1289–1303, 2005.

Das, N. N., D. Entekhabi, and E. G. Njoku, "An Algorithm for merging SMAP radiometer and radar data for high resolution soil moisture retrieval," *IEEE Trans. Geosci. Rem. Sens.*, 2011. dx.doi.org/10.1109/TGRS.2010.2089526

Das, N. N., D. Entekhabi, E. G. Njoku, J. C. Shi, J. T. Johnson, and A. Colliander, "Tests of the SMAP combined radar and radiometer algorithm using airborne field campaign observations and simulated data," *IEEE Trans. Geosci. Rem. Sens.*, vol. 52, pp. 2018–2028, 2014.

de Jeu, R., T. Holmes, R. Panciera, and J. Walker, "Parameterization of the Land Parameter Retrieval Model for L-Band Observations Using the NAFE'05 Dataset," *IEEE Geoscience and Remote Sensing Letters*, 6 (4), pp. 630–634, October 2009.

Dobson, M. C., F. T. Ulaby, M. T. Hallikainen, and M. A. El-Rayes, "Microwave dielectric behavior of wet soil – Part II: Dielectric mixing models," *IEEE Trans. Geosci. Rem. Sens.*, vol. GE-23, pp. 35–46, 1985.

Duan, X., and M. Moghaddam, "Electromagnetic scattering from arbitrary random rough surfaces using stabilized extended boundary condition method (SEBCM) for remote sensing of soil moisture," *IEEE Trans. Geosci. Rem. Sens.*, 50, pp. 87–103, 2011.

Dubois, P. C., J. J. van Zyl, and E. T. Engman, "Measuring soil moisture with imaging radars," *IEEE Trans. Geosci. Rem. Sens.*, 33, pp. 915–926, 1995.

Entekhabi, D., E. G. Njoku, P. E. O'Neill, K. H. Kellogg, W. T. Crow, W. N. Edelstein, J. K. Entin, S. D. Goodman, T. J. Jackson, J. Johnson, J. Kimball, J. R. Piepmeier, R. D. Koster, N. Martin, K. C. McDonald, M. Moghaddam, S. Moran, R. Reichle, J. C. Shi, M. W. Spencer, S. W. Thurman, L. Tsang, and J. V. Zyl, "The Soil Moisture Active Passive (SMAP) Mission," *Proceedings of the IEEE*, 98, pp. 704–716. 2010.

Fagerlund, E., B. Kleman, L. Sellin, and H. Svensson, "Physical Studies of Nature by Thermal Mapping," *Earth-Science Reviews*, 6, pp. 169–180, 1970.

Huang, S., and L. Tsang, "Electromagnetic scattering of randomly rough soil surfaces based on numerical solutions of Maxwell equations in 3 dimensional simulations using a hybrid UV/PBTG/SMCG method," *IEEE Trans. Geosci. Rem. Sens.*, 50, pp. 4025–4035. 2012.

Huang, S., L. Tsang, E. G. Njoku, and K. S. Chen, "Backscattering coefficients, coherent reflectivities, emissivities of randomly rough soil surfaces at L-band for SMAP applications based on numerical solutions of Maxwell equations in three-dimensional simulations," *IEEE Trans. Geosci. Rem. Sens.*, 48, pp. 2557–2567, 2010.

Hunt, E. R., L. Li, M. T. Yilmaz, and T. J. Jackson, "Comparison of vegetation water contents derived from shortwave-infrared and passive-microwave sensors over central Iowa," *Remote Sens. Environ.*, 115, pp. 2376–2383, 2011.

Jackson, T. and J. Kimball, "SMAP Mission Science Issues Associated with Overpass Time," SMAP Science Document No. 003, Jet Propulsion Laboratory, March 31, 2009.

Jackson, T. J. and T. J. Schmugge, "Vegetation effects on the microwave emission from soils," *Rem. Sens. Environ.*, vol. 36, pp. 203–212, 1991.

Jackson, T. J., "Measuring surface soil moisture using passive microwave remote sensing," *Hydrol. Process.*, vol. 7, pp. 139–152, 1993.

Jackson, T. J., D. Chen, M. Cosh, F. Li, M. Anderson, C. Walthall, P. Doriaswamy, and E. R. Hunt, "Vegetation water content mapping using Landsat data derived normalized difference water index for corn and soybeans," *Remote Sens. Environ.*, 92, pp. 475–482, 2004.

Jackson, T. J., D. M. Le Vine, A. Y. Hsu, A. Oldak, P. J. Starks, C. T. Swift, J. D. Isham, and M. Haken, "Soil moisture mapping at regional scales using microwave radiometry: the Southern Great Plains hydrology experiment," *IEEE Trans. Geosci. Rem. Sens.*, 37, pp. 2136–2151, 1999.

Jackson, T. J., H. McNairn, M. A. Weltz, B. Brisco, and R. Brown, "First order surface roughness correction of active microwave observations for estimating soil moisture," *IEEE Trans. Geosci. Rem. Sens.*, 35, pp. 1065–1069, 1997.

Jackson, T. J., R. Bindlish, M. H. Cosh, T. Zhao, P. J. Starks, D. D. Bosch, M. Seyfried, M.S. Moran, D.C. Goodrich, Y. H. Kerr, and D. Leroux, "Validation of Soil Moisture and Ocean Salinity Soil Moisture (SMOS) Over Watershed Networks in the U.S.," *IEEE Trans. Geosci. Rem. Sens.*, pp. 1530–1543, 2012.

Joseph, A. T., R. van der Velde, P. E. O'Neill, R. H. Lang, and T. Gish, "Soil moisture retrieval during a corn growth cycle using L-band (1.6GHz) radar observations," *IEEE Trans. Geosci. Rem. Sens.*, 46, pp. 2365–2374, 2008.

Kerr, Y., P. Waldteufel, P. Richaume, I. Davenport, P. Ferrazoli, and J.-P. Wigneron, "SMOS Level 2 Processor Soil Moisture Algorithm Theoretical Basis Document (ATBD)," Toulouse, France, CESBIO, SM-ESL (CBSA), vol. SO-TN-ESL-SM-GS-0001, v5.a, 2006.

Kim, S. B., L. Tsang, J. T. Johnson, S. Huang, J. J. van Zyl, and E. G. Njoku, "Soil moisture retrieval using time-series radar observations over bare surfaces. *IEEE Trans. Geosci. Rem. Sens.*, 50, pp. 1853–1863, 2012a.

Kim, S. B., M. Moghaddam, L. Tsang, M. Burgin, X. Xu, and E. G. Njoku, "Models of L-band radar backscattering coefficients over the global terrain for soil moisture retrieval," *IEEE Trans. Geosci. Rem. Sens.*, 52(2), 1381–1396, 2014.

Kim, S. B., R. West, and E. G. Njoku, "Effect of radar measurement error on the detection of transient inland water bodies," IGARSS, Vancouver, Canada, 2011.

Kim, Y. and J. J. van Zyl, "A time-series approach to estimate soil moisture using polarimetric radar data," *IEEE Trans. Geosci. Rem. Sens.*, 47, pp. 2519–2527, 2009.

Kim, Y., and J. J. van Zyl, "Comparison of forest estimation techniques using SAR data," *Proc. IEEE IGARSS Conf.*, pp. 1395–1397, 2001.

Kim, Y., T. J. Jackson, R. Bindlish, H. Y. Lee, and S. Y. Hong, "Radar Vegetation Index for Estimating the Vegetation Water Content of Rice and Soybean," *IEEE Geosci. Remote Sens. Lett.*, 9, pp. 564–568, 2012b.

Klein, L. A. and C. T. Swift, "An Improved Model for the Dielectric Constant of Sea Water at Microwave Frequencies," *IEEE Journal of Oceanic Engineering*, vol. 2, no. 1, January, 1977.

Mattia, F., G. Satalino, V. R. N. Pauwels, and A. Loew, "Soil moisture retrieval through a merging of multi-temporal L-band SAR data and hydrologic modelling," *Hydrol. Earth Syst. Sci.*, 13, pp. 343–356, 2009.

McNairn, H., T. J. Jackson, G. Wiseman, S. Belair, P. Bullock, A. Colliander, S. B. Kim, R. Magagi, M. Moghaddam, J. Adams, S. Homayouni, E. Ojo, T. Rowlandson, J. Shang, K. Goita, and M. Hosseini, "The Soil Moisture Active Passive Validation Experiment 2012 (SMAPVEX12): Pre-Launch Calibration and Validation of the SMAP Satellite," *IEEE Trans. Geosci. Rem. Sens.*, submitted, 2013.

Meesters, G. C., R. de Jeu, R. and M. Owe, "Analytical derivation of the vegetation optical depth from the microwave polarization difference index," *IEEE Geosci. and Remote Sensing Letters*, 2, pp. 121–123, 2005.

Mironov, V. L., L. G. Kosolapova, and S. V. Fomin, "Physically and mineralogically based spectroscopic dielectric model for moist soils," *IEEE Trans. Geosci. Rem. Sens.*, 47(7), pp. 2059–2070, 2009.

Mironov, V. L., L. G. Kosolapova, and S. V. Fomin, "Physically and mineralogically based spectroscopic dielectric model for moist soils," *IEEE Trans. Geosci. Rem. Sens.*, 47, pp. 2059–2070, 2009.

Mladenova, I. E., T. J. Jackson, R. Bindlish, and S. Hensley, "Incidence angle normalization of radar backscatter data," *IEEE Trans. Geosci. Rem. Sens.*, 51, pp. 1791–1804, 2012.

Moghaddam, M., S. Saatchi, and R. H. Cuenca, "Estimating subcanopy soil moisture with radar," *J. Geophys. Res.*, 105, pp. 14,899–814,911, 2000.

Naeimi, V., K. Scipal, Z. Bartalis, S. Hasenauer, and W. Wagner, "An improved soil moisture retrieval algorithm for ERS and METOP scatterometer observations," *IEEE Trans. Geosci. Rem. Sens.*, 47, pp. 1999–2013, 2009.

Njoku, E. and L. Li, "Retrieval of Land Surface Parameters Using Passive Microwave Measurements at 6–18 GHz," *IEEE Trans. Geosci. Rem. Sens.*, vol. 37, pp. 79–93, 1999.

Njoku, E. G. and J. A. Kong, "Theory for passive microwave remote sensing of near-surface soil moisture," *J. Geophys. Res.*, 82, 3108–3118, 1977.

Njoku, E. G. and D. Entekhabi, "Passive microwave remote sensing of soil moisture," *J. Hydrol.*, 184, pp. 101–129, 1996.

Njoku, E. G., W. J. Wilson, S. H. Yueh, S. Dinardo, F. K. Li, T. J. Jackson, V. Lakshmi, and J. Bolten, "Observations of soil moisture using a passive and active low-frequency microwave airborne sensor during SGP99," *IEEE Trans. Geosci. Rem. Sens.*, 40, pp. 2659–2673, 2002.

O'Neill, P., S. Chan, E. Njoku, T. Jackson, and R. Bindlish, "SMAP Level 2 & 3 Soil Moisture (Passive) Algorithm Theoretical Basis Document," JPL D-66480, Jet Propulsion Laboratory, Initial Release v.1, October, 2012.

O'Neill, P., M. Owe, B. Gouweleeuw, E. Njoku, J. Shi, and E. Wood, "Hydros Soil Moisture Retrieval Algorithms: Status and Relevance to Future Missions," *Proc. 2006 IEEE International Geoscience and Remote Sensing Symposium (IGARSS 2006)*, Denver, Colorado, July 31–August 4, 2006.

Oh, Y., "Robust inversion technique for retrieving soil moisture from multi-polarised backscatter of bare surface," *Electron. Lett.*, 42, pp. 414–415, 2006.

Oh, Y., K. Sarabandi, and F. T. Ulaby, "Semi-empirical model of the ensemble-averaged differential Mueller matrix for microwave backscattering from bare soil surfaces," *IEEE Trans. Geosci. Rem. Sens.*, 40, pp. 1348–1355, 2002.

Oh, Y., K. Sarabandi, and F. T. Ulaby, "An empirical model and an inversion technique for radar scattering from bare soil surfaces," *IEEE Trans. Geosci. Rem. Sens.*, 30, pp. 370–382, 1992.

Owe, M., R. de Jeu, and J. Walker, "A methodology for surface soil moisture and vegetation optical depth retrieval using the microwave polarization difference index," *IEEE Trans. Geosci. Rem. Sens.*, 39, pp. 1643–1654, 2001.

Paloscia, S., P. Pampaloni, S. Pettinato, and E. Santi, "A Comparison of Algorithms for Retrieving Soil Moisture From ENVISAT/ASAR Images," *IEEE Trans. Geosci. Rem. Sens.*, 46, pp. 3274–3284, 2008.

Pathe, C., W. Wagner, S. Sabel, M. Doubkova, and J. B. Basara, "Using ENVISAT ASAR Global Mode data for surface soil moisture retrieval over Oklahoma, USA," *IEEE Trans. Geosci. Rem. Sens.*, 47, pp. 468–480, 2009.

Shi, J. C., J. R. Wang, A. Y. Hsu, P. E. O'Neill, and E. T. Engman, "Estimation of bare surface soil moisture and surface roughness parameter using L-band SAR image data," *IEEE Trans. Geosci. Rem. Sens.*, 35, pp. 1254–1266, 1997.

SMAP project,"SMAP Algorithm Theoretical Basis Document: L2 & L3 Radiometer Soil Moisture (Passive) Products," JPL D-66480, Jet Propulsion Laboratory, Pasadena, CA, 2012. http://smap.jpl.nasa.gov/science/dataproducts/ATBD/

Tabatabaeenejad, A., M. Burgin, and M. Moghaddam, "Potential of L-band radar for retrieval of canopy and sub-canopy parameters of boreal forests," *IEEE Trans. Geosci. Rem. Sens.*, 50, pp. 2150–2160, 2012.

Ulaby, F. T., A. K. Moore, and A. K. Fung, "Microwave remote sensing: active and passive," Artech House, 1064, 1986a.

Ulaby, F. T., R. K. Moore, and A. K. Fung, "Microwave remote sensing: active and passive, volume 2: radar remote sensing and surface scattering and emission theory," Artech Inc., 1064 pp, 1986b.

Ulaby, F., P. Dubois, and J. van Zyl, "Radar mapping of surface soil moisture," *Journal of Hydrology*, 184(1-2), pp. 57–84, 1996.

Ulaby, F., R. Moore, and A. Fung, *Microwave Remote Sensing: Vols. I, II, and III*, Addison-Wesley, Reading, MA, 1982.

van Zyl, J. J., "Ch. 5—Applications: Measurement of Surface Soil Moisture," *Synthetic Aperture Radar Polarimetry*, JPL Space Science and Technology Series, J. J. van Zyl, and Y. Kim, Eds., Wiley, 312, 2011.

Verhoest, N. E. C., B. De Baets, F. Mattia, G. Satalino, C. Lucau, and P. Defourny, "A possibilistic approach to soil moisture retrieval from ERS synthetic aperture radar backscattering under soil roughness uncertainty," *Water Resour. Res.*, 43, W07435, 2007.

Wagner, W., and K. Scipal, "Large-scale soil moisture mapping in Western Africa using the ERS scatterometer," *IEEE Trans. Geosci. Rem. Sens.*, 38, pp. 1777–1782, 2000.

Wagner, W., G. Lemoine, and H. Rott, "A method for estimating soil moisture from ERS scatterometer and soil data," *Remote Sens. Environ.*, 70, pp. 191–207, 1999.

Wang, J. R. and T. J. Schmugge, "An empirical model for the complex dielectric permittivity of soils as a function of water content," *IEEE Trans. Geosci. Rem. Sens.*, 18, pp. 288–295, 1980.

Wang, J. R., "Passive microwave sensing of soil moisture content: the effects of soil bulk density and surface roughness," *Remote Sens. Environ.*, vol. 13, pp. 329–344, 1983.

Yueh, S., S. Dinardo, S. K. Chan, E. Njoku, T. Jackson, R. Bindlish, "Passive and Active L-Band System and Observations During the 2007 CLASIC Campaign," *Proc. 2008 IEEE International Geoscience and Remote Sensing Symposium (IGARSS 2008)*, Boston, Massachusetts, July 6–11, 2008.

Zhan, X., W. Crow, T. J. Jackson, P. O'Neill, "Improving Spaceborne Radiometer Soil Moisture Retrievals With Alternative Aggregation Rules for Ancillary Parameters in Highly Heterogeneous Vegetated Areas," *IEEE Trans. Geosci. Rem. Sens.*, 5(2), pp. 261–265, 2008.

Zribi, M., O. Taconet, S. Le Hegarat-Mascle, D. Vidal-Madjar, C. Emblanch, C. Loumagne, and M. Normand, "Backscattering behavior and simulation comparison over bare soils using SIR-C/X-SAR and ERASME 1994 data over Orgeval," *Remote Sens. Environ.*, 59, pp. 256–266, 1997.

# 5. The Value-Added L4_SM Soil Moisture Product

## I. Motivation and Overview

The primary SMAP measurements, land surface microwave emission at 1.41 GHz and radar backscatter at a frequency tunable from 1.215 to 1.300 GHz are directly related to surface soil moisture (in the top 5 cm of the soil column). However, several of the key applications targeted by SMAP (e.g., in agriculture and in short-term climate forecasting, among others) require knowledge of root zone soil moisture (defined here as soil moisture in the top 1 m of the soil column), which is not directly linked to SMAP observations. The foremost objective of the SMAP Level 4 Surface and Root Zone Soil Moisture (L4_SM) product is to provide estimates of root zone soil moisture that are informed by and consistent with SMAP observations. The second main objective of the L4_SM product is to provide spatially and temporally complete soil moisture to fill the spatial and temporal gaps in SMAP observations that are due to orbit and land surface characteristics. SMAP observations are only available in 1,000-km-wide swaths that cover the Earth with a 2–3 day repeat frequency and contain only limited soil moisture information in regions of dense vegetation or mountainous topography. To address these limitations in sensing depth and coverage, the L4_SM algorithm merges lower-level SMAP data with model estimates in a soil moisture data assimilation system.

At the heart of the data assimilation system is a land surface model that monitors the evolution of soil moisture, snow, and temperature states as they respond to meteorological drivers such as rainfall and incident radiation. The land surface model is driven with observation-based precipitation, which is the most important driver for soil moisture. The model also encapsulates knowledge of key land surface processes, including the vertical transfer of soil moisture between the surface and root zone reservoirs. In essence, the land model is designed to conserve both water (converting precipitation inputs into evaporation, runoff, and storage change) and energy (converting incident radiation into outgoing radiation, latent heat flux, sensible heat flux, storage change, and other miscellaneous terms). Given realistic forcing, these conservation principles ensure at least some first-order reliability in the simulation products — when it rains, for example, the modeled soil will typically get wetter. Finally, the model provides spatially and temporally complete estimates that serve as background information in the assimilation update procedure.

The assimilation updates of the L4_SM algorithm merge the model estimates with SMAP observations using weights that consider the uncertainties of each, resulting in a product that is superior to satellite or land model data alone. In the course of the data assimilation process, the subsurface assimilation updates (along with the subsurface transport formulations in the land model) effectively advect SMAP-based surface soil moisture information into deeper soil levels. Error estimates for the L4_SM product are generated as a by-product of the data assimilation system. This chapter provides a detailed description of the SMAP L4_SM product and its algorithm. Chapter 7 includes details on the validation of the L4_SM product.

## II. Assimilation System and Algorithm Flow

### A. Algorithm Overview

The L4_SM algorithm consists of two key elements adapted from the Goddard Earth Observing Model System, Version 5 (GEOS-5): (i) the GEOS-5 Catchment land surface model, which is a numerical description of the water and energy transport processes at the land–atmosphere interface, augmented with a model that describes the land surface microwave radiative transfer, and (ii) the GEOS-5 ensemble-based land data assimilation system, which is the tool that will be used to merge SMAP observations with estimates from the land model as it is driven with observation-based surface meteorological forcing data. The latter includes a soil moisture analysis based on the ensemble Kalman filter and a rule-based freeze/thaw analysis. Downscaled (9-km) brightness temperatures (L2_SM_AP) will be assimilated when and where available, supplemented with 36-km brightness temperature observations (L1C_TB; ascending and descending passes) where downscaled data are unavailable. Moreover, 3-km freeze/thaw observations (L3_FT_A) will also be assimilated.

After initialization of the system with estimates derived from a model spin-up procedure, the L4_SM algorithm steps recursively through time, alternating between model forecast (FCST) and analysis (ANA) steps. Figure 54 provides an overview of one forecast and analysis cycle. The algorithm begins with a Catchment model ensemble forecast, initialized with the analysis at time t–1 and valid at time t (labeled FCST(t) in Figure 54). For each 9-km model grid cell, the forecast freeze/thaw (F/T) state is first compared to the corresponding SMAP freeze/thaw observations (aggregated to the resolution of the model forecast). If the Catchment model forecast and the SMAP observations disagree, the model states in the 9-km grid cell in question are corrected towards the observations in a freeze/thaw analysis. If the forecast and observed freeze/thaw states agree and indicate non-frozen conditions, the grid cell in question is included in a distributed soil moisture analysis. If the model indicates non-frozen conditions and freeze/thaw observations are not available, the grid cell is also included in the soil moisture analysis. Otherwise, the analysis step is skipped for the grid cell in question. After the analysis has been completed for all grid cells, the algorithm continues with a model forecast to time t+1, and so on.
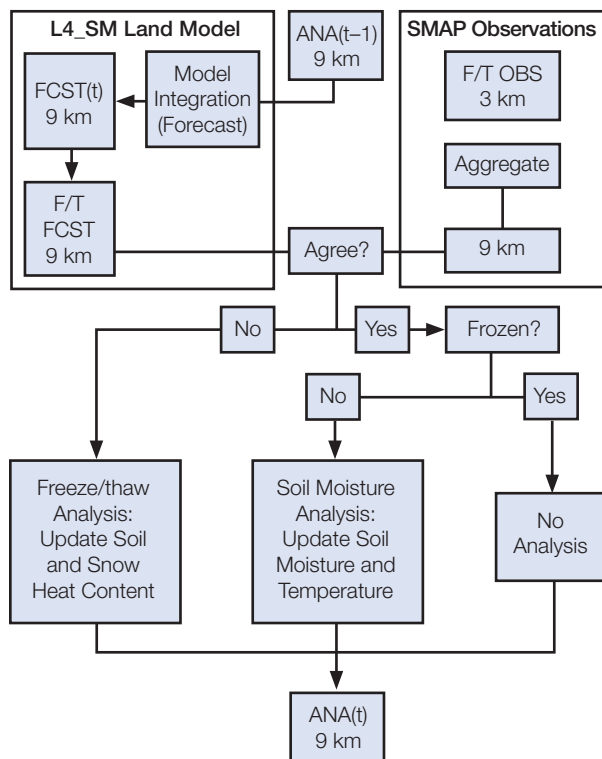
**Figure 54. L4_SM algorithm overview. See Figure 57 for a flowchart of the soil moisture analysis.**

## B. The NASA GEOS-5 Catchment Land Surface Model

Model soil moisture is obtained from integrations of the NASA Catchment Land Surface Model (hereinafter Catchment model; Koster et al., 2000; Ducharne et al., 2000). Although in standard practice the basic computational unit of the Catchment model is the hydrological catchment (or watershed), for SMAP the Earth-fixed 9-km EASE2 grid (same as that of the L2_SM_AP product) will be used to define the surface elements. The conceptual physics underlying the model, which focus on topographical variations smaller than the 9-km scale, are still important and valid for such a surface element definition.

Figure 55 provides a simplified picture of the three prognostic variables related to soil moisture: catchment deficit (CATDEF), root zone excess (RZEXC), and surface excess (SRFEXC). In effect, the vertical profile of soil moisture at each point in each computational unit (related to CATDEF; see Figure 55) is determined by the equilibrium soil moisture profile from the surface to the (spatially varying) water table (defined by a balance of gravity and capillary forces) and by two additional variables that describe deviations from the equilibrium profile: the average deviation in a 1-m root zone layer (RZEXC), and the average deviation in a 5-cm surface layer (SRFEXC). A single "root zone" depth of 1 m is chosen here to make the SMAP product more

straightforward; in nature, the depths tapped by roots vary with vegetation type.

As indicated in the bottom left of Figure 55, the Catchment model differs from traditional layer-based models by including an explicit treatment of the spatial variation of soil water and water table depth within each computational unit (that is, within each 9-km EASE grid cell for L4_SM) based on the statistics of the catchment topography. This spatial variation enters into the calculation of moisture diffusion between the root zone and lower soil moisture storage. Extensive preprocessing produces a pre-computed functional relationship between RZEXC, CATDEF, and the amount of moisture transferred between the two in a given time step, a functional relationship that is based on a spatially distributed set of one dimensional Richard's equation calculations, each representing moisture transport at some location in the catchment and each performed on a soil column fitted with high vertical resolution. The transfer of moisture between the 0–5 cm surface layer and the root zone, of particular relevance to SMAP, is computed similarly, though without a spatially distributed component; a highly-resolved, one-dimensional representation of the root zone is used to pre-compute a functional relationship between the moisture variables and the amount of moisture transferred between SRFEXC and RZEXC within the time step.

The treatment of spatial heterogeneity also allows the diagnostic separation of the catchment into saturated, unsaturated, and wilting sub-grid areas. The sizes of these three sub-grid areas vary dynamically; wetter conditions, for example, expand the saturated sub-grid area and reduce the wilting sub-grid area (if it is not already zero). The surface energy balance is computed separately for each sub-grid area using physics specific to the corresponding hydrological regime. This entails the monitoring of independent prognostic surface temperature variables for each sub-grid area (TC1, TC2, and TC4). The three surface temperature prognostic variables interact with an underlying heat diffusion model for soil temperature (consisting of six layers with depths equal to about 0.1, 0.2, 0.4, 0.75, 1.5, 10 m from top to bottom) that is common to all three sub-grid areas. The model prognostic variables for this heat diffusion model component are the ground heat contents associated with the six soil layers (GHT1, GHT2, …, GHT6).

Surface runoff processes are computed separately for each sub-grid area, again using hydrological regime-specific physics, whereas subsurface baseflow is computed directly from the diagnosed spatial distribution of water table depth. A snow model component describes the state of snow pack in terms of snow water equivalent, snow depth, and snow heat content (three layers for each variable). The time step for the model integration is 20 minutes.

## "Catchment Deficit" Variable

Consider an arbitrary point in the catchment:



Integrate: Yellow area = moisture deficit, D, at this point.

Equilibrium profile

Water table

Now integrate D across the catchment:
CATDEF = (1/A) ∫$_A$ D dA =
the average amount of water, per m$^2$, that must be added to the catchment to bring it to complete saturation, assuming equilibrium profiles.
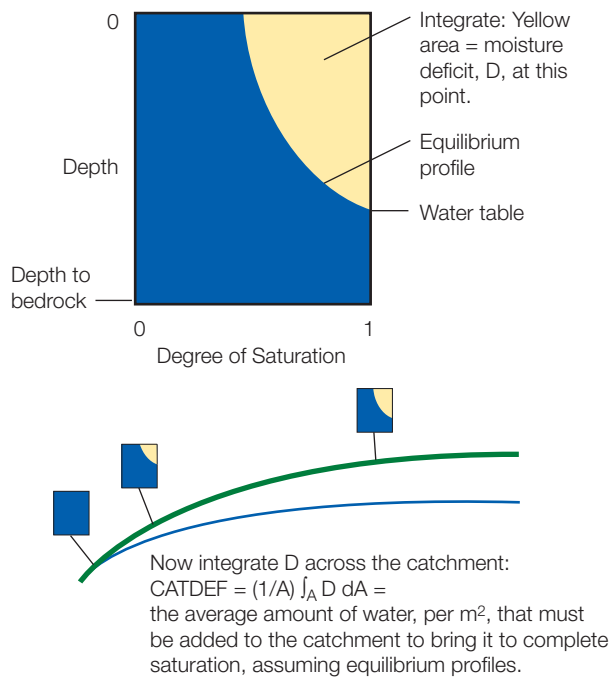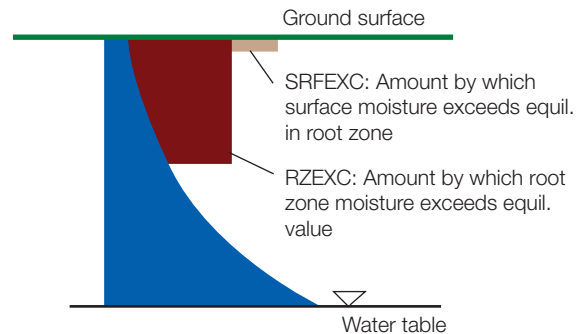
**Figure 55. Unique elements of the Catchment land surface model related to the diffusion of moisture between the 0–5 cm surface zone and the remainder of the soil profile. Shown are descriptions of the**

A salient feature of the land model integration is that it uses meteorological forcing inputs that rely on observed data as much as possible. Reichle et al. (2011), Yi et al. (2011), and Holmes et al. (2011) provide a comprehensive assessment of large-scale land surface estimates derived with the Catchment model as part of the Modern-Era Retrospective Analysis for Research and Applications (MERRA) reanalysis (Rienecker et al., 2011) and demonstrate that the Catchment model is a state-of-the-art global land surface model.

## C. The NASA GEOS-5 L-band Microwave Radiative Transfer Model

The Catchment model has been augmented with a microwave radiative transfer model that transforms the simulated surface soil moisture and temperature fields into model estimates of L-band brightness temperature (at the 9-km scale). Like the L2_SM_P and L2_SM_AP algorithms, the L4_SM algorithm uses the "tau-omega" model, an approximation of the radiative transfer processes that is appropriate for low frequency microwave emission. In this model, "tau" is the vegetation optical depth and "omega" is the scattering albedo. A layer of vegetation over the soil attenuates the emission from the soil and adds to the total radiative flux with its own emission. Assuming that

## "Root Zone Excess" and "Surface Excess" Variables: The View at a Point



Ground surface

SRFEXC: Amount by which surface moisture exceeds equil. in root zone

RZEXC: Amount by which root zone moisture exceeds equil. value

Water table

### Diffusion Calculation



Functions relating time scales of diffusion to the moisture variables are pre-computed from Richard's equation calculations at high vertical resolution. The time scales for diffusion between RZEXC and CATDEF reflect net diffusion over a spatially distributed set (across the catchment) of independent columns.

**three moisture prognostic variables (CATDEF, RZEXC, and SRFEXC) and an indication of how the transfer of moisture between the variables is computed.**

scattering within the vegetation is negligible at L-band frequencies, the vegetation may be treated mainly as an absorbing layer for the soil moisture signal.

The parameterizations of the microwave model represent a trade-off between the need to adequately simulate the key effects of surface characteristics on microwave signatures at the spatial scale of interest, and the need for a sufficiently simple representation for application to satellite retrieval algorithms. The microwave model incorporates the effects of dynamic features (including surface soil moisture and soil temperature), and static or slowly-varying features such as soil texture, soil surface roughness, land-cover and vegetation type, and vegetation water content. A comprehensive description of the model is provided by De Lannoy et al. (2013).

## D. The Ensemble Kalman Filter

The L4_SM algorithm is built on the ensemble Kalman filter (EnKF) — a Monte Carlo variant of the Kalman filter (Evensen 2003). The idea behind the EnKF is that a small ensemble of model trajectories captures the relevant parts of the error structure. Each member of the ensemble experiences perturbed instances of the input forcing fields

(representing errors in the forcing data) and/or randomly generated noise that is added to the model parameters and prognostic variables (representing errors in model physics and parameters). The error covariance matrices that are required for the filter update can then be diagnosed from the spread of the ensemble at the update time. The EnKF is flexible in its treatment of errors in model dynamics and parameters. It is also very suitable for modestly nonlinear problems and has become a popular choice for land data assimilation (Andreadis and Lettenmaier 2005; Durand and Margulis 2008; Kumar et al. 2008a,b; Pan and Wood 2006; Reichle et al. 2002a,b; Zhou et al. 2006).

The EnKF works sequentially by performing in turn a model forecast and a filter update (Figure 56). Formally, the forecast step for ensemble member i can be written as

$$x_{t,i}^- = f(x_{t-1,i}^+, q_{t,i}), \tag{33}$$

where $x_{t,i}^-$ and $x_{t-1,i}^+$ are the forecast (denoted with $^-$) and analysis (denoted with $^+$) state vectors at times t and t–1, respectively, of the i-th ensemble member. The model error (or perturbation vector) is denoted with $q_{t,i}$ and its covariance with $Q_t$. Each ensemble member represents a particular realization of the possible model trajectories with certain random errors in model parameters and/or a particular set of errors in forcing.
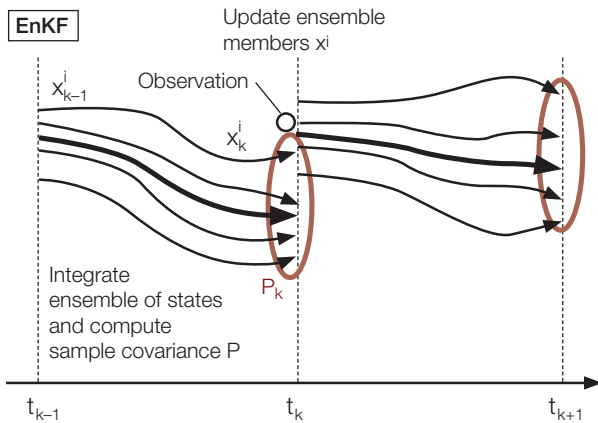


**Figure 56. The ensemble Kalman filter (EnKF).**

With the observations available at time t, the state of each ensemble member is updated to a new value. First, the filter update produces increments at time t that can be written as

$$\Delta x_{t,i} = K_t (y_{t,i} - H_t x_{t,i}^-), \tag{34}$$

where $y_{t,i}$ denotes the observation vector (suitably perturbed) and $H_t$ is the observation operator (which is written as if it was linear for ease of notation, but in practice the update is solved without explicitly computing $H_t$, [Keppenne 2000]). Next, the analyzed state vector is

obtained as $x_{t,i}^+ = x_{t,i}^- + \Delta x_{t,i}$. The Kalman gain matrix $K_t$ is given by

$$K_t = P_t H_t^T ( H_t P_t H_t^T + R_t)^{-1}, \tag{35}$$

where $P_t$ is the forecast error covariance (diagnosed from the ensemble $x_{t,i}^-$), $R_t$ is the observation error covariance, and superscript T denotes the matrix transpose. Simply put, the Kalman gain $K_t$ represents the relative weights given to the model forecast and the observations based on their respective uncertainties, along with the error correlations between different elements of the state vector. If the system is linear, if its model and observation error characteristics satisfy certain assumptions (including Gaussian, white, and uncorrelated noise), and if the input error parameters are correctly specified, the Kalman gain of Eq. (35) is optimal in the sense of minimum estimation error variance. In other words, the updated state is mathematically the best possible estimate of the state given the observations, the model prediction, and the estimated errors of both. Estimates of the model prognostic or diagnostic variables can be obtained at any time from the ensemble mean. The reduction of the uncertainty resulting from the update is reflected in the reduction of the ensemble spread. Note that the ensemble of model trajectories in the EnKF naturally yields error estimates for the assimilation products.

## E. Soil Moisture Analysis

Figure 57 summarizes the soil moisture analysis of the L4_SM algorithm. The state vector x for the soil moisture analysis consists of seven Catchment model prognostic variables (catchment deficit, root zone excess, surface excess, three surface temperature prognostic variables [one each for the saturated, unsaturated, and wilting sub-grid areas], and the first-layer ground heat content; section II.B) at each computational element (9-km grid cell) that is included in the soil moisture analysis (see also Figure 55). Formally, the forecast state vector for the soil moisture analysis is

$$x^- = \begin{bmatrix} x_1^- \\ x_2^- \\ ... \\ x_{N9}^- \end{bmatrix}, \quad \text{where} \quad x_j^- = \begin{bmatrix} SRFEXC\_FCST_j \\ RZEXC\_FCST_j \\ CATDEF\_FCST_j \\ TC1\_FCST_j \\ TC2\_FCST_j \\ TC4\_FCST_j \\ GHT1\_FCST_j \end{bmatrix}, \tag{36}$$

N9 is the number of 9-km grid cells included in the soil moisture analysis, and j=1...N9. For clarity, the subscripts for time and ensemble member are omitted.

As mentioned above, the L4_SM baseline algorithm assimilates brightness temperatures in H- and V-polarization (TBH and TBV, respectively, in Figure 57) downscaled
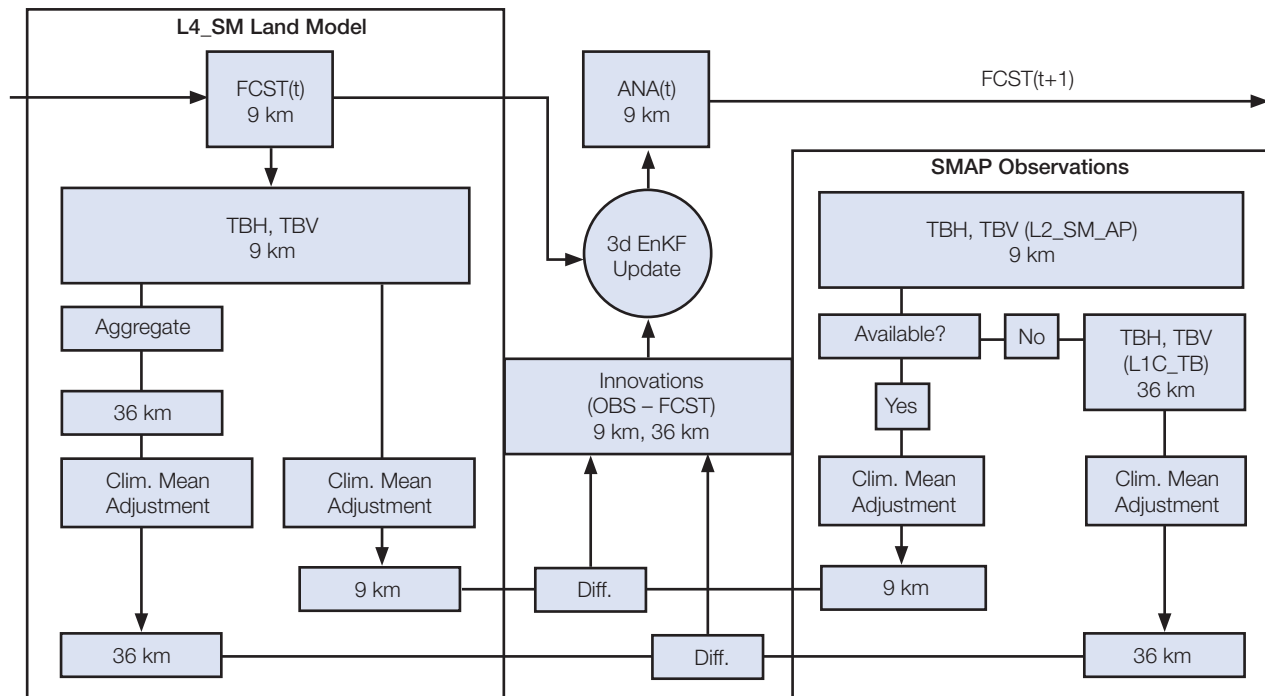
**Figure 57. The L4_SM soil moisture analysis. See text for details.**

to 9-km resolution when and where available from the L2_SM_AP product. However, high-resolution backscatter data are not always available to generate the downscaled brightness temperatures. For example, during afternoon overpasses, high-resolution radar data are collected only north of 45°N because of resource limitations. Even if high-resolution backscatter data are available, the L2_SM_AP algorithm may not always provide downscaled brightness temperatures. If, for a given time and location, downscaled (9-km) brightness temperatures are not available, the 36-km brightness temperature values from the L1C_TB product in H- and V-polarization will be assimilated. Note that we will not assimilate the 36-km brightness temperatures for a given time and location if downscaled (9-km) values are available for that time and location.

L-band brightness temperatures generated by the Catchment model and its associated microwave radiative transfer model described above have been calibrated (separately for each location) to match the climatology of SMOS observations (De Lannoy et al. 2013). While the model calibration yields largely unbiased modeled brightness temperatures (with respect to SMOS), residual model biases remain and are primarily related to seasonal variations in bias. Moreover, it is not clear to what extent the SMOS observations are impacted by low-level RFI and may themselves be biased. These unavoidable biases in the model and the observations must be addressed as part of the data assimilation system. To this end, the observed

and modeled brightness temperatures will be adjusted by subtracting their respective seasonally varying, climatological mean values (separately for H- and V-polarization) before the innovations are computed (Figure 57). Since brightness temperature is strongly impacted by surface temperature, it is important to resolve the seasonal and diurnal cycles of the climatology. The mean adjustment is therefore based on the multi-year mean value of the observed or modeled brightness temperature for a given location, day-of-year, and overpass time-of-day. SMOS brightness temperatures provide a useful early estimate of the SMAP brightness temperature climatologies. The SMOS climatology will therefore be used initially in L4_SM production until sufficient SMAP observations have been accumulated. Thereafter, a SMAP-only climatology will be used for recalibrating the land model and for generating and reprocessing the L4_SM product.

Following Eq. (34), the innovations vector $(y - Hx^-)$ will thus be computed by differencing the H- and V-polarization brightness temperatures (after the mean adjustment) from the observations and the Catchment model forecast. If downscaled (9-km) brightness temperature are available for a given 36-km grid cell, up to $2 \cdot (36/9)^2 = 32$ elements from that grid cell are included in the innovations vector (up to 16 elements each for 9-km TBH and 9-km TBV). Otherwise, the 36-km grid cell in question only contributes up to two elements to the innovations vector (36-km TBH and 36 km TBV).

The corresponding vector of model predictions of the 9-km and 36-km brightness temperature contains all the processing steps required to map the state vector x (Eq. [36]) into a model prediction of the observed values that can then be directly differenced with the observation vector y. The observation operator thus includes (i) the transformation of soil moisture and soil temperature fields into brightness temperatures via the microwave radiative transfer model at 9-km resolution, (ii) the aggregation from 9 km to 36 km only for locations where 36-km brightness temperature observations from L1C_TB are assimilated, and (iii) the climatological mean adjustment.

Finally, the increments are computed in the units of the Catchment model prognostic variables following Keppenne 2000. The L4_SM algorithm will be implemented with three-dimensional ("3d") updates (Reichle and Koster 2003; Reichle et al. 2013), that is, the increments for a given 9-km grid cell are affected by all observations within a certain radius of influence, and not just by the observations that cover the grid cell in question. The radius of influence for the "3d" algorithm is determined by the spatial error correlation scales and is expected to be no more than a few hundred kilometers (Reichle and Koster 2003). It has been shown that the ensemble filter works adequately with 12 ensemble members (Reichle et al. 2007; Liu et al. 2011). To reduce sampling errors, at least 24 ensemble members will be used (resources permitting).

### F. Freeze/Thaw Analysis

The assimilation of SMAP freeze/thaw state observations is conceptually similar to the assimilation of snow cover observations. In both cases, the observed variable is, at least at satellite footprint scale, essentially a binary measurement. Generally, binary measurements cannot be assimilated with the EnKF, because the EnKF requires continuous variables (such as water or heat reservoirs). This restriction can be circumvented, however, for snow cover observations because in land models, fractional snow cover for a given model grid cell can be related to a continuous prognostic variable (such as SWE) via a snow depletion curve. By aggregating high-resolution measurements into fractional snow cover observations (at the scale of the land model) the EnKF could still be used (De Lannoy et al. 2010; De Lannoy et al. 2011). The same does not apply to freeze/thaw observations, because there is no equivalent to the snow depletion curve for the land model's freeze/thaw state. Consequently, for the assimilation of freeze/thaw observations in the baseline L4_SM algorithm we adapt the rule-based (non-EnKF) approaches that have been developed to assimilate snow cover observations (Rodell and Houser 2004; Zaitchik and Rodell 2009).

Because the radar and radiometer measurements are not informative of soil moisture under frozen soil conditions, a given 9-km grid cell is never included simultaneously in the freeze/thaw analysis and the soil moisture analysis (Figure 54). In particular, a given 9-km grid cell will be included in the soil moisture analysis only if both the observations and the model indicate thawed conditions. If the observations and the model agree on frozen conditions, there will be no further analysis step for the 9-km grid cell in question. If the model forecast and the corresponding SMAP observations disagree on the freeze/thaw state, that is, if the model indicates frozen conditions and the observation indicates thawed conditions (or vice versa), the Catchment model prognostic variables will be adjusted towards the observed freeze/thaw state in a freeze/thaw analysis. Adjustments will primarily be made to the forecast surface soil temperatures (TC1, TC2, TC4) and the soil heat content.

## III. Ancillary Data Requirements

Aside from SMAP observations, the L4_SM system requires initialization, parameter, and forcing inputs for the Catchment land surface model and the microwave radiative transfer model, as well as input error parameters for the ensemble-based data assimilation system. This section provides an overview of the system's ancillary data requirements.

### A. Catchment Land Surface Model and Microwave Radiative Transfer Model Parameters

The Catchment land surface model requires topography, soil, and vegetation data at all computational elements in the chosen spatial discretization. A full set of these Catchment model parameters is available as part of the GEOS-5 modeling system (Rienecker et al., 2008). To the extent possible, Catchment model parameters will be adjusted for consistency with land surface parameters that are used by other SMAP products. The microwave radiative transfer parameters of the GEOS-5 modeling system are calibrated such that the long-term climatology of the modeled brightness temperatures matches that of the SMOS observations (De Lannoy et al. 2013). Key model ancillary parameter inputs are provided as part of the L4_SM data product (section IV).

Some of the soil parameters of the Catchment model may differ from those of the microwave radiative transfer model because the former requires consistent surface and root zone information whereas the latter requires only surface information, which is more readily available. Similarly, the vegetation class inputs for the Catchment model and the microwave radiative transfer model may differ because the two model components currently use slightly

different vegetation classifications. Moreover, microwave model parameters may differ between the L4_SM and the Level 2 algorithms due to algorithm-specific requirements. Most importantly, data assimilation requires unbiased estimates of modeled brightness temperatures with respect to the observations and therefore requires that microwave model parameters used for L4_SM are calibrated specifically for the L4_SM system. The SMAP team also has an ongoing task to examine consistency in the tau-omega model parameterizations between L2 and L4 soil moisture products. In any case, we expect that parameter inconsistencies between SMAP data products will be minor and will have a minimal impact on the L4_SM product.

## B. Surface Meteorological Data

The Catchment model is forced with surface meteorological data (including precipitation, downward shortwave radiation, downward longwave radiation, wind speed, near surface air temperature, near surface specific humidity, and air pressure). The input forcing data stream will mainly be provided by output from the "forward-processing" (quasi-operational) NASA GEOS-5 global atmospheric analysis system (Rienecker et al., 2008) and is based on the assimilation of a very large number (greater than $10^7$ per day) of conventional and satellite-based observations of the atmosphere into a global atmospheric model. At the time of this writing, the resolution of the "forward-processing" GEOS-5 system is 0.25° by 0.3125° in latitude and longitude, respectively. By the time the SMAP mission ends, the spatial resolution of these outputs is expected to be around 0.125° or finer. Furthermore, the forcing data are available as hourly averages or snapshots (depending on the variable) and will be interpolated to the land model time step with existing software.

Additional important corrections will be applied using gauge- and satellite-based estimates of precipitation. The specific data source for the observations-based precipitation estimates will be determined closer to the launch of SMAP based on availability. At the time of this writing, global daily gauge-based estimates are provided by the NOAA Climate Prediction Center (CPC) at a horizontal resolution of 0.5° with a latency of about 2 days (ftp://ftp.cpc.ncep.noaa.gov/precip/CPC_UNI_PRCP/GAUGE_GLB/). For the SMAP L4_SM algorithm, the observations-based precipitation estimates will be downscaled to the hourly, 9 km scale of the model forcing using the disaggregation method described in (Liu et al., 2011; Reichle et al., 2011; Reichle, 2012).

Select forcing inputs will be provided in the L4_SM data product as part of the L4_SM research output (section IV.A).

## C. Land Model Initial Conditions

The Catchment model prognostic variables will be initialized at the start of the assimilation period after forcing the model with meteorological data for a multi-year period prior to the assimilation, using forcing data extracted from the same sources used during the assimilation period. Memory of any poor initialization at the start of this "spin-up" period will be lost by the time the assimilation starts.

## D. Data Assimilation Parameters

The key feature of the EnKF is that error estimates of the model-generated results are dynamically derived from an ensemble of model integrations. Each member of the ensemble experiences slightly perturbed instances of the observed forcing fields (representing errors in the forcing data) and is also subject to randomly generated noise that is directly added to the model prognostic variables (representing errors in model physics and parameters).

Time series of cross-correlated perturbation fields are generated and applied to a subset of the meteorological forcing inputs and Catchment model prognostic variables. Collectively, these perturbations maintain an ensemble of land surface conditions that represents the uncertainty in the soil moisture state. Depending on the variable, normally distributed additive perturbations or lognormally distributed multiplicative perturbations are applied. The ensemble mean for all perturbations is constrained to zero for additive perturbations and to one for multiplicative perturbations. Moreover, time series correlations are imposed via a first-order auto-regressive model for all fields. The perturbation fields are also spatially correlated with length scales of a few hundred kilometers.

For soil moisture, soil temperature, and brightness temperature, the dominant forcing inputs are precipitation, radiation, and air temperature, and we perturb only these forcing fields. Imperfect model parameters and imperfect physical parameterizations contribute to model errors. Such errors are represented through direct perturbations to model prognostic variables (that is, model parameter values such as porosity, soil hydraulic conductivity, vegetation opacity, single scattering albedo, etc., are not separately perturbed). The key prognostic variables of the Catchment model related to soil moisture and surface soil temperature are the surface excess, the root zone excess, the catchment deficit, and the surface-layer ground heat content. Due to nonlinearities in the Catchment model, perturbations in the root zone excess typically lead to biases between the ensemble mean and the unperturbed control integration. We therefore do not perturb the root zone excess.

Cross-correlations are imposed on perturbations of the precipitation, radiation, and air temperature fields. At hourly and daily time scales, the meteorological forcing fields are ultimately based on output from atmospheric modeling and analysis systems and not on direct observations of surface precipitation and radiation. The cross-correlations are therefore motivated by the assumption that the atmospheric forcing fields represent a realistic balance between radiation, clouds, and precipitation. Under that assumption, a positive perturbation to the downward shortwave radiation tends to be associated with negative perturbations to the longwave radiation and the precipitation, and vice versa.

Forcing and model errors are difficult to quantify at the global scale. The perturbation parameter values used for L4_SM are largely based on experience. They are supported by earlier studies where model and forcing error parameters were calibrated in twin experiments (Reichle et al. 2002b; Reichle and Koster 2003) and by successful assimilation of SMMR, AMSR-E, and ASCAT satellite observations (Reichle et al. 2007; 2009; Liu et al. 2011; Draper et al. 2012), suggesting that these values are acceptable.

Observation error parameters for the assimilated SMAP brightness temperatures will be based on error estimates provided by the corresponding SMAP products. Two distinct error sources contribute to the observation error standard deviation needed in the assimilation system: (i) "instrument" measurement error (with standard deviations expected to be ~1.3 K at 36 km and ~3.6 K at 9 km for SMAP), and (ii) "representativeness" error, which accounts, for example, for the uncertainty associated with orbit-to-orbit variations in the effective support of a particular grid cell due to variations in the satellite footprint patterns. The total observation error standard deviation (including the "instrument" and "representativeness" errors) will be determined during algorithm calibration. We assume that observation errors are uncorrelated in time and space.

Again, the success of the assimilation system depends on the accurate specification of the model and observation error parameters. The improvements from data assimilation documented in section V suggest that the perturbation parameter values chosen are valid, if not necessarily optimal. The values of the perturbation parameters will be provided in the form of metadata in the L4_SM data product.

## IV. The L4_SM Data Product

### A. Data Product Overview

The SMAP L4_SM data product includes the following components (or "File Collections"):

(i) Geophysical Data, including surface soil moisture (0–5 cm vertical average), subsurface (or "root zone") soil moisture (0–100 cm vertical average), surface meteorological forcing variables, surface soil temperature, evaporative fraction, net radiation, and land surface fluxes.

(ii) Analysis Update Data, including observed, forecast, and analysis brightness temperatures (that is, innovations information), forecast and analysis surface soil moisture, root zone soil moisture, surface soil temperature, and land surface temperature (that is, analysis increment information), and error estimates for observed and forecast brightness temperatures and for analysis soil moisture and surface soil temperature.

(iii) Land Model Constants Data (time-invariant), including land cover, soil hydraulic parameters, and microwave radiative transfer model parameters such as microwave soil roughness, vegetation opacity, and vegetation scattering albedo.

### B. Spatial and Temporal Resolution, Posting, and Coverage

All L4_SM geophysical parameters will be derived at a resolution of 9 km and posted on the SMAP Earth-fixed grid with 9-km spacing (EASE grid, version 2) for all global land areas (excluding inland water and permanent ice). Three basic time steps are involved in the generation of the L4_SM product: (i) the land model integration time step (15 minutes or less), (ii) the EnKF analysis update time step, and (iii) the reporting (or output) time step for the geophysical fields and analysis update outputs provided in the L4_SM data product.

The available SMAP observations will be assimilated in an EnKF analysis update step at the nearest 3-hourly analysis time (0z, 3z, …, and 21z). The reporting time step is 3 hours, that is, geophysical data are provided as 3-hourly time averages, and analysis update data are provided as 3-hourly instantaneous estimates.

## C. Data Product Availability and Latency

After the 3-month In-Orbit Checkout (IOC) period of the SMAP observatory, the L4_SM product must be produced within 7 days of satellite data acquisition (mean latency under normal operating conditions). Based on the availability of the input daily-average precipitation observations (currently available with a latency of about 48 hours), we plan to deliver output once daily with a mean latency of ~3 days. This schedule may be adjusted according to the release schedule of the input precipitation observations that will be available after launch. Note that the latency of the L4_SM product is at least that of the lower-level SMAP input products plus processing time.

Delivery of a beta-version L4_SM product must begin 6 months after IOC, but every effort will be made to provide the L4_SM product as soon as possible after launch. Delivery of the validated L4_SM product will begin after the 12-month Calibration/Validation phase. The Calibration/Validation phase for Level 4 products covers the first twelve months after IOC.

## D. Error Estimates

The data assimilation system weighs the relative errors of the assimilated SMAP brightness temperature observations and the corresponding land model forecast (section II.D). Estimates of the error of the assimilation product are dynamically determined as a by-product of this calculation. How useful these error estimates are depends on the accuracy of the input error parameters and needs to be determined through validation. Estimates of instantaneous error fields will be provided for select variables as part of the Analysis Update Data File Collection. Specifically, the error estimates are derived from the ensemble standard deviation of the analyzed fields. These error estimates will vary in space and time.

## V. Test Plan

The L4_SM algorithm has been tested globally, to the extent possible, with satellite observations from precursor missions, including AMSR-E, ASCAT, and SMOS. Testing will continue until the SMAP launch. In each case, the outcome of the test is assessed by validating the assimilation estimates against in situ observations from existing networks and by ensuring the consistency of internal diagnostics, for example by examining the statistics of the observation-minus-forecast residuals. Additional development and testing has been conducted in the context of Observing System Simulation Experiments (OSSEs); e.g., Reichle et al. (2008).

As an example, Figure 58 shows results from the assimilation of ASCAT and AMSR-E soil moisture retrievals over 3.5 years into the NASA Catchment land surface model, using the ensemble-based GEOS-5 land assimilation system (Draper et al. 2012). Soil moisture skill from each assimilation experiment is assessed against in situ soil moisture observations from the United States Department of Agriculture SCAN and SNOTEL networks (66 sites) and the Murrumbidgee Soil Moisture Monitoring Network in Australia (19 sites). Soil moisture skill is measured as the anomaly time series correlation coefficient with the in situ data (R). Figure 58 shows the estimated R values and their 95% confidence intervals for the surface and root-zone soil moisture, from the assimilation of ASCAT, AMSR-E and both. The results are benchmarked against those from an open-loop simulation, and have been averaged by land cover type (based on MODIS land cover classifications). Across all 85 sites, assimilating ASCAT and/or AMSR-E data significantly improved the soil moisture skill (at the 5% level). In the root zone, the mean skill was increased from 0.45 for the open-loop, to 0.55 for the assimilation of ASCAT, 0.54 for the assimilation of AMSR-E, and 0.56 for the assimilation of both. Assimilating the ASCAT or AMSR-E data also improved the mean R value over each individual land cover type, in most cases significantly.

The root zone soil moisture skill of a prototype L4_SM data product that is based on brightness temperature assimilation is shown in Figure 59. The prototype product was derived at 36-km resolution using surface meteorological forcing data from the MERRA reanalysis, with precipitation forcing corrected towards gauge observations from the CPC (section III.B). Furthermore, H- and V-polarization SMOS brightness temperatures at 6 incidence angles (32.5°, 37.5°, 42.5°, 47.5°, 52.5°, and 57.5°) were assimilated.

Consistent with the formulation of the L4_SM accuracy requirement, in Figure 59 skill is measured in terms of RMSE (after removal of the long-term mean bias) versus in situ measurements. The figure shows that for most individual sites the RMSE is below 0.055 $m^3m^{-3}$. The area-average RMSE for the 142 sites shown in Figures 58 and 59 is 0.043 $m^3m^{-3}$ and thus very close to meeting the target value of 0.040 $m^3m^{-3}$. Expected enhancements in the skill of the L4_SM product after launch stem from the higher accuracy and higher resolution brightness temperature observations from SMAP (as opposed to SMOS), improvements in the surface meteorological forcing data from the more advanced and higher-resolution "forward-processing" GEOS-5 system (as opposed to
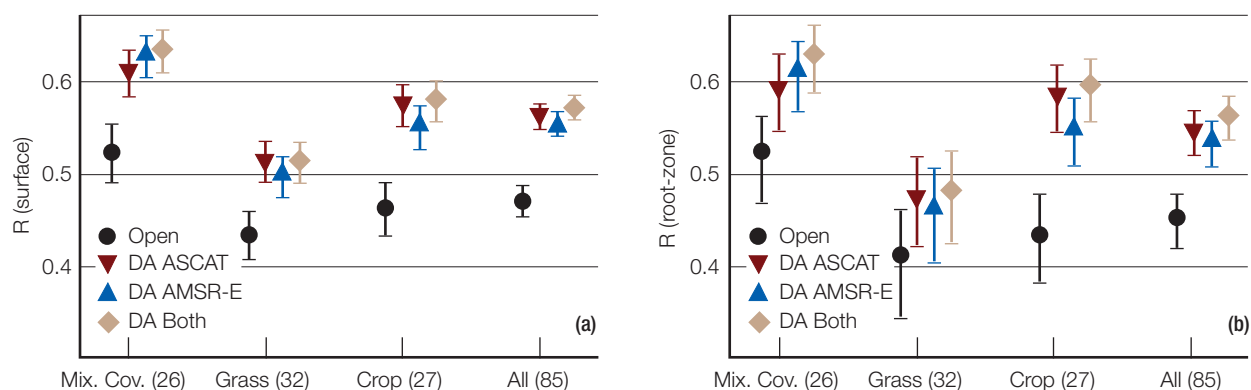
Figure 58. Mean skill for (a) surface and (b) root zone soil moisture from the open loop (ensemble mean model output, no assimilation), and the data assimilation (DA) of ASCAT, AMSR-E, and both, averaged by land cover class, with 95% confidence intervals. The number of sites in each land cover class is given in the axis labels. Skill is measured as the anomaly time series correlation coefficient (R; dimensionless) and based on all non-frozen days, from January 2007 to May 2010. (Adapted from Draper et al. 2012.)

MERRA), and the planned 9-km resolution of the land surface model (as opposed to 36 km). Moreover, the Catchment model will benefit from further improvements in the model physics and parameters and the calibration of the assimilation system will be improved. In summary, the results of this section suggest that the SMAP L4_SM data product will successfully meet its target accuracy.
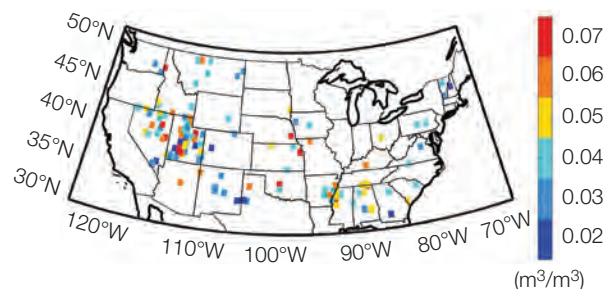


Figure 59. Root zone soil moisture RMSE ($m^3m^{-3}$) for a prototype SMAP L4_SM data product. RMSE is computed versus in situ measurements from SCAN and SNOTEL sites for March 2010 to March 2012 and after removal of the long-term mean bias.

## References

Andreadis, K. and D. Lettenmaier, "Assimilating remotely sensed snow observations into a macroscale hydrology model," *Advances in Water Resources*, 29, pp. 872–886, 2005.

De Lannoy, G. J. M., R. H. Reichle, P. R. Houser, K. R. Arsenault, N. E. C. Verhoest, and V. R. N. Pauwels, "Satellite-Scale Snow Water Equivalent Assimilation into a High-Resolution Land Surface Model," *Journal of Hydrometeorology*, 11, pp. 352–369, 2010. dx.doi.org/10.1175/2009JHM1192.1

De Lannoy, G. J. M., R. H. Reichle, K. R. Arsenault, P. R. Houser, S. V. Kumar, N. E. C. Verhoest, and V. R. N. Pauwels, "Multi-Scale Assimilation of AMSR-E Snow Water Equivalent and MODIS Snow Cover Fraction in Northern Colorado," *Water Resources Research*, 48, W01522, 2011. dx.doi.org/10.1029/2011WR010588

De Lannoy, G. J. M, R. H. Reichle, and V. R. N. Pauwels, "Global Calibration of the GEOS-5 L-Band Microwave Radiative Transfer Model over Non-Frozen Land Using SMOS Observations," *Journal of Hydrometeorology*, 14, pp. 765–785, 2013. dx.doi.org/10.1175/JHM-D-12-092.1

Draper, C. S., R. H. Reichle, G. J. M. De Lannoy, and Q. Liu, "Assimilation of passive and active microwave soil moisture retrievals," *Geophysical Research Letters*, 39, L04401, 2012. dx.doi.org/10.1029/2011GL050655

Ducharne, A., R. D. Koster, M. J. Suarez, M. Stieglitz, and P. Kumar, "A catchment-based approach to modeling land surface processes in a general circulation model, 2: Parameter estimation and model demonstration," *J. Geophys. Res*. 105(20), pp. 24823–24838, 2000.

Durand, M., and S. Margulis, "Effects of uncertainty magnitude and accuracy on assimilation of multi-scale measurements for snowpack characterization," *J. Geophys. Res.*, 113, D02105, 2008. dx.doi.org/10.1029/2007JD008662

Evensen, G., "The Ensemble Kalman Filter: theoretical formulation and practical implementation," *Ocean Dynamics*, 53, pp. 343–367, 2003. dx.doi.org/10.1007/s10236-003-0036-9

Holmes, T. R. J., T. J. Jackson, R. H. Reichle, and J. Basurea, "An Assessment of Surface Soil Temperature Products from Numerical Weather Prediction Models Using Ground-based Measurements," *Water Resources Research*, 48, W102531, 2011. dx.doi.org/10.1029/2011WR010538

Keppenne, C. L., "Data assimilation into a primitive-equation model with a parallel ensemble Kalman filter," *Mon. Weather Rev.*, 128, pp. 1971–1981, 2000.

Koster, R. D., M. J. Suarez, A. Ducharne, M. Stieglitz, and P. Kumar, "A catchment-based approach to modeling land surface processes in a general circulation model, 1: Model structure," *J. Geophys. Res.*, 105(20), pp. 24809–24822, 2000a.

Kumar, S. V., R. H. Reichle, C. D. Peters-Lidard, R. D. Koster, X. Zhan, W. T. Crow, J. B. Eylander, and P. R. Houser, "A Land Surface Data Assimilation Framework using the Land Information System: Description and Applications," *Advances in Water Resources*, 31, pp. 1419–1432, 2008a. dx.doi.org/10.1016/j.advwatres.2008.01.013

Kumar, S. V., C. Peters-Lidard, Y. Tian, R. H. Reichle, C. Alonge, J. Geiger, J. Eylander, and P. Houser, "An integrated hydrologic modeling and data assimilation framework enabled by the Land Information System (LIS)," *IEEE Computer*, 41, pp. 52–59, 2008b. dx.doi.org/10.1109/MC.2008.511

Liu, Q., R. H. Reichle, R. Bindlish, M. H. Cosh, W. T. Crow, R. de Jeu, G. J. M. De Lannoy, G. J. Huffman, and T. J. Jackson, "The contributions of precipitation and soil moisture observations to the skill of soil moisture estimates in a land data assimilation system," *Journal of Hydrometeorology*, 12, pp. 750-765, 2011. dx.doi.org/10.1175/JHM-D-10-05000.

Pan, M., and E. F. Wood, "Data Assimilation for Estimating the Terrestrial Water Budget Using a Constrained Ensemble Kalman Filter," *J. Hydrometeorol.*, 7, pp. 534–547, 2006.

Reichle, R. H., "The MERRA-Land Data Product (Version 1.2)." *GMAO Office Note no. 3*, 2012. Available at http://gmao.gsfc.nasa.gov/pubs/office_notes.

Reichle, R. H., and R. D. Koster, "Assessing the impact of horizontal error correlations in background fields on soil moisture estimation," *J. Hydrometeorol.*, 4 (6), pp. 1229–1242, 2003.

Reichle, R. H., D. McLaughlin, and D. Entekhabi, "Hydrologic data assimilation with the Ensemble Kalman filter," *Mon. Weather Rev.,* 130(1), pp. 103–114, 2002a.

Reichle, R. H., J. P. Walker, R. D. Koster, and P. R. Houser "Extended versus Ensemble Kalman filtering for land data assimilation," *J. Hydrometeorol.*, 3(6), pp. 728–740, 2002b.

Reichle, R. H., R. D. Koster, P. Liu, S. P. P. Mahanama, E. G. Njoku, and M. Owe, "Comparison and assimilation of global soil moisture retrievals from AMSR-E and SMMR," *J. Geophys. Res.*, 112, D09108, 2007. dx.doi.org/10.1029/2006JD008033

Reichle, R. H., W. T. Crow, R. D. Koster, H. Sharif, and S. P. P. Mahanama, "Contribution of soil moisture retrievals to land data assimilation products," *Geophysical Research Letters*, 35, L01404, 2008. dx.doi.org/10.1029/2007GL031986

Reichle, R. H., M. G. Bosilovich, W. T. Crow, R. D. Koster, S. V. Kumar, S. P. P. Mahanama, and B. F. Zaitchik, "Recent Advances in Land Data Assimilation at the NASA Global Modeling and Assimilation Office," in *Data Assimilation for Atmospheric, Oceanic, and Hydrologic Applications*, edited by Seon K. Park and Liang Xu, pp. 407-428, Springer Verlag, New York, 2009. dx.doi.org/10.1007/978-3-540-71056-1

Reichle, R. H., R. D. Koster, G. J. M. De Lannoy, B. A. Forman, Q. Liu, S. P. P. Mahanama, and A. Toure, "Assessment and enhancement of MERRA land surface hydrology estimates," *Journal of Climate,* 24, 6322–6338, 2011. dx.doi.org/10.1175/JCLI-D-10-05033.1

Reichle, R. H., G. J. M. De Lannoy, B. A. Forman, C. S. Draper, and Q. Liu, "Connecting Satellite Observations with Water Cycle Variables through Land Data Assimilation: Examples Using the NASA GEOS-5 LDAS," *Surveys in Geophysics*, 35, pp. 577–606, 2013. dx.doi.org/10.1007/s10712-013-9220-8

Rienecker, M. M., M. J. Suarez, R. Todling, J. Bacmeister, L. Takacs, H.-C. Liu, W. Gu, M. Sienkiewicz, R. D. Koster, R. Gelaro, I. Stajner, and J. E. Nielsen, "The GEOS-5 Data Assimilation System — Documentation of Versions 5.0.1, 5.1.0, and 5.2.0.," *Technical Report Series on Global Modeling and Data Assimilation*, 27, 2008. http://gmao.gsfc.nasa.gov/pubs/docs/Rienecker369.pdf

Rienecker, M. M. et al., "MERRA — NASA's Modern-Era Retrospective Analysis for Research and Applications," *Journal of Climate*, 24, pp. 3624–3648, 2011. dx.doi.org/10.1175/JCLI-D-11-00015.1

Rodell, M., and P. R. Houser, "Updating a land surface model with MODIS-derived snow cover," *Journal of Hydrometeorology*, 5, pp. 1064–1075, 2004.

Yi, Y., J. Kimball, L. Jones, R. H. Reichle, and K. McDonald, "Evaluation of MERRA land surface estimates in preparation for the Soil Moisture Active Passive mission," *Journal of Climate*, 24, pp. 3797–3816, 2011. dx.doi.org/10.1175/2011JCLI4034.1.

Zaitchik, B. F., and M. Rodell, "Forward-Looking Assimilation of MODIS-Derived Snow-Covered Area into a Land Surface Model," *J. Hydrometeor.*, 10, pp. 130–148, 2009. dx.doi.org/10.1175/2008JHM1042.1

Zhou, Y., D. McLaughlin, and D. Entekhabi, "Assessing the Performance of the Ensemble Kalman Filter for Land Surface Data Assimilation," *Mon. Weather Rev.*, 134, pp. 2128–2142, 2006.

# 6. Carbon Cycle Data Products

## I. Motivation and Overview

The SMAP mission provides for global mapping and monitoring of landscape freeze/thaw (FT) status and surface soil moisture conditions, with model-enhanced estimation of terrestrial carbon ($CO_2$) fluxes and underlying environmental controls. Science objectives enabled by these observations include linking terrestrial water, energy and carbon cycle processes, and reducing uncertainty regarding land-atmosphere $CO_2$ exchange and the purported missing carbon sink on land. The SMAP Level 2/3 FT product will quantify the predominant frozen or non-frozen status of the landscape at approximately 3-km resolution and 3-day fidelity. The FT retrievals will be validated to a mean spatial classification accuracy of 80%, sufficient to quantify frozen season constraints to terrestrial water mobility and the potential vegetation growing season over northern ($\geq 45°N$) land areas. The Level 4 carbon (L4_C) product uses the FT retrievals and model value-added surface and root zone soil moisture estimates with other ancillary inputs to quantify net ecosystem $CO_2$ exchange (NEE), component carbon fluxes and surface (<10 cm depth) soil organic carbon (SOC) stocks over all global vegetated land areas. The L4_C product also quantifies underlying environmental controls on these processes, including soil moisture and frozen season constraints to productivity and respiration. The L4_C NEE estimates will be validated to an RMSE requirement of 30 g C $m^{-2}$ $yr^{-1}$ or 1.6 g C $m^{-2}$ $day^{-1}$, similar to accuracy levels determined from in situ tower eddy covariance CO2 flux measurements. The L4_C research outputs include soil organic carbon (SOC), vegetation productivity, ecosystem respiration, and environmental constraint (EC) metrics clarifying FT and soil moisture related restrictions to estimated carbon fluxes. These products are designed to clarify how ecosystems respond to climate anomalies and their capacity to reinforce or mitigate global warming.

The FT signal from satellite microwave remote sensing defines the predominant frozen or non-frozen status of liquid water in the landscape, including surface vegetation, snow, and soil layer elements. The soil moisture parameter derived from satellite microwave remote sensing is a closely related measure of the relative abundance of liquid water in surface soil layers. Together, these parameters define major environmental constraints on a variety of ecosystem processes relevant to the global carbon cycle, including vegetation phenology and productivity, soil decomposition, and respiration processes (McDonald et al. 2004, Kimball et al. 2009, Kim et al. 2012). The relative importance of FT or soil moisture constraints to ecosystem processes shows strong seasonal and spatial variability in accordance with surface climate and moisture gradients. Stronger FT constraints generally occur at higher latitudes and elevations where the frozen season is a greater proportion of the annual cycle, whereas plant-available soil moisture is a major constraint to vegetation productivity and land–atmosphere carbon exchange under more arid climate conditions.

The SMAP mission provides for global mapping of soil moisture and landscape FT state dynamics with enhanced L-band (1.2/1.4 GHz) active/passive microwave sensitivity to surface soil conditions, and approximate 2–3-day temporal repeat and 3–9 km spatial resolution observations for resolving dynamic temporal changes and landscape heterogeneity in these processes. These observations enable new capabilities for global estimation and monitoring of ecosystem processes relevant to the global carbon cycle. Primary SMAP science objectives enabled by these observations include linking terrestrial water, energy and carbon cycle processes, quantifying the net carbon flux in boreal landscapes, and reducing uncertainties regarding the purported missing carbon sink on land (Entekhabi et al. 2010). The SMAP operational land products that address these carbon cycle relevant objectives include Level 2/3 FT classification (McDonald et al. 2012) and model enhanced Level 4 carbon products (Kimball et al. 2012).

## II. Freeze/Thaw Classification

### A. Science Basis for Baseline Algorithm

The timing of seasonal FT transitions generally define the duration of seasonal snow cover, frozen soils, and the timing of lake and river ice breakup and flooding in the spring (Kimball et al. 2001, 2004a). The annual non-frozen period also bounds the vegetation growing season, while annual variability in FT timing has a direct impact on net primary production and net ecosystem $CO_2$ exchange (NEE) with the atmosphere (Vaganov et al. 1999, Goulden et al. 1998). The primary science objective of the SMAP L3_FT_A product is to provide the most accurate remote sensing-based characterization of landscape FT state available at global scale supporting characterization of the spatial and temporal dynamics of landscape frozen or non-frozen condition for regions where cold temperatures are limiting for photosynthesis and respiration processes and where the timing and variability in landscape FT processes have an associated key impact on vegetation productivity and the carbon cycle. The L3_FT_A product is designed to quantify and clarify understanding of FT timing and variability to these processes over a projected three- to five-year mission cycle. The L3_FT_A product is directly relevant to a range of potential science applications, including monitoring of terrestrial carbon stocks and fluxes, flood prediction, and vegetation growth and stress. The L3_FT_A product will also help advance understanding of the effect of climate variability in the northern high latitudes.

The L3_FT_A baseline algorithm is designed to classify the land surface FT state based on a time series radar

backscatter response to the change in dielectric constant of the land surface components associated with water transitioning between solid and liquid phases. This response generally dominates the seasonal pattern of radar backscatter for regions of the global land surface undergoing seasonal FT transitions. The timing of the springtime FT state transitions corresponding to this radar backscatter response coincides with the timing of growing season initiation in boreal, alpine, and arctic tundra regions of the global cryosphere. The SMAP L3_FT_A baseline algorithm follows from an extensive heritage of previous work, initially involving truck-mounted radar scatterometer and radiometer studies over bare soils and croplands (Ulaby et al. 1986; Wegmuller 1990), followed by aircraft SAR campaigns over boreal landscapes (Way et al. 1990), and subsequently from a variety of satellite-based SAR, radiometer, and scatterometer studies at regional, continental, and global scales (e.g., Rignot and Way 1994; Way et al. 1997; Kimball et al. 2001; McDonald et al. 2004; Kim et al. 2011). These investigations have included regional, pan-boreal, and global scale efforts, supporting development of retrieval algorithms, assessment of applications of remotely sensed FT state for supporting ecologic and hydrological studies, and more recently in assembly of a satellite microwave global FT Earth System Data Record (FT-ESDR) now in distribution at the National Snow and Ice Data Center (Kim et al. 2010).

## B. Baseline Algorithm Implementation

The FT baseline algorithm is based on a seasonal threshold approach and requires only time-series radar backscatter information. The algorithm examines the time series progression of the remote sensing signature relative to signatures acquired during seasonal reference frozen and thawed states. The seasonal threshold algorithm is well-suited for application to data with temporally sparse or variable repeat-visit observation intervals and has been applied to ERS and JERS synthetic aperture radar (SAR) imagery (e.g., Rignot and Way 1994, Way et al. 1997).

A seasonal scale factor $\Delta(t)$ may be defined for an observation acquired at time t as:

$$\Delta(t) = (\sigma(t) - \sigma_{fr}) / (\sigma_{th} - \sigma_{fr}) \tag{37}$$

where $\sigma(t)$ is the measurement acquired at time t for which a FT classification is sought, and $\sigma_{fr}$ and $\sigma_{th}$ are backscatter measurements corresponding to the frozen and thawed reference states, respectively. In situations where only a single reference state is available, for example $\sigma_{fr}$, $\Delta(t)$ may be defined as a difference:

$$\Delta(t) = \sigma(t) - \sigma_{fr} \tag{38}$$

A threshold level T is then defined such that:

$$\Delta(t) > T$$
$$\Delta(t) \leq T \tag{39}$$

defines the thawed and frozen landscape states, respectively. This series of algorithms is run on a grid cell-by-cell basis for unmasked portions of the global and northern ($\geq$45°N) domains. The output from Eq. (39) is a dimensionless binary state variable designating the predominant frozen or thawed condition for each unmasked grid cell. Whereas Eq. (37) accounts for differences in the dynamic range of the remote sensing response to FT transitions driven by variations in land cover, Eq. (38) does not scale $\Delta(t)$ to account for the dynamic range in the seasonal response.

The selection of parameter T may be optimized for various land cover conditions and sensor configurations. In situations where the wintertime microwave signature is not dominated by the snow pack volume, for example for radar measurements at lower frequencies (e.g., L-band) and where shallow dry snow packs are common, $\sigma_{fr} < \sigma_{th}$ and $\Delta(t) > T$ defines the landscape thawed condition.

A major component of the SMAP baseline algorithm development has involved radar backscatter modeling and application of available satellite L-band remote sensing data from JERS-1 and ALOS PALSAR over the global terrestrial application area to develop maps of $\sigma_{fr}$, $\sigma_{th}$, and T. These activities have been used for calibration and initialization of the FT seasonal threshold algorithms prior to launch. These initial parameters will be evaluated and refined through post-launch reanalysis of the SMAP data stream.

## C. Algorithm Flow

The processing sequence for the L3_FT_A product is summarized in Figure 60. SMAP mission specifications provide for collection of global land surface observations of high-resolution (3 km) radar backscatter (L1C_S0_HiRes) for the AM (descending) orbital nodes. For the PM (ascending) orbital nodes, high-resolution backscatter (L1C_S0_HiRes) is acquired at 3-km resolution for regions north of 45°N latitude. The resulting combined L3_FT_A product will use both AM and PM overpass data in combination to delineate predominantly frozen, thawed, transitional (frozen in the AM overpass and thawed in the PM overpass) and inverse transitional (opposite of transitional) conditions. The AM overpass landscape state is provided at 3-km resolution for the global scale domain and will be used with the same seasonal threshold algorithm to delineate landscape FT status in the SMAP L3_SM_A global product. The additional PM overpass landscape state is provided at 3-km resolution north of 45°N latitude (base-

line product) for the L3_FT_A product. All renderings are posted to a 3-km EASE grid, both in global (L3_SM_A) and northern polar (L3_FT_A) projections. An example of global FT classification derived from the Special Sensor Microwave/Imager (SSM/I) is presented in Figure 61. The global domain represented in the figure corresponds to those regions of Earth's land surface where seasonal frozen temperatures are a significant constraint to annual vegetation productivity (Kim et al. 2011).

The FT classification algorithm will be applied to the radar backscatter data granules for unmasked land areas. The resulting intermediate FT products (Figure 60) will serve two purposes: (1) these data will be assembled into global daily composites in production of the L3_FT_A product, and (2) the FT product derived from global AM L1C_S0_HiRes granules will provide the binary FT state flag supporting generation of the SMAP L2 and L3 soil moisture products.
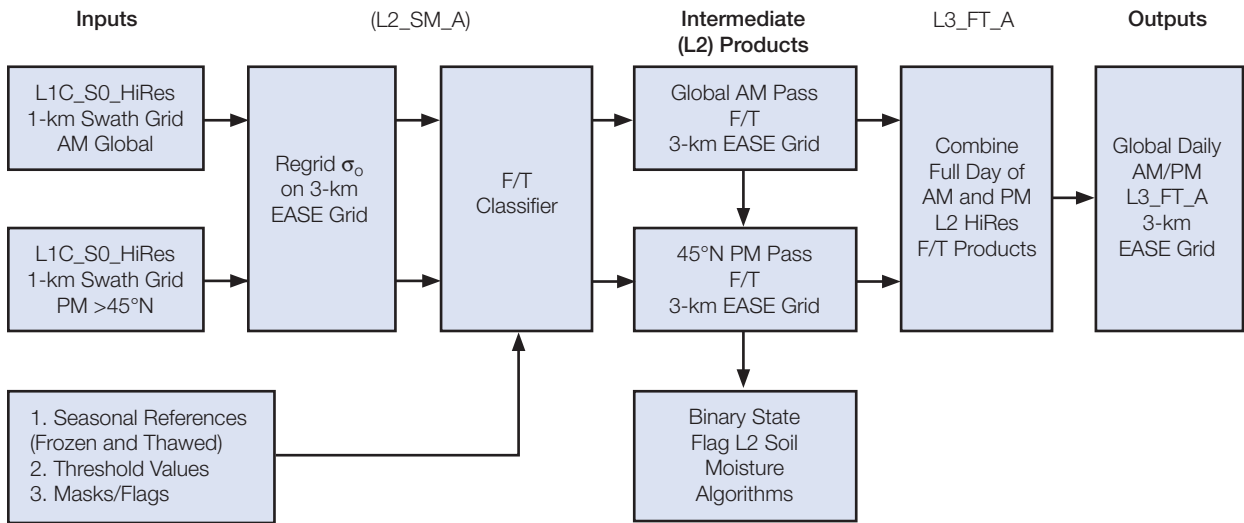


**Figure 60. Processing sequence for generation of the L3_FT_A product and the binary FT state flag to be used in generation of the SMAP soil moisture products.**
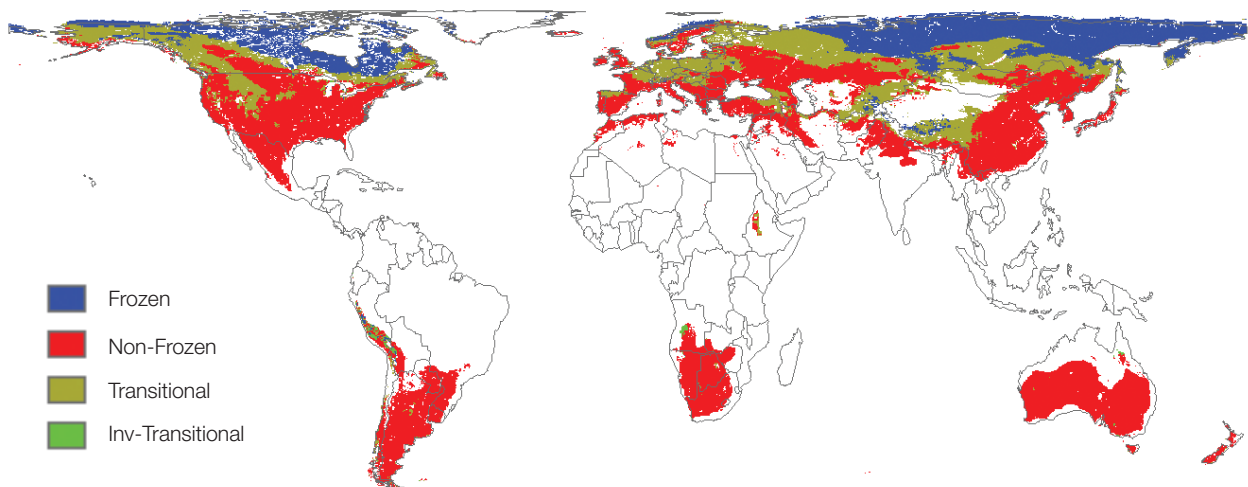


**Figure 61. Example of global daily FT product for April 10, 2004 derived from SSM/I (37 GHz channel) brightness temperature retrievals at 25 km spatial resolution (from Kim et al. 2011). Regions of frozen, thawed (here termed "non-frozen"), transitional and inverse-transitional conditions are identified.**

The FT classification algorithm is applied to the total power radar data streams, total power being the sum of HH, VV, and HV polarized backscatter. This provides the best signal-to-noise characteristic from the SMAP radar, thus optimizing product accuracy. The FT algorithm may also be employed to produce landscape FT state information from SMAP L1C_TB brightness temperature observations. Hence in the event of a failure of the SMAP radar data stream, FT data products could be produced using the L1C_TB data stream, but at a lower (~40 km) spatial resolution at the 36-km grid posting of the L1C_TB product.

Radar FT data processing will occur over unmasked portions of the global land surface domain. In addition, the FT retrieval accounts for the transient open water flag determined from the 3-km gridded backscatter in the L2_SM_A processing. No FT data processing occurs over masked areas, while "no-data" flags are used to identify masked grid cells representing ocean and inland open water bodies (static and transient), permanent ice and snow, and urban areas. The FT algorithms do not utilize ancillary data during execution and processing; however, ancillary data are used to initialize the state change thresholds that are employed in the baseline algorithm change detection scheme. Although not strictly required, prior initialization of these thresholds enhances algorithm efficiency and accuracy.

## D. Algorithm Options

Two optional temporal change detection algorithms have been identified for classification of landscape FT state dynamics using SMAP time-series L-band radar data. These options include: 1) moving window and 2) temporal edge detection FT classification algorithms. Although information from the optional algorithms may eventually prove useful for augmenting the current baseline algorithm, the use of these optional algorithms is currently unspecified.

Moving window techniques classify FT transitions based on changes in the radiometric signature relative to the temporally averaged signature computed over a moving window of specified duration. These approaches are useful when applied to temporally consistent datasets consisting of frequent (e.g., daily) observations, and for identifying multiple FT transition events. For a measurement $\sigma(t)$ acquired at time t, the difference $\delta(t)$ relative to a moving window mean may be defined as:

$$\delta(t) = \sigma(t) - \sigma_{av} \ (t - L \leq t0 \leq t - 1) \qquad (40)$$

where $\sigma_{av}$ is the average measurement (backscatter or brightness temperature) acquired over a window of duration L extending over the time interval ($t - L \leq t0 \leq t - 1$). The difference $\delta(t)$ may be compared to various thresholds, as in Eq. (39), to define the timing of critical FT

transitions. These approaches have been employed using both NSCAT and SeaWinds scatterometer data for a variety of regions (Frolking et al. 1999; Kimball et al. 2001; 2004a,b; Rawlins et al. 2005). Principal distinctions in the application of Eq. (4) have been the duration L of the moving window and the selection of thresholds applied to infer transition events.

Temporal edge detection techniques classify FT transitions by identifying pronounced step-edges in time series remote sensing data that correspond to FT transition events. As FT events induce large changes in landscape dielectric properties that tend to dominate the seasonal time-series response of the microwave radiometric signatures for the terrestrial cryosphere, edge detection approaches are suitable for identification of these events using time-series microwave remote sensing data. These techniques are based on the application of an optimal edge detector for determining edge transitions in noisy signals (Canny 1986). The timing of a major FT event is determined from the convolution applied to a time series of backscatter or brightness temperature measurements $\sigma(t)$:

$$CNV(t) = {}_\infty\!\!\int^\infty f'(x) \ \sigma \ (t - x) \ \delta x \qquad (41)$$

where $f'(x)$ is the first derivative of a normal (Gaussian) distribution. The occurrence of a step-edge transition is then given by the time when $CNV(t)$ is at a local maximum or minimum. Seasonal transition periods may involve multiple FT events. This technique accounts for the occurrence of weak edges, or less pronounced FT events, as well as larger seasonal events indicated by strong edges, and can distinguish the frequencies and relative magnitudes of these events. The variance of the normal distribution may be selected to identify step edges with varying dominance, i.e., selection of a large variance identifies more predominant step edges, while narrower variances allow identification and discrimination of less pronounced events. This approach has been applied to daily time series brightness temperatures from the SSM/I to map primary springtime thaw events annually across the pan-Arctic basin and Alaska (McDonald et al. 2004).

## E. Algorithm Performance

Refinement and testing of the FT baseline algorithm involves utilizing available satellite L-band SAR (e.g., JERS-1 SAR and ALOS PALSAR) retrievals and radar backscatter models to assess the simulated SMAP radar backscatter responses over a variety of environment, terrain, and land cover conditions in order to assess potential confusion factors and error sources. Primary sources of error and uncertainty in the FT product stem from: (1) radiometric errors due to resolution and sensor viewing geometry (azimuth); (2) geometric errors due to terrain layover and shadowing (slope/aspect); (3) within-season radar backscatter variability not accounted

for by the implementation of the constant frozen and thawed reference states employed within the baseline algorithm, and (4) variations in land cover with respect to spatial heterogeneity. Some additional errors may occur in relatively dry landscapes that contain small amounts of water such that changes in FT state result in minimal change in backscatter. Also, large precipitation events that significantly wet the land surface such that the additional surface water induces a pronounced backscatter change may induce an error in the classified FT state. Integrating JERS-1 and PALSAR datasets within the SMAP SDS test bed supports investigation of system level parameters (e.g., system noise, viewing geometry, and associated topographic effects) in the resulting FT classification error and uncertainty assessment.

The FT classification accuracy was simulated using the expected SMAP system noise vs. the difference in radar backscatter between predominantly thawed and frozen landscape states (Figure 62). A step size of at least 1.5 dB meets the targeted mean spatial classification accuracy of 80%, calculated on an annual basis.
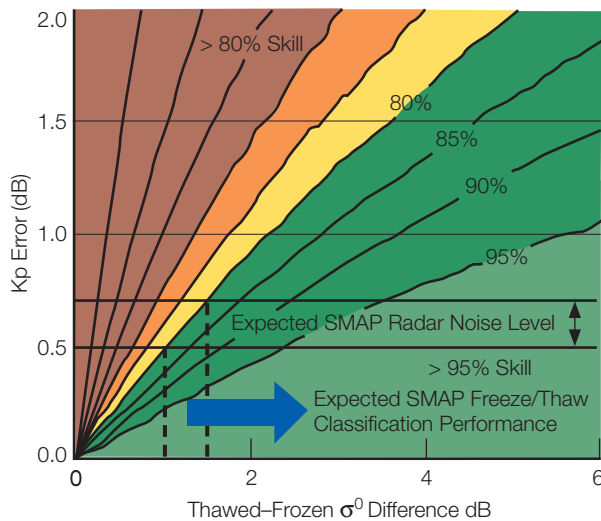


**Figure 62. Simulation of classification accuracy versus radar noise and FT state step size in backscatter. The required accuracy or skill is 80%.**

The FT algorithm performance will be assessed using the SMAP SDS algorithm test bed and available L-band microwave remote sensing datasets within the SMAP FT classification domain, including satellite based L-band observations from PALSAR and SMOS, and relatively fine scale remote sensing and biophysical data from in situ towers and airborne field campaigns (e.g. PALS, CARVE) (Jackson et al. 2011). The FT classification results will be evaluated across regional gradients in climate, land cover, terrain, and vegetation biomass through direct comparisons to existing surface biophysical measurement network observations including air/soil/vegetation temperature,

snow depth and snow water equivalent, and tower eddy covariance $CO_2$ exchange. The relationship between the algorithm FT state and the in situ sampling data will be established. Major focus areas include relations between the local/solar timing of satellite AM and PM overpasses and diurnal variability in local surface temperature and FT state dynamics, the spatial and temporal distribution and stability of L-band radar backscatter under frozen and non-frozen conditions, and the effects of sub-grid scale land cover and terrain heterogeneity on the aggregate FT signal within the sensor footprint. Biophysical measurements from in situ station measurement networks will be used to drive physical models within the SMAP algorithm test bed for spatial and temporal extrapolation of land surface dielectric and radar backscatter properties and associated landscape FT dynamics. These results will be compared with field campaign measurements and satellite based retrievals of these properties. Model sensitivity studies will be conducted to assess FT algorithm and classification uncertainties in response to uncertainties in sensor sigma-0 error and terrain and land cover heterogeneity within the sensor field of view.

## III. Net Ecosystem Carbon Exchange

### A. Science Basis for the Baseline Algorithm

Net ecosystem exchange (NEE) of $CO_2$ with the atmosphere is a fundamental measure of the balance between carbon uptake by vegetation gross primary production (GPP) and carbon losses through autotrophic ($R_a$) and heterotrophic ($R_h$) respiration. The sum of $R_a$ and $R_h$ defines the ecosystem respiration rate ($R_{eco}$), which encompasses most of the annual terrestrial $CO_2$ efflux to the atmosphere and typically represents 70-80 percent of the total magnitude of carbon uptake by GPP [Baldocchi 2008]. The NEE term provides a measure of the terrestrial biosphere capacity as a net source or sink for atmospheric $CO_2$ and its ability to offset or reinforce anthropogenic greenhouse gas emissions purported to be a major driver of global warming (IPCC 2007). NEE and its component GPP and respiration rates are spatially heterogeneous, temporally dynamic, and strongly influenced by changing environmental conditions encapsulated by the SMAP FT and soil moisture observations.

Primary science objectives of the L4_C product are to: 1) determine NEE regional patterns and temporal behavior to within the accuracy range of in situ tower eddy covariance measurement based estimates of these processes, and 2) link NEE estimates with component carbon fluxes (GPP and $R_{eco}$) and the primary environmental constraints to ecosystem productivity and respiration. The L4_C product objectives follow from the larger SMAP mission science objectives to improve understanding of processes linking terrestrial water, energy and carbon cycles, quantify the net carbon flux in boreal landscapes,

and clarify terrestrial carbon sink activity (NRC 2007: Entekhabi et al. 2010). The L4_C product is designed to quantify and improve understanding of NEE variability over a global domain, and the underlying environmental constraints to these processes over a projected three- to five-year mission cycle. The L4_C product is directly relevant to a range of potential science applications, including monitoring of terrestrial carbon stocks and fluxes, and NEE source-sink activity for atmospheric $CO_2$. The L4_C product will also advance understanding of the way in which global ecosystems, including northern boreal Arctic biomes, respond to climate variability and their capacity to reinforce or mitigate global warming.

The baseline L4_C algorithms utilize SMAP derived FT and soil moisture information to define surface water mobility constraints to NEE and underlying vegetation productivity, soil decomposition, and respiration processes. The L4_C model combines satellite data-driven light use efficiency (LUE) and three-pool soil decomposition algorithms within a terrestrial carbon flux (TCF) model framework for estimating daily carbon fluxes and surface soil organic carbon (SOC) stocks (Kimball et al. 2012; Yi et al. 2013). The L4_C model incorporates extensive heritage from the NASA EOS MODIS MOD17 operational GPP product (Zhao and Running 2010) and CASA land model (Potter et al. 1993), while the SMAP derived FT and soil moisture information is used to define frozen temperature and plant-available moisture constraints to estimated productivity and soil decomposition processes. The SMAP information is combined with other ancillary inputs, including satellite (MODIS) derived canopy fraction of photosynthetically active radiation (FPAR) and land cover information, and daily surface meteorology from observation-constrained global model reanalysis. The product domain encompasses all global vegetated land areas, while model calculations are conducted at a daily time step. The SMAP L4_SM and L3_SM_A products are used as primary environmental inputs to the L4_C algorithms, providing a direct link between SMAP product retrievals and net ecosystem $CO_2$ exchange, and underlying vegetation productivity, soil decomposition, and respiration processes.

## B. Baseline Algorithm Implementation

The L4_C algorithms utilize a TCF model to integrate SMAP mission derived FT and soil moisture inputs with ancillary MODIS FPAR and other biophysical data to estimate NEE and its component carbon fluxes (GPP and $R_{eco}$), surface (<10 cm depth) SOC stocks, and associated environmental constraints to these processes (Kimball et al. 2012). The NEE parameter is the primary (validated) product field used for demonstrating L4_C accuracy and success in meeting product science requirements (Jackson et al. 2012), though the other L4_C product fields also have strong carbon cycle science utility. The targeted

accuracy of the L4_C NEE estimate is $\leq 30$ g C m$^{-2}$ yr$^{-1}$ or 1.6 g C m$^{-2}$ d$^{-1}$ (RMSE), similar to the level of accuracy attained from in situ tower eddy covariance $CO_2$ flux measurement based NEE observations (Baldocchi 2008; Richardson and Holliger 2005; Richardson et al. 2008).

NEE (g C m$^{-2}$ d$^{-1}$) is computed on a daily basis as the residual difference between GPP and respiration from autotrophic ($R_a$) and heterotrophic ($R_h$) components:

$$NEE = (R_a + R_h) - GPP \qquad (42)$$

where positive (+) and negative (-) NEE fluxes denote the respective terrestrial loss or uptake of $CO_2$. The GPP term (g C m$^{-2}$ d$^{-1}$) represents the mean vegetation gross primary production of the dominant plant functional type (PFT) within a grid cell and is derived on a daily basis using a LUE algorithm:

$$GPP = \varepsilon * APAR \qquad (43)$$

where $\varepsilon$ is the conversion efficiency (g C MJ$^{-1}$) of photosynthetically active radiation (PAR) to vegetation biomass, and APAR (MJ m$^{-2}$ d$^{-1}$) is the amount of PAR absorbed by the canopy and available for photosynthesis. PAR (MJ m$^{-2}$ d$^{-1}$) is estimated as a constant proportion (0.45) of incident shortwave solar radiation at the surface ($R_{sw}$, MJ m$^{-2}$ d$^{-1}$) and is used with the estimated fraction of incident PAR absorbed by the vegetation canopy (FPAR) to determine APAR:

$$APAR = PAR * FPAR \qquad (44)$$

The PAR conversion efficiency ($\varepsilon$) term is derived on a daily basis from an estimated maximum rate ($\varepsilon_{mx}$, g C MJ$^{-1}$) prescribed for different plant functional types (PFT classes) (Zhao et al. 2005), and is reduced for suboptimal environmental conditions defined as the product ($\varepsilon_{mult}$) of dimensionless rate scalars ranging from no effect (1) to complete rate reduction (0) for daily minimum air temperature ($T_{mn\_scalar}$), atmosphere vapor pressure deficit ($VPD_{scalar}$), landscape FT status ($FT_{scalar}$), and integrated (0–1 m depth) surface to root zone soil moisture ($SM_{rz\_scalar}$) conditions:

$$\varepsilon_{mult} = T_{mn\_scalar} * VPD_{scalar} * FT_{scalar} * SM_{rz\_scalar} \qquad (45)$$

$$\varepsilon = \varepsilon_{mx} * \varepsilon_{mult} \qquad (46)$$

The above attenuation scalars are defined as simple switch and linear ramp functions (Kimball et al. 2012), and deviate from the MOD17 LUE logic (Zhao et al. 2005) by specifying environmental constraints for frozen landscape conditions and suboptimal root zone soil moisture ($SM_{rz}$) levels. The attenuation functions vary according to prescribed minimum and maximum constraints determined for different global biome types (Kimball et al. 2012). The primary model environmental response characteristics are

determined using control parameters defined for individual land cover PFT classes within a general Biome Properties Look-Up Table (BPLUT). A detailed set of global BPLUT parameters is summarized in the L4_C Algorithm Theoretical Basis Document (ATBD) (Kimball et al. 2012). These parameters were assembled from MODIS operational (MOD17) GPP product definitions (Zhao et al. 2005) and detailed L4_C model calibration and validation studies using in situ $CO_2$ fluxes and environmental measurements from global tower eddy covariance network (FLUXNET) monitoring sites (Kimball et al. 2009, 2012; Yi et al. 2013).

The $FT_{scalar}$ term represents the frozen temperature constraint to landscape water mobility and GPP as determined from regional comparisons between tower based GPP observations and daily FT retrievals from satellite microwave remote sensing (Kimball et al. 2004; Kim et al. 2012). The $SM_{rz\_scalar}$ term provides a direct low soil moisture constraint to GPP in addition to the atmosphere moisture deficit (VPD) constraint. These additional terms provide for a direct link between SMAP FT and soil moisture products, and associated environmental constraints to vegetation productivity and terrestrial carbon flux calculations.

The autotrophic respiration ($R_a$) term (42) represents the sum of vegetation growth and maintenance respiration, and is computed on a daily basis as a fixed proportion of GPP within individual PFT classes, based on observational evidence that variability in the ratio of Ra to GPP is conservative within individual biomes (Litton et al. 2007, Gifford 2003).

Heterotrophic respiration is computed as the sum of variable decomposition and respiration rates from three distinct SOC pools as:

$$R_h = (K_{met} * C_{met} + [1-F_{str}] * K_{str} * C_{str} + K_{rec} * C_{rec}) \qquad (47)$$

where $C_{met}$, $C_{str}$ and $C_{rec}$ (g C m$^{-2}$) represent metabolic, structural, and recalcitrant SOC pools, and $K_{met}$, $K_{str}$ and $K_{rec}$ (d$^{-1}$) are the corresponding decomposition rate parameters. The metabolic and structural SOC pools represent plant litter with relatively short (e.g., $\leq$ 5 years) turnover periods, while the recalcitrant pool represents more physically and chemically protected SOC with a longer turnover time.

The three-pool soil decomposition model approximates the complex variation of intrinsic SOC turnover rates, but has been found to produce results consistent with a wide range of observations (Knorr and Kattge 2005). Litter inputs to the $C_{met}$ and $C_{str}$ pools (47) are derived as proportions of estimated vegetation net primary production (NPP), while input to the $C_{rec}$ pool is defined as a constant proportion ($F_{str}$) of decomposed detritus from the $C_{str}$

pool (Ise and Moorcroft 2006); outputs to the SOC pools represent daily sums of the respired components:

$$dC_{met}/dt = C_{fract} * NPP - R_{h,met} \qquad (48)$$

$$dC_{str}/dt = (1 - C_{fract}) * NPP - R_{h,str} \qquad (49)$$

$$dC_{rec}/dt = F_{str} * R_{h,str} - R_{h,rec} \qquad (50)$$

where NPP is estimated as a fixed proportion of GPP (g C m$^{-2}$ d$^{-1}$) within individual PFT classes (Kimball et al. 2012; Gifford 2003; Litton et al. 2007). The $C_{fract}$ term defines the rate in which litterfall from NPP is allocated to metabolic and structural SOC pools, and is specified as a fixed rate within individual land cover classes (Potter et al. 1993; Ise and Moorcroft 2006). Values for $C_{fract}$ and proportional allocations of GPP to Ra and NPP are defined in the BPLUT for individual PFT classes (Kimball et al. 2012). This approach assumes that litter inputs to the SOC pool are proportional to NPP under long-term steady state conditions (Ise and Moorcroft 2006).

A dynamic litterfall scheme is employed for daily carbon allocation of annual NPP to the metabolic and structural SOC pools ($C_{met}$ and $C_{str}$), where the NPP litterfall fraction is evenly distributed over each annual cycle. This approach ignores potential large seasonal litterfall variability, but avoids the use of more complex phenology models that may contribute additional model complexity and uncertainty.

The L4_C algorithms employ dimensionless rate curves to account for soil temperature and moisture constraints to soil decomposition. The soil decomposition rate (K) is derived as the product of dimensionless multipliers for soil temperature ($T_{mult}$) and moisture ($W_{mult}$) and a theoretical optimum or maximum rate constant ($K_{mx}$; d$^{-1}$) under prevailing climate conditions:

$$K_{met} = K_{mx} * T_{mult} * W_{mult} \qquad (51)$$

where $T_{mult}$ and $W_{mult}$ vary between 0 (fully constrained) and 1 (no constraint). The value for $K_{mx}$ is specified as a constant within individual PFT classes, while decomposition rate parameters for $K_{str}$ and $K_{rec}$ are estimated as 40% and 1% of $K_{met}$, respectively (Ise and Moorcroft 2006). The estimation of K assumes constant soil decomposer efficiency (microbial $CO_2$ production to carbon assimilation ratio) inherent in the $K_{mx}$ term, and that soil moisture and temperature are the dominant controls on near-term (daily, seasonal, annual) decomposition rates. However, this approach also assumes that changes in litter quality (e.g., physical protection and/or chemical resistance to microbial decomposition) influence $R_h$ and NEE indirectly through associated changes in ancillary satellite (MODIS) derived FPAR inputs, especially over generally nitrogen (N) limited boreal and tundra ecosystems.

The soil decomposition rate response to temperature is defined using an Arrhenius type function [Lloyd and Taylor 1994]:

$$T_{mult} = \exp [308.56 * ((46.02 + T_{opt})^{-1} - (T_s + 46.02)^{-1})] \quad (52)$$

where $T_{opt}$ and $T_s$ are the respective reference and input daily surface soil temperatures (°C) for $T_s \leq T_{opt}$. The $T_{opt}$ term defines the optimum temperature for soil decomposition and is prescribed as a PFT-specific constant in the BPLUT. The above relationship defines a low-temperature constraint to soil decomposition; $T_{mult}$ is assumed to be unity and soil decomposition no longer temperature limited for soil temperatures above $T_{opt}$. Under these conditions, soil moisture is expected to decline with warmer soil temperatures and $W_{mult}$ becomes the primary constraint to $K_{met}$. This assumption is generally valid for most global biome types, including temperate, boreal and Arctic ecosystems (Kimball et al. 2009; Yi et al. 2013), but may not hold for warm and humid climate zones including tropical biomes (Jones et al. 2003). A variety of functional types have been used to describe temperature effects on soil respiration, while the Arrhenius model is physically based and provides a relatively accurate, unbiased estimate of soil respiration across a wide range of conditions (Lloyd and Taylor 1994; Knorr et al. 2005; Yvon-Durocher et al. 2012).

The soil decomposition rate response to soil moisture (SM) variability is defined for unsaturated (SM ≤ $SM_{opt}$) conditions as:

$$W_{mult} = [1 + a * EXP(b * SM_{opt})] / [1 + a * EXP(b * SM)] \quad (53)$$

where SM is expressed as a proportion (%/100) of soil saturation; $SM_{opt}$ is the optimum soil moisture level for heterotrophic decomposition and is prescribed for different PFT classes. The $a$ and $b$ terms are empirical fitting parameters (dimensionless) that define the decomposition rate response to soil moisture variability and are specified for different PFT classes in the BPLUT. The $W_{mult}$ term is assumed to be unity (no restriction) for SM>$SM_{opt}$, which accounts for ecosystem adaptations to wet soil conditions and a general lack of landscape level observational evidence for extended SM saturation and associated reductions in aerobic decomposition (Chimner 2004; Elberling et al. 2011). The above algorithm also assumes that mean surface soil properties are similar within individual land cover classes and relatively coarse (~9-km resolution) global satellite footprints and modeling grids.

The L4_C daily product format includes individual granules (output variables) for each grid cell representing GPP, $R_h$ and NEE fluxes (g C m$^{-2}$ d$^{-1}$), surface SOC (kg C m$^{-2}$), dimensionless (0-1) environmental constraint (EC) indices affecting the productivity and respiration calculations, and a dimensionless data quality assessment (QA) identifier for the NEE calculation. A L4_C product example for NEE is shown in Figure 63. The L4_C daily outputs are posted to a 9-km resolution global Earth grid having 1624 rows and 3856 columns, and global EASE2 grid projection format consistent with the SMAP L4_SM inputs. The L4_C global processing is conducted at a finer 1-km spatial resolution consistent with the ancillary MODIS FPAR (MOD15) and land cover classification (MOD12Q1) (Friedl et al. 2010) inputs used to define vegetation canopy attributes and BPLUT response characteristics for the model calculations. The model output parameter spatial means and variability (SD) within each 9-km resolution grid cell are defined from the underlying 1-km resolution L4_C calculations, while regional means from up to 8 global PFT classes are also represented within each cell. The (8) PFT classes and BPLUT parameters associated with these classes are enumerated elsewhere (Kimball et al. 2012). The EC granule includes four separate fields for each grid cell describing: 1) the estimated mean bulk PAR conversion efficiency constraint ($\varepsilon_{mult}$) to the LUE based GPP calculations; 2) mean soil moisture ($W_{mult}$), and 3) temperature ($T_{mult}$) constraints to the $R_h$ calculations; and 4) the proportional frozen area within each 9-km grid cell defined from the finer (3-km) resolution SMAP FT (L3_SM_A) inputs. The EC indices for $\varepsilon_{mult}$, $W_{mult}$, and $T_{mult}$ are derived from the same dimensionless multipliers used to derive GPP and $R_h$, but are rescaled in the product table to range from 0 (fully constrained) to 100 (no constraint) percent.

## C. Algorithm Flow

The baseline L4_C model structure is summarized in Figure 64 for respective LUE and carbon flux model components. The algorithm approach has structural elements similar to the Century (Parton et al. 1987; Ise and Moorcroft 2006) and CASA (Potter et al. 1993) soil decomposition models and operational MODIS MOD17 GPP algorithm (Zhao et al. 2005; Zhao and Running 2010), and is adapted for use with daily biophysical inputs derived from both global satellite and model reanalysis data (Kimball et al. 2009; Yi et al. 2012).

The L4_C model outputs are produced at a daily time step and over a global domain encompassing all vegetated land areas (Figure 63) represented by ancillary land cover classification and FPAR (MODIS) inputs. Ancillary FPAR inputs from the MODIS (MOD/MYD15) operational product stream are obtained with approximate 8-day temporal fidelity and native global sinusoidal grid tile format, and reprojected to the 1-km resolution global EASE2 grid projection format as a L4_C preprocessing step. Only best quality (QC) FPAR data are used as L4_C inputs, while missing or lower QC data for each grid cell are replaced with alternative FPAR inputs from an ancillary global mean 8-day FPAR climatology defined from the long-term (2000–2010) MODIS MOD15 best QC data record. Other dynamic daily ancillary inputs include coarser

**ENF Tower Site**
(CA-OJP, 53.92°N, 104.7°W)

r = 0.56; RMSE = 0.65 g C m⁻² d⁻¹

NEE July 15
[g C m⁻² d⁻¹]

<—1.5    —0.5    0.5    >1.5

L4_C NEE (DOY 196, g C m⁻² d⁻¹)
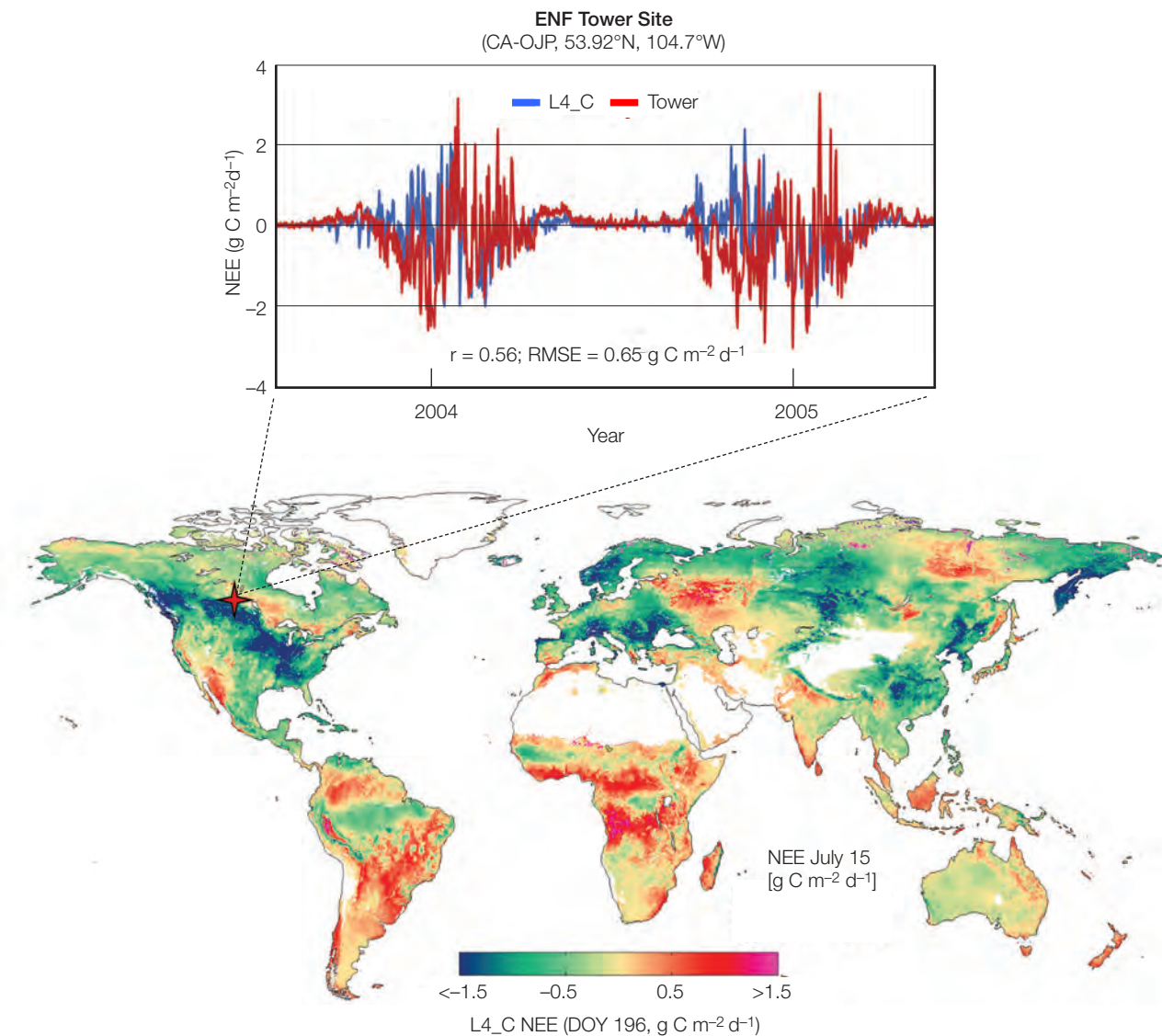
**Figure 63. L4_C global NEE product example for a selected day. The L4_C product domain encompasses all global vegetated land areas. A comparison of L4_C and tower eddy covariance measurement based daily NEE is also shown for a representative boreal coniferous evergreen** needleleaf forest (ENF) site. A negative (positive) carbon flux denotes net ecosystem uptake (loss) of atmospheric $CO_2$. Nonvegetated land and other areas outside of the processing domain are shown in white.

3-km resolution FT (L3_SM_A), 9-km resolution surface and root zone soil moisture (L4_SM), and GMAO (FP) surface meteorology. These data provide primary environmental forcings for the carbon model calculations and are subsampled to the nested 1-km resolution grid cells used for L4_C processing. The carbon model outputs are then spatially aggregated to the final 9-km resolution global EASE2 grid and HDF5 product format as a post-processing step. The L4_C product has a target mean data latency of approximately 14 days. The product latency is primarily determined by latency and availability of ancillary MODIS FPAR (~12-day latency) inputs, and accounting for an additional 2-day data processing period.

**D. Algorithm Options**

Two primary algorithm options are considered that affect the L4_C design relative to the product baseline. These options include: 1) use of lower order satellite optical-IR remote sensing based spectral vegetation index (VI) inputs to estimate FPAR for the LUE model based GPP calculations; 2) use of ancillary vegetation disturbance (fire) and recovery status inputs to perturb model SOC and carbon flux calculations from dynamic steady-state conditions.

Option 1) allows for empirical estimation of FPAR using more readily available VI inputs if an operational FPAR
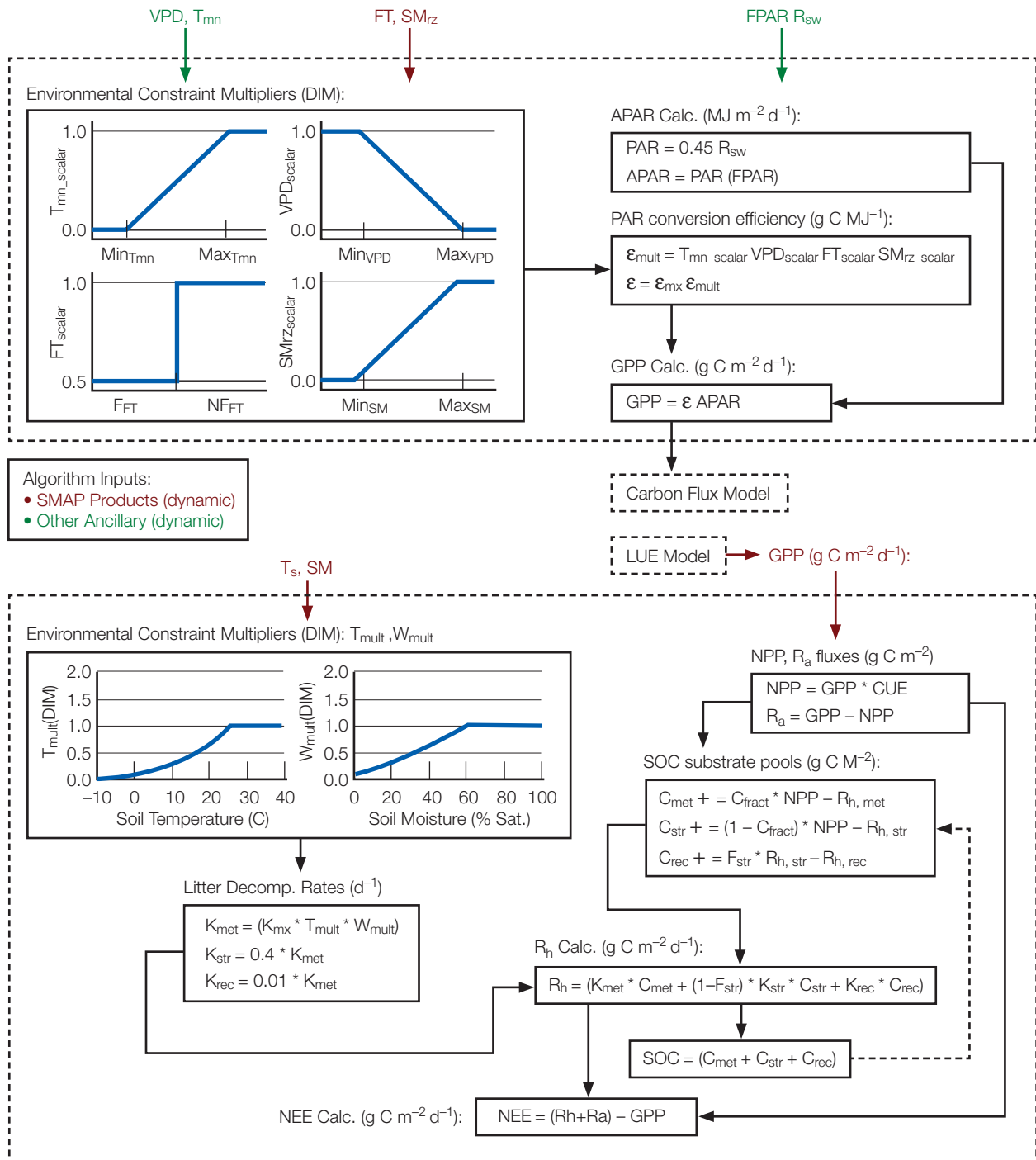
**Figure 64.** Upper graphic: Baseline L4_C LUE model structure for estimating GPP. Arrows denote the primary pathways of data flow, while boxes denote the major process calculations. Primary inputs include daily root zone soil moisture ($SM_{rz}$) and landscape freeze/thaw (FT) status from SMAP L4_SM and L3_SM_A products (in red), and other dynamic ancillary inputs (in green) including FPAR (MODIS) and land model (GMAO) data assimilation based daily surface meteorology, including vapor pressure deficit (VPD), minimum air temperature ($T_{mn}$) and incident solar shortwave radiation ($R_{sw}$). Model calculations are performed at 1-km spatial resolution using dominant PFT and BPLUT response characteristics for each grid cell defined from a global land cover classification. The resulting GPP calculation is a primary input to the carbon flux model (lower graphic). Primary carbon flux model inputs (in red) include daily GPP from the LUE model, and surface soil moisture (SM) and temperature ($T_s$) from the SMAP L4_SM product. NEE is the primary (validated) output, while GPP, Rh, SOC and EC constraint metrics are secondary (research) outputs.

product stream becomes unavailable during the SMAP mission period. The use of alternative VI inputs from other operational satellite sensors (e.g., VIIRS) potentially enhances the availability and reliability of algorithm inputs, but may degrade product accuracy and latency. However, regional and global testing of the L4_C model using alternative FPAR inputs derived from PFT specific empirical relationships between best QC MODIS 16-day composited NDVI (MOD13A2) and the FPAR (MOD15) 8-day climatology (2000–2010) showed similar accuracy as the L4_C product baseline for GPP (Kimball et al. 2012; Yi et al. 2013).

Option 2) enhances the scientific merit and potential L4_C product accuracy relative to the baseline by representing nonsteady state vegetation disturbance and recovery impacts on GPP, NEE, and SOC stocks. For the product baseline, vegetation disturbance is only partially represented by associated impacts to ancillary FPAR (MODIS) inputs. Vegetation disturbance from wildfire and other agents has a major impact on vegetation composition and function, and associated growth and respiration processes (Amiro et al. 2010; Coursolle et al. 2012), which can alter the balance between carbon sequestration and SOC storage, and NEE source/sink activity (Balshi et al. 2007; Bond-Lamberty et al. 2007). A nonsteady state disturbance recovery option for the L4_C algorithm was developed and tested over the northern (≥45°N) domain (Yi et al. 2013). Regional disturbance and recovery patterns were defined using an ancillary satellite ensemble global fire emissions database (Giglio et al. 2010), and empirical models of SOC and GPP recovery derived from MODIS VI (EVI, NDVI) inputs and boreal fire chronosequence tower site network observations of terrestrial carbon flux recovery. The disturbance recovery option resulted in improved L4_C based estimates of GPP and NEE in relation to the tower chronosequence observations. Drought and temperature variations had larger regional impacts on the carbon fluxes than fire disturbance recovery, though fire disturbances were heterogeneous, with larger impacts on carbon fluxes for some areas and years. The model performance for both baseline and estimated non steady-state conditions was generally within the targeted L4_C accuracy requirements for NEE in relation to regional tower observations. The dynamic disturbance and recovery option adds potential science utility by providing a more realistic representation of nonsteady state conditions represented by most ecosystems. However, this option increases ancillary input requirements and model complexity, while the tower chronosequence observations needed for model development and parameterization are generally lacking over the global domain.

**E. Algorithm Performance**

The L4_C algorithm performance, including variance and uncertainty estimates of model outputs, was determined during the mission pre-launch phase through model sensitivity studies using ancillary inputs similar to those used for mission operations and evaluating the resulting model simulations over the observed range of northern (≥45°N) and global conditions. Model inputs used for these studies were similar to the L4_C operational inputs and included GMAO MERRA based daily surface meteorology and soil moisture inputs (Yi et al. 2011), satellite passive microwave remote sensing based soil moisture (Kimball et al. 2009) and freeze/thaw records (Kim et al. 2012), and MODIS VI, FPAR, and GPP records (Kimball et al. 2012; Yi et al. 2013).

An estimated error budget for the L4_C NEE product is summarized in Table 15. This table quantifies the expected primary error sources and individual and cumulative error contributions to the L4_C based NEE estimates. The error budget indicates baseline L4_C product performance within the targeted accuracy guidelines (i.e., NEE RMSE ≤ 30g C m$^{-2}$ yr$^{-1}$ and 1.6 g C m$^{-2}$ d$^{-1}$). Land cover heterogeneity contributes more than half (57%) of the total product NEE uncertainty variance, while GPP, soil moisture, and temperature inputs together contribute 31% of total error variance, and the remaining 12% of the expected total error variance attributable to model parameterization uncertainty. Errors contributed by model parameterization are the least certain component of the error analysis because it is difficult to precisely quantify global parameter variability and model structural inaccuracy. The error budget is defined relative to northern biomes, which are the primary focus of L4_C science requirements and traceability. The relative (%) contributions of individual error components vary for other biomes and for variable weather and climate conditions. The error contribution of input soil moisture and temperature uncertainty is also expected to be larger for warmer and drier grasslands relative to boreal biomes.

A spatial implementation of the L4_C error (RMSE) budget over all global vegetated land areas was conducted using a forward model sensitivity analysis driven by available ancillary satellite (MODIS) and global model reanalysis (MERRA) inputs (Figure 65). These simulations included both random and systematic error components from model inputs and land cover heterogeneity effects at the 9-km spatial resolution of the global product. The resulting global NEE error budget is consistent with the previous error budget (Table 15); the global simulations indicate that the L4_C accuracy requirements are satisfied over more than 82 and 89% of respective global and northern (≥45°N) vegetated land areas, and congruent with independent NEE estimates derived from in situ tower (FLUXNET) eddy covariance network CO$_2$ flux measurements (Baldocchi 2008). Error contributions from the GPP calculations and soil moisture and temperature inputs vary with regional gradients in estimated vegetation biomass productivity.

The estimated L4_C NEE uncertainty increases in higher biomass productivity areas (e.g., forests) due to assumptions of increasing uncertainty in satellite microwave soil moisture retrievals and associated model data assimilation based soil moisture inputs. The estimated NEE uncertainty is lower than might be expected in some warmer tropical high biomass productivity areas (e.g., Amazon rainforest) because of reduced low temperature and moisture constraints to the L4_C respiration calculations so that the bulk of model uncertainty is contributed by GPP in these areas. Model NEE uncertainty in the African Congo is larger than Amazonia due to relatively drier climate conditions in central Africa defined from the GMAO MERRA surface meteorology inputs and associated uncertainty contributions from both respiration and GPP. These initial estimates will be refined during SMAP operations.

Table 15.  Estimated Total Annual NEE Error (RMSE) Budget for the SMAP L4_C Product

| Type of Error | Error Source | Source Units | Range | Value | NEE Contribution (g C m$^{-2}$ yr$^{-1}$) |
|---|---|---|---|---|---|
| Input Data | $T_s$ | °C | 1.5 – 4.0 | 3.5 | 6.2 |
| | SM | Vol. m$^3$ m$^{-3}$ | 0.04 – 0.10 | 0.05 | 5.7 |
| | GPP | g C m$^{-2}$ d$^{-1}$ | 1.0 – 2.0 | 1.5 | 14.5 |
| Model Parameterization | $K_{mx}$ | d$^{-1}$ | 0.001 – 0.01 | 0.005 | 2.9 |
| | SOC Pool | g C m$^{-2}$ | 100 – 1000 | 1000 | 9.6 |
| | Ra / GPP | Dim. | 0.05 – 0.15 | 0.1 | 2.7 |
| Heterogeneity | Land cover heterogeneity ($R_h$) | g C m$^{-2}$ yr$^{-1}$ | 0 – 60 | 16 | 22.6 |
| Total NEE Error | Inputs only | g C m$^{-2}$ yr$^{-1}$ | | | 16.7 |
| | Model only | g C m$^{-2}$ yr$^{-1}$ | | | 10.4 |
| | Inputs + Model | g C m$^{-2}$ yr$^{-1}$ | | | 19.7 |
| | Inputs + Model + Het. | g C m$^{-2}$ yr$^{-1}$ | | | 30.0 |
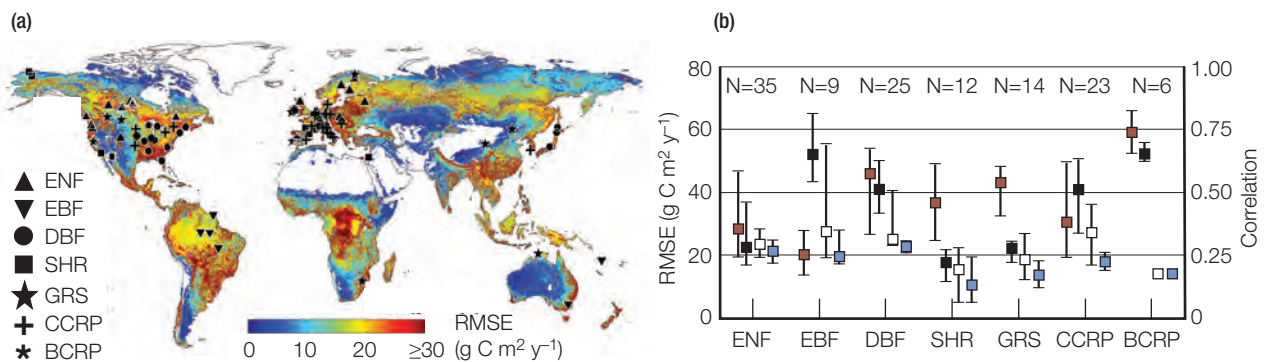


Figure 65. (a) Forward model simulations of L4_C NEE annual error (RMSE) derived using MODIS and MERRA reanalysis inputs; nonvegetated areas (in white) were masked from the analysis. Filled symbols denote selected tower (FLUXNET) validation sites for: Evergreen Needleleaf Forest (ENF), Deciduous Broadleaf Forest (DBF), Mixed Forest (MXF) & Grassland (GRS). (b) Estimated NEE error for the 124 tower sites grouped by PFT class; closed squares denote mean RMSE [■] and correlation [■] between tower observations and coincident L4_C simulations; Open squares [□] denote RMSE for each global PFT class, including random and systematic errors; Blue squares [■] denote global RMSE from random error only. Error bars denote two standard deviations. The number (N) of tower sites in each PFT class and mean correlations (R) between L4_C and tower NEE are also shown. These results indicate that the L4_C accuracy requirements (i.e., NEE RMSE ≤ 30 g C m$^{-2}$ yr$^{-1}$) are met over more than 82% and 89% of global and northern vegetated land areas, respectively.

A detailed summary of L4_C calibration and validation activities is provided elsewhere (Kimball et al. 2012; Jackson et al. 2012) and also summarized in Chapter 7 (Calibration and Validation Plan). The statistical methods and domains of validity used for testing the L4_C algorithms and for demonstrating that their performance meets the SMAP science requirements primarily involve direct comparisons between L4_C outputs and tower eddy covariance $CO_2$ flux measurements from globally distributed FLUXNET monitoring sites [Baldocchi 2008]. Approximately 80 (from >400) FLUXNET sites meet L4_C validation criteria for having spatially homogeneous land cover characteristics consistent with the overlying global PFT classification used for the L4_C carbon model calculations, and multi-year data records with well characterized uncertainty.

Initial investigations of L4_C product accuracy indicate that model performance is within the targeted accuracy requirements and at the level of tower observation uncertainty (Figure 65) (Kimball et al. 2012). A regional test of the L4_C algorithms over a northern domain showed favorable results for GPP (n=47 sites, R≥0.7, RMSD <2.5 g C m$^{-2}$ d$^{-1}$), and overall consistency for NEE (n=22, R>0.5, RMSD<2.5 g C m$^{-2}$ d$^{-1}$) in relation to daily carbon fluxes from regional tower sites (Yi et al. 2013); the model simulations of surface SOC stocks were also similar to independent SOC maps derived from regional soil inventory records. A pan-Arctic regional model intercomparison study also indicated that the L4_C model performance is similar to more detailed ecosystem process model simulations of terrestrial carbon fluxes (McGuire et al. 2012). Similar L4_C product validation efforts will occur during the SMAP post-launch period and will be used to clarify and refine model performance and product accuracy.

## F. Product Constraints, Limitations and Assumptions

The L4_C algorithms incorporate several simplifying assumptions consistent with a global satellite remote sensing product and may not sufficiently characterize all the major processes regulating land-atmosphere $CO_2$ exchange. For example, soil decomposition studies indicate that the carbon assimilation efficiency of soil microbes and associated SOC decomposition rates vary with changes in soil nitrogen availability and may not be adequately represented by a biome-specific optimum soil decomposition rate ($K_{mx}$). Soil heterotrophic respiration from deeper (e.g., >20 cm depth) soil layers can increase with soil warming, with a significant respiration contribution from older (centuries before present) SOC sources. These processes may not be adequately represented by regional GPP estimates, recent climate conditions, and near surface FT and SM dynamics from relatively coarse satellite remote sensing and model assimilation data.

The L4_C algorithms assume that the bulk of soil decomposition and $R_h$ is derived from recent litterfall and surface (<10 cm depth) soil layers. This assumption generally holds for most ecosystems, including boreal-arctic biomes, because the bulk of annual litter decomposition is composed of relatively recent (i.e., <5 years old) leaf litter that is more labile than older soil litter layers. However, deeper soil layers can contribute up to 40% or more of total $R_h$, especially later in the growing season as the seasonal warming of deeper layers progresses and lags behind shallower soil layers. The contribution of deeper SOC layers to $R_h$ may also increase over longer (decadal) time periods in boreal-arctic regions due to the large reservoir of soil carbon stored in permafrost soils, and potential warming and destabilization permafrost under global warming (Schuur et al. 2009). While the L4_C baseline algorithms are considered adequate to capture NEE seasonal and interannual variations over a 3–5 year mission life, the algorithm structure would require additional complexity to represent the $R_h$ contributions from permafrost degradation and deeper soil layers over longer time periods.

The L4_C baseline algorithms assume that surface SOC stocks are in dynamic equilibrium with estimated vegetation productivity; this steady-state assumption produces a carbon neutral biosphere (cumulative NEE = 0) over the long-term record, but represents NEE seasonal and interannual variability in response to weather and near-term climate variability (Yi et al. 2013). However, terrestrial carbon source-sink activity at most locations is impacted by disturbance history, which perturbs above and below ground carbon stocks away from steady-state conditions (Baldocchi 2008). Disturbance and recovery effects on L4_C carbon flux calculations are partially accounted for through associated impacts to ancillary FPAR or VI (option) inputs to the L4_C LUE algorithm and GPP calculation. The L4_C disturbance recovery algorithm option also provides a more explicit representation of non-steady state fire disturbance and recovery impacts to GPP, SOC and NEE estimates, and generally improved model accuracy (Yi et al. 2013), but at the expense of increased ancillary input and model parameterization requirements.

Land cover and land use change (LCLUC) from direct and indirect human impacts have a large impact on NEE over the global domain, but are expected to have less impact over sparsely populated northern land areas. Satellite remote sensing studies indicate that LCLUC from deforestation accounts for up to 1–3% yr$^{-1}$ of forested land area in tropical regions (Lepers et al. 2005); these biome level changes combined with urban and agricultural conversions have a substantial influence on global NEE patterns

and recent trends (IPCC 2007). The MODIS FPAR inputs are derived using a static global land cover classification that does not explicitly represent LCLUC impacts. Land cover changes occurring during the SMAP mission period are expected to alter biome (BPLUT) response characteristics of the affected region, which are not adequately represented using a static (baseline) ancillary land cover classification, leading to greater NEE estimation uncertainty for the affected area.

The inhibiting effects of low soil moisture on soil $CO_2$ fluxes are represented in the L4_C algorithms, primarily through a non-linear soil heterotrophic response to surface soil moisture variability. However, wetlands have been associated with reduced $CO_2$ production by aerobic decomposition and respiration processes, and enhanced methane ($CH_4$) production by anaerobic decomposition. Studies supporting $R_h$ reduction under saturated soil conditions are largely based on controlled incubation experiments and extended inundation periods, while evidence is less consistent from studies involving natural landscape level observations and heterogeneous surface conditions, including tower eddy covariance measurement footprints. Pre-launch L4_C algorithm sensitivity studies indicated decreased NEE accuracy (relative to the baseline) by imposing alternative (e.g., convex parabolic) soil moisture response functions and greater soil moisture constraints under saturated soil conditions relative to global FLUX-NET tower records (Kimball et al. 2009, 2012). The L4_C algorithms therefore assume no soil moisture constraint to $R_h$ under saturated conditions and consequently may overestimate $R_h$ and underestimate NEE carbon ($CO_2$) sink activity under extended inundation periods.

The SMAP retrievals are sensitive to surface soil moisture and water inundation, while soil moisture and temperature influence both aerobic and anaerobic respiration processes; therefore, SMAP data are potentially useful for regional mapping and monitoring of both $CO_2$ and $CH_4$ fluxes. While $CH_4$ is a significant greenhouse gas and wetlands are a major component of northern and global ecosystems, $CH_4$ is beyond the scope of current L4_C algorithm and product specifications.

The L4_C baseline algorithms define cold temperature constraints to GPP and $R_h$ calculations but apply no warm temperature constraint to estimated carbon fluxes above a biome (BPLUT) specific optimum temperature threshold. Under warmer conditions, low soil moisture is assumed to be the primary constraint to $R_h$, while large VPD and low root zone soil moisture levels are expected to be major constraints to GPP. These assumptions may not hold in warm and relatively moist climate conditions

(e.g. tropical rainforest), leading to potential overestimation of GPP and $R_h$, and enhanced soil decomposition and underestimation of SOC. The net effect of these errors on NEE accuracy is less clear, but may be partially mitigated by compensating changes in GPP and respiration components.

Sub-grid scale terrain and land cover heterogeneity is a potential source of L4_C algorithm uncertainty, and may not be adequately represented by 1-km resolution MODIS FPAR and land cover, and 3–9-km resolution FT, SM, and surface meteorological inputs used to derive mean daily carbon fluxes within each model grid cell. While the 1 km L4_C processing is similar to the sampling footprint of most in situ tower (FLUXNET) observation sites, the coarser-scale FT and meteorological inputs are expected to impart additional uncertainty to the model calculations, particularly over complex terrain and land cover areas and during seasonal FT transition periods where differences between the overlying grid cell and local environmental heterogeneity are expected to be larger.

The L4_C algorithms use a single set of land cover–specific (BPLUT) coefficients to estimate spatial and temporal variations in NEE and component carbon fluxes over a global domain. The BPLUT approach has extensive heritage, including the EOS MODIS operational (MOD17) GPP product (Zhao and Running 2010). However, use of singular coefficients to describe heterogeneous processes may lead to model prediction error where the underlying population response is skewed or multi-modal and not well represented by a single mean response characteristic. Ideally, a Bayesian approach would be better suited to represent variability and uncertainty in model response characteristics (Kimball et al. 2012). However, these approaches are computationally prohibitive for an operational global product. The characteristic distributions of many of the BPLUT parameters are also uncertain based on the current literature and sparse in situ observation networks.

Despite the above limitations, the L4_C baseline product is expected to provide NEE estimates commensurate with the accuracy attained from in situ tower eddy covariance measurement networks (Kimball et al. 2012; Yi et al. 2013). However, NEE is an incomplete representation of $CO_2$ source-sink activity because it does not account for anthropogenic carbon emissions or terrestrial carbon losses due to fire, harvesting, and other disturbances (Baldocchi 2008). The L4_C products are considered appropriate for use with sparse in situ carbon observations, and regional fire and fossil fuel emission estimates to initialize, constrain, and optimize atmospheric transport model inversions of terrestrial $CO_2$ source-sink activity

(Peters et al. 2007). The L4_C product also provides global NEE estimates with enhanced spatial resolution, temporal fidelity and accuracy over previous methods, and additional information on component carbon fluxes, SOC stocks and underlying environmental constraints to land-atmosphere $CO_2$ exchange. These new carbon products are expected to be synergistic with other overlapping satellite Earth observations, including the NASA Orbiting Carbon Observatory (OCO-2) mission. The effective analysis and integration of SMAP and OCO-2 products, including new global GPP observations from canopy fluorescence and atmospheric carbon concentrations, will require advances in model inversion and data assimilation frameworks for effective cross-sensor scaling and integration, but will likely lead to better understanding and improved model predictions of the global carbon cycle and climate feedbacks.

## References

Amiro, B. D., A. G. Barr, J. G. Barr, T. A. Black, R. Bracho, M. Brown, et al., "Ecosystem carbon dioxide fluxes after disturbance in forests of North America," *J. Geophys. Res.—Biogeo.*, vol. 115, pp. G00K02, 2010.

Baldocchi, D., "Breathing of the terrestrial biosphere: lessons learned from a global network of carbon dioxide flux measurement systems," *Austr. J. Bot.*, vol. 56, pp. 1–26, 2008.

Balshi, M. S., A. D. McGuire, Q. Zhuang, J. Melillo, D. W. Kicklighter, E. Kasischke, et al., "The role of historical fire disturbance in the carbon dynamics of the pan-boreal region: A process-based analysis," *J. Geophys. Res.—Biogeo.*, vol. 112, pp. G02029, 2007.

Bond-Lamberty, B., S. D. Peckham, D. E. Ahl, and S. T. Gower, "Fire as the dominant driver of central Canadian boreal forest carbon balance," *Nature*, vol. 450, pp. 89–92, 2007.

Canny, J. F., "A computational approach to edge detection." *IEEE Trans. Pattern Anal. Mach. Intell.*, vol. 8, pp. 679–698, 1986.

Chimner, R. A., "Soil respiration rates of tropical peatlands in Micronesia and Hawaii," *Wetlands*, vol. 24, pp. 51–56, 2004.

Coursolle, C., H. A. Margolis, M. A. Giasson, P. Y. Bernier, B. D. Amiro, M. A. Arain, et al., "Influence of stand age on the magnitude and seasonality of carbon fluxes in Canadian forests," *Agr. Forest Meteorol.*, vol. 165, pp. 136–148, 2012.

Elberling, B., L. Askaer, C. J. Jørgensen, H. P. Joensen, M. Kühl, R. N. Glud, and F. R. Lauritsen, "Linking Soil O2, CO2, and CH4 concentrations in a wetland soil: Implications for CO2 and CH4 fluxes," *Environ. Sci. Technol.*, vol. 45, pp. 3393–3399, 2011.

Entekhabi, D., E.G. Njoku, P. E. O'Neill, K. H. Kellogg, W. T. Cros, W. N. Edelstein, et al., "The soil moisture active passive (SMAP) mission," *Proceedings of the IEEE*, vol. 98, pp. 704–716, 2010.

Friedl, M. A., D. Sulla-Menashe, B. Tan, A. Schneider, N. Ramankutty, A. Sibley, et al., "MODIS Collection 5 global land cover: Algorithm refinements and characterization of new datasets," *Rem. Sens. Environ.*, vol. 114, pp. 168–182, 2010.

Frolking, S., K. McDonald, J. Kimball, R. Zimmermann, J. B. Way, and S. W. Running, "Using the space-borne NASA Scatterometer (NSCAT) to determine the frozen and thawed seasons of a boreal landscape," *J. Geophy. Res.*, vol. 104, pp. 27,895–27,907, 1999.

Gifford, R. M., "Plant respiration in productivity models: conceptualization, representation and issues for global terrestrial carbon-cycle research," *Funct. Plant Biol.*, vol. 30, pp. 171–186, 2003.

Giglio, L., J. T. Randerson, G. R. van der Werf, P. S. Kasibhatla, G. J. Collatz, and R. S. DeFries, "Assessing variability and long-term trends in burned area by merging multiple satellite fire products," *Biogeosciences*, vol. 7, pp. 1171–1186, 2010.

Goulden, M. L., S. C. Wofsy, J. W. Harden, S. E. Trumbore, P. M. Crill, S. T. Gower, et al., "Sensitivity of Boreal Forest Carbon Balance to Soil Thaw," *Science*, vol. 279, pp. 214–217, 1998.

IPCC, *Climate Change 2007: The Physical Science Basis. Contribution of Working Group I to the Fourth Assessment Report of the Intergovernmental Panel on Climate Change*, eds. S. Solomon, D. Qin, M. Manning, Z. Chen, M. Marquis, K. B. Averyt, et al., Cambridge Univ. Press: Cambridge, UK, 2007.

Ise, T. and P. R. Moorcroft, "The global-scale temperature and moisture dependencies of soil organic carbon decomposition: an analysis using a mechanistic decomposition model," *Biogeochemistry*, vol. 80, pp. 217–231, 2006.

Jackson, T., A. Colliander, J. Kimball, R. Reichle, W. Crow, D. Entekhabi, et al., "SMAP Science Data Calibration and Validation Plan," SMAP Project, JPL D-52544, Jet Propulsion Laboratory, Pasadena CA, 96 pp., 2012.

Jones, C. D., P. Cox, and C. Huntingford, "Uncertainty in climate-carbon-cycle projections associated with the sensitivity of soil respiration to temperature," *Tellus*, vol. 55, pp. 642–648, 2003.

Kim, Y., J. S. Kimball, J. Glassy, and K. C. McDonald, "MEaSUREs Global Record of Daily Landscape Freeze/Thaw Status, Version 2, [1979–2010]," Boulder, Colorado, USA: NASA DAAC at the National Snow and Ice Data Center. Digital media (http://nsidc.org/data/nsidc-0477.html), 2010, updated 2012.

Kim, Y., J. S. Kimball, K. C. McDonald, and J. Glassy, "Developing a global data record of daily landscape freeze/thaw status using satellite passive microwave remote sensing," *IEEE Trans. Geosci. Rem. Sens.*, vol. 49, pp. 949–960, 2011.

Kim, Y., J. S. Kimball, K. Zhang, and K. C. McDonald, "Satellite detection of increasing Northern Hemisphere non-frozen seasons from 1979 to 2008: Implications for regional vegetation growth," *Rem. Sens. Environ.*, vol. 121, pp. 472–487, 2012.

Kimball, J. S., R. Reichle, K. C. McDonald, and P. E. O'Neill, "SMAP Algorithm Theoretical Basis Document, Release V.1: L4 Carbon Product," SMAP Project, JPL D-66484, Jet Propulsion Laboratory, Pasadena CA., 73 pp., 2012.

Kimball, J. S., K. C. McDonald, A. R. Keyser, and S. W. Running, "Application of the NASA scatterometer (NSCAT) for determining the daily frozen and non-frozen landscape of Alaska," *Rem. Sens. Environ.*, vol. 75, pp. 113–126, 2001.

Kimball, J. S., K. C. McDonald, S. Frolking, and S. W. Running, "Radar remote sensing of the spring thaw transition across a boreal landscape," *Rem. Sens. Environ.*, vol. 89, pp. 163–175, 2004.

Kimball, J. S., K. C. McDonald, S. W. Running, and S. E. Frolking, "Satellite radar remote sensing of seasonal growing seasons for boreal and subalpine evergreen forests," *Rem. Sens. Environ.*, vol. 90, pp. 243–259, 2004a.

Kimball, J. S., L. A. Jones, K. Zhang, F. A. Heinsch, K. C. McDonald, and W. C. Oechel, "A satellite approach to estimate land—atmosphere $CO_2$ exchange for boreal and Artic biomes using MODIS and AMSR-E," *IEEE Trans. Geosci. Rem. Sens.*, vol. 47, pp. 569–587, 2009.

Knorr W. and J. Kattge, "Inversion of terrestrial ecosystem model parameter values against eddy covariance measurements by Monte Carlo sampling," *Global Change Biol.*, vol. 11, pp. 1333–51, 2005.

Knorr, W., I. C. Prentice, J. I. House, and E. A. Holland, "Long-term sensitivity of soil carbon turnover to warming," *Nature*, vol. 433, pp. 298–301, 2005.

Lepers, E., E. F. Lambin, A. C. Janetos, R. DeFries, et al., "A synthesis of information on rapid land-cover change for the period 1981–2000," *Bioscience*, vol. 55, 2, pp. 115–124, 2005.

Litton, C. M., J. W. Raich, and M. G. Ryan, "Carbon allocation in forest ecosystems," *Glob. Change Biol.*, vol. 13, pp. 2089–2109, 2007.

Lloyd, J. and J. A. Taylor, "On the temperature dependence of soil respiration," *Functional Ecol.*, vol. 8, pp. 315–323, 1994.

McDonald, K. C., R. Dunbar, E. Podest, and J. S. Kimball, "SMAP Algorithm Theoretical Basis Document: L3 Radar Freeze/Thaw (Active) Product," SMAP Project, JPL D-66482, Jet Propulsion Laboratory, Pasadena, CA., 60 pp., 2012.

McDonald, K. C., J. S. Kimball, E. Njoku, R. Zimmermann, and M. Zhao, "Variability in springtime thaw in the terrestrial high latitudes: Monitoring a major control on the biospheric assimilation of atmospheric $CO_2$ with spaceborne microwave remote sensing," *Earth Interactions*, vol. 8, pp. 1–23, 2004.

McGuire, A. D., T. R. Christensen, D. Hayes, A. Heroult, E. Euskirchen, J. S. Kimball, et al., "An assessment of the carbon balance of Arctic tundra: comparisons among observations, process models, and atmospheric inversions," *Biogeosciences*, vol. 9, pp. 3185–3204, 2012.

Parton, W. J., D. S. Schimel, C. V. Cole, and D. S. Ojima, "Analysis of factors controlling soil organic matter levels in Great Plains grasslands," *Soil Sci. Soc. Am. J.*, vol. 51, pp. 1173–1179, 1987.

Peters, W., A. R. Jacobson, C. Sweeney, A. E. Andrews, et al., "An atmospheric perspective on North American carbon dioxide exchange: CarbonTracker," *PNAS*, vol. 104(48), pp. 18925–18930, 2007.

Potter, C. S., J. T. Randerson, C. B. Field, P. A. Matson, P. M. Vitousek, H. A. Mooney, and S. A. Klooster, "Terrestrial ecosystem production: A process model based on global satellite and surface data," *Global Change Biol.*, vol. 7, 4, pp. 811–841, 1993.

Rawlins, M. A., K. C. McDonald, S. Frolking, R. B. Lammers, M. Fahnestock, J. S. Kimball, et al., "Remote sensing of snow thaw at the pan-Arctic scale using the SeaWinds scatterometer," *J. Hydrol.*, vol. 312, pp. 294–311, 2005.

Reichle, R., W. Crow, R. Koster, J. Kimball, and G. De Lannoy, "SMAP Algorithm Theoretical Basis Document: L4 Surface and Root-Zone Soil Moisture Product," SMAP Project, JPL D-66483, Jet Propulsion Laboratory, Pasadena, CA, 76 pp., 2012.

Richardson, A. D. and D. Y. Hollinger, "Statistical modeling of ecosystem respiration using eddy covariance data: Maximum likelihood parameter estimation, and Monte Carlo simulation of model and parameter uncertainty applied to three simple models," *Agr. Forest Meteorol.*, 131, pp. 191–208, 2005.

Richardson, A. D., M. D. Mahecha, E. Falge, J. Kattge, A. M. Moffat, D. Papale, et al., "Statistical properties of random CO2 flux measurement uncertainty inferred from model residuals," *Agr. Forest Meteorol.*, vol. 148, pp. 38–50, 2008.

Rignot, E. and J. B. Way, "Monitoring freeze—thaw cycles along North—South Alaskan transects using ERS-1 SAR," *Remote Sens. Environ.*, vol. 49, pp. 131–137, 1994.

Schuur, E.A.G., J. G. Vogel, K. G. Crummer, H. Lee, J. O. Sickman, and T. E. Osterkamp, "The effect of permafrost thaw on old carbon release and net carbon exchange from tundra," *Nature*, vol. 459, pp. 556-559, 2009.

Ulaby, F. T., R. K. Moore, and A. K. Fung, "Microwave Remote Sensing: Active and Passive," vol. 1-3, Dedham, MA: Artec House, 1986.

Vaganov, E. A., M. K. Hughes, A. V. Kirdyanov, F. H. Schweingruber, and P. P. Silkin, "Influence of snowfall and melt timing on tree growth in subarctic Eurasia," *Nature*, vol. 400, pp. 149–151, 1999.

Way, J., J. Paris, E. Kasischke, C. Slaughter, L. Viereck, N. Christensen, et al., "The effect of changing environmental conditions on microwave signatures of forest ecosystems: preliminary results of the March 1988 Alaskan aircraft SAR experiment," *International Journal of Remote Sensing*, vol. 11, pp. 1119–1144, 1990.

Way, J., R. Zimmermann, E. Rignot, K. McDonald, and R. Oren, "Winter and spring thaw as observed with imaging radar at BOREAS," *J. Geophys. Res.–Atmos.*, vol. 102, pp. 29673–29684, 1997.

Wegmuller, U., "The effect of freezing and thawing on the microwave signatures of bare soil," *Remote Sens. Environ.*, vol. 33, pp. 123–135, 1990.

Yi, Y., J. S. Kimball, L. A. Jones, R. H. Reichle, and K. C. McDonald, "Evaluation of MERRA land surface estimates in preparation for the Soil Moisture Active Passive Mission," *J. Climate*, vol. 24, pp. 3797–3816, 2011.

Yi, Y., J. S. Kimball, L. A. Jones, R. H. Reichle, R. Nemani, and H. A. Margolis, "Recent climate and fire disturbance impacts on boreal and arctic ecosystem productivity estimated using a satellite-based terrestrial carbon flux model," *J. Geophys. Res.–Biogeo.*, vol. 118, pp. 1–17, 2013.

Yvon-Durocher, G., J. M. Caffrey, A. Cescatti, M. Dossena, P. d. Giorgio, J. M. Gasol, et al., "Reconciling the temperature dependence of respiration across timescales and ecosystem types," *Nature*, vol. 487, 472–476, 2012.

Zhao, M. and S. W. Running, "Drought-induced reduction in global terrestrial net primary production from 2000 through 2009," *Science*, vol. 329, 5994, pp. 940–943, 2010.

Zhao, M., F. A. Heinsch, R. R. Nemani, and S. W. Running, "Improvements of the MODIS terrestrial gross and net primary production global dataset," *Rem. Sens. Environ.*, vol. 95, 2, pp. 164–175, 2005.

# 7. Science Data Calibration and Validation

## I. Introduction

### A. Objectives

SMAP mission science requirements are contained in the Level 1 science requirements document: Science Requirements and Mission Success Criteria (SRMSC). Included in this document are requirements for accuracy, spatial resolution, and temporal revisit for the soil moisture and freeze/thaw measurements, and mission duration, for both baseline and minimum missions. Also stated in the SRMSC is the requirement that a Calibration and Validation (Cal/Val) Plan be developed and implemented to minimize and assess random errors and spatial and temporal biases in the soil moisture and freeze/thaw estimates, and that the SMAP validation program shall demonstrate that SMAP retrievals of soil moisture and freeze/thaw state meet the stated science requirements.

The SMAP Cal/Val Plan includes pre-launch and post-launch activities starting in Phase A and continuing after launch and commissioning through the end of the mission (Phase E). The scope of the Cal/Val plan is the set of activities that enable the pre- and post-launch Cal/Val objectives to be met.

The pre-launch objectives of the Cal/Val program are to:

- Acquire instrument data necessary for the calibration of SMAP Level 1 L-Band sensor products (brightness temperatures and backscatter cross-section);

- Acquire and process data with which to calibrate, test, and improve models and algorithms used for retrieving SMAP Level 2-4 science data products;

- Develop and test the infrastructure and protocols for post-launch validation; this includes establishing an in situ observation strategy for the post-launch phase.

The post-launch objectives of the Cal/Val program are to:

- Verify and improve the performance of the sensor and science algorithms;

- Validate the accuracy of the science data products.

### B. Cal/Val Program Deliverables

The deliverables of the SMAP Cal/Val Program fall in the following six categories:

- SMAP Science Cal/Val Plan document;

- Implementation plans for identified pre- and post-launch field campaigns;

- Reports documenting results, archival, and analyses of pre-launch field campaigns and data acquisitions;

- Beta Release and Validation report for L1 data accompanying archived data (at IOC plus three and six months, respectively);

- Beta Release and Validation report for L2-L3 data accompanying archived data (at IOC plus three and twelve months, respectively);

- Validation report for L4 data (accompanying archived data at post-IOC plus twelve months).

## II. Overview of Validation Methodology

### A. Background

In developing the Cal/Val plan for SMAP there are precedents and experiences that were utilized. The Committee on Earth Observation Satellites (CEOS) Working Group on Calibration and Validation (WGCV) (see http://calvalportal.ceos.org/CalValPortal/welcome.do) has established standards that provided a starting point for SMAP. The Land Products Sub-Group (see http://lpvs.gsfc.nasa.gov) has expressed the perspective that "A common approach to validation would encourage widespread use of validation data, and thus help toward standardized approaches to global product validation. With the high cost of in situ data collection, the potential benefits from international cooperation are considerable and obvious."

Cal/Val has become synonymous in the context of remote sensing with the suite of processing algorithms that convert raw data into accurate and useful geophysical or biophysical quantities that are verified to be self-consistent. Another activity that falls in the gray area is vicarious calibration, which refers to techniques that make use of natural or artificial sites on the surface of the Earth for the post-launch calibration of sensors.

A useful reference in developing a validation plan is the CEOS Hierarchy of Validation (http://lpvs.gsfc.nasa.gov):

- Stage 1: Product accuracy is assessed from a small (typically < 30) set of locations and time periods by comparison with in situ or other suitable reference data.

- Stage 2: Product accuracy is estimated over a significant set of locations and time periods by comparison with reference in situ or other suitable reference data. Spatial and temporal consistency of the product and with similar products has been evaluated over globally representative locations and time periods. Results are published in the peer-reviewed literature.

- Stage 3: Uncertainties in the product and its associated structure are well quantified from comparison with reference in situ or other suitable reference data. Uncertainties are characterized in a statistically

robust way over multiple locations and time periods representing global conditions. Spatial and temporal consistency of the product and with similar products has been evaluated over globally representative locations and periods. Results are published in the peer-reviewed literature.

- Stage 4: Validation results for stage 3 are systematically updated when new product versions are released and as the time-series expands.

A validation program would be expected to transition through these stages over the mission life span.

The SMAP mission is linked by a common L-band frequency with the SMOS, Aquarius, ALOS-2 and SAOCOM missions, and by its soil moisture products with the GCOM-W and ASCAT missions (operating at C-band and higher frequencies). All of these missions could be generating soil moisture products at the same time; therefore, SMAP will attempt to cooperate in their validation activities to improve the efficiency and robustness of its Cal/Val.

## B. Definitions

In order for the Cal/Val Plan to effectively address the mission requirements, a unified definition base is needed. The SMAP Cal/Val Plan uses the same source of terms and definitions as the SMAP Level 1 and Level 2 requirements. These are documented in the SMAP Science Terms and Definitions document (in draft, 2010), where Calibration and Validation are defined as follows:

- Calibration: The set of operations that establish, under specified conditions, the relationship between sets of values or quantities indicated by a measuring instrument or measuring system and the corresponding values realized by standards.

- Validation: The process of assessing by independent means the quality of the data products derived from the system outputs.

The L2 product requirements are interpreted in Reichle et al. 2010 for computing the validation quality metric.

Before releasing validated products the mission is required to release beta products. The maturity of the products in the beta release is defined as follows:

- Early release used to gain familiarity with data formats.

- Intended as a test bed to discover and correct errors.

- Minimally validated and still may contain significant errors.

- General research community is encouraged to participate in the QA and validation, but need to be aware that product validation and QA are ongoing.

- Data may be used in publications as long as the fact that it is beta quality is indicated by the authors. Drawing quantitative scientific conclusions is discouraged. Users are urged to contact science team representatives prior to use of the data in publications, and to recommend members of the instrument teams as reviewers.

- The estimated uncertainties will be documented.

- May be replaced in the archive when an upgraded (provisional or validated) product becomes available.

## C. Validation Methods, Resources, and Data Availability

A valuable lesson learned in global land imaging has been that validation is critical for providing the accuracy and credibility required for widespread product usage. Supporting information must be based on quantitative estimates of uncertainty for all products. For satellite-based retrievals, this should include direct comparison with independent correlative measurements. The assessment of uncertainty must also be conducted and presented to the community in normally used metrics in order to facilitate acceptance and implementation. SMAP will utilize a wide range of methodologies in calibrating and validating the mission science products, these include:

- Stable, known, homogeneous targets

- In situ networks

- Satellite products

- Model-based products

- Field experiments (tower- and aircraft-based SMAP instrument simulators)

Some of these methodologies will be better suited to a specific product than others. Matching these to SMAP products will be addressed in later sections. The following section discusses each of these techniques in more detail.

Another important consideration in developing the Cal/Val Plan is that SMAP will provide global products. Therefore, product validation should be representative of a wide range of global climate and vegetation conditions. Obviously the logistics and potential costs of conducting a fully comprehensive program may be beyond the capabilities available. Success will require partnerships that leverage ongoing programs, both within the U. S. and internationally.

### 1) Stable, Known, Homogeneous Targets

During post-launch Level 1 calibration, the observation of external calibration targets will commence in order to remove calibration biases, tune calibration algorithms, and track and remove long-term instrumental drifts. These "standards" will either 1) be used directly for calibration by employing a modeled value of their brightness or backscatter, or 2) be the intermediate means of transfer from the calibration of another satellite system operating at L-Band (such as SMOS, Aquarius, or PALSAR). Either way, the ultimate "absolute calibration" of the SMAP Level 1 products will be against these selected external standards. Because these standards are assumed to have known brightness temperature or NRCS values and stability characteristics, long-term drifts can also be detected and removed. These targets shall include, but are not necessarily limited to, cold sky background, the open ocean, Antarctica, and the Amazon.

### 2) In Situ Networks

In situ soil moisture, surface and air temperature, surface flux, and additional land surface characteristic observations will be important in validating science products from the SMAP mission. These data will also be valuable throughout the development phase of the mission to support field campaigns, modeling, and synergistic studies using AMSR 2, PALSAR, SMOS, and Aquarius.

The characteristics of an ideal in situ validation resource for SMAP will depend upon the product. However, the following features apply to all;

- Represents a spatial domain approximately the size of the retrieval grid product (3, 9, and 36 km). Since in situ observations typically represent an area much smaller than the satellite product, this means that scaling must be addressed using multiple sample sites that satisfy statistical criteria or with an alternative technique.

- Includes numerous domains in a variety of climate/geographic regions.

- Provides data in near real time with public availability.

- Has the potential for continued operation.

- Includes a wide range of related meteorological measurements.

The L2 through L4 soil moisture products share common features (measurements of soil moisture); however, the requirements of the L3_FT_A and L4_C are different from these and each other. Therefore, each will be discussed separately.

Another important consideration for SMAP Cal/Val implementation (which will utilize data from a variety of observing programs with varying objectives) is establishing global consistency in the correlative data. In the case of freeze/thaw, there are many potential sites but much of the data will come from operational meteorological observatories that have well established standards. For net ecosystem $CO_2$ exchange (NEE), most of the data come from national and international surface flux observing networks. Although there are a limited number of these sites, collaboration has resulted in standards for the relevant variables. The most problematic in situ observations are those of soil moisture. Almost every soil moisture installation and network has some variation in its instrumentation and design that must be taken into consideration. As a result, the SMAP project has devoted more time and attention to resolving issues associated with soil moisture observations than with FT and NEE, which have established standards. Additional details for soil moisture, freeze/thaw, and related resources are provided in the following sections.

**Soil Moisture.** Based upon the SMAP mission requirements, in addition to the list of characteristics above, an ideal in situ soil moisture resource would include verified surface layer (5 cm soil depth) as well as the 0–100 cm profile observations. An initial survey of available resources conducted in 2008 indicated that very few could meet the requirements for an ideal validation site and that the overall number of sites was limited.

The resources identified in the survey can be grouped into two distinct categories;

- Sparse networks that provide only one site (or possibly a few sites) within a satellite grid product.

- Dense networks that provide multiple sampling sites within a spatial domain matching a SMAP product grid product.

Sparse networks are often operational and satisfy data latency and availability requirements. At the time of the initial survey, the only dedicated soil moisture program was the Soil Climate Analysis Network (SCAN) operated by the U. S. Department of Agriculture (USDA) Natural Resources Conservation Service. Covering almost every state in the U. S. (Schaefer et al., 2007), SCAN satisfied many of the requirements mentioned above with two exceptions; they are single point measurements with no supporting scaling studies and have not been rigorously verified.

Another example of a sparse network is the Oklahoma Mesonet (http://www.mesonet.org/) that provides soil moisture and a wide range of other variables at over 90 stations in the state of Oklahoma. In the case of the Oklahoma Mesonet, there are also issues with the real time

and public availability of the data. Over the past few years, the National Oceanic and Atmospheric Administration (NOAA) has implemented the Climate Reference Network (CRN) (http://www.ncdc.noaa.gov/crn/), which shares many of the features of SCAN (>100 sites in the U. S.) and includes a wide range of additional measurements.

**Freeze/Thaw.** Ideally, the freeze/thaw (FT) in situ validation resources should include reference (2 m height) air temperature, vegetation (stem and canopy) temperature and surface (<10 cm depth) soil temperature measurements with high temporal fidelity (daily or better) sampling and representation over the observed range of climate, terrain, land cover and vegetation biomass conditions. As noted for soil moisture, these measurements should also satisfy the general requirements listed above. Unlike soil moisture measurements, reference air temperature observations are readily available from global operational meteorological networks and are subject to international standards. In addition, air temperature is not expected to exhibit as much spatial variability as soil moisture. However, vegetation and soil temperature observations are available at relatively few sites with variable standards; these measurements also exhibit larger characteristic spatial heterogeneity than surface air temperature.

Although standard meteorological networks can be used for validation of FT, there is a need for some observations using dense networks with additional surface measurements. Almost all FT resources are sparse networks.

**Net Ecosystem Exchange.** Surface flux towers are the primary requirement for validating the L4 C product. As noted for soil moisture, these measurements should also satisfy the general requirements listed above. Surface flux observations include direct eddy covariance measurements of NEE and measurement based estimates of component carbon fluxes including gross primary production (GPP) and ecosystem respiration (Reco). The tower site observations include other environmental measurements (e.g. air and soil temperature, humidity, solar radiation, wind direction and velocity, sensible and latent energy flux) designed for characterizing the surface energy balance, and the environmental drivers and constraints on vegetation photosynthetic activity. The carbon flux data involve time integrated measurements of land-atmosphere $CO_2$ exchange at frequent (e.g., half-hourly) intervals, which can be aggregated over longer (e.g., daily) time periods. Sensor malfunctions, maintenance activities, and data quality control and screening procedures can result in temporal gaps in the carbon flux measurement record; the resulting data records are then gap-filled using relatively standardized procedures, including physical and empirical modeling of missing data from supporting environmental data in order to obtain complete observa-

tional records, which can then be temporally aggregated to daily and longer time periods. The current global tower network now involves more than several hundred individual sites representing most vegetation biome types and climate regimes. These data are available from national and international cooperating networks with agreed upon standards for instrumentation, data processing and distribution. Many of these sites, particularly those with longer (>1 yr) operational records, have relatively well documented measurement accuracy and uncertainty. Most tower flux observations are representative of a local (~1-km resolution) sampling footprint that may not reflect regional conditions within the overlying (~9-km resolution) SMAP product footprint, particularly in areas with heterogeneous land cover and terrain conditions. Selection of suitable tower validation sites will involve pre-screening of sites on the basis of having relatively homogeneous land cover and terrain conditions within the overlying SMAP product window.

### 3) Synergistic Satellite Observations

Observations by other satellite instruments both before and after launch can be utilized for calibration and validation of SMAP. For pre-launch calibration and validation the primary role of spaceborne observations will be the testing of algorithms, using Level 1 products to produce SMAP Level 2 and 3. Level 2 products (soil moisture) from these missions can be used to evaluate the SMAP algorithm performance. For post-launch calibration and validation the alternative mission observations will provide products that can be compared with those from SMAP.

The following lists some of the most relevant satellite products that could be used before and/or after the launch for SMAP calibration and validation (responsible agency and launch year in parenthesis):

- SMOS (ESA, 2009): Global L-band horizontal and vertical polarization brightness temperature and surface soil moisture; pre-launch and post-launch

- ALOS PALSAR (JAXA, 2006): Multiple resolution backscatter product based on L-band SAR; pre-launch

- MetOp ASCAT (ESA, 2006) and Sentinal-1 (ESA, 2013): Soil moisture index based on C-band backscatter; pre-launch and post-launch

- Aquarius (NASA/CONAE, 2011): Simultaneous L-band brightness temperature and backscatter; experimental soil moisture product; pre-launch and post-launch

- GCOM-W AMSR 2 (JAXA, 2012): Soil moisture product based on C- and X-band brightness temperature; pre-launch and post-launch

- SAOCOM (CONAE, 2015): Backscatter and soil moisture products based on L-band SAR; post-launch

- ALOS-2 PALSAR (JAXA, 2014): Multiple resolution backscatter product based on L-band SAR; possibly pre-launch and post-launch

These satellite programs measure either brightness temperature or backscatter at L-band (Aquarius provides both) and/or produce a soil moisture product from their observations. The options and the value of these other satellites depend largely on the overlap of the mission with SMAP. However, for example, in the case of SMOS the measurements of brightness temperature will be extremely valuable, even if the data are limited to the pre-launch period, because they represent the first L-band brightness temperature measurements from space.

Cross-calibration exercises between different satellite instruments have been successfully carried out improving the quality of the time series created by the instruments in question (e.g., Atlas et al. 2008; Liu et al. 2008). For inter-comparisons between the satellites, the product accuracy requirements of the other missions are of significance. The most relevant intercomparison mission is SMOS (since it is L-band and has a soil moisture product at the same spatial resolution), which has soil moisture accuracy requirements equivalent to SMAP.

The limitations of this type of comparison are the quality of the alternative product, differences in overpass times/days, and accounting for system differences affecting the soil moisture product. In the case of GCOM-W, which has a 01:30 AM / 01:30 PM overpass time, confusion factors would include data at a different time of day (from the SMOS/SMAP overpass time of 06:00 AM) and contributing depth issues associated with GCOM-W's C-band frequency (Jackson 2007). The SMAP team has actively participated in the validation of these alternative products during the SMAP pre-launch period, which has provided us with knowledge of the quality of both the SMOS and GCOM-W soil moisture.

### 4) Model-Based Validation Approaches

Validation based on land surface modeling and data assimilation will be used to complement in situ and satellite-based validation. As discussed in previous sections, validation against in situ observations is difficult because the observation sites include limited geographic regions and environmental settings and is complicated by the mismatch between the point-scale of the in situ measurements and the distributed (order of km) scale of the SMAP data products. Hydrological land surface models and data assimilation approaches provide continuous (in space and time) soil moisture products that match the spatial support of SMAP soil moisture products. Model-based validation can start immediately upon launch and thereby offers a key advantage for meeting the ambitious IOC+12-month validation deadline.

Several Numerical Weather Prediction (NWP) centers (including ECMWF, NCEP, and NASA/GMAO) routinely produce operational or quasi-operational soil moisture fields at a scale comparable to the SMAP radiometer product. These data products rely on the assimilation of a vast number of atmospheric observations (and select land surface observations) into General Circulation Models (GCMs). Although there are many caveats that need to be considered in using these data, they are readily available and they are consistent with the atmospheric forcing (precipitation and radiation) and land use information that determine the spatial and temporal patterns in soil moisture fields. Moreover, surface temperature from at least one NWP system will be used in the generation of the SMAP L2_SM_P data product. Output from these systems is necessary for the application the validation activities described below. In this context, NWP data may be used directly or as forcing inputs to more customized hydrological modeling systems.

**Land Surface Modeling Comparisons.** In the simplest case, land surface models (either embedded in a NWP system or in off-line mode) can be used to generate soil moisture products at larger (basin-wide and continental) scales using land surface and meteorological forcing datasets that are independent of the SMAP remote sensing data. The resulting soil moisture fields can then be compared with the remotely sensed soil moisture product at validation sites over diurnal and seasonal cycles. These model-derived soil moisture fields can also be used to extend the comparisons to larger space and time domains than available from in situ observations. Model-based soil moisture fields can also be used to derive brightness temperature and backscatter using forward modeling. These estimates can be valuable in validating the Level 1 SMAP products.

The inherent uncertainty in any model-based soil moisture product is an obvious limitation to such a validation approach. However, recent work has extended the application of so-called "Triple Collocation" (TC) approaches to soil moisture validation activities (Scipal et al. 2008; Miralles et al. 2010; Dorigo et al. 2010). These approaches are based on cross-averaging three independently acquired estimates of soil moisture to estimate the magnitude of random error in each product. A viable soil

moisture product triplet could consist of a passive remote sensing product, an active remote sensing product, and a model product (Scipal et al. 2008; Dorigo et al. 2010). In situ observations can also be used in place of one of these. If successfully applied, TC can correct model versus SMAP soil moisture comparisons for the impact of uncertainty in model product. However, TC cannot provide viable bias information and, therefore, only assesses the random error contribution to total RMSE. Note that TC can also be applied to reduce the impact of sampling error when up-scaling sparse in situ measurements during validation against ground-based soil moisture observations.

**Data Assimilation Approaches.** The development of land surface modeling and data assimilation tools for SMAP synergistically provides an important framework for the supplemental calibration and validation of SMAP data products as well as the option to generate Level 4 data products.

An ensemble-based data assimilation system produces internal diagnostics that can be used to indirectly validate its output. One such diagnostic consists of the "innovations" (or "observation-minus-forecast" residuals) that contrast the model-based forecast values directly with the observations. The assimilation system also produces corresponding error estimates. Specifically, the statistics of appropriately normalized innovations can be examined (Reichle et al. 2007; see also discussion of adaptive filtering in the L4_SM chapter). Through minor customizations of the assimilation system, this approach can be applied to brightness temperature as well as soil moisture retrievals.

Data assimilation and land surface modeling systems also provide an opportunity to convert the impact of soil moisture information into a more readily-measurable quantity. For example, Crow et al. (2010) develops and verifies a quasi-global soil moisture evaluation system that effectively substitutes rain gauge measurements for ground-based soil moisture observations. The approach is based on evaluating the correlation coefficient between antecedent rainfall error and analysis increments (i.e.. the net addition or subtraction of modeled soil water accompanying the assimilation of a single soil moisture estimate) that are produced by a land data assimilation system. This correlation coefficient provides a reliable linear metric for the ability of a given soil moisture product to accurately characterize soil moisture anomalies. The use of rain observations as a source of verification expands potential soil moisture validation locations from isolated sites to much broader regions in which rain-gauge measurements are available for retrospective analysis. Bolten et al. (2010) uses a similar methodology to assess the added utility of assimilating AMSR-E soil moisture retrievals for root-zone soil moisture

monitoring in the presence of uncertain precipitation forcing into a land surface model.

### 5) Field Experiments

Field experiments can provide very detailed information; however, the costs and logistics limit how extensive these can be spatially and temporally. During pre-launch field experiments datasets served a valuable role by providing diverse but controlled condition data that was used for developing algorithms, establishing algorithm parameterization, and defining validation site scaling properties. The most relevant pre-SMAP soil moisture campaigns are summarized in Colliander et al. (2012). During its development period, SMAP conducted or collaborated in several soil moisture campaigns that culminated in the extensive SMAPVEX12. Table 16 summarizes these campaigns and provides links to more detailed descriptions and data archives. In addition, overviews of CanEx10 (Magagi et al. 2013), SMAPVEX12 (McNairn et al. 2014), and SMAPEx (Panciera et al. 2014) are published. Post-launch airborne field experiments will also be valuable in validating SMAP products and resolving, receiving anomalies, and improving algorithms. Further details are provided in a later section.

### III. Calibration and Validation Requirements of SMAP Products

Assessing whether the requirements of the SMAP products are met is the primary objective of the Cal/Val Plan. The requirements for the algorithms, i.e. ATBDs, flow down from the product. In the ATBDs, each product algorithm team identifies what calibration and validation activities are needed to meet the product requirements. These activities then become another set of requirements for the Cal/Val Plan. This section focuses on detailing the requirement defined by the ATBDs.

Subsequent sections describe how the Cal/Val Program addresses these requirements together with the other mission requirements.

### A. Level 1 — Sensor Products

Level 1 SMAP science products are the calibrated sensor outputs (brightness temperature and radar backscatter). The accuracy of these products depends on the pre-launch calibration model and the calibration algorithm and coefficients applied in the post-launch processing.

Table 17 lists the Level 1 products, their requirements for spatial resolution and accuracy, and associated pre-launch and post-launch Cal/Val requirements. Products L1B_TB and L1C_TB are time-ordered and swath- and Earth-gridded (collocated with radar) brightness temperatures, respectively. Products L1B_S0_LoRes and L1C_

Table 16. Field campaigns relevant to SMAP Cal/Val.

| Name | Definition | Time Period | Location | Aircraft Sensors | Archive |
|---|---|---|---|---|---|
| SGP99 | Southern Great Plains 1999 | 1999 | Oklahoma | PALS | Will be posted at National Snow and Ice Data Center (nsidc.org) |
| SMEX02 | Soil Moisture Experiment 2002 | 2002 | Iowa | PALS AIRSAR | National Snow and Ice Data Center (nsidc.org) |
| CLASIC | Cloud Land Surface Interaction Campaign | 2007 | Oklahoma | PALS | Will be posted at National Snow and Ice Data Center (nsidc.org) |
| SMAPVEX08 | Soil Moisture Active Passive Validation Experiment 2008 | 2008 | Maryland | PALS | Will be posted at National Snow and Ice Data Center (nsidc.org) |
| CanEx10 | Soil Moisture Validation Experiment 2008 | 2010 | Saskatchewan | UAVSAR EC L-band radiometer | University of Sherbrooke (pages. usherbrooke.ca/canexsm10) |
| SMAPVEX11 | Soil Moisture Active Passive Validation Experiment 2011 | 2011 | Oklahoma | PALS | Will be posted at National Snow and Ice Data Center (nsidc.org) |
| SMAPEx | Soil Moisture Active Passive Validation Experiments | 2011 | Australia | PBMR PLMR | www.smapex.monash.edu.au |
| SMAPVEX12 | Soil Moisture Active Passive Validation Experiment 2012 | 2012 | Manitoba | PALS UAVSAR | University of Sherbrooke (pages. usherbrooke.ca/smapvex12) Will be posted at National Snow and Ice Data Center (nsidc.org) |
| Midwest Drought | | 2012 | USA | UAVSAR | Jet Propulsion Laboratory (uavsar.jpl.nasa.gov) |

S0_HiRes (West et al. 2012) are the low-resolution (real aperture) and high-resolution (synthetic aperture) radar cross-sections, respectively.

A separate document has been prepared that describes the calibration and validation that will be used for the Level 1 products (Hudson and Peng 2010).

**B. Level 2 and 3 — Geophysical Products**

Level 2 products contain derived geophysical parameters (soil moisture, freeze/thaw) whose accuracy depends on the accuracy of the input Level 1 sensor data, ancillary data, and the Level 2 geophysical retrieval algorithms. (See Table 18 for Level 2/3 products.)

*1) Metrics*

The soil moisture accuracy requirements will be satisfied by the L2 and L3 soil moisture products at the corresponding horizontal resolution. Specifically, the requirement implies that for the selected areas for which validating in situ observations are available from verified sites, the SMAP surface (0–5 cm) soil moisture products must satisfy RMSE<0.04 $m^3/m^3$ (after removal of long-term mean bias) in the case of active/passive and passive products and RMSE<0.06 $m^3/m^3$ (after removal of long-term mean bias) in the case of the active product.

The L3 freeze/thaw product will provide estimates of land surface freeze/thaw state expressed as a binary (frozen or thawed) condition. The baseline L3 freeze/thaw product will be provided for land areas north of 45ºN with a mean classification accuracy of 80% at 3-km spatial resolution and 2-day average temporal fidelity. The accuracy of the L3 product is determined by comparison of the freeze/thaw state map to selected in situ temperature measurement networks within northern (≥45°N) vegetated land areas for the baseline product.

Table 17. Level 1 products and associated Cal/Val requirements. The columns are divided for product type; spatial resolution of the instrument output for L1B_TB, L1B_S0, L1C_S0 and grid resolution for L1C_TB; accuracy for horizontal and vertical polarization, and for 3rd Stokes parameter of radiometer and HV-combination of radar; and pre-launch and post-launch Cal/Val requirements.

| Level 1 Products | Resolution (km) | Accuracy Requirement | Information and data required for performing Cal/Val | |
| --- | --- | --- | --- | --- |
| | | | Pre-Launch | Post-Launch |
| L1B_TB | 40 | 1.3 K (H, V)– | • High-level output coaxial noise source, 0.3 K accuracy (to be modified from existing source called RATS)<br>• Polarimetric coaxial noise source: existing source called CNCS (Peng and Ruf 2008)<br>• L-band warm blackbody (for feed horn) with return loss >35 and thermal stability of 0.2°C (existing)<br>• L-band LN2-cooled blackbody, 1 K accuracy (existing)<br>• Controlled thermal environment<br>• Antenna pattern and reflector emission verified by antenna team [1] | • Pre-launch calibration parameters<br>• Sky TB map for cold sky calibration<br>• Ocean and land target RTM with overall 0.4 K uncertainty<br>• Geolocation: Antenna pointing information; ocean RTM; coastlines<br>• Faraday rotation: IRI and IGRF databases; Aquarius and SMOS values; Rotation angles from astronomers, geostationary satellites and GPS satellites<br>• Atmospheric correction: global temperature and humidity profiles<br>• Antenna pattern correction: Nominal antenna pattern; Antenna pointing information; SMAP TB Forward Simulator [2,3]<br>• Aquarius radiometer brightness temperatures<br>• SMOS radiometer brightness temperatures<br>• Aircraft-based observations during field campaigns |
| L1C_TB | 40 | 1.3 K (H, V) | • C-band AMSR-E data over Florida region<br>• Prototype SMAP-like dataset from the Testbed over Florida region | • SMAP L1B and L1C data over coastlines and high TB contrast locations |
| L1B_S0 | 30 | | • TBD | • Sky TB map for CSC<br>• Pre-launch calibration parameters<br>• Established uniform, isotropic, stable Earth targets<br>• Data from contemporaneous radars (Aquarius, PALSAR, UAVSAR, SAOCOM, etc.)<br>• Aircraft-based observations during field campaigns<br>• Receive only data acquisition (for RFI) |
| L1C_S0 | 3 | 1 dB (HH, VV); 1.5 dB (X-pol) | • TBD | • L1B_S0<br>• Checks for scalloping … |

(1) The radiometer development, implementation and calibration is the responsibility of GSFC. The antenna development, implementation, testing, and characterization is the responsibility of JPL.

(2) SMAP Brightness Temperature (TB) Forward Simulator: based on ocean and land surface radiative transfer model (RTM). The simulator includes the following sources and effects:

• Solar direct, reflected
• Lunar direct, reflected
• Galactic direct, reflected
• Land, atmosphere, ocean
• Faraday rotation
• Antenna sidelobes

(3) Assumptions in current error budget

• Earth sidelobe scene known to 6 K
• Cross-pol TB known to 2 K
• Space scene known to 1 K
• Solar flux known to 20 s.f.u.

Table 18. Level 2/3 products and associated Cal/Val requirements. The columns are divided by product type; grid resolution; accuracy requirement of the product; revisit time; pre-launch and post-launch Cal/Val requirements.

| Level 2/3 Products | Grid (km) | Accuracy | Rep (d) | Information and data required for performing Cal/Val | |
|---|---|---|---|---|---|
| | | | | **Pre-Launch** | **Post-Launch** |
| L2_SM_P | 36 | 0.04 m³/m³ | 3 | • Ancillary datasets needed by baseline and option algorithms<br>• Global Testbed (GloSim) retrieval simulations using synthetic observation conditions<br>• Field experiment data (SGP99, SMEX02, CLASIC, SMAPVEX08, CanEx-SM10, SMAPVEX12) for surface SM [1]<br>• SMOS brightness temperature and soil moisture products, ancillary data and validation products | • Algorithm parameterization established<br>• In situ core validation sites [2]<br>• In situ sparse networks<br>• SMOS, GCOM-W and ASCAT soil moisture products<br>• Independent hydrologic model outputs<br>• Field experiments [1] |
| L2_SM_A | 3 | 0.06 m³/m³ | 3 | • Ancillary datasets needed by baseline and option algorithms<br>• Global Testbed (GloSim) retrieval simulations using synthetic observation conditions<br>• Field experiment data (SGP99, SMEX02, CanEx-SM10, SMAPVEX12 and tower-based campaigns) for surface SM [1,1b]<br>• Satellite (PALSAR) data | • Algorithm parameterization established<br>• In situ core validation sites [2]<br>• In situ sparse networks;<br>• ALOS-2 and SAOCOM soil moisture products<br>• Independent hydrologic model outputs<br>• Field experiments [1] |
| L2_SM_A/P | 9 | 0.04 m³/m³ | 3 | • Ancillary datasets needed by baseline and option algorithms<br>• Global Testbed (GloSim) retrieval simulations using synthetic observation conditions<br>• SGP99, SMEX02, CLASIC, SMAPVEX08, SMAPVEX12 datasets<br>• Multi-scale and long-duration airborne field experiment [1] data capturing temporal soil moisture and diversity of land cover type | • Algorithm parameterization established<br>• In situ core validation sites [2]<br>• In situ sparse networks<br>• Independent hydrologic model outputs<br>• Field experiments [1] |
| L3_FT_A | 3 | 80% | 2 | • Ancillary datasets needed by baseline and option algorithms<br>• Global Testbed (GloSim) retrieval simulations using synthetic observation conditions<br>• Testbed simulations with in situ sparse networks (NRCS SNOTEL and SCAN, FLUXNET, ALECTRA, WMO) frozen/non-frozen status and SMOS and PALSAR<br>• SMOS, PALSAR, PALS time series data over test regions<br>• Field experiments over complex terrain and land cover [3] | • Algorithm parameterization established<br>• In situ sparse networks (NRCS SNOTEL, SCAN, FLUXNET, ALECTRA, WMO) frozen/non-frozen status<br>• Field experiments (e.g., PALS) with in situ sparse network sites (e.g., FLUXNET) |

**Table 18. Footnotes**

(1) Surface soil moisture (SM) experiments have the following baseline requirements (subsite is a part of the experiment domain, such as a field):

- The soil moisture in the top 5 cm can be determined with dielectric probes with point location specific calibration through bulk density and thermo-gravimetric core sampling, which yields sample uncertainty no more than 0.04 m³/m³.

- The spatial sampling of surface SM is done following the methodology established for that specific location

- The soil texture is to be determined for each sampling point specifically through bulk density core samples.

- The land cover is classified according to the classes used for the SMAP products.

- The vegetation is classified according to the classes used for the SMAP products.

- The vegetation water content measurements are calibrated through destructive thermo-gravimetric sampling.

- Soil temperature is determined at each sampling point. Site specific meteorological state is determined for air temperature and precipitation.

Some geophysical input parameters have greater impact on the radar soil moisture error (as opposed to the radiometer soil moisture) than others (such as roughness, and information on vegetation geometric and dielectric properties [see L2_SM_A ATBD for the complete list]). Therefore, this information should be available from the pre-launch field experiments to develop the algorithms. The procedures for doing this need to be established in the pre-launch phase. Furthermore, radar is more sensitive to the incidence and azimuth angle of the measurement than radiometers primarily because of the high spatial resolution of radar needs to be considered in the experiments.

(2) In situ core validation sites (meaning an intense measurement site with established scaling from point measurements to satellite grid product) used in the post-launch soil moisture validation need to satisfy the following requirements:

- The soil moisture measured must provide an estimate of the state of the top 5 cm with well defined uncertainty brackets

- For L2_SM_A, surface roughness measurements at appropriate time & spatial scales are highly desired.

- The spatial sampling of the site must be such that a defined resolution scaling scheme can be applied.

(3) In situ frozen/non-frozen status will be determined as a composite ensemble of vegetation, soil and air temperature measurements where available, and will be compared to coincident grid product L3 freeze/thaw measurements for areas of the globe where seasonally frozen temperatures are a major constraint to hydrological and ecosystem processes. The fulfillment of the requirements will be assessed by comparing SMAP freeze/thaw classification results and in situ frozen or non-frozen status. The in situ resource should provide a strategy for spatial up-scaling of in situ measurements commensurate with the 3-km spatial scale of the satellite retrieval. Attention should be given to landscape heterogeneity within the scope of the validation site or sites in the upscaling strategy.

Measurements supporting freeze/thaw Cal/Val activities should meet the following minimum requirements:

- Measurement of surface (screen height) air temperature.

- Measurement of surface (up to 10 cm depth) and profile (up to 1 m depth) soil temperatures.

- Measurement of vegetation temperature (when significant vegetation present).

- In situ temperature measurements should be sufficient to characterize the variability in local microclimate heterogeneity within a spatial scale compatible with the SMAP freeze/thaw product.

- To provide uniformity across sites, the local land cover of the site should be consistent with a global (IGBP-type) land cover classification.

- Each land cover class within the validation site should be captured within the suite of temperature measurements such that the local vegetation and land cover heterogeneity is represented.

- Measurements should have sufficient temporal fidelity to capture seasonal and diurnal temperature and freeze/thaw patterns.

Desired methods for measuring air, soil, and vegetation temperatures include thermocouple type measures of physical temperatures and thermal IR type measurements of surface "skin" temperatures with consistent and well documented accuracy and error sources over a large (e.g., –30°C to 40°C) temperature range.

### 2) Information and Data Required for Cal/Val

Table 18 shows the Level 2/3 products, their requirements for spatial resolution, accuracy, and revisit time, and the associated Cal/Val requirements. Products L2_SM_P, L2_SM_A and L2_SM_AP are soil moisture products (top 5 cm of soil), based on radiometer-only, radar-only, and combined radar-radiometer data, respectively. Product L3_FT_A is the freeze/thaw state product is based on radar data only.

## C. Level 4 — Geophysical Products

Level 4 products contain geophysical parameters whose accuracies depend on the accuracies of the input Level 1 and Level 2–3 data products, other input data, and the model and assimilation technique.

### 1) Metrics

The soil moisture accuracy requirements will be satisfied by the L4 soil moisture product at the 9-km horizontal resolution. Specifically, the requirement implies that for the selected areas for which validating in situ observa-

tions are available from verified sites, the SMAP surface (0–5 cm) and root zone soil moisture products must satisfy RMSE<0.04 m³/m³ (after removal of long-term mean bias).

The net ecosystem exchange (NEE) estimates from the L4_C product will be validated at 9-km resolution against the selected in situ observations from flux towers. Specifically, the requirement will be satisfied if the median RMSE against the validation is less than 30 g C m$^{-2}$ yr$^{-1}$ or 1.6 g C m$^{-2}$ d$^{-1}$ after removal of long-term mean bias.

### 2) Information, Data, and Processing Required for Cal/Val

Table 19 shows the two Level 4 products, their requirements for spatial resolution, accuracy, revisit time, and

the associated Cal/Val requirements. L4_SM is a surface and root-zone soil moisture product, and L4_C is a net ecosystem exchange (NEE) product.

## IV. Infrastructure Development for Validation

A major activity during the pre-launch phase of the SMAP mission was developing the infrastructure needed to conduct post-launch validation in an efficient manner. During the earlier stages of developing the SMAP Cal/Val Plan, Table 20 was developed to summarize the methodologies that would be used in Cal/Val and outstanding issues associated with these.

Of these issues, three demanded immediate actions by SMAP if they were going to be resolved. These all involved the in situ observations; 1) intercalibration between differ-

**Table 19. Level 4 products and associated Cal/Val requirements. The columns are divided by product type; grid resolution; accuracy requirement of the product; revisit time; pre-launch and post-launch Cal/Val requirements.**

| Level 4 Products | Grid (km) | Accuracy | Rep (d) | Information and data required for performing Cal/Val | |
|---|---|---|---|---|---|
| | | | | **Pre-Launch** | **Post-Launch** |
| L4_SM | 9 | 0.04 m³/m³ | 3 | • Testbed simulations<br>• Satellite observations (SMOS, Aquarius, PALSAR)<br>• In situ core sites and sparse networks<br>• Internal data assimilation diagnostics | • Surface SM: see Level 2<br>• Root-zone SM: Core and Supplemental Validation Sites (incl. SCAN, CEOP, Oklahoma Mesonet, USCRN, GPS, COSMOS)<br>• Precipitations observations<br>• Internal data assimilation diagnostics |
| L4_C | 9 | 30 gC/m²/yr | 3 | • Satellite data (e.g., MOD17 product)<br>• GEOS-5<br>• In situ CO$_2$ eddy flux (e.g., FLUXNET)<br>• Internal data assimilation diagnostics | • SMAP L4 SM<br>• In situ CO2 eddy flux (e.g., FLUXNET) [1] |

(1) The accuracy of the L4_C outputs, including NEE and component carbon fluxes, will be established in relation to in situ tower eddy flux CO$_2$ measurements and associated carbon budgets within regionally dominant vegetation classes following established protocols. The fulfillment of the NEE requirement will be assessed by comparing SMAP L4_C NEE output with in situ measurement-based CO$_2$ flux estimates.

In order for a flux tower to be useful for NEE validation, it has to provide at minimum the following measurements:

• Continuous daily (cumulative 24-hr) estimates of gross primary production (GPP), ecosystem respiration (Reco), and NEE with well defined and documented accuracy, including both systematic and random errors.

• Relatively homogeneous land cover and vegetation conditions within an approximate 9-km x 9-km footprint commensurate with the resolution of the SMAP L4_C product.

• To provide uniformity across sites, the local land cover of the site should be compatible with a global (IGBP-type) land cover classification.

• The local site should have a minimum level of supporting meteorological measurements including air temperature and humidity, surface (≤10 cm depth) soil moisture and soil temperature, precipitation, and snow depth (if present); these measurements should be continuously monitored and sufficient to capture local microclimate heterogeneity within the tower footprint.

• The local site should have a minimum level of supporting biophysical inventory measurements including surface (≤10 cm depth) soil organic carbon stocks, vegetation stand age class, land use, and disturbance history.

**Table 20. Overview of the SMAP Cal/Val methodologies.**

| Methodology | Role | Issues | Actions |
|---|---|---|---|
| Core Validation Sites | Accurate estimates of products at matching scales for a limited set of conditions | • In situ sensor calibration<br>• Limited number of sites | • In Situ Testbed<br>• Cal/Val Partners |
| Sparse Networks | One point in the grid cell for a wide range of conditions | • In situ sensor calibration<br>• Up-scaling<br>• Limited number of sites | • In Situ Testbed<br>• Scaling methods<br>• Cal/Val Partners |
| Satellite Products | Estimates over a very wide range of conditions at matching scales | • Validation<br>• Comparability<br>• Continuity | • Validation Studies<br>• Distribution matching |
| Model Products | Estimates over a very wide range of conditions at matching scales | • Validation<br>• Comparability | • Validation Studies<br>• Distribution matching |
| Field Experiments | Detailed estimates for a very limited set of conditions | • Resources<br>• Schedule Conflicts | • Airborne simulators<br>• Partnerships |

ent sensors used in different in situ networks, 2) up-scaling of the point-wise in situ measurement to the SMAP footprint scale, and 3) increasing the number and quality of the core validation sites. These efforts will be described in subsequent sections.

## A. Comments on In Situ Soil Moisture Measurement

In situ measurement and scaling of soil moisture presents many challenges. As a result, there are a wide range of measurement techniques and protocols that have been adopted in practice. The value of an observing program to SMAP validation will depend upon (a) the quality of the measurements, (b) how the measurement relates to the validation criteria (in particular the depths and scales), and (c) the availability of the data in a timely manner. The following discussion focuses on the first two issues.

Although the providers of in situ data are likely to have conducted an assessment of the quality of their measurements, if adequate calibration has not been conducted the SMAP project will have to make an assessment before using the data for validation.

In situ resources that will be the most relevant for SMAP soil moisture calibration and validation would provide an estimate of the volumetric soil moisture over the surface 5 cm and the 100 cm depth of soil. In general, this will involve two steps: 1) establishing that the sensor provides the equivalent of the volumetric soil moisture that would be obtained using a reference standard, and 2) if the sensor does not actually measure the defined layer, providing verification that the sensor values are well correlated to the mission product depths (0–5 and 0–100 cm). It should be noted that the 0–5 cm measurement is the highest

priority and that this measurement is logistically easier to obtain and verify than the 0–100 cm depth measurement.

The recommended reference standard for characterizing volumetric soil moisture is the thermo-gravimetric (usually shortened to gravimetric) measurement method (Chapter 3.1.2.1 in Dane and Topp 2002). This technique is time consuming to implement operationally; therefore, it is usually only used for calibration of sensors and in field campaigns. The soil moisture in a known volume ($cm^3$) is characterized by weighing, then drying, and weighing again to obtain the mass of water (g). With a specific density of 1 $cm^3/g$ for water, the result is the volumetric soil moisture ($cm^3/cm^3$).

Most sensor manufacturers provide a calibration function for converting the sensor signal to soil moisture (some do not actually provide volumetric soil moisture but an alternative variable such as moisture–tension). These calibrations are often based on limited laboratory studies and are often soil type specific; thus requiring site characterization for a more accurate estimate. Some operational networks have conducted supplemental laboratory analyses to improve their products. An advantage of laboratory calibration is that a full range of soil moisture can be examined.

An alternative, or in some cases a complement, to laboratory calibration is site-specific calibration. The advantage of a site-specific calibration is that it incorporates soil type correction and peculiarities associated with the installation. As described later, it can also be used to correct for measurement depth differences. Disadvantages include repetitive site visits to capture a range of conditions and potential impacts from destructive sampling. Also, this approach is much easier to implement for surface layer measurements than the full profile.

The most straightforward way to provide both items above is to sample the 0–5 cm soil layer using a volume extraction method, such as a ring coring tool.

The other aspect that must be considered regarding the use of in situ observations for SMAP validation is how the measurement relates to the depths defined in validation criteria. Each type of sensor measures a different volume and different networks utilize different installation protocols that can result in incompatibility. SMAP is supporting studies, specifically the In Situ Sensor Testbed, described below, to provide a basis for normalizing these different methods and protocols.

Performing a site-specific calibration against a standard of gravimetric measurement of the 0–5 cm soil layer (and 0–100 cm if possible) is the recommended protocol for calibration and normalizing an in situ network for integration into the SMAP validation data base.

### 1) Soil Moisture In Situ Sensor Testbed

A testbed was established to test and calibrate various soil moisture probes provided by different manufacturers. Specifically, the SMAP Marena Oklahoma In Situ Sensor Testbed (MOISST) will provide answers to the following set of questions: (1) How do different soil moisture sensors perform given the same hydrologic inputs of rainfall and evaporation? (2) How do different sampling intervals impact the soil moisture estimates, given instantaneous measurements versus time averaged measurements? (3) How do the orientations of installation influence the data record and effectiveness of the sensor? (4) How can networks which measure soil moisture by different fundamental methods, capacitance, frequency domain reflectometry (FDR), and time domain reflectometry (TDR), be compared to a standard of gravimetric validation? (5) How can the measurements from different sensors with different sampling scales, particularly the COSMOS (http://cosmos.hwr.arizona.edu) and GPS systems (Larson et al. 2010) of soil moisture monitoring, compare given the variation in scale of measurement? Answering these questions is important for establishing a standard for soil moisture measurement in situ sites across the globe.

The site is located in Marena, Oklahoma and managed by the Oklahoma State University (OSU) Range Research Station. The Oklahoma Mesonet MARE site is located 400 m from the site and two NOAA CRN stations are located nearby. The landscape of the site is characterized as rangeland and pasture. OSU Department of Plant and Soil Science will provide additional local support.

The site consists of four separate sets of installations situated around Subsite A so they have radially increasing distance from Subsite A. Figure 66 shows the locations of
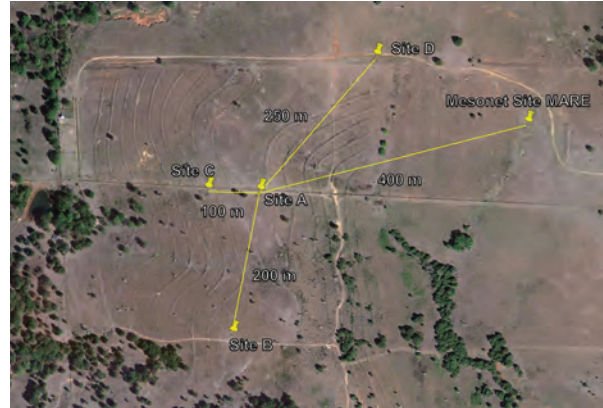


Figure 66. Geographic configuration of the SMAP MOISST and its subsites.

the subsites: Subsite C is at a distance of 100 m, Subsite B at 200 m, Subsite D at 300 m and Mesonet MARE site additionally at a distance of 400 m from Subsite A.

Each subsite has a set of soil moisture sensors. Table 21 shows which sensors are installed at which subsite, the number of sensors at each subsite and the depths of the installations at those subsites. A Passive Distributed Temperature Sensor (DTS) System (Steele-Dunne et al. 2010) is installed between Subsites A and B. For investigation of the effect of the sampling interval each sensor is sampling with enhanced one-minute interval for five minutes every hour. Additionally, the vegetation water content, surface roughness and soil characteristics will be determined for the domain over the course of the experiment.

## B. Soil Moisture Up-Scaling Study

Up-scaling is a key issue in utilization of in situ measurements for calibration and validation. Therefore, one of the pre-launch cal/val objectives is to define a standard methodology on how to transfer point-wise ground measurements of in situ resources to the SMAP footprint scale. A SMAP working group focused on providing systematic scaling guidelines for the SMAP Cal/Val program. This effort has resulted in a paper "Upscaling sparse ground-based soil moisture observations for the validation of coarse-resolution satellite soil moisture products" (Crow et al. 2012).

## C. Core Validation Sites

The SMAP project chose to follow the approach used in previous satellite validation programs (MODIS, AMSR-E, and SMOS) and to establish a set of Core Validation Sites (CVS). The scientific objective of these sites is to provide very high quality in situ observations that can be used to estimate soil moisture, freeze/thaw, or NEE accurately at the spatial resolution of the L2–L4 products, while satisfying all the other requirements described in subsequent

Table 21. Soil moisture sensor types, subsites where they are installed, number of sensors per subsite, and depths of installations at those subsites.

| Configuration | Sites | No. | Depths (cm) |
|---|---|---|---|
| Stevens Water Hydra Probes | A,B,C,D | 6 | 2.5, 5, 10, 20, 50, 100 |
| Delta-T Theta Probes | A,B,C,D | 5 | 5, 10, 20, 50, 100 |
| Decagon EC-TM probes | A,B,C,D | 5 | 5, 10, 20, 50, 100 |
| Sentek EnviroSMART | A,B,C,D | 4 | 10 , 20, 50, 100 |
| Acclima Sensor | A,B,C,D | 5 | 5, 10, 20, 50, 100 |
| Campbell CS 229-L heat dissipation sensors (OK Mesonet) | A,B,C,D | 5 | 5, 10, 20, 50, 100 |
| Campbell CS615/CS616 TDRs | A,B,C,D | 5 | 5, 10, 20, 50, 100 |
| Passive Distributed Temperature Sensor (DTS) System | A-B | 1 | 10 cm |
| GPS reflectometers | A, C, D | 1 | |
| COSMOS system | A | 1 | |
| Climate Reference Network Station | B, D | 6 | 2.5, 5 |
| Traditional TDR System | A | 4 | 5, 10, 50, 100 |
| ASSH System (Mongolia) | A | | |

sections. Linking the in situ observations to the SMAP product grid sizes is a key aspect of the CVS. Overall the highest priority in situ resources for SMAP Cal/Val are the Core Validation Sites (CVS). CVS have been an important component of previous efforts to use remote sensing to estimate soil moisture (AMSR-E [Jackson et al. 2010], SMOS [Jackson et al. 2012]) and other land parameters.

In particular, it was suggested that it is highly desirable that the soil moisture Core Validation Site design included multiple sites that would provide a statistically reliable estimate; however, the use of an established alternative method for scaling would be considered, especially for sparse networks. In the case of sparse networks, if the basic data provided has been verified, the SMAP project can collaborate on alternative scaling methods. The selected Core Validation Sites would be the focus of intensive ground and aircraft field campaigns to further verify scaling. Extensive ancillary datasets would be established to support algorithm development and implementation at multiple scales and water, energy, and carbon models and other synergistic science.

### 1) General Requirements for CVS

The following minimum criteria are desired for a CVS of any of the data products:

- Accessible to researchers

- Has existing infrastructure including access and utilities

- Heritage of scientific studies to build from

- An area that is homogeneous or has a uniform mixture of land covers at the product scale

- Represents an extensive or important biome

- Complements the overall set of sites

- Operational by 2013 with infrastructure support through 2017

- Formal arrangement with the SMAP project

In situ methods provide point observations and the volume contributing to each point is different from satellite grid products value (depending on the product). A variety of techniques can be used to establish the scaling of the points and grids. Each participating CVS will have associated a description of the methods that will be used to scale its in situ measurements up to a SMAP grid cell size.

### 2) Specific Requirements for a Soil Moisture CVS

Explicit requirements set out for soil moisture CVS are the following:

- Depths: Minimum 0–5 cm, desirable 0–5 and 0–100 cm

- Sensors that have been calibrated to volumetric soil moisture using the thermo-gravimetric method (verification)

- A dense network of sensors (Minimum 6, desired 15) over a SMAP grid cell

— Acceptable: Scaling using an established alternative technique

— Desirable: Three nested levels of extent (3, 9, and 36 km)

- Supporting studies to establish the representative-ness of the network using more intensive sampling

- Data available in 1 to 4 weeks to the validation team

- Supporting information on soils, vegetation, and meteorology

Sites distributed geographically and representative of a range of climate and vegetation types are desirable. Data access, latency, and verification of calibration and scaling must be satisfied if a site is to be a CVS. Networks that cannot satisfy all of the requirements will be supplemental resources for validation.

Although it is highly desirable that the soil moisture CVS design includes multiple sites that provide a statistically reliable estimate, the use of an established alternative method for scaling will be considered, especially for sparse networks.

### 3) Selection and Engagement of CVS

During the early Phase A of the SMAP project the existing in situ resources were not in the state that they alone could provide all the information needed to conduct SMAP validation. Most of the readily available resources were sparse and lacked an explicit scaling to SMAP grid

cell spatial resolutions. When combined with variations between instruments and installations, it would have been difficult to conduct the analyses necessary for global consistency. There were a few candidate dense networks; however, even these would have needed to adapt to the spatial scales of SMAP.

Increasing the number and improving the quality of in situ observations available to SMAP was identified as a significant issue by the Cal/Val Working Group and actions were initiated to address these problems. One specific action taken was to release a Dear Colleague Letter (DCL) for In Situ Validation through NASA. This announcement solicited responses that involved no exchange of funds, allowed international participation, provided guidance and minimum requirements, and applied to all types of in situ observations.

Collaboration has also been also solicited outside the DCL-process and in the end all participants who must enter into a formal agreement with the project regarding cooperation in the calibration and validation of the mission products will be recognized as SMAP Cal/Val Partners. CVS will be selected from Cal/Val Partners' sites based on the parameters of the sites, as discussed above. Other sites not meeting all requirements will be referred to as Supplemental Validation Sites.

### 4) List of Potential SMAP Core Validation Sites

The current set of candidate CVS is shown in Figure 67 and listed in Table 22. These included good geographic coverage and were mostly focused on soil moisture.
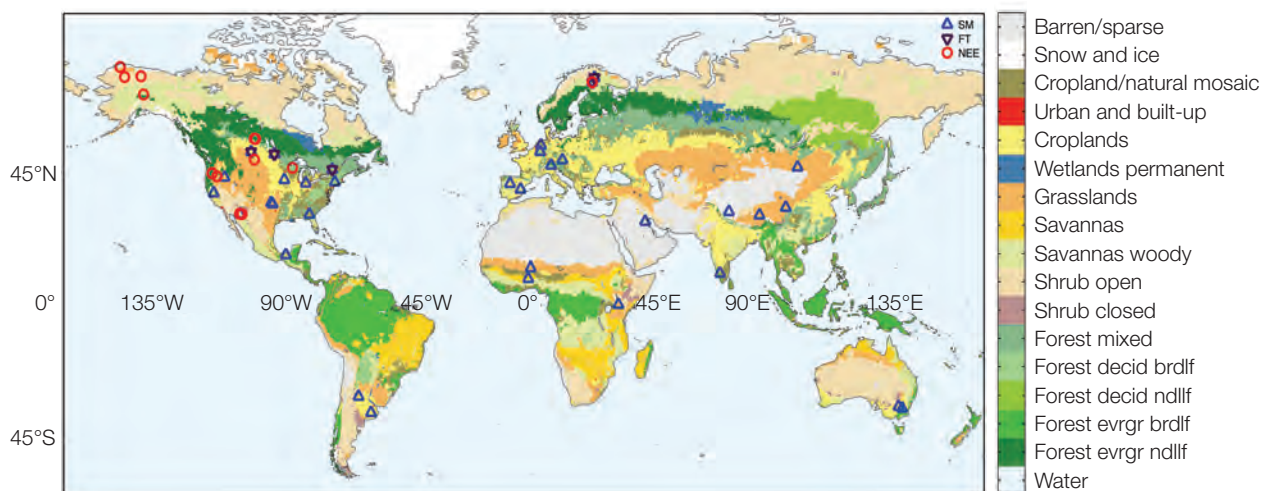


Figure 67. The distribution of Cal/Val partners that are candidates for SMAP Core Validation Sites.

**Table 22. SMAP Cal/Val partners that are candidates for SMAP Core Validation Sites.**

| Site/Network | PI Last Name | Location (Number) | Type | L2/3 SM | L3 FT | L4 SM | L4 C | L1 |
|---|---|---|---|---|---|---|---|---|
| USDA ARS Research Watershed Networks | M. Cosh | USA (6) | Dense | X | | | | |
| Reynolds Creek Experimental Watershed | M. Seyfried | Idaho | Dense | X | | X | | |
| SoilSCAPE Wireless Network | M. Moghaddam | California (3) | Dense | X | | X | | |
| Soil moisture and freeze/thaw network in the Northeast | M. Temimi | New York | Dense | X | | X | | |
| Saskatchewan and Ontario Soil Moisture Networks | A. Berg | Canada (2) | Dense | X | X | X | | |
| Agri-Food Canada In Situ Networks | H. McNairn | Canada (3) | Dense | X | X | X | | |
| Mexican Riverine Ecosystem | J. Ramos Hernandez | Mexico | Dense | X | | X | | |
| Murrumbidgee Catchment Core Validation Site | J. Walker | Australia | Dense | X | | X | | X |
| Kuwait Desert Terrain | K. Al Jassar | Kuwait | Dense | X | | | | X |
| FMI-ARC | J. Pulliainen | Finland | Dense | X | X | X | X | |
| CCRN Networks | H. Wheatear | Canada | Dense | | X | | | |
| Twente NL and Tibetan Plateau Sites | Z. Su | Netherlands and Tibet (4) | Dense | X | | X | | |
| Argentina Forest and Agriculture | H. Karszenbaum | Argentina | Dense | X | | X | | |
| Argentina SAOCOM Sites | M. Thibeault | Argentina | Dense | X | | | | |
| Mpala Hydrological Observatory, Kenya | K. Caylor | Kenya | Dense | X | | X | X | |
| REMEDHUS | J. Martinez-Fernandez | Spain | Dense | X | | X | | |
| TERENO | C. Montzka | Germany | Dense | X | | | | X |
| HOAL | W. Dorigo | Austria | Dense | X | | X | | |
| Valencia | E. Lopez-Baeza | Spain | Dense | X | | | | |
| MAHASRI | I. Kaihotsu | Mongolia | Dense | X | | | | |
| AMMA | T. Pellarin | Niger, Benin (2) | Dense | X | | | | |
| EURAC | C. Notarnicola | Italy | Dense | X | | | | |
| Metolius and Burns, Oregon | B. Law | USA, Oregon | Tower | | | X | | |
| BERMS | H. Wheater | Canada | Tower | | | X | | |
| Imnavait Watershed & Bonanza Crk | E. Euskirchen | USA, Alaska | Tower | | | X | | |
| Park Falls | A. Desai | USA, Wisconsin | Tower | | | X | | |
| Fort Peck | T. Miers | USA, Montana | Tower | | | X | | |
| Sky Oaks, Ivotuk, Atqusuk | W. Oechel | USA | Tower | | | X | | |
| Santa Rita, Walnut Gulch | R. Scott | USA, Arizona | Tower | | | X | | |
| Tonzi Ranch | D. Baldocchi | USA | Tower | | | X | | |

## D. Supplemental Validation Sites

Supplemental Validation Sites are those that do not fulfill all the requirements of the CVS but are nevertheless seen as very important for the SMAP calibration and validation activities. In most cases these are measurements provided by sparse networks that do not have calibration and scaling information. Table 23 lists the sparse networks

that will be Supplemental Validation Sites. Several of the key networks in the U.S. are illustrated in Figure 68. In addition, candidate CVS described above may be moved to this category pending ongoing evaluations.

Additionally, several groups have indicated that they will support SMAP Cal/Val with tower- and aircraft-based observations of brightness temperature and soil moisture. These collaborators are summarized in Table 24.
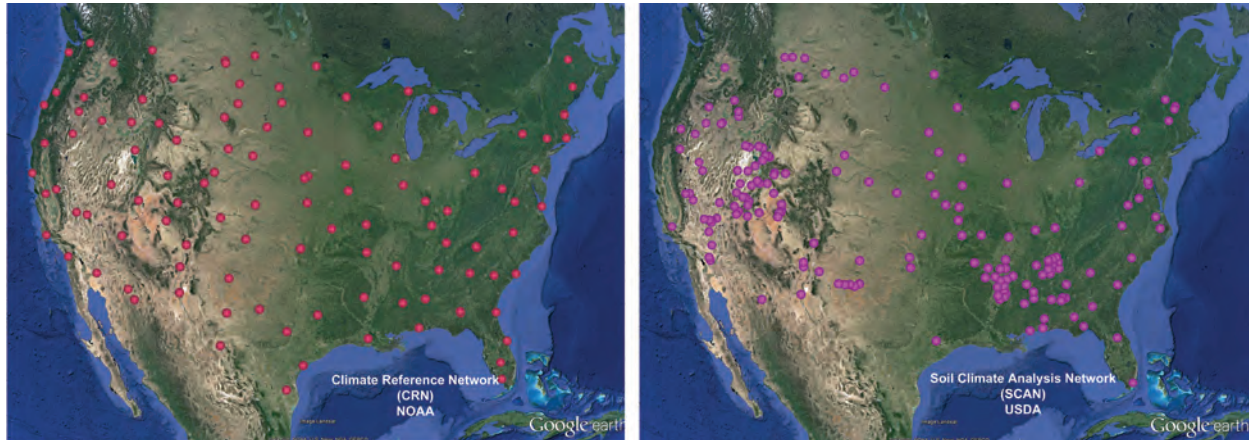


Figure 68. Map of several key sparse networks that will be SMAP Supplemental Validation Sites.

Table 23. The list of selected partners for SMAP Supplemental Validation Sites.

| Site/Network | PI Last Name | Location | Type | L2 SM | L3 FT | L4 SM | L4 C | L1 |
|---|---|---|---|---|---|---|---|---|
| SMOSMANIA | J. Calvet | France | Sparse | X | | X | | |
| SCAN/SNOTEL | | USA | Sparse | X | X | X | | |
| CRN | M. Palecki | USA | Sparse | X | | X | | |
| GPS Interferometric Reflectometry Network | E. Small | Western USA | Sparse | X | | | | |
| Southern Sierra Critical Zone Observatory | J. Hopmans | California | Sparse | X | | X | X | |

Table 24. SMAP Cal/Val team L-band tower and aircraft-based sensors.

| Group | Tower Instruments | Aircraft Instruments |
|---|---|---|
| NASA GSFC | Active and Passive (ComRAD) | |
| JPL | | Active and Passive (PALS) |
| JPL | | Active (UAVSAR) |
| University of Monash, Australia | | Active (PLIS) and Passive (PLMR) |
| University of Julich, Germany | Passive (Julbara) | Active (?) and Passive (PLMR) |
| SAOCOM | | Active |
| CREST | Passive | |
| University of Florida | Active and Passive | |
| Kuwait University | Active and Passive | |

## V. Post-Launch Activities

### A. Overview

In the post-launch period, the calibration and validation activities will address directly the measurement requirements for the L1-L4 data products. Each data product has quantifiable performance specifications to be met over the mission lifetime, with calibration and validation requirements addressed in their respective ATBDs.

Post-launch calibration and validation activities are divided into four main parts following the IOC phase after launch:

- Release of beta (or provisional) versions of L1 and L2 products

- Six-month sensor product Cal/Val phase, after which delivery of validated L1 products to the public archive will begin.

- Twelve-month geophysical product Cal/Val phase, after which delivery of validated L2 through L4 products to the public archive will begin.

- Extended monitoring phase (routine science operations) lasting for the remainder of the science mission. During this period, additional algorithm upgrades and reprocessing of data products can be implemented if found necessary (e.g., as a result of drifts or anomalies discovered during analysis of the science products).

Figure 69 shows the draft timeline (placeholders, and without commitment to dates) for the Cal/Val in the post-launch phase (Phase E). The timeline shows the key Cal/Val activities and relevant project schedule items. Phase E of the mission is divided into the IOC phase, Science Cal/Val phase, and Routine Operations phase. This is reflected at the top of the table. In the Cal/Val Phase there are two important milestones: (1) release of validated L0 and L1 data, and (2) release of validated L2 through L4 data.

In situ validation sites, networks and field campaigns are the core of the science product cal/val in the post-launch phase. The table highlights the operation and occurrence of these.

Coordination of post-launch Cal/Val and Science Data System (SDS) activities is important since the SDS produces the science products, provides storage and management of Cal/Val data, provides data analysis tools, and performs reprocessing and metadata generation of algorithm and product versions. The Level 2 requirements state that the cumulative mission science data shall be reprocessed up to three times (if necessary) to improve the data quality and that the final reprocessing shall be used to generate consistently-processed set for the complete mission one month after the end of prime (3-year) science mission. The figure shows placeholders for these milestones. Additionally, Figure 69 includes other relevant satellite missions taking place simultaneously with the SMAP mission. Note that in the case of Aquarius and SMOS that they will be extended if still operational.
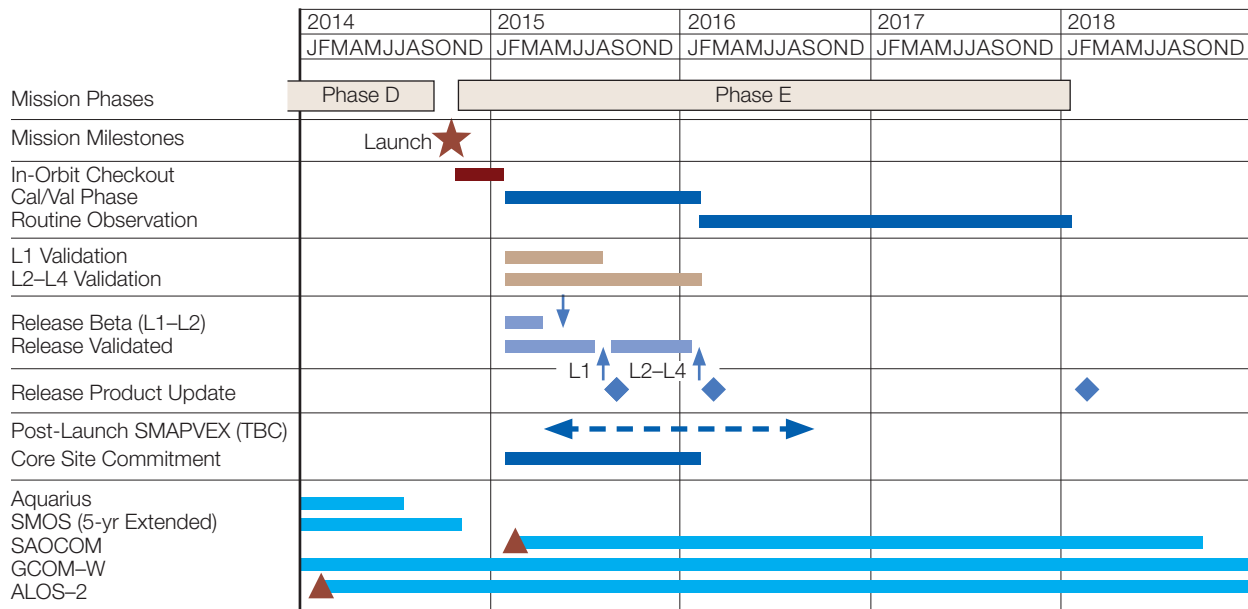


Figure 69. Post-launch Cal/Val timeline.

## B. Sensor Products

### 1) Radiometer Brightness Temperature

The calibration approach of the SMAP radiometer requires that the absolute calibration is done on orbit after launch. The specific objectives of the radiometer post-launch calibration and validation activities are to:

• Provide any necessary tuning of pre-launch calibration, including bias removal, and set calibration-related parameters that can only be determined on-orbit

• Calibrate drifts in the measured brightness temperature

• Validate instrument performance i.e. determine radiometer performance figures

• Validate brightness temperature product i.e. determine overall uncertainty

• Validate brightness temperature gridding to Earth grid

The following subsections break these objectives down to separable components of the radiometer operation and calibration. Table 25 provides an overview.

**Geolocation.** Standard geolocation techniques for scanning instruments that have been previously developed and inherited from other missions (e.g., QuikSCAT, SSMI) are carefully documented in existing documents. These algorithms account for spacecraft position, pointing, and attitude; antenna scan angle; curvature of Earth and measurement timing.

The baseline geolocation will be established based on the spacecraft ephemeris and the nominal scan geometry. The SMAP radar provides ranging and Doppler information, which can be used to remove antenna pointing biases to high accuracy. The measured brightness temperatures will be utilized in several ways to refine the baseline. Flat targets, such as large open ocean regions, can be used to determine pitch and roll bias utilizing the measured brightness temperature over the full 360° scan. The scan cone angle can also be solved and used to adjust the nominal cone angle. Alignment of coastlines and water bodies can be used to determine the best fit of the two-dimensional brightness temperature image vs. known geography. Coastline crossings can be also be utilized but the scan position needs to be addressed (as opposed to the case of fixed beam instruments such as Aquarius). Finally, the radiometer geolocation can be compared against the SAR geolocation, which, however, needs to account for the latency in the processing.

**Faraday Rotation Correction.** The validation of the Faraday rotation correction will be accomplished by comparing the estimated Faraday rotation with the Faraday rotation obtained from ionosphere electron density (International Reference Ionosphere [IRI] database) and magnetic field data (International Geomagnetic Reference Field [IGRF] database). The rotation angle can also be compared with the estimation by SMOS (Yueh 2000). This validation will be particularly important for calibration data collected over the ocean, where 3rd Stokes parameter is generated both by Faraday rotation and by the azimuthal asymmetry of ocean wave fields, although ocean-generated third Stokes parameter is expected to be less than 1 K.

**Atmospheric Correction.** The effect of the atmosphere is expected to be very small at L-band. Nevertheless, a correction will be applied to the brightness temperature measurement. The atmospheric correction will be carried out by applying global temperature and humidity profiles (from forecast data) to a radiative transfer model of standard clear-sky case, at least over ocean. Over land, an application of path delay measured by other microwave instruments is considered to improve accuracy.

**Antenna Pattern Correction.** The SMAP Brightness Temperature Forward Simulator will be used to calculate an estimate of the effect of the sidelobes on the brightness temperature. The method will be validated utilizing known scenes.

Table 25. SMAP Cal/Val methodologies and their roles in the L1B_TB product validation.

| Methodology | Data Required | Importance | Metrics |
|---|---|---|---|
| External Targets | Grid cell averages for each overpass | Primary | RMSE, SDEV, Drift |
| Satellite Products | TB matchups with SMOS and Aquarius | Primary | Relative RMSE, SDEV, Drift, spatial and temporal correlation |
| Model Products | Antarctic, ocean, and cold space expected TBs | Primary | RMSE, SDEV, Drift, spatial and temporal correlation |
| Field Experiments | Aircraft- and ground-based radiometer measurements | Secondary | Spatial and temporal variability of sites |

**RFI and Post-Launch Calibration.** For validation of RFI mitigation, RFI detection flags will be compared with known RFI sites (such as FAA radars). The SMAP brightness temperature product will be compared with brightness temperature products of the Aquarius and SMOS missions (at about 40° incidence angle) and also the RFI detection flags will be compared with the RFI records generated by Aquarius and SMOS. RFI mitigation can also be validated by comparing soil moisture retrieval quality measures to RFI detection flags; poor retrieval quality could be due to missed RFI.

**Absolute Calibration and Drift Monitoring and Correction.** After applying the corrections listed in the previous paragraphs, the Cal/Val activities listed in Table 10 will be implemented. Post-launch absolute calibration and drift correction of the radiometer is centered on the measurements of three external targets: the "cold" cosmic microwave background (CMB), the "cool" ocean, and the "warm" Antarctica ice sheets. By applying these reference targets the absolute error and drift of the brightness temperature measurements is corrected to less than 0.4 K This requires that the radiometer is to be calibrated with accuracy of better than 2 K in the pre-launch phase. The radiometer will acquire data in high data rate mode (RFI detection) over the external calibration targets in order to calibrate all sub-channels for optimal RFI detection and removal.

The CMB is measured in the Cold Sky Calibration (CSC) maneuver. In CSC the instrument is pointed at the galactic pole. The maneuver will be carried out monthly or as required. The effect of the thermal changes during the maneuver will also be evaluated and accounted for. The absolute accuracy of the aggregate CMB and galactic source models are on the order of 0.1 K, the brightness temperature of CMB being at the 2.73 K level.

The ocean target is a bounded geographical area specified by latitude and longitude limits (an area in the Southeast Pacific has been preliminarily identified). In order to have an accurate value for the brightness temperature over the ocean target a radiative transfer model (RTM) will be developed (utilizing experience from Aquarius). The RTM will exploit buoy measurements (such as TOGA-TAO and Argo arrays) and regional averages based on environmental reanalysis models to obtain accurate input values for physical temperature, wind, salinity etc. The RTM will account for surface roughness, atmospheric effects, reflections of celestial objects, etc. where applicable. The performance of the RTM of the target area will be confirmed in pre-launch. The absolute accuracy of the ocean target RTM is expected to be better than 0.4 K with better relative accuracy (for stability monitoring). However, achieving this accuracy would mean discarding of data obtained during less than ideal conditions (e.g., high winds). The expected brightness temperature is in

the 80–150 K range, depending mostly on the polarization and ocean temperature.

The Antarctica ice sheets contain areas with seasonally highly stable L-band brightness temperature. In particular, the area around the Dome-C on eastern Antarctica has been under study and this region has been preliminarily identified as a calibration target (a latitude and longitude mask has been specified around Dome-C). Intensive ground based studies at L-band suggest that the stability would be in the order of 0.1 K. The Dome-C site is equipped with meteorological measurements but the RTM from snow and ice layers needs more development before absolute accuracies at levels better than 1 K can be reliably achieved. An option to increase the absolute accuracy would be continuous ground-based measurements of the brightness temperature, which would then be upscaled to footprint size. The brightness temperature level of the Antarctica is around 200 K.

The calibration data from the ocean and Antarctica targets will be acquired on every overpass. For Antarctica, this means almost every orbit. The ocean target will be measured a few times a day. In comparison to the CSC maneuver, which is expected to be carried out monthly, the observation frequency of the terrestrial calibrations targets is very high. Hence, the calibration strategy involves two elements: activity related to the proximity of CSC maneuvers and activity related to the frequent observations of the terrestrial calibration targets between CSC maneuvers.

The absolute calibration of the brightness temperature measurements is determined around the CSC events. The CSC observation together with the observations of the terrestrial targets (within one day of the CSC maneuver [TBC]) is used to find the best fit between calibration parameters and the targets. In this case, the CSC value is fixed and the radiometer calibration parameters are adjusted. However, through analysis of the measurements of the terrestrial calibration targets it may be possible that also the RTM parameters of the terrestrial targets are adjusted to find the best fit.

Between the CSC events, the RTM parameters of the terrestrial calibration targets remain fixed and the RTM values are used to monitor the stability of the radiometer and detect any drifts and correct for them. It is important to note that when monitoring the stability of the radiometer, the absolute value of the target is not essential as long as the changes of the target, if any, are known. Therefore, although the absolute accuracy of the RTM values for the terrestrial targets may not always meet the requirement, they should meet the requirement in the sense of stability.

There is a feedback from Level 2 product validation to Level 1 product validation. The observations over the

Level 2 validation site are used to detect any systematically behaving biases which could possibly be attributed to the radiometer calibration parameters rather than Level 2 retrieval algorithm parameterization.

Intersatellite calibration will also be employed if other L-band radiometer instruments will be available, such as SMOS and Aquarius. The process for utilizing these observations is TBD.

The process described above constitutes the calibration and validation activity of the brightness temperature and is intended 1) to ensure that the L1B_TB product meets its requirement, and 2) to provide the performance characteristics of the L1B_TB product.

**Gridding.** The accuracy of the gridding algorithms will be evaluated by viewing coastlines, islands, and inland lakes.

*2) Radar Backscatter Cross-Section*

The post-launch calibration objectives for the radar measured backscatter cross-section are to remove channel-to-channel, pixel-to-pixel biases and the absolute bias. Another purpose of the cross-section validation is to show that the requirements for L1_S0_LoRes and L1_S0_HiRes have been met, and also to use this information to optimize the accuracy of the final cross-section products. Table 26 summarizes the methodologies that will be utilized.

**Pointing and Geolocation.** In order to meet the pointing requirements, the antenna spin axis must be closely aligned with the nadir vector. It has been demonstrated, both by experience with SeaWinds and by modeling of SMAP, that the radar returns provide a highly accurate means of determining pointing biases on-orbit. The plan is therefore to observe the radar echo return as the antenna rotates and derive the roll/pitch biases. The S/C attitude control system will then be adjusted by ground command to null out these biases, and the biases in the "cone angle" about nadir can be deduced. Geolocation of radar

data will be further confirmed using the location of known physical features on the ground as well as the location of large corner reflectors in the California desert.

**Radiometric Calibration and Bias Removal.** The post-launch external calibration of the radar receive and transmit operation consists of several components. It is expected that man-made targets are by themselves insufficient to complete the calibration. This is due to the fact that the pixel size is too large for corner reflectors (however, they are inexpensive and may be helpful in geolocation validation) and the transponder accuracy is insufficient. Instead, the statistical analysis of large, uniform, isotropic and well-characterized, stable scenes (such as Amazon) are applied. Additionally, cross-calibrations with other contemporaneously flying radars are used. These will include ALOS-2, Aquarius, and possibly UAVSAR measurements over distributed targets and over targets where these comparison sensors can be calibrated with corner reflectors. Furthermore, calibrations based on natural targets have been demonstrated to be very accurate. For example, JPL Ku-band scatterometers removed channel-to-channel and pixel-to-pixel biases to 0.2 dB, and JERS-1 demonstrated that Amazon is stable to less than 0.2 dB at L-band. The polarimetric backscatter reciprocity can also be utilized in the calibration. Calibration stability over time can be assessed using the above described tropical rain forest targets, as well as the ocean (after it has been corrected for the effects of wind speed and direction). The ocean presents a target that has excellent measurement statistics and is present at all latitudes.

**Faraday Rotation Correction.** The L1B and L1C radar processors will estimate Faraday rotation using forecasts of the ionospheric total electron content (TEC) derived from GPS measurements and supplied by IGS. A study was performed pre-launch, and it was found that about 3% of the land surface points will not meet accuracy requirements if no Faraday rotation correction is applied. The errors in the IGS forecasts of TEC are small enough that applying a correction based on them will lower all residual Faraday rotation errors under the error budget.

**Table 26. SMAP Cal/Val methodologies and their roles in the L1B/C_S0 product validation.**

| Methodology | Data Required | Importance | Metrics |
|---|---|---|---|
| Stable Scattering Targets | Amazon reference area radar observations over time | Primary | SDEV, drift vs. time, channel, cross-track position |
| Satellite Products | $\sigma^o$ cross-calibration with (PALSAR, JERS, Aquarius) over the Amazon | Primary | Minimize biases |
| Geolocation by Shoreline Fitting | Known shoreline maps vs. highest resolution radar map | Primary | Mean displacement along/cross track |
| Swath Oriented Artifact Detection | Full-res swath image over isotropic targets (Amazon, Ice) | Primary | Visible swath oriented discontinuities |

Validation of the Faraday rotation correction will be performed by comparing the Faraday rotation angle derived by the SMAP Radiometer with the value derived from the IGS supplied TEC value.

**RFI Mitigation.** During Instrument In-Orbit Checkout (IOC), there will be a period of time referred to as the "RFI Survey" where the radar transmit will be disabled, and the radar will run in a receive only mode for an 8-day orbit repeat cycle. During this time, the transmit frequency will be rastered continually over the entire tuned range. By so doing, data will be collected by sampling the RFI environment as a function of geographic position. This dataset will be used to select the optimum frequencies to use to avoid RFI. It might be necessary to implement a regular "frequency hopping" scheme so that the SMAP radar does not interfere with other terrestrial services. After selecting the "optimum" frequency, residual levels or RFI are expected to be present, and will be detected and removed in ground processing. Validation of the RFI removal algorithm will be performed during L1 Cal/Val by comparing output products with the RFI mitigation algorithm switched on and off. With the removal algorithm switched off, RFI will show up as bright areas in the backscatter image. With the removal algorithm switched on, the RFI flags will show where RFI was detected and where it was considered correctable.

## C. Geophysical Products

This section describes the post-launch calibration and validation of the geophysical products, L2–L4. Note that the Cal/Val of L2 soil moisture products automatically calibrates and validates the L3 soil moisture products, since they are just compilations of L2 products.

### 1) Soil Moisture Passive (L2/3_SM_P)

Table 27 summarizes the methodologies that will be used to validate L2/3_SM_P. Each of these was described previously. The primary validation will be a comparison of retrievals at for a 36-km product with ground-based observations that have been verified as providing a spatial average of soil moisture at this scale, the CVS. However, other types of observations or products will contribute to post-launch validation. The following subsections describe these in more detail.

**Core Validation Sites.** As noted previously, the baseline validation (Stage 1) for the L2_SM_P soil moisture will be a comparison of retrievals for a 36-km product with ground-based observations that have been verified as providing a spatial average of soil moisture at the same scale, referred to as Core Validation Sites. Many of these sites have been used in AMSR-E and SMOS validation (Jackson et al. 2010; Jackson et al. 2012; Jones et al., 2007; Kimball et al. 2009). Some of these sites will also be the focus of

intensive ground and aircraft field campaigns to further verify the accuracy of the collected data.

The footprint-scale soil moisture estimates of Core Validation Sites will be compared against the SMAP L2_SM_P products to produce an RMSE assessment of the accuracy of the product over these sites.

**Supplemental Validation Sites.** The intensive network validation described above can be complemented by sparse networks as well as by new/emerging types of networks included in the Supplemental Validation Sites. Due to the scaling issues of most of these networks, the data are more likely to be used as part of the statistical triple co-location analysis (Scipal et al. 2008; Dorigo et al. 2010) as opposed to exact comparisons of in situ value and the product.

**Satellite Products.** Depending upon mission timing and life, it is possible that both SMOS and JAXA's GCOM-W will be producing global soil moisture products at the same time as SMAP.  Both of these products are at the same nominal spatial resolution as the SMAP L2_SM_P soil moisture and are supported by validation programs, which should be mature by the SMAP launch date. In addition, an Aquarius soil moisture product will be available at a coarser spatial resolution.

Post-launch soil moisture product comparisons with SMOS and GCOM-W are a very efficient means of validation over a wide range of conditions. If confidence in these products is high, they will provide a good resource for Stage 2 SMAP validation.

Post-launch validation will consist of comparisons between the SMAP / SMOS / GCOM-W soil moisture estimates that include:

- Core Validation Sites

- Extended homogeneous regions

- Global maps

For the core validation sites and extended homogeneous regions, statistical comparisons will be conducted (Root Mean Square Difference, RMSD, will be used instead of RMSE because the alternative satellite products are not considered to be "ground truth").

Comparisons will be initiated as soon as SMAP soil moisture products become available; however, a sufficient period of record that includes multiple seasons will be necessary before any firm conclusions can be reached. It should also be noted that only dates when both satellites cover the same ground target at the same time will be useful. The overlap of the swaths will vary by satellite. The morning (and evening) orbits of SMAP and SMOS cross

**Table 27. SMAP Cal/Val methodologies and their roles in the L2/3_SM_P product validation.**

| Methodology | Data Required | Importance | Metrics |
|---|---|---|---|
| Core Validation Sites | Grid cell averages for each overpass | Primary | RMSE, Bias, Correlation |
| Supplemental Validation Sites | Spatially scaled grid cell values for each overpass | Secondary: Pending results of scaling analyses | RMSE, Bias, Correlation |
| Satellite Products | Orbit-based match-ups (SMOS, GCOM-W, Aquarius) | Primary: Pending assessments and continued operation | RMSD, Bias, Correlation |
| Model Products | Orbit-based match-ups (NCEP, GEOS-5, ECMWF) | Secondary | RMSD, Bias, Correlation |
| Field Experiments | Detailed estimates for a very limited set of conditions | Primary | RMSE, Bias, Correlation |

(the SMOS 6 AM overpass is ascending while the SMAP 6 AM overpass is descending). Obviously, coverage of a specific site by both satellites will be infrequent.

Although data collected over the CVS will be of the greatest value, the Supplemental Validation Sites with concurrent satellite observations will also be useful, especially for regions that are relatively homogeneous in terms of land cover/vegetation and soils. One example would be the Sahara region.

Another role for the satellite products is in providing a synoptic perspective. Global image comparisons will be used to identify regions and / or time periods where the soil moisture products from the different satellites diverge.

Assessments will be conducted periodically throughout the SMAP post-launch period to assess, monitor, and possibly correct bias offsets between SMAP products and SMOS/GCOM-W products. In order to fully exploit SMOS/GCOM-W soil moisture products for SMAP validation, it will be necessary for SMAP team members to participate in the assessment and validation of these products and to secure access to the data through ESA and JAXA.

**Model-Based Products.** In the simplest case, land surface models (either embedded in a Numerical Weather Prediction (NWP) system or in off-line mode) can be used to generate soil moisture products at larger (basin-wide and continental) scales using land surface and meteorological forcing datasets that are independent of the SMAP remote sensing data. As in the case of satellite products, the resulting soil moisture fields can then be compared with the remotely sensed soil moisture product at validation sites (or synoptically) over diurnal and seasonal cycles. These model-derived soil moisture fields can also be used to extend comparisons to larger space and time domains than available from in situ observations, thus supporting Stage 2 validation. The spatial resolution of

the L2_SM_P matches the typical spatial resolution of the NWP products. An advantage of the model-based products is that they produce a synoptic global product every day, which means that more frequent comparisons to SMAP and ground-based observations are possible.

Several NWP centers (including ECMWF, NCEP, and NASA/GMAO) routinely produce operational or quasi-operational soil moisture fields at a scale comparable to the SMAP radiometer product that could be used in SMAP validation. (This is distinct from the GMAO generation of the SMAP L4_SM surface and root zone soil moisture product, which uses an EnKF to merge SMAP observations with soil moisture estimates from the NASA Catchment land surface model.) The NWP-derived data products rely on the assimilation of a vast number of atmospheric observations (and select land surface observations) into General Circulation Models (GCMs). Although there are many caveats that need to be considered in using these data, they are readily available and they are consistent with the atmospheric forcings (precipitation and radiation) and land use information that determine the spatial and temporal patterns in soil moisture fields.

There is significant inherent uncertainty in any model-based soil moisture product since this is not one of the NWP primary variables. In addition, the models typically simulate a thicker surface soil layer than the layer that dominates the satellite measurement. Little effort has put so far into validating the soil moisture products of these models. Therefore, while these model products are useful, they must be used very carefully. As a result, they are considered to be a secondary resource for validating L2_SM_P soil moisture.

**Field Experiments.** Post-launch field experiments will play an important role in a robust validation of the L2_SM_P data product. These experiments provide critical information that can be used to independently assess the contributions of radiometer calibration, algorithm

structure and parameterization, and scaling on performance. Field experiments require numerous elements that include ground and aircraft resources, which involve many participants and associated financial support. However, they provide moderate-term intensive measurements of soil moisture and other surface characteristics at SMAP product scales.

While it is desirable to acquire such information as soon as possible after launch, the uncertainties of the actual launch date, the relationship of the launch date to the season, and the logistics of allocating fiscal year resources require that such commitments be conservative. Therefore, the field experiments should be scheduled for some time post-launch and used as part of the more robust validation of the SMAP products. Based on an October 2014 launch, one major extended post-launch field campaign that should include one or core validation sites (such as Oklahoma) is scheduled for summer 2015 or 2016.

**Combining Techniques.** Recent work has extended the application of the "Triple Collocation" (TC) approach to soil moisture validation activities (Scipal et al. 2008; Dorigo et al. 2010). These approaches are based on cross-averaging three independently-acquired estimates of soil moisture to estimate the magnitude of random error in each product. One viable product-triplet is the use of passive-based remote sensing, active-based remote sensing and a model-based soil moisture product (Dorigo et al. 2010; Crow et al. 2010). If successfully applied, TC can correct model versus SMAP soil moisture comparisons for the impact of uncertainty in the model product. However, TC cannot provide viable bias information and, therefore, only assesses the random error contribution to total RMSE. Note that TC can also be applied to reduce the impact of sampling error when up-scaling sparse in situ measurements during validation against ground-based soil moisture observations.

## 2) Soil Moisture Active (L2/3_SM_A)

The baseline validation will be a comparison of retrievals at 3 km with ground-based observations that have been verified as providing a spatial average of soil moisture at this scale. However, as indicated in Table 28, there are other types of observations or products will contribute to post-launch validation. The validation approach of the L2_SM_A product follows that of the L2_SM_P: the scaling issue is only adjusted to the finer 3-km resolution and there are some issues which require different amount of attention due to the different observing instrument (radar as opposed to radiometer). The following subsections discuss the use of the various methodologies.

**Core and Supplemental Validation Sites.** The usefulness of soil moisture in situ networks for satellite product validation was discussed previously. In terms of utilization of in situ core sites and the sparse networks the L2_SM_A product validation follows mostly the approach of the L2_SM_P product. However, the scaling process of the point has different parameters, since the pixel size of the L2_SM_A product is only 3 km.

The footprint-scale soil moisture estimates from the Core and Supplemental Validation Sites will be compared with the radar-based soil moisture products. In this process the model based techniques will be used to minimize the upscaling errors, broaden the temporal and spatial domain of the validation and to provide more insight into the parameters of the hydrological cycle at the network locations. First comparisons will be made before the release of the beta release. The full comparison and evaluation will be completed by the end of Cal/Val Phase. The comparison between the in situ estimates and the product will also be used to refine the algorithm and its parameterization.

Table 28. SMAP Cal/Val Methodologies and Their Roles in the L2/3_SM_A Product Validation

| Methodology | Data Required | Importance | Metrics |
|---|---|---|---|
| Core Validation Sites | Grid Cell averages for each overpass | Primary | RMSE, Bias, Correlation |
| Supplemental Validation Sites | Spatially scaled grid cell values for each overpass | Secondary: Pending results of scaling analyses | RMSE, Bias, Correlation |
| Satellite Products | Orbit-based match-ups (Aquarius, PALSAR-2, SAOCOM, GCOM-W, SMOS) | Secondary: Pending assessments and continued operation | RMSD, Bias, Correlation |
| Model Products | Orbit-based match-ups (NCEP, GEOS-5, ECMWF) | Secondary | RMSD, Bias, Correlation |
| Field Experiments | Detailed estimates for a very limited set of conditions | Primary | RMSE, Bias, Correlation |

The validation metric (mean of site-specific RMSE, see Reichle et al. 2010) is determined separately for sparse networks and core sites due to their different upscaling properties.

The land surface data assimilation framework will be utilized for retrieving additional performance metrics (innovation statistics) for the soil moisture product and also for the exercise where the in situ soil moisture observations are substituted for ground-based measurements of rain rate, which enables the utilization of rain gauge networks with large coverage.

**Satellite and Model Products.** The utility of other satellite products for the validation of a SMAP product was described in a previous section. Radar cross-section measured by ALOS PALSAR (or ALOS-2) and SAOCOM may be obtained to test the algorithms. The resolutions of these radars are very high, which can be utilized in the validation of the mitigation of pixel heterogeneity effects. However, care must be taken regarding the various polarimetric modes and incidence angles of PALSAR and SAOCOM. Assessments will be conducted to estimate, monitor, and correct bias offsets between SMAP products and ALOS-2 and SAOCOM products over the validation sites.

The first tests against SAOCOM soil moisture products will be performed by the end of Cal/Val Phase, and the monitoring will continue as long as these products are available. They are not a priority for the beta release.

Efforts are underway to develop model-based products.

**Field Experiments.** As in the case of L2_SM_P, the field experiments provide critical information that can be used to independently assess the contributions of radar calibration, algorithm structure and parameterization, and scaling on performance for the L2_SM_A product validation. They provide moderate-term intensive measurements of soil moisture and other surface characteristics at L2_SM_A pixel scales. However, due to the relatively small pixel size of the L2_SM_A product the significance of the airborne field experiments in terms of scaling properties of a pixel is not as disparate as in the case of L2_SM_P (36-km pixel).

Post-Launch SMAPVEX is planned to include airborne radar observations. While Post-Launch SMAPVEX is scheduled as soon as possible after launch, the uncertainties of the actual date, the relationship to the season, and other logistics require that time-wise commitments for utilization of the campaign data be conservative. Therefore, Post-Launch SMAPVEX and other potential field experiments shall be used as part of the more robust validation of the SMAP products. Post-Launch SMAPVEX and other

post-launch field campaigns are discussed more in a later section. The analysis will focus on matching up airborne observation with satellite products and to produce RMSE on a product scale, and also regarding variability within the product footprint.

The field experiment data will be processed and analyzed for the final validation report. The beta release will not include results from the field experiments not only due to the processing time but also due to the timing of the campaign, which cannot be guaranteed to take place within three months after completion of the IOC.

**Combining Different Validation Sources.** Each above-mentioned validation component produces a separate quantified validation result. The primary, and most emphasized, value is given by the core sites, which is complemented by the result from the sparse networks to add coverage and diversity of validation conditions. The field campaign results will be used to augment this value by giving additional insight to the breakdown of error sources in in situ measurements and scaling process.

The role of other satellite products is to establish the product relative to these products and will not directly add to the validity of the product. Additionally, the land surface data assimilation framework will be used to obtain innovation statistics as an additional performance metric.

The beta release will include only assessment based on selection of core sites and sparse networks. The validation release will include input from all validation sources.

### 3) Soil Moisture Active/Passive (L2/3_SM_AP)

The baseline validation will be a comparison of retrievals at 9 km with ground-based observations that have been verified as providing a spatial average of soil moisture at this scale. However, as shown in Table 29, other types of observations or products will contribute to the post-launch validation. The validation approach of the L2_SM_AP product takes into account the validation efforts of both L2_SM_P and L2_SM_A, as L2_SM_AP combines both radiometer and radar measurements for retrieval. The following subsections discuss use of long-term measurement networks, field experiments, utilization of other satellite products, and hydrological modeling.

**Core and Supplemental Validation Sites.** The utility of soil moisture in situ networks for satellite product validation was described in a previous section. The utilization of in situ dense sampling sites and sparse networks for the L2_SM_AP product validation mostly follows the approach of the L2_SM_P product. However, the scaling process of the point measurements has different parameters, since the pixel size of the L2_SM_AP product is only

Table 29. SMAP Cal/Val methodologies and their roles in the L2/3_SM_A/P product validation.

| Methodology | Data Required | Importance | Metrics |
|---|---|---|---|
| Core Validation Sites | Grid cell averages for each overpass (time-continuous) | Primary | RMSE, Bias, Anomaly Correlation |
| Supplemental Validation Sites | Spatially scaled grid cell values for each overpass (time-continuous) | Secondary: Pending results of scaling analyses | RMSE, Bias, Anomaly Correlation |
| Satellite Products | Orbit-based match-ups (SMOS, GCOM-W, Aquarius) | Secondary: Pending assessments and continued operation | Pattern matching, Correlation |
| Model Products | Global model outputs (NCEP, GEOS-5, ECMWF) | Secondary | Correlation |
| Field Experiments | Detailed estimates for a very limited set of conditions | Primary | RMSE, Bias, Correlation |

9 km and the pixel is formed by a combination of 36-km radiometer pixels and 3-km radar pixels.

The footprint-scale soil moisture estimates from the Core and Supplemental Validation Sites will be compared with the radiometer-based soil moisture products. In this process, the model-based techniques will be used to minimize the upscaling errors, broaden the temporal and spatial domain of the validation, and to provide more insight into the parameters of the hydrological cycle at the network locations. First comparisons will be made before the release of the beta release. The full comparison and evaluation will be completed by the end of Cal/Val Phase. The comparison between the in situ estimates and the product will also be used to refine the algorithm and its parameterization.

The validation metric (mean of site-specific RMSE, see Reichle et al. 2010) is determined separately for sparse networks and core sites due to their different upscaling properties.

The land surface data assimilation framework will be utilized for retrieving additional performance metrics (innovation statistics) for the soil moisture product and also for the exercise where the in situ soil moisture observations are substituted for ground-based measurements of rain rate, which enables the utilization of rain gauge networks with large coverage.

**Satellite and Model-Based Products.** The testing of the L2_SM_AP directly with other satellite data products is limited due to the unique nature of combining L-band radiometer and L-band radar with synthetic aperture processing. However, it may be possible to carry out some algorithm level tests by combining data from L-band radiometers (such as SMOS) and L-band radar (such as ALOS-2) flying on different platforms. The direct comparisons of soil moisture products on a 9-km scale can

be carried out against SAOCOM by aggregating its soil moisture products.

The first tests against these other satellite products will be performed by the end of Cal/Val Phase, and the monitoring will continue as long as these products are available. They are not a priority for the beta release.

Efforts are underway to develop model-based products.

**Field Experiments.** As in the case of L2_SM_P, the field experiments provide critical information that can be used to independently assess the contributions of radar and radiometer calibration, algorithm structure and parameterization, and scaling on performance for the L2_SM_AP product validation. They provide moderate-term intensive measurements of soil moisture and other surface characteristics at L2_SM_AP pixel scales. The collection of field experiment data is combined for all soil moisture algorithms to campaigns occurring as has been laid out for L2_SM_P.

Post-Launch SMAPVEX is planned to include combined airborne radar and radiometer observations. While Post-Launch SMAPVEX is scheduled as soon as possible after launch, the uncertainties of the actual date, the relationship to the season, and other logistics require that time-wise commitments for utilization of the campaign data be conservative. Therefore, Post-Launch SMAPVEX and other potential field experiments shall be used as part of the more robust validation of the SMAP products. Post-Launch SMAPVEX and other post-launch field campaigns are discussed more in a later section. The analysis will focus on matching up airborne observation with satellite products and produce RMSE on product scale and also regarding variability within the product footprint.

The field experiment data will be processed and analyzed for the final validation report. The beta release will not

include results from the field experiments not only due to the processing time but also due to the timing of the campaign which cannot be guaranteed to take place within 3 months after completion of the IOC.

**Combining Different Validation Sources.** Each above-mentioned validation component produces a separate quantified validation result. The primary, and most emphasized, value is given by the Core Sites, which is complemented by the result from the sparse networks to add coverage and diversity of validation conditions. The field campaign results will be used to augment this value by giving additional insight to the breakdown of error sources in in situ measurements and scaling process.

The role of other satellite products is to establish the product relative to these products and will not directly add to the validity of the product. Additionally, the land surface data assimilation framework will be used to obtain innovation statistics as an additional performance metric.

The beta release will include only assessment based on selection of core sites and sparse networks. The validation release will include input from all validation sources.

### 4) Freeze/Thaw State (L3_FT_A)

The baseline validation will be a comparison of freeze/thaw state retrievals with ground-based observations that have been verified as providing a spatial average of freeze/thaw state at this scale. However, as shown in Table 30, other types of observations or products will contribute to the post-launch validation. The following subsections discuss the use of long-term measurement networks and field experiments.

**Core and Supplemental Validation Sites.** Success criteria for the L3_FT_A product will be assessed relative to in situ network measurements of frozen and non-frozen status for northern (≥45°N) biophysical monitoring stations within the major land cover and climate regimes.

In situ frozen/non-frozen status will be determined as a composite ensemble of vegetation, soil and air temperature measurements, and will be compared to coincident footprint scale L3 freeze/thaw measurements. The fulfillment of the requirements will be assessed by comparing SMAP freeze/thaw classification results and in situ frozen or non-frozen status.

The full comparison and evaluation of the L3 freeze/thaw product accuracy will be completed by the end of the mission Cal/Val Phase. The comparison between the in situ temperature observations and the freeze/thaw product will also be used to refine the classification algorithm and its parameterization.

### 5) Satellite and Model-Based Products

**Field Experiments.** Additional L3 freeze/thaw validation activities may involve field campaigns using relatively fine scale airborne (e.g., PALS) and tower-based L-band remote sensing in conjunction with detailed biophysical measurements from in situ station networks (e.g., FLUXNET). Particular focus areas for these activities include examining sub-grid scale spatial heterogeneity in radar backscatter and freeze/thaw characteristics within the SMAP footprint; verifying spatial and temporal stability in L-band radar backscatter for reference frozen and non-frozen conditions; verifying linkages between L3 freeze/thaw dynamics, vegetation productivity and seasonal patterns in land-atmosphere $CO_2$ exchange. The results of these validation activities may then be used to refine pre-launch algorithms and ancillary datasets to improve L3 freeze/thaw product accuracy.

Table 30. SMAP Cal/Val methodologies and their roles in the L3_FT product validation.

| Methodology | Data Required | Importance | Metrics |
|---|---|---|---|
| Core Validation Sites | Grid cell averages for each overpass | Primary | F/T flag agreement (%); false hits/omission (%); primary freeze/melt onset bias (days) |
| Supplemental Validation Sites | Spatially scaled grid cell values for each overpass | Primary: Pending results of scaling analyses | F/T flag agreement (%); false hits/omission (%); primary freeze/melt onset bias (days) |
| Satellite Products | PALSAR-2, ASCAT, SMOS, AMSR-E | Secondary: Pending assessments and continued operation | F/T flag agreement (%); false hits/omission (%); primary freeze/melt onset bias (days) |
| Model Products | GEOS-5 | Secondary | F/T flag agreement (%); false hits/omission (%); primary freeze/melt onset bias (days); correlation, bias, and RMSE of fractional frozen area |
| Field Experiments | Detailed estimates for a very limited set of conditions | Secondary | F/T flag agreement (%); false hits/omission (%); primary freeze/melt onset bias (days) |

**Combining Different Validation Sources.** Each above-mentioned validation component produces a separate quantified validation result. The primary, and most emphasized, value is given by the Core Sites, which is complemented by the result from the sparse networks to add coverage and diversity of validation conditions. The field campaign results will be used to augment this value by giving additional insight to the breakdown of error sources in in situ measurements and scaling process.

### 6) Soil Moisture Data Assimilation Product (L4_SM)

The overall approach that will be used to validate L4_SM is summarized in Table 31. For certain applications, such as the initialization of soil moisture reservoirs in atmospheric forecasting systems, the absolute error in the soil moisture estimates is not necessarily relevant (Crow et al. 2005). Since scaling of soil moisture data is usually required prior to their use in model-based applications (if only because of deficiencies in the modeling system), time-invariant biases in the moments of the L4_SM product become meaningless. For model applications, the temporal correlation of soil moisture estimates with independent observations is therefore a more relevant validation metric. By focusing on the correlation metric, evaluation problems stemming from the inconsistency between point and area-averaged quantities are, to some extent, ameliorated. Entekhabi et al. 2008 provides a detailed discussion of the relationship between RMSE and correlation metrics.

**Validation with In Situ Observations.** Validation of the surface soil moisture estimates from the L4_SM product against in situ observations will be identical to that of the L2_SM_A/P surface soil moisture product, including validation against measurements from dedicated field experiments.

The root zone soil moisture estimates of the L4_SM product will be validated with in situ observations from Core and Supplemental Sites.

Land surface flux, surface temperature, and other estimates from the L4_SM product will be evaluated against in situ observations as much as possible but will be considered research products. The availability of land surface flux data for validation is very limited. A comparably large collection of such data is provided free of charge by FLUXNET (http://fluxdata.org).

**Validation with Data Assimilation Approaches.** Relative to the coverage of the satellite and model soil moisture estimates, few in situ data are available. The validation of the L4_SM product based on in situ observations will thus be complemented with model-based validation approaches. Specifically, the soil moisture data assimilation system produces internal diagnostics that will be used to indirectly validate its output. Specifically, the statistics of appropriately normalized innovations will be examined. Moreover, we will use also use independent precipitation observations to evaluate the surface and root zone soil moisture increments that are produced by the L4_SM algorithm.

### 7) NEE Product (L4_C)

The overall approach that will be used to validate the L4_C product is summarized in Table 32. The statistical methods and domains of validity envisaged for testing the L4_C algorithms and for demonstrating that their performance meets the SMAP science requirements will involve direct comparisons between model outputs and tower eddy covariance $CO_2$ flux measurements from available FLUXNET tower sites representing the dominant global biome types (Baldocchi 2008). Similar protocols have

**Table 31. SMAP Cal/Val methodologies and their roles in the L4_SM product validation.**

| Methodology | Data Required | Importance | Metrics |
|---|---|---|---|
| Core Validation Sites | Observed grid cell averages (time-continuous surface and root zone soil moisture) | Primary | Anomaly correlation, RMSE, Bias |
| Supplemental Validation Sites | Observed values (time-continuous surface and root zone soil moisture) | Primary | Anomaly correlation |
| Satellite Products | Orbit-based match-ups for surface soil moisture (SMOS, ASCAT, Aquarius, GCOM-W) | Secondary: Pending assessments and continued operation | Anomaly correlation, RMSD, Bias |
| Model Products | Global modeling and data assimilation systems (ECMWF, NCEP), surface and root zone soil moisture | Primary | Anomaly correlation, Assimilation diagnostics, RMSD, Bias |
| Field Experiments | Detailed estimates of surface and root zone soil moisture for a very limited set of conditions | Secondary | Anomaly correlation, RMSE, Bias |

Table 32. SMAP Cal/Val methodologies and their roles in the L4_C product validation.

| Methodology | Data Required | Importance | Metrics |
| --- | --- | --- | --- |
| Core Validation Sites | Observed grid cell averages (time-continuous) | Primary | Correlation, RMSE, Bias |
| Contributing Validation Sites | Observed values (time-continuous) | Primary | Correlation |
| Satellite Products | Orbit-based match-ups (SMOS, ALOS-2…) | Secondary: Pending continued operation | Anomaly correlation, RMSD, Bias |
| Model Products | Site and global modeling systems, model inversions (CarbonTracker) | Primary | Sensitivity diagnostics, correlation, RMSD, Bias |
| Field Experiments | Detailed estimates for a very limited set of conditions | Secondary | Correlation, RMSE, Bias |

been successfully implemented for validating the MODIS MOD17 GPP products (Heinsch et al. 2006; Running et al. 1999; Baldocchi et al. 2001; Turner et al. 2006). The L4_C performance and error budgets will also be determined through model perturbation and sensitivity analyses spanning the range of observed northern environmental conditions and using model input accuracy information. If the L4_C algorithms are implemented within the GMAO assimilation framework, this will enable robust error tracking and quantification of the value of SMAP inputs relative to L4_C calculations derived solely from unconstrained model reanalysis inputs. The model reanalysis framework will also enable L4_C products to be generated well before initiation of the SMAP data stream and will provide a standard from which improved model calculations using SMAP derived inputs can be assessed.

L4_C model parameters and initial SOC pool sizes will be determined prior to launch through model simulations and sensitivity studies using GMAO LIS assimilation-based soil moisture and temperature inputs and MODIS GPP inputs over the observed range of Northern Hemisphere ($\geq$45 °N) variability. These estimates will be refined post-launch following initiation of the SMAP data stream and associated production of the input GMAO L4_SM fields. If the L4_C algorithms are implemented within the GMAO assimilation framework, the value of SMAP inputs will be quantified relative to L4_C NEE calculations derived solely from unconstrained model reanalysis inputs.

The accuracy of the L4_C outputs, including NEE and component carbon fluxes for GPP and Rtot will be also be established in relation to in situ $CO_2$ eddy flux measurements and associated carbon budgets from available tower network observations (e.g., FLUXNET) within regionally dominant vegetation classes following established protocols (e.g., Heinsch et al. 2006; Kimball et al. 2009).

The fulfillment of the NEE requirement will be assessed by comparing SMAP L4_C NEE output with FLUXNET NEE estimates.

## D. Dedicated Post-Launch Field Campaigns

The purpose of the post-launch field campaigns is to provide critical information needed for the validation of the products. Each product identified a strategy for the validation in the preceding sections and whether field campaigns are required to carry out this strategy. This section presents a summary of coordinated efforts which answer these needs of each product.

Field experiments typically require considerable coordination between different groups, such as the project team, SDT working groups, government agencies, research institutions and universities. This imposes relatively long lead time for the planning of campaigns and may affect the timing of the campaign. At the same time, the field campaigns need to be concluded so that the collected data can be used in the calibration and validation of the data products in a constructive way. Moreover, there is also optimum seasonal timing to carry out soil moisture and freeze/thaw state field campaigns.

A field campaign dedicated to calibration and validation of SMAP soil moisture products is planned to be carried out in North America sometime after the completion of IOC, depending on the launch date.

Considering the launch date of early November 2014 (which would mean the end of IOC in early February 2015), the campaign could be carried out in the May to October timeframe in 2015 or 2016 to coincide with a favorable season for soil moisture validation. The location of the campaign is to be determined but it will be carried out over one or more of the soil moisture core validation sites in North America.

The airborne instrumentation will include at least an airborne L-band radar and radiometer; possibly PALS and UAVSAR. Post-launch field campaigns will require the rapid mapping of spatial domains on the scale of the SMAP products (up to 36 km) concurrent with satellite overpasses. In general, this will require coverage within a time window of 1 to 3 hours in order to minimize the effects of naturally occurring geophysical changes. In addition, several geographic domains will be required. These requirements make it critical that the airborne simulator be an efficient mapping instrument installed on an aircraft platform with higher speed and possibly altitude capabilities than have been available in pre-launch campaigns. Planning for this campaign will have to be coordinated with AirMOSS and possibly other concurrent projects, which utilize these airborne resources as well. Alternative resources should be identified for potential risk mitigation.

The aim of the campaign is to capture a range of soil moisture and vegetation conditions and this is accounted for in the timing and planning of the location of the campaign. One potential design is shown in Figure 70.



**Figure 70. Example of a possible Post-Launch SMAPVEX design.**

The in situ sampling needs to account for the different sensitivities of the radiometer and radar algorithms on different surface and vegetation components. Since the radar is more sensitive to these parameters, the requirements of the radar-based algorithms are driving the design.

### E. Satellite Data

#### 1) SMOS

ESA provides data from missions such as SMOS through an ongoing proposal process. The SMAP project has subscribed for the Level 1C product over land (L-band brightness temperature on Earth grid) and Level 2 soil moisture product with necessary ancillary data products through this process. The data is utilized to support algo-rithm pre-launch development, calibration and validation and preparation to post-launch calibration and validation activities.

#### 2) Aquarius

Data from Aquarius is publically available through NASA's DAACs.

#### 3) GCOM-W

JAXA has provided data from its missions to NASA in the past. At the present, there are ongoing discussions between NASA and JAXA that are specifically related to GCOM-W that include the AMSR-2 instrument. If these are not formalized by the time of the GCOM-W launch, the SMAP project will attempt to establish scientific collaboration directly in order to acquire soil moisture products. It is also possible that the current NASA AMSR-E program algorithms may be adapted for GCOM-W to continue this data stream.

#### 4) SAOCOM

SAOCOM will provide data to groups based upon a proposal process. CONAE released a pre-launch announcement of opportunity that the SMAP project responded to. When the post-launch announcement of opportunity is released, the SMAP project will submit a proposal for the acquisition of data to support Cal/Val.

#### 5) ASCAT

EUMETSAT Advanced Scatterometer (ASCAT) provides soil moisture index product based on C-band radar measurements. The data is available through the data portal of EUMETSAT.

#### 6) ALOS-2 PALSAR-2

PALSAR-2 will provide data to groups based upon a proposal process. JAXA released a pre-launch announcement of opportunity that SMAP team members responded to for the acquisition of data to support Cal/Val.

### References

Atlas, R., R. N. Hoffman, J. Ardizzone, M. Leidner, and J. C. Jusen, "A New Cross-Calibrated, Multi Ocean Surface Wind Product," *Proc. IEEE International Geoscience and Remote Sensing Symposium 2008*, Boston, MA, USA, July 6–11, 2008.

Baldocchi, D., "Breathing of the terrestrial biosphere: lessons learned from a global network of carbon dioxide flux measurement systems," *Austr. J. Bot.*, vol. 56, pp. 1–26, 2008.

Baldocchi, D., E. Falge, L. Gu, R. Olson, D. Holinger, S. Running, et al., "FLUXNET: A new tool to study the temporal and spatial variability of ecosystem-scale carbon dioxide, water vapor, and energy flux densities," *Bulletin of the American Meteorological Society*, vol. 82, pp. 2415–2434, 2001.

Bolten, J., W. T. Crow, X. Zhan, T. J. Jackson, and C. A. Reynolds, "Evaluating the Utility of Remotely Sensed Soil Moisture Retrievals for Operational Agricultural Drought Monitoring," *IEEE J. Selected Topics Applied Earth Obs. Remote Sens.*, vol. 3, no. 1, pp. 57–66, 2010.

Colliander, A., S. Chan, S. Kim, N. Das, S. Yueh, M. H. Cosh, R. Bindlish, T. J. Jackson, and E. Njoku, "Long-Term Analysis of PALS Soil Moisture Campaign Measurements for Global Soil Moisture Algorithm Development," *Remote Sensing of Environment*, 121, pp. 309–322, 2012.

Crow, W. T., A. A. Berg, M. H. Cosh, A. Loew, B. P. Mohanty, R. Panciera, P. de Rosnay, D. Ryu, and J. P. Walker, "Upscaling Sparse Ground-Based Soil Moisture Observations for the Validation of Coarse-Resolution Satellite Soil Moisture Products," *Rev. Geophys.*, vol. 50, RG2002, 2012. dx.doi.org/10.1029/2011RG000372

Crow, W. T., D. G. Miralles, and M. H. Cosh, "A quasi-global evaluation system for satellite-based surface soil moisture retrievals," *IEEE Trans. Geosci. Remote Sens.*, 48(6), pp. 2516–2527, 2010. dx.doi.org/10.1109/IGARSS.2008.4779051

Crow, W. T., R. D. Koster, R. H. Reichle, and H. O. Sharif, "Relevance of time-varying and time-invariant retrieval error sources on the utility of spaceborne soil moisture products" *Geophys. Res. Lett.*, vol. 32, no. 24, Art. no. L24405, 2005.

Dane, J. H. and C. Topp, *Methods of Soil Analysis. Part 4. Physical Methods*, Soil Science Society of America Book Series, vol. 5, 2002.

Dorigo, W. A., K. Scipal, R. Parinussa, Y. Liu, W. Wagner, R. de Jeu, and V. Naeimi, "Error Characterisation of Global Active and Passive Microwave Soil Moisture Datasets," *Hydrol. Earth Syst. Sci.*, 14, pp. 2605–2616, 2010.

Entekhabi, D., R. H. Reichle, W. T. Crow, and R. D. Koster, "Performance metrics for soil moisture retrievals and application requirements," *Journal of Hydrometeorology*, 11, pp. 832–840, 2010. dx.doi.org/10.1175/2010JHM1223.1

Heinsch, F. A., M. Zhao, S. W. Running, J. S. Kimball, R. R. Nemani, et al., "Evaluation of Remote Sensing Based Terrestrial Productivity From MODIS Using Region-al Tower Eddy Flux Network Observations," *IEEE Trans. Geosci. Rem. Sens.*, vol. 44, no. 7, pp. 1908–1925, 2006.

Hudson, D. and J. Peng, "SMAP Radiometer (minus reflector) Pre-Launch Calibration Plan," NASA Goddard Space Flight Center, September 8, 2010.

Jackson, T. J., M. Cosh, R. Bindlish, P. Starks, D. Bosch, M. Seyfried, D. Goodrich, S. Moran, and J. Du, "Validation of Advanced Microwave Scanning Radiometer Soil Moisture Products," *IEEE Trans. Geosci. Rem. Sens.*, vol. 48, no. 12, pp. 4256–4272, 2010.

Jackson, T. J., R. Bindlish, M. H. Cosh, T. Zhao, P. J. Starks, D. D. Bosch, M. Seyfried, M. S. Moran, D. C. Goodrich, Y. H. Kerr, and D. Leroux, "Validation of Soil Moisture and Ocean Salinity (SMOS) Soil Moisture Over Watershed Networks in the U.S.," *IEEE Trans. Geosci. Rem. Sens.*, vol. 50, no. 5, pp. 1530–1543, 2012.

Jackson, T., "SMAP Soil Moisture Overpass Time Considerations," SMAP Workshop Report, NASA, 2007.

Jones, L. A., J. S. Kimball, K. C. McDonald, S. K. Chan, E.G., Njoku, and W. C. Oechel, "Satellite Microwave Remote Sensing Of Boreal And Arctic Soil Temperatures from AMSR-E," *IEEE Trans. Geosci. Remote Sens.*, vol. 45, no. 7, pp. 2004–2018, 2007.

Kimball, J. S., L. A. Jones, K. Zhang, F. A. Heinsch, K. C. McDonald, and W. C. Oechel, "A Satellite Approach To Estimate Land-Atmosphere CO2 Exchange for Boreal And Arctic Biomes Using MODIS and AMSR-E," *IEEE Trans. on Geosci. Rem. Sens.*, vol. 47, no. 2, pp. 569–587, 2009.

Larson, K. M., J. J. Braun, E. E. Small, V. U. Zavorotny, E. D. Gutmann, and A. L. Bilich, "GPS Multipath and Its Relation to Near-Surface Soil Moisture Content," *IEEE J. Sel. Topics in Applied Earth Obs. Rem. Sens.*, vol. 3, no. 1, pp. 91–99, 2010.

Liu, J., X. Zhan, and T. J. Jackson, "Soil Moisture Retrieval from WindSat Using the Single Channel Algorithm Toward a Blended Global Soil Moisture Product from Multiple Microwave Sensors," *Proc. SPIE 2008*, vol. 7085, 2008.

Magagi, R., A. Berg, K. Goita, S. Belair, T. J. Jackson, B. Toth, A. Walker, H. McNairn, P. O'Neill, M. Moghaddam, I. Gherboudj, A. Colliander, M. H. Cosh, J. Belanger, M. Burgin, J. Fisher, S. Kim, L. Rousseau, N. Djamaï, J. Shang, and A. Merzouki, "A Canadian Experiment for Soil Moisture in 2010 (CanEX-SM10): Overview and Preliminary Results," *IEEE Trans. Geosci. Rem. Sens.*, 51, pp. 347–363, 2013.

McNairn, H., T. J. Jackson, G. Wiseman, S. Bélair, A. Berg, P. Bullock, A. Colliander, M. H. Cosh, S. Kim, R. Magagi, M. Moghaddam, J. R. Adams, S. Homayouni, E. Ojo, T. Rowlandson, J. Shang, K. Goïta, and M. Hosseini, "The Soil Moisture Active Passive Validation Experiment 2012 (SMAPVEX12): Pre-Launch Calibration and Validation of the SMAP Satellite," *IEEE Trans. Geosci. Rem. Sens.*, 2014.

Miralles, D. G., W. T. Crow, and M. H. Cosh, "A technique for estimating spatial sampling errors in coarse-scale soil moisture estimates derived from point-scale observations," *Journal of Hydrometeorology*, 11(6), pp. 1404–1410, 2010. dx.doi.org/10.1175/2010JHM1285.1

Panciera, R., J. Walker, T. J. Jackson, D. Ryu, D. Gray, A. Monerris, H. Yardley, M. Tanese, C. Rudiger, X. Wu, Y. Gao, and J. Hacker, " The Soil Moisture Active Passive Experiments (SMAPEx): Towards Soil Moisture Retrieval from the SMAP Mission, *IEEE Trans. Geosci. Rem. Sens.*, 2014.

Peng, J. and C. S. Ruf, "Calibration Method for Fully Polarimetric Microwave Radiometers Using the Correlated Noise Calibration Standard," *IEEE Trans. Geosci. Rem. Sens.*, vol. 46, no. 10, October 2008.

Reichle, R. et al., "Skill Metrics for Validation of SMAP Data Products," SMAP SDT Memo, April 13, 2010.

Reichle, R. H., R. D. Koster, P. Liu, S. P. P. Mahanama, E. G. Njoku, and M. Owe, "Comparison and Assimilation of Global Soil Moisture Retrievals from AMSR-E and SMMR," *J. Geophys. Res.*, vol. 112, D09108, 2007.

Running, S. R., D. D. Baldocchi, D. P. Turner, S. T. Gower, P. S. Bakwin, and K. A. Hibbard, "A global terrestrial monitoring network integrating tower fluxes, flask sampling, ecosystem modeling and EOS satellite data," *Remote Sensing of Environment*, vol. 70, pp. 108–128, 1999.

Schaefer, G. L., M. H. Cosh, and T. J. Jackson, "The USDA Natural Resources Conservation Service Soil Climate Analysis Network (SCAN)," *Journal of Atmospheric and Oceanic Technology*, vol. 24, pp. 2073–2077, 2007.

Scipal, K., T. Holmes, R. de Jeu, V. Naeimi, W. Wagner, "A Possible Solution for the Problem of Estimating the Error Structure of Global Soil Moisture Dataset," *Geophys. Res. Lett.*, vol. 35, 2008.

Steele-Dunne, S. C., M. M. Rutten, D. M. Krzeminska, M. Hausner, S. W. Tyler, J. Selker, T. A. Bogaard, and N. C. van de Giesen, "Feasibility of soil moisture estimation using passive distributed temperature sensing," *Water Resource Research*, vol. 46, no. 3, 2010.

Turner, D. P., W. D. Ritts, W. B. Cohen, S. T. Gower, S. W. Running, M. Zhao, M. H. Costa, A. A. Kirschbaum, J. M. Ham, S. R. Saleska, and D. E. Ahl., "Evaluation of MODIS NPP and GPP products across multiple biomes," *Remote Sensing of Environment*, vol. 102, pp. 282–292, 2006.

West, R. et al., "Algorithm Theoretical Basis Document (ATBD): L1B_S0_LoRes and L1C_S0_HiRes," Initial Release, v.1, October 1, 2012. Available at http://smap.jpl.nasa.gov/science/dataproducts/ATBD/

Yueh, S., "Estimates of Faraday Rotation with Passive Microwave Polarimetry for Microwave Remote Sensing of Earth Surfaces," *IEEE Trans. Geosci. Rem. Sens.*, vol. 38, no. 5, September 2000.

# 8. The NASA Soil Moisture Active Passive (SMAP) Applications Program

## I. Introduction

The purpose of this chapter is

- To provide the scope and activities of the SMAP Applications Program; and

- To offer guidance to other missions initiating pre-launch applications programs.

The document is organized to provide an introductory SMAP mission and science overview in the context of SMAP applications (Sections II and III), followed by a SMAP Applications Program overview (Section IV). Pre-launch activities and post-launch plans are summarized in Sections V and VI. The document concludes with a summary of the deliverables and timeline for SMAP Applications Program activities in relation to other SMAP mission milestones (Section VII).

### A. Applications Program Scope and Objectives

The SMAP Applications Program was initiated in 2007, seven years before the scheduled launch of SMAP in late 2014. The overall goal of the SMAP Applications Program is to engage SMAP end users and build broad support for SMAP applications through a transparent and inclusive process. The sub-goals of the program are to:

- Develop a community of users and decision makers that understand SMAP capabilities and are interested in using SMAP products in their applications (SMAP Community of Practice);

- Reach out to users that are unfamiliar with SMAP capabilities but have the potential to benefit from SMAP products in their applications (SMAP Community of Potential);

- Provide information about SMAP applications to the broad science community to build support for SMAP applications (SMAP Community of Support);

- Facilitate feedback between SMAP user communities and the SMAP Mission and Science Definition Teams; and

- Identify Early Adopters who will partner with SMAP to optimize their use of SMAP products before launch as part of SMAP testbed and SMAP calibration/validation activities.

Related to the last bullet, the SMAP Early Adopter Program was developed in 2010 to facilitate feedback on SMAP products pre-launch, and accelerate the use of SMAP products post-launch. This program provided specific non-financial support to Early Adopters who committed to engage in pre-launch applied research with quantitative metrics.

### B. Definitions

There are a number of terms that will be used throughout this chapter. SMAP — the acronym — is defined as Soil Moisture Active Passive. The SMAP Project is the entity formed to develop, launch, and operate the SMAP Observatory, and the SMAP Mission is the broad name given to everything related to SMAP. The SMAP Science Definition Team (SDT) functioned from FY2008 through FY2013 to advise the Project, and the SMAP Science Team (ST) will function starting October 1, 2013, to provide calibration/validation support and research guidance.

Specific definitions are also used in the description of the SMAP Applications Program. Applications are defined as innovative uses of SMAP data products in decision-making activities for societal benefit. Applied research will provide fundamental knowledge of how SMAP data products can be scaled and integrated into users' policy, business and management activities to improve decision-making efforts. Users include individuals or groups in the public or private sectors with national or international applications at local to global scales. Early Adopters are a subset of users who have a direct or clearly defined need for SMAP-like soil moisture or freeze/thaw data, and who are planning to apply their own resources (funding, personnel, facilities, etc.) to demonstrate the utility of SMAP data for their particular system or model.

The SMAP Applications Program has hosted a number of workshops, tutorials, focus sessions, and town halls. These activities had different purposes and formats, resulting in a set of formal general definitions for events. SMAP Applications Workshops provide an update of the mission and its progress to the community of interest and are set up to exchange information about SMAP soil moisture and freeze/thaw state products on a broad scale. These workshops, which are organized annually or every 2 years, seek to engage a broad segment of the diverse SMAP user community and provide feedback to the SMAP mission about SMAP product applications. SMAP Applications Focus Sessions provide a forum for a well-defined user group to receive specific support and information on the utility of SMAP soil moisture and freeze/thaw state products for thematic mission objectives. Focus sessions are concentrated one-day events focused on a thematic or disciplinary community. NASA Applications Tutorials are organized to discuss products and applications of multiple NASA decadal survey missions. Tutorials are hosted by an end user group but are organized and managed by the decadal mission or the

SMAP Applications Team. SMAP Applications Town Halls are gatherings organized by the SMAP Applications Team to inform users of SMAP products and discuss applications in an informal setting. Town Halls are associated with large technical meetings like the American Geophysical Union (AGU), American Meteorological Society (AMS), and the International Geosciences and Remote Sensing Symposium (IGARSS) annual conferences.

## II. SMAP Mission and Science Overview

SMAP is one of four first-tier missions recommended in the Decadal Survey report of the National Research Council's Committee on Earth Science and Applications from Space (2007). The Decadal Survey was composed of six disciplinary panels. Five of the six panels cited applications and applied science uses for SMAP data (Table 33). This broad and multi-disciplinary recognition of the value of soil moisture and freeze/thaw data resulted in the placing of SMAP in the first tier of priority Earth science missions.

The SMAP Science Definition Team (SDT) defined five major science goals for driving the mission measurement requirements: 1) estimate global water and energy fluxes at the land surface; 2) extend weather forecast skill; 3) develop flood and drought predictions; 4) quantify net carbon flux in boreal landscapes; and 5) link terrestrial water, energy and carbon cycle processes. With these science drivers, the SDT identified applications that were also major components of the mission (Section III). These driving science and the priority application goals for the project were the basis for a set of common measurement requirements, leading to the SMAP science data products (see Chapter 2, Table 4).

## III. SMAP Applications

The application areas directly addressed by SMAP measurements of soil moisture and freeze/thaw state, acquired globally and at high spatial and temporal resolutions, are (Entekhabi et al., 2010):

### 1) Weather and Climate Forecasting



Soil moisture variations affect the evolution of weather and climate over continental regions. Initialization of numerical weather prediction and seasonal climate models with accurate soil moisture information enhances their prediction skills and extends their skillful lead times. Information about saturated soils and inundated wetlands can improve estimates of terrestrial methane ($CH_4$) emission, which is the third most important greenhouse gas after water vapor and carbon dioxide. Information about freeze and thaw is used to determine the distribution of frozen ground to improve the assessment of land surface conditions in global forecasting systems. Improved seasonal climate predictions will benefit climate-sensitive socioeconomic activities, including water management, agriculture, fire, flood, and drought hazards monitoring.

Table 33. NRC Decadal Survey Panel citation of SMAP applications.

| Decadal Survey Panel | Cited SMAP Applications |
|---|---|
| Water Resources and Hydrological Cycle | 1. Floods and Drought Forecasts |
| | 2. Available Water Resources Assessment |
| | 3. Link Terrestrial Water, Energy, and Carbon Cycles |
| Climate Variability and Change | 4. Longer-Term and More Reliable Atmospheric Forecasts |
| Weather Science and Applications | 5. Longer-Term and More Reliable Atmospheric Forecasts |
| Human Health and Security | 6. Heat Stress and Drought |
| | 7. Vector-Borne and Water-Borne Infectious Disease |
| Land Use, Ecosystems, and Biodiversity | 8. Ecosystem Response (Variability and Change) |
| | 9. Agricultural and Ecosystem Productivity |
| | 10. Wildfires |
| | 11. Mineral Dust Production |

## 2) Droughts and Wildfires



Soil moisture strongly affects plant growth and hence agricultural productivity, especially during conditions of water shortage and drought. Currently, there is no global in situ network for soil moisture monitoring. Global estimates of soil moisture and plant water stress must be derived from models. These model predictions (and hence drought monitoring) can be greatly enhanced through assimilation of space-based soil moisture observations. Improvements in the ability to monitor and forecast agricultural drought (i.e., the lack of root zone soil moisture) will improve famine early warning in the most food-insecure countries in the world. Soil moisture information can be used to predict wildfires, determine prescribed burning conditions, and estimate smoldering combustion potential of organic soils. Improvements in wildfire information with SMAP soil moisture products can provide more useful and accurate data on toxic air-quality events and smoke white-outs (thus increasing transportation safety) and can inform prescribed fire activities (increasing efficiency).

## 3) Floods and Landslides



Soil moisture is a key variable in water-related natural hazards, including floods and landslides. High-resolution observations of soil moisture and landscape freeze/thaw status will lead to improved flood forecasts, especially for intermediate to large watersheds where most flood damage occurs. Surface soil moisture state is key to the partitioning of precipitation into infiltration and runoff, and thus is one of the major pieces of information which drives flood prediction modeling. Similarly, soil moisture in mountainous areas is one of the most important determinants of landslides. In cold land regions, the timing of thawing (which can be derived from satellite radar measurements) is coincident with the onset of seasonal snowmelt, soil

thaw, and ice breakup on large rivers and lakes. Hydrologic forecast systems initialized with mapped high-resolution soil moisture and freeze/thaw fields will therefore open up new capabilities in operational flood forecasting and flash flood analysis. In turn, this will improve the response of government agencies and emergency managers to a full range of emergencies and disasters, and potentially provide insurance brokers with an up-to-date indicator of the likelihood of flooding, landslides, droughts, and wildfires in risk models related to business decisions.

## 4) Agricultural Productivity



SMAP will provide information on water availability and environmental stress for estimating plant productivity and potential yield. The availability of direct observations of soil moisture status and the timing and extent of potential frost damage from SMAP will enable significant improvements in operational crop productivity and water stress information systems by providing realistic soil moisture and freeze/thaw observations as inputs for agricultural prediction models. Improved models will provide crucial information for decision-makers managing water and other resources, especially in data-sparse regions. Even without simulation models, farmers can also use soil moisture and freeze/thaw information directly as a proxy for field readiness (i.e., determining when the soil is dry enough for driving heavy machinery). At the global scale, a better grasp of the impact of agricultural drought on crop yield provides better crop supply and demand information for use by producers, commodity markets, traders, and policy makers. Forecasts of the impact of climate fluctuations on crop yields with ongoing measurements of soil moisture and freeze/thaw will also improve management of agriculturally important pests and disease in developing countries.

## 5) Human Health

Improved seasonal soil moisture forecasts using SMAP data will directly benefit famine early warning systems, particularly in sub-Saharan Africa and South Asia, where hunger remains a major human health factor and the population harvests its food from rain-fed agriculture in highly monsoonal (seasonal) conditions. In the temperate and extra-tropical latitudes, freeze/thaw measurements from SMAP will benefit environmental risk models and early warning systems related to the potential expansion of many disease vectors that are constrained by the timing and duration of seasonal frozen temperatures. SMAP will also benefit the emerging field of landscape epidemiology (aimed at identifying and mapping vector habitats for human diseases such as malaria) where direct observations of soil moisture and freeze/thaw status can provide valuable information on vector population dynamics. Soil moisture in the upper layer has a direct effect on dust generation and air quality in desert and arid environments. Indirect benefits will also be realized as SMAP data will enable better weather forecasts that lead to improved predictions of heat stress and virus spreading rates. Better flood forecasts will lead to improved disaster preparation and response. Soil moisture provides more accurate information on the state of saturated soils that impacts stream flow, nutrient loading, and turbidity; and these both lead to better management of urban water supply and quality.

*6) National Security*



Information on surface soil moisture and freeze/thaw is critical to evaluating ground trafficability and mobility. The integration of soil moisture has been determined to be the single most critical parameter in state-of-the-ground models. Soil moisture and freeze/thaw data are also key to a broad array of military and civil works capabilities including road and bridge building, dam and levee assessment/construction, and tactical decision aid design and development. Weather models need maps of the soil moisture and freeze/thaw variables to initialize forecasts for low-level fog, aviation density altitude, and dust generation. SMAP soil moisture and freeze/thaw information exceed current capability in terms of resolution, sensitivity, coverage, and sensing depth. Furthermore, radar obser-

vations over oceans and water bodies yield information on ice cover at high resolution and regardless of illumination.

## IV. SMAP Applications Program Overview

The SMAP Applications Program was initiated to integrate applications needs into mission planning as encouraged by the U. S. Congress, the National Research Council, and the NASA Earth Science Division. Roles and responsibilities evolved as the Program developed and as needs became apparent. The SMAP Applications Program follows an Applications Plan that is updated continuously as the SMAP mission proceeds through its development and operational phases.

### A. Requirements

The SMAP Applications Program requirements are outlined by the NASA Authorization Act of 2005 (P.L. 109-155, Sec. 313), National Research Council Decadal Survey Report on "Earth Science and Applications from Space," the NASA Earth Sciences Division "Applied Sciences Program Strategic Plan," and the Program-Level Requirements for the SMAP Project, where:

- NASA Authorization Act of 2005 (P.L. 109-155), SEC. 313 entitled "Pilot projects to encourage public sector applications" states "The Administrator shall establish a program of grants for competitively awarded pilot projects to explore the integrated use of sources of remote sensing and other geospatial information to address State, local, regional, and tribal agency needs. In Sec. 314(a), "The Administrator shall establish an advisory committee, consisting of individuals with appropriate expertise in State, local, regional, and tribal agencies, the university research community, and the remote sensing and other geospatial information industries, to monitor the program established under section 313."

- National Research Council Decadal Survey Report "Earth Science and Applications from Space" Chapter 1 states "A fundamental challenge for the coming decade is to ensure that established societal needs help to guide scientific priorities more effectively and that emerging scientific knowledge is actively applied to obtain societal benefits. New observations and analyses … broadened community participation and improved means for dissemination and use of information are all required." It further states that "... addressing the environmental challenges will not be possible without increased collaboration between Earth scientists and researchers in other disciplines including the social, behavioral, and economic sciences and policy experts. It is necessary now to

build on the paradigm of Earth system science and strengthen its dual role of science and applications. This duality has always been an element of Earth science, but it must be leveraged more effectively than in the past..."

- NASA Earth Sciences Division "Applied Sciences Program Strategic Plan" states the goal to "evaluate the potential for current and planned NASA missions to meet societal needs through applied sciences participation in mission science teams" and provide Mission applications support to "integrate applications needs into mission planning."

- The SMAP Project "Program-Level Requirements for the SMAP Project" states in section 4.5.2 that "Beginning in Phase C, the SMAP Project shall organize and host a SMAP data product applications workshop annually. The workshop will share information on the SMAP science data applications and define potential applications that can be supported within existing SMAP data requirements. Results will be provided to the SMAP science team and at other SMAP workshops and meetings."

## B. Roles and Responsibilities

The SMAP Applications Program is a group effort with hundreds of partners ranging from users to NASA managers (Table 34). The SMAP Applications Team is a smaller group that works closely to plan and prioritize SMAP applications activities. At the time of this writing, the SMAP Applications Team is composed of the SMAP Applications Coordinators (Molly Brown and Vanessa Escobar), SMAP Applications Working Group Chair (Susan Moran), SMAP Science Definition Team Leader (Dara Entekhabi), SMAP Project Scientist (Simon Yueh / Eni Njoku), SMAP Deputy Project Scientist (Peggy O'Neill), SMAP Project Manager (Kent Kellogg), SMAP Science Data Systems Representative (Barry Weiss), NSIDC DAAC Deputy Manager (Amanda Leon), NASA Headquarters Applied Sciences Program Manager (Brad Doorn), and NASA Headquarters SMAP Program Scientist (Jared Entin).

## C. Applications Plan

As stated earlier, the goal of the SMAP Applications Program is to engage SMAP end users and build broad support for SMAP applications through a transparent and

**Table 34.  Leaders, partners, and roles in the SMAP Applications Program.**

| Title | Person(s)* | Role |
|---|---|---|
| SMAP Applications Working Group (AppWG) | Over 300 members and growing | SMAP applications development and feedback to the SMAP mission |
| SMAP Applications Working Group (AppWG), Chair | Susan Moran | Serve as liaison between SMAP SDT and SMAP AppWG |
| SMAP Applications Coordinator | Molly Brown and Vanessa Escobar | Develop and implement SMAP Applications Plan; plan and conduct workshops, focus sessions, and tutorials |
| SMAP Applications Team | See list in Section IV.B | Plan and prioritize SMAP applications activities |
| SMAP Early Adopters | 30+ Users (Table 36) | Partner with SDT for applied research |
| SMAP Science Team (ST) | Entekhabi et al.** | Partner with Early Adopters for applied research |
| SMAP Cal/Val Working Group, Chair | Tom Jackson | Coordinate with AppWG |
| SMAP Algorithms Working Group, Chair | Mahta Moghaddam | Coordinate with AppWG |
| SMAP Mission Project Manager | Kent Kellogg | Programmatic Support |
| NASA Applied Science Program, Program Manager | Brad Doorn | Integrate applications needs into mission planning |
| NASA Headquarters, SMAP Program Scientist | Jared Entin | Programmatic Support |
| NASA Flight Program, Earth Science Division, Assoc. Director | Steve Volz | Coordination of Decadal Survey mission applications activities |

*Persons associated with titles and roles are those in place at the time of this writing.

**http://smap.jpl.nasa.gov/people/sciencepeople/

inclusive process. Toward this goal, the SMAP mission formed an open-community SMAP Applications Working Group (AppWG) and held the 1st SMAP Applications Workshop on September 9–10, 2009. Presentations and discussions at that workshop provided the basis for development of the SMAP Applications Plan. The SMAP Applications Plan is a living document that will be updated continuously as the SMAP mission proceeds through its development and operational phases (http://smap.jpl. nasa.gov/files/smap2/SMAP_Apps_Plan_120706.pdf). It outlines the goals, strategic partners, implementation strategy, and evaluation plan for the SMAP Applications Program. The plan is accompanied by annual work plans that are developed in collaboration with the Applications Team and implemented by the Applications Coordinators.

## V. Pre-Launch Activities

The pre-launch activities of the SMAP Applications Program are a pioneering effort that has redefined how to engage users during the development of a NASA mission. The next sections describe key elements of the SMAP Applications Program, including the SMAP Applications Working Group (AppWG), the SMAP Early Adopter Program, interactions with other components of the SMAP Mission, and inter-mission collaboration.

### A. Applications Working Group (AppWG)

The open-community SMAP AppWG was initiated in 2008. It is chaired by a Science Definition Team member and populated through networking and invitation. As SMAP Applications workshops were conducted, the attendees were notified that they would be added to the AppWG. Members have also been added at their request through registration on the SMAP website at http://smap. jpl.nasa.gov/science/wgroups/applicWG/. Through these avenues, the SMAP AppWG membership has increased from 0 in Jan. 2009 to 150 by Aug. 2010, to 270 by June 2011, and to its current number of over 350 members.

Two key roles for members of the SMAP AppWG are 1) SMAP application development, and 2) feedback to the SMAP mission. The objectives of the AppWG are to:

- Assess current applications benefits and requirements for SMAP products;

- Develop a community of end users that understand SMAP capabilities and are interested in using SMAP products in their application;

- Foster Early Adopters who can work with the SMAP project during the pre-launch period, particularly to assess impacts on their applications;

- Provide information about SMAP and its products to the broad user and science community; and

- Provide guidance to future NASA solicitation processes.

Interaction between the mission and the AppWG has been largely through regular emails, Applications Workshops, and multiple Focus Sessions and Town Halls. All SMAP Applications activities are documented with reports that are approved by the Applications Team, and subsequently posted on the SMAP website. The report is meant to engage with those who were not able to attend the meeting or learn about the event after it has occurred. Through these activities (Table 35), potential applications were identified (http://smap.jpl.nasa.gov/files/smap2/ Workshop_Report_100309_final.pdf); user feedback was provided to the mission on agriculture, climate, hydrology, disasters, and public health (http://smap.jpl.nasa.gov/ files/smap2/Workshop_Report_final_2.pdf; Escobar et al. 2011); a Memorandum of Understanding (MOU) was drafted between NASA and USDA; SMAP Early Adopters were engaged and Summaries of Activities (SOAs) signed (section V.B); interaction between applications and the SMAP Cal/Val and Algorithm Development teams and the Distributed Active Archive Center (DAAC) was defined (section V.C); and joint-mission tutorials were planned (section V.D).

A study based on questionnaires was conducted in order to appropriately target the activities occurring in the years before launch (Brown and Escobar 2013). The objective of this study was to solicit data requirements, accuracy needs and current understanding of the SMAP mission from the potential user community. The study showed areas where soil moisture research is highly valued and thematically exclusive, thus bringing awareness and future actions to broaden the mission's reach before launch. It also demonstrated that the spatio-temporal requirements of the community for soil moisture data will be met by SMAP, although they vary by application and organization.

### B. Early Adopter Program

The Early Adopters are a subset of the SMAP AppWG. As stated earlier, the goal of the SMAP Early Adopter Program is to provide specific support to Early Adopters in pre-launch applied research to facilitate feedback on SMAP products pre-launch, and accelerate the use of SMAP products post-launch. In a written, signed Summary of Activities (SOA), Early Adopters agree to:

- Engage in pre-launch research that will enable integration of SMAP data after launch in their application;

Table 35. SMAP workshops, tutorials, focus sessions, and town halls.

| Event | Description | Outcome |
|---|---|---|
| 1st Applications Workshop at NOAA, Sept. 2009 | Defining the role of the SMAP AppWG, the DAAC and engaging the user community | Potential applications identified* |
| Town Hall at GEOSS Meeting in Chile, 2010 | Discussion with the Chilean Space Agency and University of Las Serenas | Interest in joining with SMAP for grape/wine production in Santiago, Chile, participation in UAVSAR field campaign |
| 2nd Applications Workshop at USDA, October 2011 | Understanding who the users are, how they use data, and what their data needs are; presentations by 7 Early Adopters | Feedback from the thematic groups: agriculture, climate, hydrology, disaster, and public health* |
| SMAP/USDA Focus Session at USDA, October 2011 | Presentations by USDA subagencies on research and applications related to soil moisture and freeze/thaw information | An MOU signed between NASA and USDA; 3 Early Adopters SOAs |
| Focus Session for Dept. of Defense, Tucson, 2011 | Discussion of SMAP applications with diverse DoD community | Engagement in the Early Adopter Program; 2 Early Adopter SOAs |
| Town Hall at World Water Forum in France, 2011 | Panel discussion about SMAP applications in hydrology | Early engagement of international users for transboundary water issues |
| Focus Session at Palo Verde Nuclear Power Plant, Arizona, 2012 | Use SMAP with other environmental datasets for emergency decision making | Emergency operation product development |
| Focus Session for Urban Modeling Community at ASU, Arizona, 2012 | Understanding how SMAP data combine with urban models | Joining AppWG and using SMAP-like data in water budget/policy modeling |
| Town Hall at IGARSS in Munich, Germany, 2012 | Pre-launch analysis of the SMAP mission in the user community | Planned a Joint Mission Tutorial between SMOS and SMAP |
| 1st Joint Mission Tutorial, SMAP/ICESat-2, at ASF, Sept. 2012 | Focus on SMAP freeze/thaw and connection with ICESat-2 altimetry | New collaborative products and data formatting approaches** |
| 2nd Joint Mission Tutorial, SMAP/GRACE/GPM/SWOT at USGS, October 2012 | Explore collaborative opportunities for use of SMAP, GPM, GRACE-FO and SWOT data | New collaborative products and data formatting approaches** |
| Applications Workshop on Health at CDC, January 2014 | Discussion of soil moisture data impacts on health and health related applications | TBD |
| 3rd Joint Mission Tutorial, SMAP/SMOS Tutorial at AMS Meeting, February 2014 | Discuss continuity of soil moisture data (from SMOS to SMAP) for Operational Numerical Weather Prediction | TBD |
| 3rd Applications Workshop, Boulder, CO, April 2014 | Focusing on results of Early Adopter research | TBD |
| Focus sessions on Health and DoD, Spring 2014 | Detailed follow-up to thematic discussions from previous meetings | TBD |
| 4th Applications Workshop, 2016 | Discussion of the uses of SMAP data and the value of SMAP pre-launch applications effort | TBD |

*Full reports available at http://smap.jpl.nasa.gov/science/wgroups/applicWG/appsWkshp/

**Escobar (2013).

- Complete the project with quantitative metrics prior to launch;

- Join the SMAP Applications Team to participate in discussions of SMAP mission data products related to application needs; and

- Participate in the implementation of the SMAP Applications Plan by taking lead roles in SMAP applications research, meetings, workshops, and related activities.

In turn, the SMAP Project agrees to:

- Incorporate the Early Adopter contributions into the SMAP Applications Plan;

- Provide Early Adopters with simulated SMAP data products via the SMAP Science Data System (SDS) Testbed; and/or

- Provide Early Adopters with planned pre-launch calibration and validation (cal/val) data from SMAP field campaigns, modeling, and synergistic studies.

The Early Adopter nomination and selection process begins with the request for nomination (RFN) made to the SMAP AppWG, posted on the SMAP website, and sent to relevant list servers. The first RFN was scheduled to follow the establishment of the SMAP AppWG at the 1st SMAP Applications Workshop. Subsequent announcements were made annually. After two announcements, an open request for nomination was instituted, accepting nominations at any time with an ad hoc review and selection by the Applications Team.

A "SMAP Point of Contact" associated with the SMAP Mission was assigned to each new Early Adopter to help the Early Adopters get access to and resolve issues with SMAP pre-launch datasets; to facilitate their research and receive feedback to the SMAP project on research metrics; and to report on Early Adopter successes, challenges and progress during SMAP SDT meetings.

Twenty-one Early Adopters have been selected to date (Table 36, updates at http://smap.jpl.nasa.gov/files/smap2/All%20EA%20table.pdf). Interaction is facilitated through quarterly conference calls with all Early Adopters, Project Scientists, and the SMAP SDT. The applied research underway by Early Adopters provides fundamental knowledge of how SMAP data products can be scaled and integrated into users' policy, business, and management activities to improve decision-making efforts (some examples on page 155–156). A Special Collection of J. of Hydrometeorology is planned to report pre-launch

applications research by Early Adopters and other SMAP users, to be published at the time of launch.

## C. Interaction with SMAP Cal/Val, Algorithm Development and the SMAP DAACs

SMAP is the first NASA mission to promote pre-launch applied research by making simulated products and Cal/Val data available to users through a NASA DAAC before launch. This has required careful coordination between the SMAP Cal/Val and Algorithm Working Groups and the DAACs. Early in project planning, NASA Headquarters selected the National Snow and Ice Data Center (NSIDC) and the Alaska Satellite Facility (ASF) DAACs to be responsible for SMAP products and other mission data.

In the Early Adopter Program, users are offered access to simulated SMAP data products generated pre-launch by algorithm teams and observing system simulation experiments conducted on the SMAP Science Data System (SDS) Testbed. The most reasonable way to provide Early Adopters with these data is through the DAAC. The DAAC's mandate is to provide products after launch, yet for the SMAP Applications Program, the NSIDC DAAC is now providing data to select users before launch. Recently, the NASA Applied Sciences Advisory Group (ASAG) suggested to the NASA Earth Science Subcommittee (memo dated 25 Nov. 2012) that "the responsibilities of the DAACs be broadened to include providing access to pre-launch test data for applications research supporting mission development."

To clarify the process of pre- and post-launch data access, a policy has been outlined by the SMAP Project to define data categories and data user categories for providing access to pre-launch and post-launch SMAP data via the NSIDC and ASF DAACs. A preliminary data access matrix is currently under review.

## D. Inter-Mission Collaboration

The NRC Decadal Survey recommended 15 new space missions for NASA (including one joint mission with NOAA) and three missions for NOAA (including the one joint mission). A goal of the SMAP Applications Program is to coordinate SMAP applications with other planned NASA and NOAA Decadal Survey Missions (http://www.nap.edu/catalog.php?record_id=11820). This has been accomplished through SMAP Joint Mission Tutorials (Table 35). These discussions resulted in several new collaborations including a sea-ice product and a groundwater recharge product, shared datasets, and more.

Escobar (2013) noted that "Joint mission tutorials … are important to NASA as well as to end users. NASA provides huge amounts of remotely sensed data for Earth

science; getting these data into the hands of those who can make the most of them to address practical applications that impact society requires engagement and interaction with end users. To ensure that NASA maximizes the impact of its data, it is necessary for users with diverse perspectives to use these data. Leveraging the pool of information that NASA has available is important; working to achieve this goal before missions are launched increases the potential for significant use in a timely fashion after data are made available."

## Early Adopter Pre-Launch Research

*Example:* EFFECT OF SOIL MOISTURE ON DUST EMISSION

Soil moisture is a dynamic variable that has a critical impact on the dust emission mechanism. AERONET aerosol optical depth (AOT870) data were correlated to SMOS soil moisture data collected from 2010 to 2011 over the Cinzana dust source region (south Sahel). The results show that as the SMOS soil moisture increases, the AERONET AOT decreases up to a threshold moisture content above which no dust emission takes place. The threshold moisture content seems to be dependent on the climatic change over the dust source area. The incorporation of the soil moisture parameter in estimating the AOT would improve its estimation.
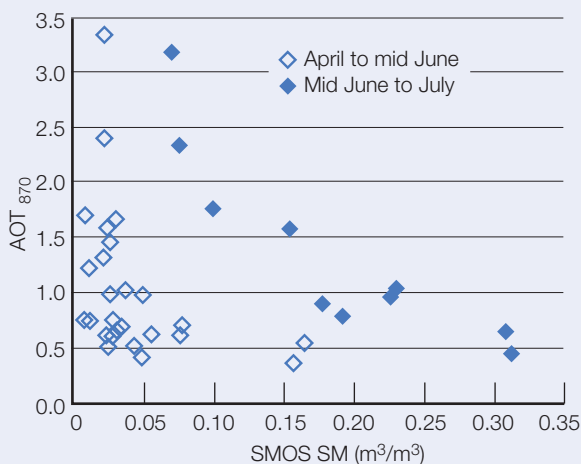


*Example:* NUMERICAL WEATHER PREDICTION

Soil moisture is a very important variable in numerical weather prediction systems. For drier soils, cooling caused by evaporation is generally limited, leading to increased warming and mixing in the atmospheric boundary layer. This directly affects near-surface air humidity, air pollutants, and production of clouds and precipitation. This figure illustrates the positive impact of soil moisture initial conditions on numerical weather predictions in 2001 in the Canadian Meteorological Centre (Bélair et al. 2003). The new system with improved soil moisture initial conditions (blue lines) shows decreased biases for 24–48h precipitation accumulations compared to the control (magenta lines).
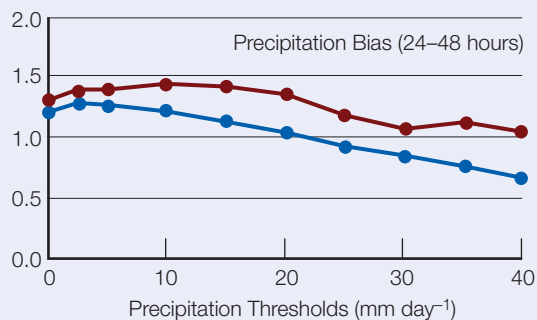


*Example:* GLOBAL INSURANCE and RE-INSURANCE

Willis Global Analytics is merging satellite data from NASA into existing risk identification and analysis systems for insurance and reinsurance, engaging end users to enhance decision making with SMAP products.

*Example:* NATIONAL SOIL MOISTURE MONITORING

The USDA National Agricultural Statistical Service (NASS) has launched a web-based U.S. crop vegetation condition assessment and monitoring application: VegScape (http://nassgeodata.gmu.edu/VegScape/). This web-based application has been designed to be a platform for accessing, visualizing, assessing and disseminating crop soil moisture condition derivative data products produced using SMAP data.

*Example:* GLOBAL NEAR-REAL-TIME MONITORING OF SOIL MOISTURE

Operational monitoring of active and passive data gives information on systematic differences between model and satellite observations.

### Example: CROP YIELD MODELING

Agricultural models have been developed to predict the yield of various crops at field and regional scales. One key input of the agricultural models is soil moisture. The conceptual diagram relates variation in regional domain-averaged soil moisture to variation in total crop yield. Statistical analysis would lead to the development of probability distributions of crop yield as a transformation of the probability distribution of domain averaged soil moisture at the beginning of the growing season.
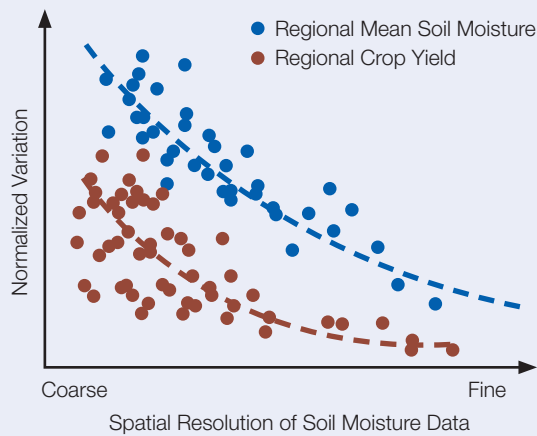


### Example: NUMERICAL WEATHER PREDICTION

The NASA Short-term Prediction Research and Transition (SPoRT) Center is implementing the assimilation of SMOS into the Weather Research and Forecasting numerical weather prediction (NWP) model through coupling with the Land Information System to 1) investigate the impact of soil moisture observations on NWP models, and 2) understand the mechanics

needed to assimilate soil moisture from the upcoming SMAP mission. By assimilating soil moisture observations, modelers can improve a land surface model's ability to simulate evapotranspiration and latent and sensible heating at the surface, important inputs to NWP models. In addition, knowledge of the soil moisture helps calculate surface emissivity, improving the utilization of satellite observations of atmospheric temperature and water vapor within the data assimilation system, further improving weather forecasts.

### Example: AGRICULTURAL DROUGHT

Areas of the world where assimilation of AMSR-E surface soil moisture retrievals significantly impacts the sampled cross-correlation between soil moisture anomalies for month i and NDVI anomalies for month $i$-1. As a result, red areas correspond to regions where the availability of satellite-based surface soil moisture retrievals significantly improves our ability to forecast agricultural drought using off-line water balance modeling. Assimilation model is the standard USDA Foreign Agricultural Service, 2-Layer Palmer water balance model and plotted values are sigma-levels of statistical significance for changes in cross-correlation relative to a model-only baseline (Bolten et al., 2013).

### Example: VEHICLE MOBILITY

The DoD plans to use SMAP to improve ground vehicle mobility predictions. In a scenario in which a unit wants to assess its river crossing capability during a flood event, vehicle mobility is limited by bank geometry, water depth and velocity, and soil conditions. Soil moisture is used both in the soil strength model and in the flood model that determines water depth and velocity. SMAP soil moisture estimates will provide a greater confidence level in these assessments.

Table 36. SMAP Early Adopters, SMAP project contacts, and applied research topics. Many Early Adopters cross multiple applications (updates at http://smap.jpl.nasa.gov/science/wgroups/applicWG/EarlyAdopters/).

| Early Adopter PI and Institution | Applied Research Topic |
|---|---|
| **Weather and Climate Forecasting** | |
| Stephane Bélair, Meteorological Research Division, Environment Canada (EC) | Assimilation and impact evaluation of observations from the SMAP mission in Environment Canada's Environmental Prediction Systems |
| Lars Isaksen and Patricia de Rosnay, European Centre for Medium-Range Weather Forecasts (ECMWF) | Monitoring SMAP soil moisture and brightness temperature at ECMWF |
| Xiwu Zhan, Michael Ek, John Simko, and Weizhong Zheng, NOAA National Centers for Environmental Prediction (NCEP), NOAA National Environmental Satellite Data and Information Service (NOAA-NESDIS) | Transition of NASA SMAP research products to NOAA operational numerical weather and seasonal climate predictions and research hydrological forecasts |
| Michael Ek, Marouane Temimi, Xiwu Zhan, and Weizhong Zheng, NOAA National Centers for Environmental Prediction (NCEP), NOAA National Environmental Satellite Data and Information Service (NOAA-NESDIS), City College of New York (CUNY) | Integration of SMAP freeze/thaw product line into the NOAA NCEP weather forecast models |
| John Galantowicz, Atmospheric and Environmental Research, Inc. (AER) | Use of SMAP-derived inundation and soil moisture estimates in the quantification of biogenic greenhouse gas emissions |
| Jonathan Case, Clay Blankenship, and Bradley Zavodsky, NASA Short-term Prediction Research and Transition (SPoRT) Center | Data assimilation of SMAP observations, and impact on weather forecasts in a coupled simulation environment |
| Lars Kaleschke, Institute of Oceanography, University of Hamburg, Germany | SMOS to SMAP migration for cryosphere and climate application |
| **Droughts and Wildfires** | |
| Jim Reardon and Gary Curcio, U. S. Forest Service (USFS) | Use of SMAP soil moisture data to assess the wildfire potential of organic soils on the North Carolina Coastal Plain |
| Chris Funk, Amy McNally, and James Verdin, USGS and UC Santa Barbara | Incorporating soil moisture retrievals into the FEWS Land Data Assimilation System (FLDAS) |
| Brian Wardlow and Mark Svoboda, Center for Advanced Land Management Technologies (CALMIT), National Drought Mitigation Center (NDMC) | Evaluation of SMAP soil moisture products for operational drought monitoring; potential impact on the U. S. Drought Monitor (USDM) |
| Kashif Rashid, UN World Food Programme | Application of a SMAP-based index for flood forecasting in data-poor regions |
| Uma Shankar, The University of North Carolina at Chapel Hill | Enhancement of a bottom-up fire emissions inventory using Earth observations to improve air quality, land management, and public health decision support |
| **Floods and Landslides** | |
| Rafael Ameller, StormCenter Communications, Inc. | SMAP for enhanced decision making |
| Konstantine Georgakakos, Hydrologic Research Center | Development of a strategy for the evaluation of the utility of SMAP products for the Global Flash Flood Guidance Program of the Hydrologic Research Center |
| Fiona Shaw, Willis, Global Analytics | A risk identification and analysis system for insurance; eQUIP suite of custom catastrophe models, risk rating tools, and risk indices for insurance and reinsurance purposes |
| Steven Quiring, Texas A&M University | Hurricane power outage prediction |

| Early Adopter PI and Institution | Applied Research Topic |
| --- | --- |
| *Agricultural Productivity* | |
| Catherine Champagne, Agriculture and Agri-Food Canada (AAFC) | Soil moisture monitoring in Canada |
| Zhengwei Yang and Rick Mueller, USDA National Agricultural Statistical Service (NASS) | U. S. national cropland soil moisture monitoring using SMAP |
| Amor Ines and Stephen Zebiak, International Research Institute for Climate and Society (IRI), Columbia University | SMAP for crop forecasting and food security early warning applications |
| Jingfeng Wang, Rafael Bras, Aris Georgakakos, and Husayn El Sharif, Georgia Institute of Technology (GT) | Application of SMAP observations in modeling energy/water/carbon cycles and their impact on weather and climatic predictions |
| Curt Reynolds, USDA Foreign Agricultural Service (FAS) | Enhancing USDA's global crop production monitoring system using SMAP soil moisture products |
| Alejandro Flores, Boise State University | Data fusion and assimilation to improve applications of predictive ecohydrologic models in managed rangeland and forest ecosystems |
| Barbara S. Minsker, University of Illinois and sponsored by John Deere Inc. | Comprehensive, large-scale agriculture and hydrologic data synthesis |
| *Human Health* | |
| Hosni Ghedira, Masdar Institute, UAE | Estimating and mapping the extent of Saharan dust emissions using SMAP-derived soil moisture data |
| James Kitson, Andrew Walker, and Cameron Hamilton, Yorkshire Water, UK | Using SMAP L-2 soil moisture data for added value to the understanding of land management practices and impact on water quality |
| Luigi Renzullo, Commonwealth Scientific and Industrial Research Organisation (CSIRO), Australia | Preparing the Australian Water Resources Assessment (AWRA) system for the assimilation of SMAP data |
| Kyle McDonald and Don Pierson, City College of New York (CUNY) and CREST Institute, New York City Dept. of Environmental Protection | Application of SMAP freeze/thaw and soil moisture products for supporting management of New York City's potable water supply |
| *National Security* | |
| John Eylander and Susan Frankenstein, U. S. Army Engineer Research and Development Center (ERDC) Cold Regions Research and Engineering Laboratory (CRREL) | U. S. Army ERDC SMAP adoption for USACE civil and military tactical support |
| Kyle McDonald, City College of New York (CUNY) | Integration of SMAP datasets with the NRL environmental model for operational characterization of cryosphere processes across the north polar land–ocean domain |
| Georg Heygster, Institute of Environmental Physics, University of Bremen, Germany | SMAP-Ice: use of SMAP observations for sea ice remote sensing |
| Gary McWilliams, Army Research Laboratory (ARL); George Mason, U. S. Army Engineer Research and Development Center (ERDC) Geotechnical and Structures Laboratory (GSL); Li Li, Naval Research Laboratory (NRL); and Andrew Jones, Colorado State University (CSU) | Exploitation of SMAP data for Army and Marine Corps mobility assessment |
| *General* | |
| Srini Sundaram, Agrisolum Limited, UK | Application of SMAP data products in Agrisolum, a Big Data social agritech platform |
| Thomas Harris, Exelis Visual Information Solutions | Utilization of SMAP Products in ENVI, IDL and SARscape — Products L1 to L4 |

## VI. Post-Launch Activities

Plans are currently being made for the post-launch (Phase E) Applications Program. The goal will be to expand the depth and diversity of data uses through a broad and committed community of users after the satellite is launched. Other primary activities will be continuing the Early Adopter Program and conducting the SMAP Applications Program Evaluation.

### A. Applications Working Group

Post-launch, the SMAP Applications Team will expand its reach to smaller conferences and meetings to engage more thematic users in operational and decision-making environments. The SMAP Applications Program will work to increase the visibility and participation of policy and decision-making communities who use satellite data in pre-launch applications activities to ensure the maximum use of SMAP products after launch. Another goal of the post-launch applications program is the demonstration of SMAP science data products for research and applications, and liaison with the broader science and applications communities. Applied research results will be documented through articles in the peer-reviewed literature or in newsletters. These lessons learned will be compiled in one location on the SMAP website for easy access.

### B. Early Adopter Program

Post-launch activities will be partly determined by the schedule for SMAP Cal/Val and product release. During the first 3 months after launch (i.e., the In-Orbit Commissioning [IOC]), no science data will be available for the user community. The instruments may only be "on" intermittently during significant portions of this period. The availability of data for science begins at the end of IOC (EIOC — an acronym for convenience here) as follows:

- Cal/Val:

    — Launch to Launch+3 months: IOC

    — EIOC to EIOC+6 months: validation of L1 products

    — EIOC to EIOC+12 months: validation of L2-L4 products

- Product Release to the general public via the DAAC:

    — EIOC+3 months: Beta L1 products released

    — EIOC+6 months: Beta L2-L4 products released and validated L1 products released

    — EIOC+12 months: Validated L2-L4 products released

Access to preliminary data will be restricted to selected Early Adopters during the period before beta products are released to the general public via the DAAC.

### C. SMAP Applications Program Evaluation

Key issues for the evaluation of the SMAP Applications Program include answering the following questions: What is the overall result of the SMAP Applications Program in mission planning? How can we show the "applications value" of the SMAP mission? Has SMAP's engagement with the applications community increased the overall value of the mission to NASA and to the broader community? Has the community of data users been expanded (in terms of theme, research type, and operational/policy type) due to the investment in the Applications Program? How has the SMAP Applications Program changed the type and level of engagement with potential users during different mission phases? Has long-term engagement with the mission ground system and DAAC from before-to after-launch maximized societal benefit of the mission? How has mission science benefited from having pre-launch efforts (Early Adopter Program, pre-launch SMAP data access, exploratory user product development, etc.)?

We plan to provide lessons learned and evaluation of the SMAP applications program for future missions by focusing on four metrics:

1. Comparison of actual SMAP application activities with the SMAP Level 1 guidelines;

2. SMAP Applications Working Group composition and activities 2 years before launch and 1 year after launch;

3. Results of pre-launch applications research; and

4. Use of SMAP data for applications post-launch.

An evaluation report on the SMAP Applications Program will be completed after the 4th SMAP Applications Workshop in 2016.

## VII. Deliverables, Timeline, Budget, and Summary

The SMAP Applications Program has tested new concepts, definitions, and activities that could provide guidance to other missions initiating pre-launch applications programs. The deliverables have been organized by mission phase (Table 37) with a timeline in relation to other mission milestones (Figure 71). The evaluation of the SMAP Applications Program in 2016 will provide a report of lessons learned.

The SMAP Applications Program was supported by a small budget that covered the travel and activities of the SMAP SDT member who served as the SMAP Applications Working Group Chair, along with salary support (part-time FTEs) for the SMAP Applications Coordinators

throughout the mission lifetime. Workshops, Tutorials, Focus Sessions and Town Halls were hosted by users (donating facilities and amenities) with no registration fee or travel allowances. The SMAP Applications Team organized each event. Hosting events at users' institutions minimized expenses to the SMAP Project, but also provided wide exposure to the host.

In summary, the SMAP mission is committed to the dual role — science and applications — defined by the NRC Decadal Survey. Through the SMAP Applications Program activities, the SMAP mission has and will continue to be listening, learning, and striving to be of maximum value to applications. The deliverables from this effort should enhance the applications value of not only the SMAP mission, but all current and upcoming NASA missions. The evaluation of the SMAP Applications Program 2 years after launch will refine the approaches and lead to a better understanding of how to increase the overall value of the mission to NASA and to the broader community.

Table 37. SMAP Applications Program deliverables organized by mission phase.

| Mission Phase | Application Program Deliverables |
|---|---|
| **Pre-Phase A**<br>Establish Level 1 requirements and science goals and prepare a preliminary scientific conception of the mission | • Tables 34 and 35 |
| **A: Preliminary Analysis**<br>Create a preliminary design and proof of concept specifying instrument design, orbit, altitude, ground data systems, etc. | • Applications website<br>• 1st Applications Workshop<br>• Applications Working Group (AppWG)<br>• Draft Applications Plan<br>• Applications Coordinator hired |
| **B: Definition**<br>Convert the preliminary plan into a technical solution. Requirements are defined, schedules determined, and teams established around hardware. SDT is chosen. | • Early Adopters selected<br>• 2nd Applications Workshop<br>• Expanded AppWG<br>• Multiple Focus Sessions and Town Halls |
| **C/D: Design/Development**<br>Finalize ATBD and select algorithms; finalize cal/val plan and conduct cal/val rehearsal; complete mission CDR and SIR | • Final Applications Plan<br>• 2nd round of Early Adopters selected<br>• Inter-Mission Tutorials<br>• 3rd Applications Workshop<br>• Publication of EA applied research<br>• Plan for phase E |
| **E: Operations**<br>Operating the spacecraft and obtaining the data; processing and delivering data to the community. | • 4th Applications Workshop<br>• Report on Early Adopter Program<br>• Report on Applications Program |
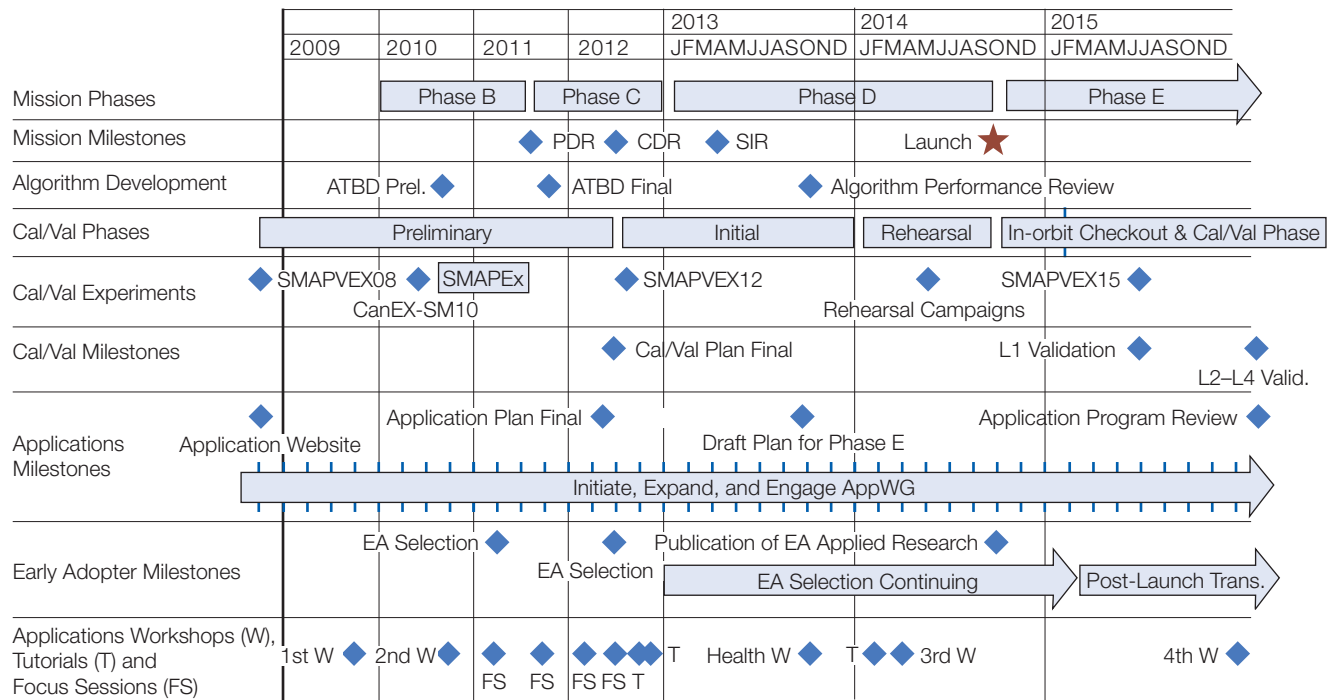
**Figure 71. Timeline of mission phases and milestones.**

## References

Bélair, S., L.-P. Crevier, J. Mailhot, et al., "Operational implementation of the ISBA land surface scheme in the Canadian regional weather forecast model. Part I: Warm season results," *Journal of Hydrometeorology*, 4:352-370, 2003. dx.doi.org/10.1175/1525-7541(2003)42003

Bolten, J. D. and W. T. Crow, "Improved prediction of quasi-global vegetation conditions using remotely-sensed surface soil moisture," *Geophysical Research Letters*, 39, L19406, 2012. dx.doi.org/10.1029/2012GL053470

Brown, M. E. and V. M. Escobar, "Assessment of soil moisture data requirements by the potential SMAP data user community: Review of SMAP mission user community," *IEEE Journal of Selected Topics in Applied Earth Observations and Remote Sensing*, 7:277–283, 2014. dx.doi.org/10.1109/JSTARS.2013.2261473

Entekhabi, D., E. Njoku, P. O'Neill, K. Kellogg, K., W. Crow, W. Edelstein, J. Entin, S. Goodman, T. Jackson, J. Johnson, J. Kimball, J. Peipmeier, R. Koster, K. McDonald,M. Moghaddam, M. S. Moran, R. Reichle, J. Shi, M. Spencer, and S. Thurman, S., "The Soil Moisture Active and Passive (SMAP) Mission," *Proceedings of the IEEE*, 98(5), pp. 704–716, 2010.

Escobar, V., M. Brown, and M. S. Moran, "The Soil Moisture Active Passive (SMAP) Applications Program and the 2011 SMAP Applications Workshop," *The Earth Observer*, 23(6), pp. 24–25, 2011.

Escobar, V., "SMAP Applications Joint Mission Tutorial: Working across mission boundaries to join thematic applications, observations, mission scientists and end users," *The Earth Observer,* 25(1), pp. 14–19, 2013.

Moran, M. S., P. E. O'Neill, D. Entekhabi, E. G. Njoku, and K. H. Kellogg, "Fostering applications opportunities for the NASA Soil Moisture Active Passive (SMAP) Mission," *Proceedings of the 2010 IEEE International Geoscience and Remote Sensing Symposium*, July 25, 2010, Honolulu, HI, pp. 2571–2574, 2010.

National Research Council, *Earth Science and Applications from Space: National Imperatives for the Next Decade and Beyond*, Washington, D.C., The National Academies Press, 2007.

# 9. SMAP Project Bibliography

## List of SMAP-Related Publications by the Project and Science Teams

Aksoy, M. and J. T. Johnson, "A comparative analysis of low-level radio frequency interference in SMOS and Aquarius microwave radiometer measurements," *IEEE Trans. Geosci. Rem. Sens.*, vol. 51, no. 10, pp. 4983–4992, 2013a.

Aksoy, M. and J. T. Johnson, "A study of SMOS RFI over North America," *IEEE Geoscience and Remote Sensing Letters*, vol. 10, pp. 515–519, 2013b.

Albergel, C., W. Dorigo, R. H. Reichle, G. Balsamo, P. de Rosnay, J. Munoz-Sabater, L. Isaksen, R. de Jeu, and W. Wagner, "Skill and global trend analysis of soil moisture from reanalyses and microwave remote sensing," *Journal of Hydrometeorology*, vol. 14, no. 4, pp. 1259–1277, 2013. dx.doi.org/10.1175/JHM-D-12-0161.1

Bao, Q., Y. Liu, J. Shi and G. Wu, "Comparisons of soil moisture datasets over the Tibetan Plateau and application to the simulation of Asia summer monsoon onset," *Advances in Atmospheric Sciences*, vol. 27, no. 2, pp. 303–314, 2010. dx.doi.org/10.1007/s00376-009-8132-5

Bateni, S. M., C. Huang, S. Margulis, E. Podest, and K. McDonald,"Feasibility of Characterizing Snowpack and the Freeze-Thaw State of Underlying Soil Using Multifrequency Active/Passive Microwave Data," *IEEE TGARS*, vol. 51, no. 7, 2013.

Bindlish, R., W. T. Crow, and T. J. Jackson, "Role of passive microwave remote sensing in improving flood forecasts," *IEEE Geoscience and Remote Sensing Letters*, vol. 6, no. 1, pp. 112–116, 2009a.

Bindlish, R., T. J. Jackson, A. J. Gasiewski, B. Stankov, M. Klein, M. H. Cosh, I. Mladenova, C. Watts, E. Vivoni, V. Lakshmi, and T. Keefer, "Aircraft-based soil moisture retrievals under mixed vegetation and topographic conditions," *Remote Sensing of Environment*, vol. 112, pp.375–390, 2008.

Bindlish, R., T. Jackson, R. Sun, M. Cosh, S. Yueh, and S. Dinardo, "Combined passive and active microwave observations of soil moisture during CLASIC," *IEEE Geoscience and Remote Sensing Letters*, vol. 6, pp. 644–648, 2009b.

Bolten, J. D. and W. T. Crow, "Improved prediction of quasi-global vegetation conditions using remotely-sensed surface soil moisture," *Geophysical Research Letters*, vol. 39, no. 19, L19406, 2012. dx.doi.org/10.1029/2012GL053470

Bolten, J. D., W. T. Crow, T. J. Jackson, X. Zhan, and C. A. Reynolds, "Evaluating the utility of remotely-sensed soil moisture retrievals for operational agricultural drought monitoring," *IEEE Journal of Selected Topics in Applied Earth Observations and Remote Sensing*, vol. 3, pp. 57–66, 2010. dx.doi.org/10.1109/JSTARS.2009.2037163

Brown, M. E. and V. M. Escobar, "Assessment of soil moisture data requirements by the potential SMAP data user community: Review of SMAP mission user community," *IEEE Journal of Selected Topics in Applied Earth Observations and Remote Sensing*, 7, pp. 277–283, 2014. dx.doi.org/10.1109/JSTARS.2013.2261473

Brown, M. E., V. M. Escobar, M. Macauley, J. Aschbacher, M. P. Milagro-Perez, B. Doorn, and L. Friedl, "Policy for robust space-based Earth science, technology, and applications," *Space Policy*, vol. 29, no. 1, pp. 76–82, 2013b.

Brown, M., V. Escobar, S. Moran, D. Entekhabi, P. O'Neill, E. Njoku, B. Doorn, and J. Entin, "NASA's Soil Moisture Active Passive (SMAP) mission and opportunities for applications users," *Bulletin of the American Meteorological Society*, vol. 94, pp.1125–1127, 2013c.

Brucker, L., E. Dinnat, and L. S. Koenig, "Weekly-gridded Aquarius L-band radiometer/scatterometer observations and salinity retrievals over the polar regions: applications for cryospheric studies," *The Cryosphere Discuss.*, vol. 7, pp. 5921–5970, 2013. dx.doi.org/10.5194/tcd-7-5921-2013

Burgin, M., D. Clewley, R. Lucas, and M. Moghaddam, "A generalized radar backscattering model based on wave theory for multilayer multispecies vegetation," *IEEE Trans. Geosci. Rem. Sens.*, vol. 49, pp. 4832–4845, 2011.

Champagne, C., A. Berg, J. Belanger, H. McNairn, and R. de Jeu, "Evaluation of Soil Moisture Derived from Passive Microwave Remote Sensing Over Agricultural Sites in Canada Using Ground-based Soil Moisture Monitoring Networks," *International Journal of Remote Sensing*, 31(14), pp.3669–3690, 2010.

Chen, F., W. T. Crow, P. J. Starks, and D. N. Moriasi, "Improving hydrologic predictions of a catchment model via assimilation of surface soil moisture," *Advances in Water Resources*, vol. 34, no. 4, pp. 526–536, 2011.

Chen, K. S., A. K. Fung, J. Shi, and H. W. Lee, "Interpretation of backscattering mechanisms from non-gaussian correlated randomly rough surfaces," *Journal of Electromagnetic Waves and Applications*, vol. 20, no. 1, pp. 2233–2246, 2006.

Chen, L., J. Shi, J. P. Wigneron, K. S. Chen, L. Jiang, and J. Du, "A parameterized surface emission model at L-band for soil moisture retrieval," *IEEE Geoscience and Remote Sensing Letters*, vol. 7, no. 1, pp. 127–130, 2010.

Chen, K. S., L. Tsang, J. Shi, and H. C. Huang, "Microwave emission from two-dimensional inhomogeneous dielectric rough surfaces based on physics-based two-grid methods," in *Electromagnetic Research*, vol. 67, pp. 181–203, 2007.

Chen, K. S., T. D. Wu, L. Tsang, Qin Li, J. Shi and A. K. Fung, "The emission of rough surfaces calculated by the integral equation method with a comparison to a three-dimensional moment method simulations," *IEEE Trans. Geosci. Rem. Sens.*, vol. 1, no. 1, pp. 90–101, 2003.

Colliander, A., S. Chan, S. Kim, N. Das, S. Yueh, M. H. Cosh, R. Bindlish, T. J. Jackson, and E. Njoku, "Long-term analysis of PALS soil moisture campaign measurements for global soil moisture algorithm development," *Remote Sensing of Environment*, vol. 121, pp. 309–322, 2012a.

Colliander, A., K. McDonald, R. Zimmermann, R. Schroeder, J. Kimball, and E. Njoku, "Application of QuikSCAT backscatter to SMAP validation planning: Freeze/thaw over ALECTRA sites in Alaska from 2000 to 2007," *IEEE Trans. Geosci. Rem. Sens.*, vol. 50, pp. 461–468, 2012b.

Cosh, M. H., A. Kabela, B. Hornbuckle, M. L. Gleason, T. J. Jackson, and J. H. Prueger, "Observations of dew amount using in situ and satellite measurements in an agricultural landscape," *Agricultural and Forest Meteorology*, vol. 49, pp. 1082–1086, 2009.

Cosh, M. H., T. J. Jackson, S. Moran, and R. Bindlish, "Temporal persistence and stability of surface soil moisture in a semi-arid watershed," *Remote Sensing of Environment*, vol. 112, pp. 304–313, 2008.

Cosh, M. H., T. J. Jackson, C. Smith, B. Toth, and A. Berg, "Validating the BERMS in situ soil water content data record with a large-scale temporary network," *Vadose Zone Journal*, vol. 12, no. 2, 2013. dx.doi.org/10.2136/vzj2012.0151

Cosh, M. H., J. Tao, T. J. Jackson, L. G. McKee, and P. O'Neill, "Vegetation water content mapping in a diverse agricultural landscape: The national airborne field experiment 2006," *Journal of Applied Remote Sensing*, vol. 4, no. 1, 043532, 2010. dx.doi.org/10.1117/1.3449090

Crow, W. T., A. A. Berg, M. H. Cosh, A. Loew, B. P. Mohanty, R. Panciera, P. de Rosnay, D. Ryu, and J. P. Walker, "Upscaling sparse ground-based soil moisture observations for the validation of coarse-resolution satellite soil moisture products," *Reviews of Geophysics*, vol. 50, no. 2, RG2002, 2012. dx.doi.org/10.1029/2011RG000372

Crow, W. T., T. Chan, D. Entekhabi, P. R. Houser, A. Hsu, T. J. Jackson, E. Njoku, P. E. O'Neill, J. Shi, and X. Zhan, "An observing system simulation experiment for Hydros radiometer soil moisture products," *IEEE Trans. Geosci. Rem. Sens.*, vol. 43, no. 6, pp. 1289–1303, 2005a.

Crow, W. T., D. Entekhabi, R. D. Koster, and R. H. Reichle, "Multiple spaceborne water cycle observations would aid modeling," *EOS*, vol. 87, no. 15, p. 149 and 153, 2006.

Crow, W. T., G. F. Huffman, R. Bindlish, and T. J. Jackson, "Improving satellite rainfall accumulation estimates using spaceborne soil moisture retrievals," *Journal of Hydrometeorology*, vol. 10, pp. 199–212, 2009a.

Crow, W. T., R. D. Koster, R. H. Reichle, and H. Sharif, "Relevance of time-varying and time-invariant retrieval error sources on the utility of spaceborne soil moisture products," *Geophysical Research Letters*, vol. 32, no. 24, L24405, 2005b. dx.doi.org/10.1029/2005GL024889

Crow, W. T., D. G. Miralles, and M. H. Cosh, "A quasi-global evaluation system for satellite-based surface soil moisture retrievals," *IEEE Trans. Geosci. Rem. Sens.*, vol. 48, no. 6, pp. 2516–2527, 2010a. dx.doi.org/10.1109/TGRS.2010.2040481

Crow, W. T. and R. H. Reichle, "Comparison of adaptive filtering techniques for land surface data assimilation," *Water Resources Research*, vol. 44, no. 8, W08423, 2008. dx.doi.org/10.1029/2008WR006883

Crow, W. T. and D. Ryu, "A new data assimilation approach for improving runoff prediction using remotely-sensed soil moisture retrievals," *Hydrologic and Earth System Sciences*, vol. 13, pp. 1–16, 2009b.

Crow, W. T. and M. J. van den Berg, "An improved approach for estimating observation and model error parameters for soil moisture data assimilation," *Water Resources Research*, vol. 46, W12519, 2010b. dx.doi.org/10.1029/2010WR009402

Crow, W. T., M. J. van den Berg, G. F. Huffman, and T. Pellarin, "Correcting rainfall using satellite-based surface soil moisture retrievals: The soil moisture analysis rainfall tool (SMART)," *Water Resources Research*, vol. 47, no. 8, W08521, 2011. dx.doi.org/10.1029/2011WR010576-

Das, N., D. Entekhabi, and E. Njoku, "Algorithm for merging SMAP radiometer and radar data for high-resolution soil moisture retrieval," *IEEE Trans. Geosci. Rem. Sens.*, vol. 49, no. 5, pp. 1504–1512, 2011.

Das, N. N., D. Entekhabi, E. G. Njoku, J. C. Shi, J. T. Johnson, and A. Colliander, "Tests of the SMAP combined radar and radiometer algorithm using airborne field campaign observations and simulated data," *IEEE Trans. Geosci. Rem. Sens.*, vol. 52, pp. 2018–2028, 2014.

Das, N. N., B. P. Mohanty, M. H. Cosh, and T. J. Jackson, "Modeling and assimilation of root zone soil moisture using remote sensing observations in Walnut Gulch Watershed during SMEX04," *Remote Sensing of Environment*, vol. 112, pp. 415–429, 2008.

De Lannoy, G. J. M., R. H. Reichle, P. R. Houser, V. R. N. Pauwels, and N. E. C. Verhoest, "Correcting for forecast bias in soil moisture assimilation with the ensemble Kalman filter," *Water Resources Research*, vol. 43, no. 9, W09410, 2007. dx.doi.org/10.1029/2006WR005449

De Lannoy, G. J. M., R. H. Reichle, and V. R. N. Pauwels, "Global calibration of the GEOS-5 L-band microwave radiative transfer model over non-frozen land using SMOS observations," *Journal of Hydrometeorology*, vol. 14, no. 3, pp. 765–785, 2013. dx.doi.org/10.1175/JHM-D-12-092.1

De Lannoy, G. J. M., R. H. Reichle, and J. A. Vrugt, "Uncertainty Quantification of GEOS-5 L-Band Radiative Transfer Model Parameters using Bayesian Inference and SMOS Observations," *Remote Sensing of Environment*, vol. 148, pp. 146–157, 2014. dx.doi.org/10.1016/j.rse.2014.03.030

Demir, M. A., J. T. Johnson, and T. Zajdel, "A study of the fourth-order small perturbation method for scattering from two-layer rough surfaces," *IEEE Trans. Geosci. Rem. Sens.*, vol. 50, pp. 3374–3382, 2012.

Dhital, Y., Q. Tang, and J. Shi, "Hydroclimatological changes in the Bagmati River Basin, Nepal," *Journal of Geographical Sciences*, vol. 23, no. 4, pp. 612–626, 2013. dx.doi.org/10.1007/s11442-013-1032-8

Dorigo, W. A., W. Wagner, R. Hohensinn, S. Hahn, C. Paulik, C., M. Drusch, S. Mecklenburg, P. van Oevelen, A. Robock, and T. Jackson, "The International Soil Moisture Network: A data hosting facility for global in situ soil moisture measurements," *Hydrology and Earth System Sciences*, vol. 15, pp. 1675–1698, 2011.

Draper, C. S., R. H. Reichle, R. de Jeu, V. Naeimi, R. Parinussa, and W. Wagner, "Estimating root mean square errors in remotely sensed soil moisture over continental scale domains," *Remote Sensing of Environment*, vol. 137, pp. 288–298, 2013. dx.doi.org/10.1016/j.rse.2013.06.013

Draper, C. S., R. H. Reichle, G. J. M. De Lannoy, and Q. Liu, "Assimilation of passive and active microwave soil moisture retrievals," *Geophysical Research Letters*, vol. 39, no. 4, L04401, 2012. dx.doi.org/10.1029/2011GL050655

Du, J., T. J. Jackson, R. Bindlish, M. H. Cosh, L. Li, B. Hornbuckle, and E. Kabela, "Effect of dew on aircraft-based passive microwave observations over an agricultural domain," *Journal of Applied Remote Sensing*, vol. 6, no. 1, 063571, 2012. dx.doi.org/10.1117/1.JRS.6.063571

Du, J. Y. and J. Shi, "A method to rebuild historical satellite-derived soil moisture products based on retrievals from current L-band satellites," *IEEE Geoscience and Remote Sensing Letters*, vol. 9, no. 5, pp. 910–914, 2012.

Du, Y. J. Shi, Y. Li, and J. A. Kong, "Analyzing EM scattering from random rough surfaces using the stochastic second-degree iterative method, sparse matrix algorithm, and Chebyshev approximation," *Electronics Letters*, vol. 45, no. 6, pp. 292–293, 2009.

Du, J., J. S. Kimball, M. Azarderakhsh, R. S. Dunbar, M. Moghaddam, and K. C. McDonald, "Classification of Alaska spring thaw characteristics using satellite L-band radar remote sensing," *IEEE TGARS*, 99, pp. 1–15, 2014.

Du, J. Y., J. Shi, and R. Sun, "The development of HJ SAR soil moisture retrieval algorithm," *International Journal of Remote Sensing*, vol. 31, no. 14, pp. 3691–3705, 2010. dx.doi.org/10.1080/01431161.2010.483486

Du, J. Y., J. Shi, S. Tjuatja, and K. S. Chen, "A combined method to model microwave scattering from a forest medium," *IEEE Trans. Geosci. Rem. Sens.*, vol. 44, no. 4, pp. 815–824, 2006.

Du, Y., W. Z. Yan, J. Shi, Z. Y. Li, and E. X. Chen, "Electromagnetic scattering from a corn canopy at L and C bands," *Progress in Electromagnetics Research*, vol. 114, pp. 33–49, 2011.

Duan, X. and M. Moghaddam, "Stabilized extended boundary condition method for Vector electromagnetic scattering from arbitrary random rough surfaces for remote sensing of soil moisture," *IEEE Trans. Geosci. Rem. Sens.*, vol. 50, no. 1, pp. 87–103, 2012.

Dunne, S. and D. Entekhabi, "An ensemble-based reanalysis approach to land data assimilation," *Water Resources Research*, vol. 41, no. 2, W02013, 2005. dx.doi.org/10.1029/2004WR003449

Dunne, S., D. Entekhabi, and E. Njoku, "Impact of multi-resolution active and passive measurements on soil moisture estimation using the ensemble Kalman smoother," *IEEE Trans. Geosci. Rem. Sens.*, vol. 45, no. 4, pp. 1016–1028, 2007.

Entekhabi, D. and M. Moghaddam, "Mapping recharge from space: Roadmap to meeting the grand challenge," *Journal of Hydrogeology*, vol. 15, pp. 105–116, 2007.

Entekhabi, D., E. Njoku, P. Houser, M. Spencer, T. Doiron, J. Smith, R. Girard, S. Belair, W. Crow, T. Jackson, Y. Kerr, J. Kimball, R. Koster, K. McDonald, P. O'Neill, T. Pultz, S. Running, J. C. Shi, E. Wood, and J. van Zyl, "The Hydrosphere State (HYDROS) mission concept: An Earth system pathfinder for global mapping of soil moisture and land freeze/thaw," *IEEE Trans. Geosci. Rem. Sens.*, vol. 42, no. 10, pp. 2184–2195, 2004.

Entekhabi, D., E. G. Njoku, P. E. O'Neill, K. H. Kellogg, W. T. Crow, W. N. Edelstein, J. K. Entin, S. D. Goodman, T. J. Jackson, J. Johnson, J. Kimball, J. R. Peipmeier, R. D. Koster, K. C. McDonald, M. Moghaddam, M. S. Moran, R. Reichle, J. C. Shi, M. W. Spencer, and S. W. Thurman, "The soil moisture active and passive (SMAP) mission," *Proceedings of the IEEE*, vol. 98, pp. 704–716, 2010a. dx.doi.org/10.1109/JPROC.2010.2043918

Entekhabi, D., R. H. Reichle, R. D. Koster, and W. T. Crow, "Performance metrics for soil moisture retrievals and application requirements," *Journal of Hydrometeorology*, vol. 11, no. 3, pp. 832–840, 2010b. dx.doi.org/10.1175/2010JHM1223.1

Famiglietti, J. S., D. Ryu, A. Berg, M. Rodell, and T. J. Jackson, "Field observations of soil moisture variability across scales," *Water Resources Research*, vol. 44, no. 1, W01423, 2008. dx.doi.org/10.1029/2006WR005804

Flores, A., D. Entekhabi, and R. L. Bras, "Application of a hillslope-scale soil moisture data assimilation system to military trafficability assessment," *Journal of Terramechanics*, vol. 51, pp. 53–66, 2014. dx.doi.org/10.1016/j.jterra.2013.11.004

Flores, A. N., D. Entekhabi and R. L. Bras, "Hydrologic data assimilation with a hillslope-scale resolving model and L-band radar observations: Synthetic experiments with the ensemble Kalman filter," *Water Resources Research*, vol. 48, no. 8, 2012. dx.doi.org/10.1029/2011WR011500

Flores, A. N., V. Y. Ivanov, D. Entekhabi, and R. L. Bras, "Impact of hillslope-scale organization of topography, soil moisture, soil temperature and vegetation on modeling surface microwave radiation emission," *IEEE Trans. Geosci. Rem. Sens.*, vol. 47, no. 8, pp. 2557–2571, 2009.

Frankford, M. and J. T. Johnson, "Compensation of Faraday rotation in multi-polarization scatterometry," *IEEE Trans. Geosci. Rem. Sens.*, vol. 48, pp. 358–364, 2010.

Galantowicz, J. F., D. Entekhabi, and E. G. Njoku, "Estimation of soil type heterogeneity effects in the retrieval of soil moisture from radiobrightness," *IEEE Trans. Geosci. Rem. Sens.*, vol. 38, no. 1, pp. 312–316, 2000.

Guner, B., M. T. Frankford, and J. T. Johnson, "A study of the Shapiro-Wilk test for the detection of pulsed sinusoidal radio frequency interference," *IEEE Trans. Geosci. Rem. Sens.*, vol. 47, pp. 1745–1751, 2009.

Guo, Y., J. Shi, X. Li, and J. Du, "Evaluation of terrain effect on microwave radiometer measurement and its correction," *International Journal of Remote Sensing*, vol. 32, no. 24, pp. 889–8913, 2011. dx.doi.org/10.1080/01431161.2011.591844

Hain, C. R., W. T. Crow, J. R. Mecikalski, M. C. Anderson, and T. Holmes, "An intercomparison of available soil moisture estimates from thermal-infrared and passive microwave remote sensing and land-surface modeling," *Journal of Geophysical Research—Atmospheres*, vol. 116, no. D15, D15107, 2011. dx.doi.org/10.1029/2011JD015633

Hain, C. R., W. T. Crow, M. C. Anderson, and J. R. Mecikalski, "An ensemble Kalman filter dual assimilation of thermal-infrared and microwave satellite observations of soil moisture into the Noah land surface model," *Water Resources Research*, vol. 48, no. 11, W11517, 2012. dx.doi.org/10.1029/2011WR011268

Heathman, G. C., M. H. Cosh, E. Han, T. J. Jackson, L. G. McKee, and S. McAfee, "Field scale spatiotemporal analysis of surface soil moisture for evaluating point-scale in situ networks," *Geoderma*, vol. 170, pp. 195–205, 2012.

Holmes, T., W. Crow, T. Yilmaz, T. Jackson, and J. Basara, "Enhancing model-based land surface temperature estimates using multi-platform microwave observations," *Journal of Geophysical Research—Atmospheres*, vol. 118, pp. 577–591, 2013.

Holmes, T. R. J., T. J. Jackson, R. H. Reichle, and J. Basara, "An assessment of surface soil temperature products from numerical weather prediction models using ground-based measurements," *Water Resources Research*, vol. 48, no. 2, W02531, 2012. dx.doi.org/10.1029/2011WR010538

Huang, S. and L. Tsang, "Electromagnetic scattering of randomly rough soil surfaces based on numerical solutions of Maxwell equations in 3-dimensional simulations using a hybrid UV/PBTG/SMCG method," *IEEE Trans. Geosci. Rem. Sens.*, vol. 50, pp. 4025–4035, 2012.

Huang, S., L. Tsang, E. G. Njoku, and K. S. Chen, "Backscattering coefficients, coherent reflectivities, emissivities of randomly rough soil surfaces at L-band for SMAP applications based on numerical solutions of Maxwell equations in three-dimensional simulations," *IEEE Trans. Geosci. Rem. Sens.*, vol. 48, pp. 2557–2567, 2010.

Hudson, D., J. R. Piepmeier, and D. L. Long, "Polarization rotation correction in radiometry: An error analysis," *IEEE Trans. Geosci. Rem. Sens.*, vol. 45, no. 10, pp. 3212–400, 2007.

Hunt, E. R. Jr., L. Li, M. T. Yilmaz, and T. J. Jackson, "Comparison of vegetation water contents derived from shortwave-infrared and passive-microwave sensors over central Iowa," *Remote Sensing of Environment*, vol. 115, pp. 2376–2383, 2011.

Jackson, T. J., R. Bindlish, M .H. Cosh, T. Zhao, P. J. Starks, D. D. Bosch, M. S. Moran, M. S. Seyfried, Y. Kerr, and D. Leroux, "Validation of soil moisture and ocean salinity (SMOS) soil moisture over watershed networks in the U.S.," *IEEE Trans. Geosci. Rem. Sens.*, vol. 50, pp. 1530–1543, 2012.

Jackson, T. J., M. H. Cosh, R. Bindlish, P. J. Starks, D. D. Bosch, M. S. Seyfried, D. C. Goodrich, and M. S. Moran, "Validation of advanced microwave scanning radiometer soil moisture products," *IEEE Trans. Geosci. Rem. Sens.*, vol. 48, pp. 4256–4272, 2010.

Jackson, T. J., M. S. Moran, and P. E. O'Neill, "Introduction to soil moisture experiments 2004 (SMEX04)," *Remote Sensing of Environment*, vol. 112, pp. 301–303. 2008.

Johnson, J. T. and J. D. Ouellette, "Polarization features in bistatic scattering from rough surfaces," *IEEE Trans. Geosci. Rem. Sens.*, vol. 52, no. 3, pp. 1616–1626, 2014.

Johnson, J. T. and L. C. Potter, "Performance study of detection algorithms for pulsed sinusoidal interference in microwave radiometry," *IEEE Trans. Geosci. Rem. Sens.*, vol. 47, no. 2, pp. 628–636, 2009.

Joseph, A., P. O'Neill, R. van der Velde, R. Lang, and T. Gish, "Effects of corn on C- and L-band radar backscatter: A correction method for soil moisture retrieval," *Remote Sensing of Environment*, vol. 114, pp. 2417–2430, 2010a. dx.doi.org/10.1016/j.rse.2010.05.017

Joseph, A., R. van de Velde, P. O'Neill, B. Choudhury, S. Liang, R. Lang, E. Kim, T. Gish, and P. Houser, "L-band observations over a corn canopy during the entire growing season," *Sensors*, vol. 10, pp. 6980–7001, 2010b. dx.doi.org/10.3390/S100706980

Kim, Y., J. S. Kimball, K. Didan, and G. M. Henebry, "Response of vegetation growth and productivity to spring climate indicators in the conterminous United States derived from satellite remote sensing data fusion," *Agricultural and Forest Meteorology*,194, pp. 132–143, 2014.

Kim, Y., J. S. Kimball, K. Zhang, K. Didan, I. Velicogna, and K. C. McDonald, "Attribution of divergent northern vegetation growth responses to lengthening non-frozen seasons using satellite optical-NIR and microwave remote sensing," *International Journal of Remote Sensing*, 35(10), pp. 3700–3721, 2014.

Kim, S.-B., M. Moghaddam, L. Tsang, M. Burgin, X. Xu, and E. G. Njoku, "Models of L-band radar backscattering coefficients over the global terrain for soil moisture retrieval," *IEEE Trans. Geosci. Rem. Sens.*, vol. 52, pp. 1381–1396, 2014.

Kim, S.-B., L. Tsang, J. T. Johnson, S. Huang, J. J. van Zyl, and E. G. Njoku, "Soil moisture retrieval using time-series radar observations over bare surfaces," *IEEE Trans. Geosci. Rem. Sens.*, vol. 50, no. 5, pp. 1853–1863, 2012.

Kim, Y., T. Jackson, R. Bindlish, H. Lee, and S. Hong, "Monitoring of soybean growth using L, C, X-band scatterometer data," *International Journal of Remote Sensing*, vol. 34, pp. 4069-4082, 2013.

Kim, Y., T. Jackson, R. Bindlish, H. Lee, and S. Hong, "Radar vegetation indices for estimating the vegetation water content of rice and soybean," *IEEE Geoscience and Remote Sensing Letters*, vol. 9. pp. 564–568, 2012a.

Kim, Y., J. S. Kimball, K. C. McDonald, and J. Glassy, "Developing a global data record of daily landscape freeze/thaw status using satellite passive microwave remote sensing," *IEEE Trans. Geosci. Rem. Sens.*, vol. 49, no. 3, pp. 949–960, 2011. dx.doi.org/ 10.1109/ TGRS.2010.2070515

Kim, Y., J. S. Kimball, K. Zhang, and K. C. McDonald, "Satellite detection of increasing northern hemisphere non-frozen seasons from 1979 to 2008: Implications for regional vegetation growth," *Remote Sensing of Environment*, vol. 121, pp. 472–487, 2012b.

Kim, Y. and J. J. van Zyl, "A time-series approach to estimate soil moisture using polarimetric radar data," *IEEE Trans. Geosci. Rem. Sens.*, vol. 47, pp. 2519–2527, 2009.

Kimball, J. S., L. A. Jones, K. Zhang, F. A. Heinsch, K. C. McDonald, and W. C. Oechel, "A satellite approach to estimate land–atmosphere $CO_2$ exchange for Boreal and Arctic biomes using MODIS and AMSR-E," *IEEE TGARS*, 47(2), pp. 569–587, 2009.

Konings, A., D. Entekhabi, S. Chan and E. Njoku, "Effect of radiative transfer uncertainty on L-band radiometric soil moisture retrieval," *IEEE Trans. Geosci. Rem. Sens.*, vol. 49, no. 7, pp. 2686–2698, 2011.

Koster, R. D., et al., "The second phase of the Global Land–Atmosphere Coupling Experiment," *J. Hydromet.*, vol. 12, pp. 805–822, 2011.

Koster, R. D., Z. Guo, R. Yang, P. A. Dirmeyer, K. Mitchell, and M. J. Puma, "On the nature of soil moisture in land surface models," *Journal of Climate*, vol. 22, pp. 4322–4335, 2009.

Koster, R. D., S. P. P. Mahanama, B. Livneh, D. P. Lettenmaier, and R. H. Reichle, "Skill in streamflow forecasts derived from large-scale estimates of soil moisture and snow," *Nature Geoscience*, vol. 3, pp. 613–616, 2010a. dx.doi.org/10.1038/NGEO944

Koster, R. D., S.P.P. Mahanama, T. J. Yamada, G. Balsamo, A. A. Berg, et al., "Contribution of land surface initialization to subseasonal forecast skill: First results from a multi-model experiment," *Geophysical Research Letters*, vol. 37, no. 2, L02402, 2010b. dx.doi.org/10.1029/2009GL041677

Koster, R. D., M. J. Suarez, P. Liu, U. Jambor, A. A. Berg, M. Kistler, R. H. Reichle, M. Rodell, and J. Famiglietti, "Realistic initialization of land surface states: Impacts on subseasonal forecast skill," *Journal of Hydrometeorology*, vol. 5, no. 6, pp. 1049–1063, 2004. dx.doi.org/10.1175/ JHM-387.1

Koster, R. D., G. K. Walker, S. P. P. Mahanama, and R. H. Reichle, "Soil Moisture Initialization Error and Subgrid Variability of Precipitation in Seasonal Streamflow Forecasting," *Journal of Hydrometeorology*, vol. 15, pp. 69–88, 2013. dx.doi.org/10.1175/JHM-D-13-050.1

Krajewski, W., M. Anderson, W. Eichinger, D. Entekhabi, B. Hornbuckle, P. Houser, G. Katul, W. Kustas, J. Norman, C. Peters-Lidard, and E. Wood, "A remote sensing observatory for hydrologic sciences: A genesis for scaling to continental hydrology," *Water Resources Research*, vol. 42, no. 7, W07301, 2006. dx.doi.org/10.1029/2005WR004435

Kumar, S. V., C. D. Peters-Lidard, D. Mocko, R. H. Reichle, Y. Liu, K. R. Arsenault, Y. Xia, M. Ek, G. Riggs, B. Livneh, and M. Cosh, "Assimilation of passive microwave-based soil moisture and snow depth retrievals for drought estimation," *Journal of Hydrometeorology*, 2014. dx.doi.org/10.1175/JHM-D-13-0132.1

Kumar, S. V., R. H. Reichle, K. W. Harrison, C. D. Peters-Lidard, S. Yatheendradas, and J. A. Santanello, "A comparison of methods for a priori bias correction in soil moisture data assimilation," *Water Resources Research*, vol. 48, no. 3, W03515, 2012. dx.doi.org/10.1029/2010WR010261

Kumar, S. V., R. H. Reichle, R. D. Koster, W. T. Crow, and C. D. Peters-Lidard, "Role of subsurface physics in the assimilation of surface soil moisture observations," *Journal of Hydrometeorology*, vol. 10, no. 6, pp. 1534–1547, 2009. dx.doi.org/10.1175/2009JHM1134.1

Kurum, M., P. O'Neill, R. Lang, M. Cosh, A. Joseph, and T. Jackson, "Impact of conifer forest litter on microwave emission at L-band," *IEEE Trans. Geosci. Rem. Sens.*, vol. 50, no. 4, pp. 1071–1084, 2012a. dx.doi.org/10.1109/ TGRS.2011.2166272

Kurum, M., R. Lang, P. O'Neill, A. Joseph, T. Jackson, and M. Cosh, "L-band radar estimation of forest canopy attenuation for active/passive soil moisture inversion," *IEEE Trans. Geosci. Rem. Sens.*, MicroRad08 Special Issue, vol. 47, no. 9, pp. 3026–3040, 2009. dx.doi.org/10.1109/TGRS.2009.2026641

Kurum, M., R. Lang, P. O'Neill, A. Joseph, T. Jackson, and M. Cosh, "A first-order radiative transfer model for microwave radiometry of forest canopies at L-band," *IEEE Trans. Geosci. Rem. Sens.*, MicroRad10 Special Issue, vol. 49, no. 9, pp. 3167–3179, 2011. dx.doi.org/10.1109/TGRS.2010.2091139

Kurum, M., P. E. O'Neill, R. H. Lang, A. T. Joseph, T. J. Jackson, and M. H. Cosh, "Effective tree scattering and opacity at L-band," *Remote Sensing of Environment*, vol. 118, pp. 1–9, 2012b. dx.doi.org/10.1016/j.rse.2011.10.024

Li, F., W. T. Crow, and W. P Kustas, "Towards the estimation of root-zone soil moisture via the simultaneous assimilation of thermal and microwave soil moisture retrievals," *Advances in Water Resources*, vol. 33, pp. 201–214, 2010. dx.doi.org/10.1016/j.advwatres.2009.11.007

Li, Q., J. Shi, and K. S. Chen, "A generalized power law spectrum and its applications to the backscattering of soil surface on the integral equation model," *IEEE Trans. Geosci. Rem. Sens.*, vol. 40, no. 2, pp. 271–280, 2002.

Liu, Q., R. H. Reichle, R. Bindlish, M. H. Cosh, W. T. Crow, R. de Jeu, G. J. M. De Lannoy, G. J. Huffman, and T. J. Jackson, "The contributions of precipitation and soil moisture observations to the skill of soil moisture estimates in a land data assimilation system," *Journal of Hydrometeorology*, vol. 12, no. 5, 12, pp. 750–765, 2011. dx.doi.org/10.1175/JHM-D-10-05000.1

Magagi, R., A. Berg, K. Goita, S. Belair, T. Jackson, B. Toth, A. Walker, H. McNairn, P. O'Neill, M. Moghaddam, I. Gherboudj, A. Coliander, M. Cosh, J. Belanger, M. Burgin, J. Fisher, S. Kim, LP Rousseau, N. Djamai, J. Shang, and A. Merzouki, "Canadian experiment for soil moisture in 2010: overview and preliminary results," *IEEE Trans. Geosci. Rem. Sens.*, vol. 51, no. 1, part 2, pp. 347–363, 2013. dx.doi.org/10.1109/TGRS.2012.2198920

Maggioni, V., E. N. Anagnostou, and R. H. Reichle, "The impact of model and rainfall forcing errors on characterizing soil moisture uncertainty in land surface modeling," *Hydrology and Earth System Sciences*, vol. 16, pp. 3499–3515, 2012a. dx.doi.org/10.5194/hess-16-3499-2012

Maggioni, V., R. H. Reichle, and E. N. Anagnostou, "The effect of satellite-rainfall error modeling on soil moisture prediction uncertainty," *Journal of Hydrometeorology*, vol. 12, no. 3, pp. 413–428, 2011. dx.doi.org/10.1175/2011JHM1355.1

Maggioni, V., R. H. Reichle, and E. N. Anagnostou, "The efficiency of assimilating satellite soil moisture retrievals in a land data assimilation system using different rainfall error models," *Journal of Hydrometeorology*, vol. 14, no. 1, pp. 368–374, 2013. dx.doi.org/10.1175/JHM-D-12-0105.1

Maggioni, V., R. H. Reichle, and E. N. Anagnostou, "The impact of rainfall error characterization on the estimation of soil moisture fields in a land data assimilation system," *Journal of Hydrometeorology*, vol. 13, no. 3, pp. 1107–1118, 2012b. dx.doi.org/10.1175/JHM-D-11-0115.1

Mahanama, S. P. P., B. Livneh, R. D. Koster, D. Lettenmaier, and R. H. Reichle, "Soil moisture, snow, and seasonal streamflow forecasts in the United States," *Journal of Hydrometeorology*, vol. 13, no. 1, pp. 189–203, 2012. dx.doi.org/10.1175/JHM-D-11-046.1

Mahanama, S. P. P., R. D. Koster, R. H. Reichle, and L. Zubair, "The role of soil moisture initialization in subseasonal and seasonal streamflow prediction: A case study in Sri Lanka," *Advances in Water Resources*, vol. 31, no. 10, pp. 1333–1343, 2008. dx.doi.org/10.1016/j.advwatres.2008.06.004

Manns, H. and A. Berg, "Importance of soil organic carbon on surface soil water content variability among agricultural fields," *Journal of Hydrology*, 516, pp. 297–303, 2014.

Manns, H., A. Berg, P. Bullock, and H. McNairn, "Impact of soil surface characteristics on soil water content variability in agricultural fields," *Hydrological Processes*, 2014. dx.doi.org/10.1002/hyp.10216

Margulis, S., D. Entekhabi, D. McLaughlin, "Spatiotemporal disaggregation of remotely sensed precipitation for ensemble hydrologic modeling and data assimilation," *Journal of Hydrometeorology*, vol. 7, no. 3, pp. 511–533, 2006. dx.doi.org/10.1175/JHM492.1

Margulis, S. A., D. B. McLaughlin, D. Entekhabi, and S. Dunne, "Land data assimilation and estimation of soil moisture using measurements from the Southern Great Plains 1997 field experiment," *Water Resources Research*, vol. 38, no. 12, p. 1299, 2002.

McColl, K. A., D. Entekhabi, and Maria Piles, "Uncertainty analysis of soil moisture and vegetation indices using Aquarius scatterometer observations," *IEEE Trans. Geosci. Rem. Sens.*, vol. 52, no. 7, pp. 4259–4272, 2014.

McGuire, A. D., T. R. Christensen, D. Hayes, A. Heroult, E. Euskirchen, J. S. Kimball, C. Koven, P. Lefleur, P. A. Miller, W. Oechel, P. Peylin, M. Williams, and Y. Yi, "An assessment of the carbon balance of Arctic tundra: Comparisons among observations, process models, and atmospheric inversions," *Biogeosciences*, vol. 9, pp. 3185–3204, 2012. dx.doi.org/10.5194/bg-9-3185-2012

McLaughlin, D., Y. Zhou, D. Entekhabi, and V. Chat-darong, "Computational issues for large-scale land surface data assimilation problems," *Journal of Hydro-meteorology*, vol. 7, no. 3, pp. 494–510, 2006. dx.doi.org/10.1175/JHM493.1

Merlin, O., J. Walker, R. Panciera, M. J. Escorihuela, and T. Jackson, "Assessing the SMOS soil moisture retrieval parameters with high-resolution NAFE'06 data," *IEEE Geoscience and Remote Sensing Letters*, vol. 6, pp. 635–639, 2009.

Miralles, D. G., W. T. Crow, and M. H. Cosh, "Estimating spatial sampling errors in coarse-scale soil moisture esti-mates derived from point-scale observations," *Journal of Hydrometeorology*, vol. 11, no. 6, pp. 1404–1410, 2010. dx.doi.org/10.1175/2010JHM1285.1

Misra, S., P. N. Mohammed, B. Guner, C. S. Ruf, J. R. Piepmeier, and J. T. Johnson, "Microwave radiom-eter radio-frequency interference detection algorithms: A comparative study," *IEEE Trans. Geosci. Rem. Sens.*, vol. 47, no. 11, pp. 3742–3754, 2009a.

Misra, S., P. N. Mohammed, B. Guner, C. S. Ruf, J. R. Piepmeier, and J. T. Johnson, "Radio frequency in-terference detection algorithms in microwave radiometry: A comparative study," *IEEE Trans. Geosci. Rem. Sens.*, vol. 47, pp. 3742–3754, 2009b.

Mladenova, I., T. J. Jackson, R. Bindlish, and S. Hensley, "Incidence angle normalization of radar backscatter data," *IEEE Trans. Geosci. Rem. Sens.*, vol. 51, pp. 1791–1804, 2013.

Moghaddam, M., D. Entekhabi, Y. Goykhman, K. Li, M. Liu, A. Mahajan, A. Nayyar, D. Shuman, and D. Teneketzis, "A wireless soil moisture smart sensor web using physics-based optimal control: Concept and initial demonstrations," *IEEE Journal of Selected Topics in Applied Earth Observations and Remote Sensing*, vol. 3, no. 4, pp. 522–535, 2010.

Molotch, N. P., P. D. Brooks, S. P. Burns, M. Litvak, J. R. McConnell, R. K. Monson, and K. Musselman, "Ecohydrological controls on snowmelt partitioning in mixed-conifer sub-alpine forests," *Ecohydrology*, vol. 2, no. 2, pp. 129–142, 2009. dx.doi.org/10.1002/eco.48

Moran, M. S., L. Alonso, J. Moreno, M. P. Cendrero Mateo, F. de la Cruz, and A. Montoro, "A RADARSAT-2 quad-polarized time series for monitoring crop and soil conditions in Barrax, Spain," *IEEE Trans. Geosci. Rem. Sens.*, vol. 50, pp. 1057–1070, 2012. dx.doi.org/10.1109/TGRS.2011.2166080

Narvekar, P. S., G. Heygster, T. J. Jackson, R. Bindlish, G. Macelloni, and J. Notholt, "Passive polarimetric micro-wave signatures observed over Antarctica," *IEEE Trans. Geosci. Rem. Sens.*, vol. 48, pp. 1059–1075, 2010.

Nearing, G. S., W. T. Crow, K. R. Thorp, M. S. Moran, R. H. Reichle, and H. V. Gupta, "Assimilating remote sensing observations of leaf area index and soil moisture for wheat yield estimates: An observing system simulation experiment," *Water Resources Research*, vol. 48, no. 5, W05525, 2012a. dx.doi.org/10.1029/2011WR011420

Nearing, G. S., M. S. Moran, C. Holifield Collins, K. R. Thorp, and S. C. Slack, "An improved strategy for assimilating synthetic aperture radar imagery into modeled estimations of soil moisture through parameter optimization," *Remote Sensing of Environment*, vol. 114, pp. 2564–2574, 2010.

Nearing, G. S., M. S. Moran, and R. L. Scott, "Coupling diffusion and maximum entropy models to estimate ther-mal inertia," *Remote Sensing of Environment*, vol. 119, pp. 222–231, 2012b.

O'Neill, P., T. J. Jackson, D. Entekhabi, and E. Njoku, "Survey of L-band tower and airborne sensor systems relevant to upcoming soil moisture missions," *IEEE Geoscience and Remote Sensing Newsletter*, vol. 151, pp. 13–16, 2009.

Ouellette, J. D., J. T. Johnson, S. Kim, J. van Zyl, M. Spencer, M. Moghaddam, L. Tsang, and D. Entekhabi, "A simulation study of compact polarimetry for radar re-trieval of soil moisture," *IEEE Trans. Geosci. Rem. Sens.*, 2014. dx.doi.org/ 10.1109/TGRS.2013.2294133

Pan, M., E. F. Wood, D. B. McLaughlin, D. Entekhabi, and L. Luo, "A multiscale ensemble filtering system for hydro-logic data assimilation: 1. Implementation and synthetic experiment," *Journal of Hydrometeorology*, vol. 10, no. 3, pp. 794–806, 2009.

Panciera, R., J. Walker, T. J. Jackson, D. Ryu, D. Gray, A. Monerris, H. Yardley, M. Tanese, C. Rudiger, X. Wu, Y. Gao, and J. Hacker, "The Soil Moisture Active Passive Experiments (SMAPEx): Towards soil moisture retriev-al from the SMAP mission," *IEEE Trans. Geosci. Rem. Sens.*, vol. 51, no. 1, pp. 490–507, 2014.

Panegrossi, G., R. Ferretti, L. Pulvirenti, N. Pierdicca: "Impact of ASAR soil moisture data on the MM5 precipitation forecast for the Tanaro flood event of April 2009," *Natural Hazards and Earth System Sciences*, vol. 11, issue 12, pp. 3135–3149, 2011.

Parinussa, R., T. Holmes, and W. T. Crow, "The impact of land surface temperature on soil moisture anomaly detection from passive microwave observations," *Hydrology and Earth Systems Sciences*, vol. 15, pp. 3135–3151, 2011. dx.doi.org/10.5194/hess-15-3135-2011

Park, J., J. T. Johnson, N. Majurec, N. Niamsuwan, J. Piepmeier, P. Mohammed, C. Ruf, S. Misra, S. Yueh, and S. Dinardo, "Airborne L-band radio frequency interference observations from the SMAPVEX08 campaign and associated flights," *IEEE Trans. Geosci. Rem. Sens.*, vol. 49, pp. 3359–3370, 2011.

Peng, J. and C. S. Ruf, "Calibration Method for Fully Polarimetric Microwave Radiometers Using the Correlated Noise Calibration Standard," *IEEE Trans. Geosci. Remote Sens.*, vol. 46, no. 10, October 2008.

Piepmeier, J. R., J. T. Johnson, P. N. Mohammed, D. Bradley, C. Ruf, M. Aksoy, R. Garcia, D. Hudson, L. Miles, and M. Wong, "Radio-Frequency Interference (RFI) Mitigation for the Soil Moisture Active Passive (SMAP) Microwave Radiometer," *IEEE Trans. Geosci. Rem. Sens.*, vol. 56, no. 1, part 2, pp. 761–775, January 2014.

Piepmeier, J. R., D. G. Long, and E. G. Njoku, "Stokes antenna temperatures," *IEEE Trans. Geosci. Rem. Sens.*, vol. 46, no. 2, pp. 516–527, 2008.

Pierdicca, N., L. Pulvirenti, and C. Bignami, "Soil moisture estimation over vegetated terrains using multitemporal remote sensing data," *Remote Sensing of Environment*, vol. 114, pp. 440–448, 2010.

Pierdicca, N., L. Pulvirenti, C. Bignami, and F. Ticconi, "Monitoring soil moisture in an agricultural test site using SAR data: design and test of a pre-operational procedure," *IEEE Journal of Selected Topics in Applied Earth Observations and Remote Sensing*, vol. 6, no. 3, pp. 1199–1210, 2013. dx.doi.org/10.1109/JSTARS.2012.2237162

Pierdicca, N., L. Pulvirenti, F. Fascetti, R. Crapolicchio, and M. Talone, "Analysis of two years of ASCAT- and SMOS-derived soil moisture estimates over Europe and North Africa," *European Journal of Remote Sensing*, vol. 46, pp. 759–773, 2013. dx.doi.org/10.5721/EuJRS20134645

Pierdicca, N., L. Pulvirenti, and G. Pace, "A Prototype Software Package to Retrieve Soil Moisture from Sentinel 1 Data by Using a Bayesian Multitemporal Algorithm," *IEEE Trans. Geosci. Rem. Sens.*, vol. 7, no. 1, pp.153–166, 2014. dx.doi.org/10.1109/JSTARS.2013.2257698

Piles, M., D. Entekhabi, and A. Camps, "A change detection algorithm for retrieving high-resolution soil moisture from SMAP radar and radiometer observations," *IEEE Trans. Geosci. Rem. Sens.*, vol. 47, no. 12, pp. 4125–4131, 2009.

Pinel, N., J. T. Johnson, and C. Bourlier, "Fully polarimetric scattering from random rough layers under the geometric optics approximation: Geoscience applications," *Radio Science*, vol. 46, RS0E20, 2011.

Podest, E., K. C. McDonald, and J. S. Kimball, "Multisensor Microwave Sensitivity to Freeze/Thaw Dynamics Across a Complex Boreal Landscape," *IEEE TGARS*, vol. 52, no. 11, 2014.

Ponce Campos, G. E., M. S. Moran, A. Huete, Y. Zhang, C. Bresloff, T. E. Huxman, D. Eamus, D. D. Bosch, A. R. Buda, S. A. Gunter, T. Heartsill Scalley, S. G. Kitchen, M. P. McClaran, W. H. McNab, D. S. Montoya, J. A. Morgan, D.P.C. Peters, E. J. Sadler, M. S. Seyfried, and P. J. Starks, "Ecosystem resilience despite large-scale altered hydroclimatic conditions," *Nature*, vol. 494, pp. 3439–352, 2013. dx.doi.org/10.1038/nature11836

Reichle, R. H., "Data assimilation methods in the Earth sciences," *Advances in Water Resources*, vol. 31, no. 11, pp. 1411–1418, 2008. dx.doi.org/10.1016/j.advwatres.2008.01.001

Reichle, R. H., M. G. Bosilovich, W. T. Crow, R. D. Koster, S. V. Kumar, S. P. P. Mahanama, and B. F. Zaitchik, "Recent Advances in Land Data Assimilation at the NASA Global Modeling and Assimilation Office," in *Data Assimilation for Atmospheric, Oceanic and Hydrologic Applications*, edited by Seon K. Park and Liang Xu, pp. 407–428, Springer Verlag, New York, 2009. dx.doi.org/10.1007/978-3-540-71056-1.

Reichle, R. H., W. T. Crow, and C. L. Keppenne, "An adaptive ensemble Kalman filter for soil moisture data assimilation," *Water Resources Research*, vol. 44, no. 3, W03423, 2008a. dx.doi.org/10.1029/2007WR006357

Reichle, R. H., W. T. Crow, R. D. Koster, H. Sharif, and S. P. P. Mahanama, "Contribution of soil moisture retrievals to land data assimilation products," *Geophysical Research Letters*, vol. 35, no. 1, L01404, 2008b. dx.doi.org/10.1029/2007GL031986

Reichle, R. H., G. J. M. De Lannoy, B. A. Forman, C. S. Draper, and Q. Liu, "Connecting Satellite Observations with Water Cycle Variables through Land Data Assimilation: Examples Using the NASA GEOS-5 LDAS," *Surveys in Geophysics*, vol. 35, pp. 577–606, 2014. dx.doi.org/10.1007/s10712-013-9220-8

Reichle, R. H., D. Entekhabi, and D. B. McLaughlin, "Downscaling of radio brightness measurements for soil moisture estimation: A four-dimensional variational data assimilation approach," *Water Resources Research*, vol. 37, no. 9, pp. 2353–2364, 2001. dx.doi.org/10.1029/2001WR000475

Reichle, R. H. and R. D. Koster, "Assessing the impact of horizontal error correlations in background fields on soil moisture estimation," *Journal of Hydrometeorology*, vol. 4, no. 6, pp. 1229–1242, 2003. dx.doi.org/10.1175/1525-7541

Reichle, R. H. and R. D. Koster, "Bias reduction in short records of satellite soil moisture," *Geophysical Research Letters*, vol. 31, no. 19, L19501, 2004. dx.doi.org/10.1029/2004GL020938

Reichle, R. H. and R. D. Koster, "Global assimilation of satellite surface soil moisture retrievals into the NASA Catchment land surface model," *Geophysical Research Letters*, vol. 32, no. 2, L02404, 2005. dx.doi.org/10.1029/2004GL021700

Reichle, R. H., R. D. Koster, J. Dong, and A. A. Berg, "Global soil moisture from satellite observations, land surface models, and ground data: Implications for data assimilation," *Journal of Hydrometeorology*, vol. 5, no. 3, pp. 430–442, 2004. dx.doi.org/10.1175/1525-7541(2004)005<0430:GSMFSO>2.0.CO;2

Reichle, R. H., R. D. Koster, P. Liu, S. P. P. Mahanama, E. G. Njoku, and M. Owe, "Comparison and assimilation of global soil moisture retrievals from the Advanced Microwave Scanning Radiometer for the Earth Observing System (AMSR-E) and the Scanning Multichannel Microwave Radiometer (SMMR)," *Journal of Geophysical Research—Atmospheres*, vol. 112, no. D9, D09108, 2007. dx.doi.org/10.1029/2006JD008033

Reichle, R. H., D. B. McLaughlin, and D. Entekhabi, "Hydrologic data assimilation with the ensemble Kalman filter," *Monthly Weather Review*, vol. 130, pp. 103–114, 2002.

Reichle, R. H., D. B. McLaughlin, and D. Entekhabi, "Variational data assimilation of microwave radiobrightness observations for land surface hydrology applications," *IEEE Trans. Geosci. Rem. Sens.*, vol. 39, no. 8, pp. 1708–1718, 2001. dx.doi.org/10.1109/36.942549

Reichle, R. H., J. P. Walker, R. D. Koster, and P. R. Houser, "Extended vs. ensemble Kalman filtering for land data assimilation," *Journal of Hydrometeorology*, vol. 3, no. 6, pp. 728–740, 2002. dx.doi.org/10.1175/1525-7541(2002)003<0728:EVEKFF>2.0.CO;2

Rowlandson, T. L., A. A. Berg, P. R. Bullock, E. R Ojo, H. McNairn, G. Wiseman, and M. H. Cosh, "Evaluation of Several Calibration Procedures for a Portable Soil Moisture Sensor," *Journal of Hydrology*, vol. 498, pp. 335–344, 2013. dx.doi.org/10.1016/j.jhydrol.2013.05.021

Sahoo, A. K., G. J. M. De Lannoy, R. H. Reichle, and P. R. Houser, "Assimilation and downscaling of satellite observed soil moisture over the Little River Experimental Watershed in Georgia, USA," *Advances in Water Resources*, vol. 52, pp. 19–33, 2013. dx.doi.org/10.1016/j.advwatres.2012.08.007

Shi, J., K. S. Chen, Q. Li, T. J. Jackson, P. E. O'Neill, and L. Tsang, "A parameterized surface reflectivity model and estimation of bare surface soil moisture with L-band radiometer," *IEEE Trans. Geosci. Rem. Sens.*, vol. 40, no. 12, pp. 2674–2686, 2002.

Shi, J., T. Jackson, J. Tao, J. Du, R. Bindlish, L. Lu, and K. S. Chen, "Microwave vegetation indices for short vegetation covers from satellite passive microwave sensor AMSR-E," *Remote Sensing of Environment*, vol. 112, no. 12, pp. 4285–4300, 2008.

Shi, J., L. M. Jiang, L. X. Zhang, K. S. Chen, J. P Wigneron, and A. Chanzy, "A parameterized multifrequency-polarization surface emission model," *IEEE Trans. Geosci. Rem. Sens.*, vol. 43, no. 12, pp. 2831–2841, 2005.

Shi, J., L. M. Jiang, L. X. Zhang, K. S. Chen, J. P. Wigneron, A. Chanzy, and T. Jackson, "Physically based estimation of bare surface soil moisture with the passive radiometers," *IEEE Trans. Geosci. Rem. Sens.*, vol. 44, no. 11, pp. 3145–3153, 2006.

Shuman, D., A. Nayyar, A. Mahajan, Y. Goykhman, K. Li, M. Liu, D. Teneketzis, M. Moghaddam, and D. Entekhabi, "Measurement scheduling for soil moisture sensing: From physical models to optimal control," *Proceedings of IEEE*, vol. 98, no. 11, pp. 1918–1933, 2010.

Silva, A., M. Liu, and M. Moghaddam, "Power-management techniques for wireless sensor networks and similar low-power communication devices based on non-rechargeable batteries," *Journal of Computer Networks and Communications*, vol. 2012, article ID 757291, 10 pages, 2012. dx.doi.org/10.1155/2012/757291

Silva, A., M. Liu, and M. Moghaddam, "Ripple-2: A non-collaborative, asynchronous, and open architecture for highly-scalable and low duty-cycle WSNs," *ACM Mobile Computing and Communications Review*, 17(1), pp. 55–60, 2013.

Spencer, M., C. Chen, H. Ghaemi, S. Chan, and J. Belz, "RFI Characterization and Mitigation for the SMAP Radar," *IEEE Trans. Geosci. Remote Sens.*, vol. 51, no. 10, pp. 4973–4982, October 2013.

Tabatabaeenejad, A., M. Burgin, and M. Moghaddam, "Potential of L-band radar for retrieval of canopy and sub-canopy parameters of boreal forests," *IEEE Trans. Geosci. Remote Sens.*, vol. 50, no. 6, pp. 2150–2160, 2012.

Tabatabaeenejad, A. and M. Moghaddam, "Retrieval of surface and deep soil moisture and effect of moisture profile on inversion accuracy," *IEEE Geoscience and Remote Sensing Letters*, vol. 8, no. 3, pp. 477–481, 2011.

Tsang, L., I. Koh, T. H. Liao, SH Huang, X. Xu, E. Njoku, and Y. Kerr, "Active and passive vegetated surface models with rough surface boundary conditions from NMM3D," *IEEE Journal of Selected Topics in Applied Earth Observations and Remote Sensing*, vol. 6, no. 3, pp. 1698–1709, 2013.

van den Hurk, B., F. Doblas-Reyes, G. Balsamo, R. D. Koster, S. Seneviratne, and H. Camargo Jr., "Soil moisture effects on seasonal temperature and precipitation forecast scores in Europe," *Climate Dynamics*, vol. 38, no. 1-2, pp. 349–362, 2012. dx.doi.org/ 10.1007/s00382-010-0956-2

van Zyl, J. J., "Applications: Measurement of Surface Soil Moisture," Chapter 5, *Synthetic Aperture Radar Polarimetry*, JPL Space Science and Technology Series, J. J. van Zyl and Y. Kim, Eds., p. 312, Wiley, 2011.

Vivoni, E. R., M. Gebremichael, C. J. Watts, R. Bindlish, and T. J. Jackson, "Comparison of ground-based and remotely-sensed surface soil moisture estimates over complex terrain during SMEX04," *Remote Sensing of Environment*, vol. 112, pp. 314–325, 2008.

Wagner, W., L. Brocca, V. Naeimi, R. H. Reichle, C. S. Draper, R. de Jeu, D. Ryu, C.-H. Su, A. Western, J.-C. Calvet, Y. H. Kerr, D. J. Leroux, M. Drusch, T. J. Jackson, S. Hahn, W. Dorigo, and C. Paulik, "Clarifications on the 'Comparison Between SMOS, VUA, ASCAT, and ECMWF Soil Moisture Products Over Four Watersheds in U.S.'," *IEEE Trans. Geosci. Rem. Sens.*, 52, pp. 1901–1906, 2014. dx.doi.org/10.1109/ TGRS.2013.2282172

Watts, J. D., J. S. Kimball, F.-J. W. Parmentier, T. Sachs, J. Rinne, D. Zona, W. Oechel, T. Tagesson, M. Jackowicz-Korczynski, and M. Aurela, "A satellite data driven biophysical modeling approach for estimating northern peatland and tundra CO2 and CH4 fluxes," *Biogeosciences*, vol. 11, pp. 1961–1980, 2014.

Wigneron, J.-P., A. Chanzy, Y. Kerr, J. C. Shi, M-J Escorihuela, A. Mialon, F. Demontoux, H. Lawrence, P. de Rosnay, and K. Saleh, "Evaluating an improved parameterization of the soil emission in L-MEB," *IEEE Trans. Geosci. Remote Sens.*, vol. 49, no. 4, pp. 1177–1189, 2011.

Wu, T.-D., K.-S. Chen, J. Shi, H.-W. Lee, and A. K. Fung, "A study of an AIEM model for bistatic surface scattering from randomly rough surfaces," *IEEE Trans. Geosci. Rem. Sens.*, vol. 46, no. 9, pp. 2584–2598, 2008. dx.doi.org/10.1109/TGRS.2008.919822

Yan, W. Z., Y. Du, Z. Li, E. Chen and J. Shi, "Characterization of the validity region of the extended T-matrix method for scattering from dielectric cylinders with finite length," *Progress in Electromagnetics Research*, vol. 96, pp. 309–328, 2009.

Yi, Y., J. Kimball, L. Jones, R. H. Reichle, and K. McDonald, "Evaluation of MERRA land surface estimates in preparation for the Soil Moisture Active Passive mission," *Journal of Climate*, vol. 24, no. 15, pp. 3797–3816, 2011. dx.doi.org/10.1175/2011JCLI4034.1

Yi, Y., J. S. Kimball, L. A. Jones, R. H. Reichle, R. Nemani, and H. A. Margolis, "Recent climate and fire disturbance impacts on boreal and arctic ecosystem productivity estimated using a satellite-based terrestrial carbon flux model," *Journal of Geophysical Research—Biogeosciences*, vol. 118, no. 2, pp. 606–622, 2013. dx.doi.org/10.1002/ jgrg.20053

Yi, Y., J. S. Kimball, and R. H. Reichle, "Spring Hydrology Determines Summer Net Carbon Uptake in Northern Ecosystems," *Environmental Research Letters*, vol. 9, no. 6, 064003, 2014. dx.doi.org/10.1088/1748-9326/9/6/064003

Yilmaz, M. T. and W. T. Crow, "The optimality of potential rescaling approaches in land data assimilation," *Journal of Hydrometeorology*, vol. 14, no. 2, pp. 650–660, 2013. dx.doi.org/10.1175/JHM-D-12-052.1

Yilmaz, M. T., W. T. Crow, M. C. Anderson, and C. Hain, "An objective methodology for merging satellite and model-based soil moisture products," *Water Resources Research*, vol. 48, no. 11, W11502, 2012. dx.doi.org/10.1029/2011WR011682

Yilmaz, M. T., E. R. Hunt, L. D. Goins, S. L. Ustin, V. C. Vanderbilt, and T. J. Jackson, "Vegetation water content during SMEX04 from ground data and Landsat 5 thematic mapping imagery," *Remote Sensing of Environment*, vol. 112, pp. 350–362. 2008a.

Yilmaz, M. J., E. R. Hunt Jr., and T. J. Jackson, "Remote sensing of vegetation water content from equivalent water thickness using satellite imagery," *Remote Sensing of Environment*, vol. 112, pp. 2514–2522, 2008b.

Zhan, X., W. T. Crow, T. J. Jackson, and P. O'Neill, "Improving space-borne radiometer soil moisture retrievals with alternative aggregation rules for ancillary parameters in highly heterogeneous vegetated areas," *IEEE Geoscience and Remote Sensing Letters*, vol. 2, pp. 261–265, 2008.

Zhang, K., J. S. Kimball, Y. Kim, and K. C. McDonald, "Changing freeze-thaw seasons in northern high latitudes and associated influences on evapotranspiration," *Hydrological Processes*, vol. 25, pp. 4142–4151, 2011.

Zhang, Y., M. S. Moran, M. A. Nearing, Guillermo E. Ponce Campos, A. R. Huete, A. R. Buda, D. D. Bosch, S. A. Gunter, S. G. Kitchen, W. H. McNab, J. A. Moran, M. P. McClaran, D. S. Montoya, D. P. C. Peters, and P. J. Starks, "Extreme precipitation patterns reduced terrestrial ecosystem production across biomes during 2000–2009," *Journal of Geophysical Research—Biogeosciences*, vol. 118, pp. 1–10, 2013. dx.doi.org/10.1029/2012JG002136

Zhang, S. L., J. Shi, and Y. J. Dou, "A soil moisture assimilation scheme based on the microwave land emissivity model and the community land model," *International Journal of Remote Sensing*, vol. 33, no. 9, pp. 2770–2797, 2012. dx.doi.org/10.1080/01431161.2011.620032

Zhang, Z. J., J. Shi, and J. Z. Luan, "The microwave scattering and absorption characteristics of vegetation," *Journal of Remote Sensing*, vol. 10, no. 4, pp. 537–541, 2006.

Zhou, Y., D. McLaughlin, and D. Entekhabi, "Assessing the performance of the ensemble Kalman filter for land surface data assimilation," *Monthly Weather Review*, vol. 134, no. 8, pp. 2128–2142, 2006.

Zhou, Y., D. McLaughlin, D. Entekhabi and G.-H. C. Ng, "An ensemble multiscale filter for large nonlinear data assimilation problems," *Monthly Weather Review*, vol. 136, pp. 678–698, 2008.

Zhao, T., L. X. Zhang, J. Shi, and L. Jiang, "A physically based statistical methodology for surface soil moisture retrieval in the Tibetan Plateau using microwave vegetation indices," *Journal of Geophysical Research—Atmospheres*, vol. 116, no. D8, D08116, 2011. dx.doi.org/10.1029/2010JD015229

# Abbreviations and Acronyms

| | |
|---|---|
| **A** | Active |
| **AAFC** | Agriculture and Agri-Food Canada |
| **ACE** | Flight controller |
| **AER** | Atmospheric and Environmental Research, Inc. |
| **AERONET** | Aerosol Robotic Network |
| **AGU** | American Geophysical Union |
| **AirMOSS** | Airborne Microwave Observatory of Subcanopy and Subsurface |
| **AIRS** | Atmospheric Infrared Sounder |
| **AIRSAR** | Airborne Synthetic Aperture Radar |
| **ALECTRA** | Alaska Ecological Transect |
| **ALOS PALSAR** | Advanced Land Observing Satellite Phased Array L-band SAR |
| **AMMA** | African Monsoon Multidisciplinary Analyses |
| **AMR** | Advanced Microwave Radar |
| **AMS** | American Meteorological Society |
| **AMSR-E** | Advanced Multichannel Scanning Radiometer–EOS |
| **ANA** | Analysis |
| **AOT** | Aerosol Optical Thickness |
| **AP** | Active-Passive |
| **APAR** | Absorbed Photosynthetically Active Radiation |
| **AppWG** | Applications Working Group |
| **ARL** | Army Research Laboratory |
| **ARS** | Agricultural Research Service |
| **ASA** | American Society of Agronomy |
| **ASAG** | Applied Sciences Advisory Group |
| **ASAR** | Advanced Synthetic Aperture Radar |
| **ASCAT** | Advanced Scatterometer |
| **ASF** | Alaska Satellite Facility |
| **ASRIS** | Australian Soil Research Information System |

| | |
|---|---|
| **ASSH** | Automatic Station for Soil Hydrology |
| **ASU** | Arizona State University |
| **ATBD** | Algorithm Theoretical Basis Document |
| **BERMS** | Boreal Ecosystem Research and Monitoring Sites |
| **BFPQ** | Block Floating Point Quantized |
| **BPLUT** | Biome Properties Look-Up Table |
| **CALMIT** | Center for Advanced Land Management Information Technologies |
| **CanEx10** | Canadian Experiment for Soil Moisture 2010 |
| **CARVE** | Carbon in Arctic Reservoirs Vulnerability Experiment |
| **CASA** | Carnegie Ames Stanford Approach |
| **CATDEF** | Catchment Deficit |
| **CCRN** | Changing Cold Regions Network |
| **CDC** | Centers for Disease Control |
| **C&DH** | Command and Data Handling |
| **CDR** | Critical Design Review |
| **CEOP** | Coordinated Energy and Water Cycle Observations Project |
| **CEOS** | Committee on Earth Observation Satellites |
| **CF** | Climate and Forecast |
| **CIRES** | Cooperative Institute for Research in Environmental Sciences |
| **CLASIC** | Cloud Land Surface Interaction Campaign |
| **CMB** | Cosmic Microwave Background |
| **CMD** | Command |
| **CNCS** | Correlated Noise Calibration Standard |
| **CNS** | Coupled Noise Source; Correlated Noise Source |
| **ComRAD** | Combined Radar/Radiometer |
| **CONAE** | Comisión National de Actividades Especiales |

| | | | | |
|---|---|---|---|---|
| CONUS | Continental United States | | ECS | EOSDIS Core System |
| COSMOS | Cosmic-ray Soil Moisture Observing System | | EDOS | EOS Data and Operations System |
| COTS | Commercial Off-The-Shelf | | EESS | Earth Exploration Satellite Service |
| CPC | Climate Prediction Center | | EFOV | Effective Field of View |
| CREST | Cooperative Remote Sensing Science and Technology Center | | EIOC | End of In-Orbit Commissioning |
| | | | EMS | ESDIS Metrics System |
| CRN | Climate Reference Network | | ENF | Evergreen Needleleaf Forest |
| CRREL | Cold Regions Research and Engineering Laboratory | | EnKF | Ensemble Kalman Filter |
| | | | Envisat | Environmental Satellite |
| CSA | Canadian Space Agency | | EOM | End of Mission |
| CSC | Cold Space Calibration; Cold Sky Calibration | | EOS | Earth Observing System |
| | | | EOSDIS | Earth Observing System Data and Information System |
| CSU | Colorado State University | | | |
| CUNY | City College of New York | | ERDC | Engineer Research and Development Center |
| CVS | Core Validation Site | | | |
| | | | ERS | European Remote Sensing Satellite |
| DAAC | Distributed Active Archive Center | | ESA | European Space Agency |
| DBA | Distorted Born Approximation | | ESDIS | Earth Science Data and Information System |
| DBD | Deciduous Broadleaf Forest | | | |
| DCA | Dual-Channel Algorithm | | ESSP | Earth System Science Pathfinder |
| DCL | Dear Colleague Letter | | EUMETSAT | European Organisation for the Exploitation of Meteorological Satellites |
| DEM | Digital Elevation Model | | | |
| DIP | Diplexer | | EURAC | European Academy of Bozen/Bolzano |
| DoD | Department of Defense | | | |
| DS | Decadal Survey | | FAA | Federal Aviation Administration |
| DSMC | Data Services Management Center | | FAS | Foreign Agricultural Service |
| DTS | Distributed Temperature Sensor | | FCST | Forecast |
| | | | FDF | Flight Dynamics Facility |
| EA | Early Adopters | | FDR | Frequency Domain Reflectometry |
| EASE2 | Equal-Area Scalable Earth–2 (Grid) | | FEWS | Famine Early Warning Systems Network |
| EC | Environmental Constraint; Environment Canada | | FLDAS | FEWS Land Data Assimilation System |
| | | | FLUXNET | Global Network Monitoring $CO_2$, Water, and Energy Flux |
| ECHO | EOS Clearing House | | | |
| ECMWF | European Centre for Medium-Range Weather Forecasts | | FMI-ARC | Arctic Research Center of Finnish Meteorological Institute |

| | |
|---|---|
| **FOT** | Flight Operations Team |
| **FPAR** | Fraction of Photosynthetically Active Radiation |
| **FPGA** | Field-Programmable Gate Array |
| **FT; F/T** | Freeze/Thaw |
| **FTE** | Full-Time Equivalent |
| **FT-ESDR** | Freeze/Thaw Earth System Data Record |
| **FTP** | File Transfer Protocol |

| | |
|---|---|
| **GCM** | General Circulation Model |
| **GCMD** | Global Change Master Directory |
| **GCOM-W** | Global Change Observation Mission –Water |
| **GDS** | Ground Data System |
| **GEOS-5** | Goddard Earth Observing Model System, Version 5 |
| **GEOSS** | Global Earth Observation System of Systems |
| **GloSim** | Global-Scale Simulation |
| **GMAO** | Global Modeling and Assimilation Office |
| **GNSS** | Global Radio Navigation Satellite |
| **GPM** | Global Precipitation Measurement |
| **GPP** | Gross Primary Production |
| **GPS** | Global Positioning System |
| **GRACE** | Gravity Recovery and Climate Experiment |
| **GRACE-FO** | Gravity Recovery and Climate Experiment Follow-On |
| **GRS** | Grassland |
| **GSL** | Geotechnical and Structures Laboratory |
| **GSFC** | Goddard Space Flight Center |
| **GRUMP** | Global Rural–Urban Mapping Project |
| **GT** | Georgia Institute of Technology |
| **GTOPO30** | Global 30 Arcsecond Elevation (DEM) |

| | |
|---|---|
| **H** | Horizontal |
| **HDF5** | Hierarchical Data Format Version 5 |
| **HOAL** | Hydrological Open Air Laboratory |
| **Hydros** | Hydrosphere State |
| **HWSD** | Harmonized World Soil Database |

| | |
|---|---|
| **IceSAT-2** | Ice, Cloud, and land Elevation Satellite-2 |
| **IF** | Intermediate Frequency |
| **IFOV** | Instantaneous Field of View |
| **IGARSS** | International Geosciences and Remote Sensing Symposium |
| **IGBP** | International Geosphere-Biosphere Programme |
| **IGRF** | International Geomagnetic Reference Field |
| **IOC** | In-Orbit Checkout; In-Orbit Commissioning |
| **IMS** | Interactive Multisensor Snow and Ice Mapping System |
| **IONEX** | Ionosphere Map Exchange |
| **IPCC** | Intergovernmental Panel on Climate Change |
| **IR** | Infrared |
| **IRI** | International Research Institute for Climate and Society; International Reference Ionosphere |
| **ISO** | International Organization for Standardization |
| **ISST** | In Situ Sensor Testbed |

| | |
|---|---|
| **JAXA** | Japan Space Agency |
| **JERS** | Japanese Earth Resources Satellite |
| **JPL** | Jet Propulsion Laboratory |

| | |
|---|---|
| **LCLUC** | Land Cover and Land Use Change |
| **LIS** | Land Information System |
| **LPRM** | Land Parameter Retrieval Model |

| | |
|---|---|
| **LR** | Little River |
| **LST** | Local Solar Time |
| **LUE** | Light Use Efficiency |
| **LW** | Little Washita |
| **LZPF** | Level Zero Processing Facility |

| | |
|---|---|
| **MAHASRI** | Monsoon Asian Hydro-Atmospheric Scientific Research and Prediction Initiative |
| **MARE** | Marena, Oklahoma, Mesonet Site |
| **MDOT** | Mission Data Operations Team |
| **MEaSUREs** | Making Earth System Data Records for Use in Research Environments |
| **MERRA** | Modern-Era Retrospective Analysis for Research and Applications |
| **MGS** | McMurdo Station, Antarctica, antenna |
| **MOC** | Mission Operations Center |
| **MODIS** | Moderate Resolution Imaging Spectroradiometer |
| **MOISST** | Marena Oklahoma In Situ Sensor Testbed |
| **MOS** | Mission Operations System |
| **MOU** | Memorandum of Understanding |
| **MPD** | Maximum Probability of Detection |
| **MPDI** | Microwave Polarization Difference Index |
| **MPRA** | Microwave Polarization Ratio Algorithm |
| **MXF** | Mixed Forest |

| | |
|---|---|
| **N** | Nitrogen |
| **NAIF** | Navigation and Ancillary Information Facility |
| **NASA** | National Aeronautics and Space Administration |
| **NASS** | National Agricultural Statistical Service |
| **NCEP** | National Centers for Environmental Prediction |

| | |
|---|---|
| **NDMC** | National Drought Mitigation Center |
| **NDVI** | Normalized Difference Vegetation Index |
| **NEDT** | Noise Equivalent Delta Temperature |
| **NEE** | Net Ecosystem Exchange |
| **NEN** | Near-Earth Network |
| **NESDIS** | National Environmental Satellite Data and Information Service (NOAA) |
| **NL** | Netherlands |
| **NOAA** | National Oceanic and Atmospheric Administration |
| **NPOESS** | National Polar Orbiting Operational Environmental Satellite System |
| **NPP** | Net Primary Production |
| **NPP/JPSS** | NPOESS Preparatory Project/Joint Polar Satellite System |
| **NRC** | National Research Council |
| **NRCS** | Natural Resources Conservation Service; Normalized Radar Cross-Section |
| **NRL** | Naval Research Laboratory |
| **NSD** | National Soil Database |
| **NSIDC** | National Snow and Ice Data Center |
| **NWP** | Numerical Weather Prediction |

| | |
|---|---|
| **OCO-2** | Orbiting Carbon Observatory–2 |
| **OMT** | Orthomode Transducer |
| **OSSE** | Observing System Simulation Experiment |
| **OSU** | Oklahoma State University |

| | |
|---|---|
| **P** | Passive |
| **PALS** | Passive Active L-Band System; Passive Active L-band Sensor |
| **PALSAR** | Phased Array L-Band SAR |
| **PAR** | Photosynthetically Active Radiation |
| **PBMR** | Pushbroom Microwave Radiometer |
| **PDR** | Preliminary Design Review |

| | | | | |
|---|---|---|---|---|
| **PFT** | Plant Functional Types | | **RZEXC** | Root Zone Excess |
| **PLIS** | Polarimetric L-Band Imaging Scatterometer | | **SAC-D** | Satélite de Aplicaciones Científicas–D |
| **PLMR** | Polarimetric L-band Multibeam Radiometer | | **SAOCOM** | Satélite Argentino de Observatión con Microondas |
| **PLO-OSC** | Phase-Locked Oscillator | | **SAR** | Synthetic Aperture Radar |
| **PRF** | Pulse Repetition Frequency | | **S/C** | Spacecraft |
| **PRI** | Pulse Repetition Interval | | **SCA** | Single-Channel Algorithm |
| **PTL** | Product Team Lead | | **SCA-H (V)** | Single-Channel Algorithm at H Polarization (V Polarization) |
| **PWR** | Power | | **SCAN** | Soil Climate Analysis Network (USDA) |
| **QA** | Quality Assessment | | **SCH** | Spherical Coordinate System |
| **QC** | Quality | | **SDEV** | Standard Deviation |
| **QuikSCAT** | Quick Scatterometer | | **SDS** | Science Data System |
| | | | **SDT** | Science Definition Team |
| **RATS** | (Heritage Noise Source) | | **s.f.u.** | Solar Flux Unit |
| **RBA** | Reflector Boom Assembly | | **SGP** | Southern Great Plains Experiment |
| **RBE** | Radio Frequency Back-End | | **SGS** | Svalbard, Norway, antenna |
| **RC** | Reynolds Creek | | **SIA** | Spun Instrument Assembly |
| **RDE** | Radiometer Digital Electronics | | **SIR** | System Integration Review |
| **Reco** | Ecosystem Respiration | | **SIR-C** | Spaceborne Imaging Radar–C |
| **REMEDHUS** | Red de Medición de la Humedad del Suelo | | **SM** | Soil Moisture |
| **RF** | Radio Frequency | | **SMAP** | Soil Moisture Active Passive |
| **RFE** | Radiometer Front-End | | **SMAPEx** | SMAP Experiments |
| **RFI** | Radio Frequency Interference | | **SMAPVEX** | Soil Moisture Active Passive Validation Experiment |
| **RFN** | Request for Nomination | | **SMEX** | Soil Moisture Experiment |
| **RHS** | Right-Hand Side | | **SMEX02** | Soil Moisture Experiment 2002 |
| **RMS** | Root Mean Square | | **SMMR** | Scanning Multichannel Microwave Radiometer |
| **RMSD** | Root Mean Square Difference | | | |
| **RMSE** | Root Mean Square Error | | **SMOS** | Soil Moisture and Ocean Salinity |
| **RSS** | Residual Sum of Squares | | **SMOSMANIA** | Soil Moisture and Ocean Salinity Meteorological Automatic Network Integrated Application |
| **RTM** | Radiative Transfer Model | | | |
| **RVI** | Radar Vegetation Index | | **SN** | Space Network |

| | |
|---|---|
| **SNOTEL** | Snow Telemetry |
| **SNR** | Signal-to-Noise Ratio |
| **SOA** | Summary of Activities |
| **SOC** | Soil Organic Carbon |
| **SPDM** | Science Processing and Data Management |
| **SPoRT** | Short-term Prediction Research and Transition (Center) |
| **SRC** | Source |
| **SRFEXC** | Surface Excess |
| **SRMSC** | Science Requirement and Mission Success Criteria |
| **SRTM** | Shuttle Radar Topography Mission |
| **SSM/I** | Special Sensor Microwave Imager |
| **SSS** | Sea Surface Salinity |
| **SST** | Sea Surface Temperature |
| **ST** | Science Team |
| **STT** | Slow-Time Thresholding |
| **STATSGO-US** | State Soil Geographic Data Base for the Conterminous United States |
| **S/W** | Software |
| **SWE** | Snow Water Equivalent |
| **SWOT** | Surface Water Ocean Topography |

| | |
|---|---|
| **TB** | Brightness Temperature |
| **TBD** | To Be Determined |
| **TBH** | Brightness Temperature in Horizontal Polarization |
| **TBV** | Brightness Temperature in Vertical Polarization |
| **TC** | Triple Collocation |
| **TCF** | Terrestrial Carbon Flux |
| **TDR** | Time Domain Reflectometry |
| **TDRS** | Tracking and Data Relay Satellite |
| **TDRSS** | Tracking and Data Relay Satellite System |

| | |
|---|---|
| **TEC** | Total Electron Content; Total Electron Count |
| **TERENO** | Terrestrial Environmental Observatories |
| **TLM** | Telemetry |
| **TOGA-TAO** | Tropical Ocean Global Atmosphere/ Tropical Atmosphere Ocean |

| | |
|---|---|
| **UAF** | University of Alaska Fairbanks |
| **UAVSAR** | Uninhabited Aerial Vehicle Synthetic Aperture Radar |
| **URS** | User Registration System |
| **URSA** | User Remote Sensing Access |
| **USACE** | U. S. Army Corps of Engineers |
| **USCRN** | U. S. Climate Reference Network |
| **USDA** | U. S. Department of Agriculture |
| **USDM** | U. S. Drought Monitor |
| **USFS** | U. S. Forest Service |
| **USGS** | U. S. Geological Survey |

| | |
|---|---|
| **V** | Vertical |
| **VI** | Vegetation Index |
| **VIIRS** | Visible Infrared Imaging Radiometer Suite |
| **VPD** | Vapor Pressure Deficit |
| **VWC** | Vegetation Water Content |

| | |
|---|---|
| **WG** | Walnut Gulch |
| **WGS** | Wallops antennas; World Geodetic System |
| **WMO** | World Meteorological Organization |
| **WSC** | White Sands Complex |

| | |
|---|---|
| **XML** | Extensible Markup Language |